Decoding Algorithms for Some Non-Coherent Space-Time Codes

Antonio Maria Cipriano

Algorithmes de Décodage pour des Codes Espace-Temps Non Cohérents

Antonio Maria Cipriano

École Nationale Supérieure des Télécommunications

Thèse en cotutelle avec l'Université de Padoue, Italie

8 mars 2005

Ringraziamenti

Il mio primo pensiero va al Prof. Gianfranco Cariolaro, che mi ha incoraggiato a seguire la via della ricerca e mi ha insegnato il gusto e l'esigenza del lavoro di gruppo. Oltre a lui sono ben presenti nella mia mente Tomaso Erseghe, Paolo Villoresi, Francesco De Pellegrini e Nicola Laurenti, a cui sono riconoscente fra l'altro per aver svolto spesso il ruolo del "confessore". Un ringraziamento particolare va sicuramente ai miei compagni di ufficio Gabriele, Valentina, Khalid, Tommaso, Mino per le numerose discussioni tecniche ma ancor più per l'atmosfera calorosa e umana che non hanno mai fatto mancare. Vorrei poi ringraziare Filippo, Antonio, Daniele, Giambattista, Federico, Mauro, Federica e tutti coloro che ho dimenticato di citare ma che con la loro personalità hanno arricchito le mie giornate.

Infine, ringrazio la mia famiglia, Angelo e Marine per la loro continua presenza e sostegno.

Je tiens aussi à remercier mon directeur de thèse à l'E.N.S.T. Georges Rodriguez Guisantes qui a accepté d'encadrer ma recherche en France, il a su avoir la patience de m'écouter et me soutenir tant moralement que financièrement quand il le fallait. Le travail de recherche ici réalisé a bénéficié de son éclairage ainsi que de celui de Jean–Claude Belfiore, Inès Kammoun, Olivier Rioul, Slim Chabbou, Nicolas Gresset, Philippe Ciblat. Ce présent document doit aussi beaucoup aux courageux correcteurs: Slim, Danilo, Sylvain, Marine.

Un grand merci à tous les gens (et ils sont nombreux) qui ont contribué à rendre agréables les longues journées de travail: Lydia, Slim, Ghalid, Ghassan, Ghaya, Nicolas, Chantal, Fatma, Hans–Martin, Cédric, Bruno, Daniel, João, Ioannis, David, Oliver, Elena, Anne–Laure, Ihsan, Adel, Axel, Sébastien, etc.. Enfin, une pensée pleine de gratitude pour mes copains de bureau: Sylvain, Emilio, Elie, Elias, Frédéric.

Contents

Tables of Abbreviations and Notations

Abbreviations:

AWGN	Additive White Gaussian Noise
BER	Bit Error Probability
CD	Compact Decomposition
co–ML–tg	coherent Maximum Likelihood decoder on the tangent space
CPM	Continuous Phase Modulation
CS	Cosine–Sine (form or representation)
CSI	Channel State Information
EP codes	noncoherent codes obtained via exponential map
E–D	Estimation–Detection
FER	Frame Error Probability
GLRT	Generalized Likelihood Ratio Test
mCD	modified Compact Decomposition
MD	Minimal Decomposition
MIMO	Multiple Input Multiple Output
ML	Maximum Likelihood
PAM	Pulse Amplitude Modulation
PEP	Pairwise Error Probability
SIMO	Single Input Multiple Output
SISO	Single Input Single Output
SNR	Signal to Noise Ratio
STB	Space–Time Block (code)
SVD	Singular Value Decomposition
TAST	Threaded Algebraic Space–Time (code)
TSVD	Thin Singular Value Decomposition

Notations:

$\mathbb{C}^T$	vector space of complex vectors of length T
$\mathbf{I}_M$	$M \times M$ identity matrix
$\mathbf{0}_M$	$M \times M$ null matrix
$\mathbf{I}_{T,M}$	$T \times M$ matrix $\mathbf{I}_{T,M}^t = [\mathbf{I}_M \ \mathbf{0}_{T-M}]$, $T \geq M$
$\mathbf{x}$	(complex) column vector
$\mathbf{X}$	(complex) matrix
$\mathbf{X}^t$	transpose matrix
$\mathbf{X}^*$	conjugate matrix
$\mathbf{X}^\dagger$	transpose conjugate matrix
$\mathrm{vec}(\mathbf{X})$	column vector built with the columns of $\mathbf{X}$
$\mathrm{rank}(\mathbf{X})$	the rank of matrix $\mathbf{X}$
$\mathrm{null}(\mathbf{X})$	the null space of matrix $\mathbf{X}$
span($\mathbf{X}$), $\Omega_{\mathbf{X}}$	vector subspace spanned by the columns of $\mathbf{X}$
$\dim(\Omega_{\mathbf{X}})$	the dimension of vector subspace $\Omega_{\mathbf{X}}$, i.e. rank($\mathbf{X}$)
$\lvert\mathbf{A}\rvert$, det($\mathbf{A}$)	the determinant of the complex square matrix $\mathbf{A}$
$\mathrm{tr}\,\mathbf{A}$	the trace of the complex square matrix $\mathbf{A}$, i.e. the sum of its diagonal elements
$\lVert\mathbf{A}\rVert_F$	Frobenius norm of matrix $\mathbf{A}$, equal to $(\mathrm{tr}(\mathbf{A}\,\mathbf{A}^\dagger))^{-1/2}$
$\lVert\mathbf{A}\rVert_2$	spectral norm of $\mathbf{A}$, equal to $\sqrt{\lambda}$, with λ the maximum eigenvalue of $\mathbf{A}^\dagger\mathbf{A}$
$\otimes$	matrix Kronecker product
$\mathcal{U}_M$	group of the $M \times M$ unitary matrices
$\mathcal{U}_{T,M}$	set of the $T \times M$ complex matrices with orthonormal columns
$\mathfrak{u}_T$	set of the $T \times T$ skew–Hermitian matrices
$G_{T,M}$	Grassmann manifold of M–dimensional vector subspaces of $\mathbb{C}^T$
Ω_{ref}, $\mathbf{X}_{ref}$	reference subspace
$\Omega_{\mathbf{X}} + \Omega_{\mathbf{Y}}$	sum between subspaces, i.e. span$[\mathbf{X}\ \mathbf{Y}]$
$\Omega_{\mathbf{X}} \cap \Omega_{\mathbf{Y}}$	subspace intersection
$\exp$	the exponential map
$\exp^{-1}$	the exponential map inverse
$t\pi_\Omega$	tangent space to the Grassmannian at the subspace Ω
$t\pi_{ref}$	tangent space to the Grassmannian at the reference subspace
$B_{\pi/2}$	open subset of $t\pi_{ref}$ in which the exponential map is invertible
$\mathbb{U}$	unit circle in the complex plane, i.e. $\{v \in \mathbb{C} : \lvert v\rvert = 1\}$
$\mathbb{U}_T^{T-n}(\mathbf{u}_1, .., \mathbf{u}_n)$	unit hyperphere in $\mathbb{C}^T$ orthogonal to subspace span($\mathbf{U}$) where $\mathbf{U} = [\mathbf{u}_1, \ldots, \mathbf{u}_n]$, i.e. $\{\mathbf{v} \in \mathbb{C}^T : \lVert\mathbf{v}\rVert = 1, \mathbf{v}^\dagger\mathbf{U} = \mathbf{0}\}$
$\mathcal{B}$, $\mathcal{B}'$	coherent space–time code
$\mathcal{C}$ ($\mathcal{C}_\mathcal{B}$)	non–coherent EP code (obtained from $\mathcal{B}$)
$\mathcal{T}$ ($\mathcal{T}_\mathcal{B}$)	non–coherent training–based code (obtained from $\mathcal{B}$)
$\lvert\mathcal{C}\rvert$, L	code cardinality
$d_c(\Omega_{\mathbf{X}}, \Omega_{\mathbf{Y}})$	chordal distance between $\Omega_{\mathbf{X}}$ and $\Omega_{\mathbf{Y}}$
$d_{cF}(\Omega_{\mathbf{X}}, \Omega_{\mathbf{Y}})$	chordal Frobenius distance between $\Omega_{\mathbf{X}}$ and $\Omega_{\mathbf{Y}}$
$d_p(\Omega_{\mathbf{X}}, \Omega_{\mathbf{Y}})$	product distance between $\Omega_{\mathbf{X}}$ and $\Omega_{\mathbf{Y}}$

$d_{arc}(\Omega_{\mathbf{X}}, \Omega_{\mathbf{Y}})$	geodesic distance between $\Omega_{\mathbf{X}}$ and $\Omega_{\mathbf{Y}}$
$d_c(\mathcal{C})$	minimum chordal distance of code $\mathcal{C}$
$d_{cF}(\mathcal{C})$	minimum chordal Frobenius distance of code $\mathcal{C}$
$d_p(\mathcal{C})$	minimum product distance of code $\mathcal{C}$
$d_{arc}(\mathcal{C})$	minimum geodesic distance of code $\mathcal{C}$
$\mathcal{CN}(\mathbf{m}, \mathbf{K})$	circularly symmetric, complex Gaussian random variable of mean $\mathbf{m}$ and covariance $\mathbf{K}$
P_e	average supersymbols error probability or FER (Frame Error Probability)
P_{ij}	pairwise error probability between sent codeword $\mathbf{X}_i$ and received codeword $\mathbf{X}_j$ inthe case that $\mathcal{C} = \{\mathbf{X}_i, \mathbf{X}_j\}$
$d^{alg}(\mathcal{C})$	algebraic diversity of code $\mathcal{C}$
$d^{co-ML}(\mathcal{B})$	PEP–based diversity of code $\mathcal{B}$ with respect to coherent ML rule
$d^{nc-ML}(\mathcal{B})$	PEP–based diversity of code $\mathcal{B}$ with respect to non–coherent ML rule
$d^{GRLT}(\mathcal{C})$	PEP–based diversity of code $\mathcal{C}$ with respect to GLRT
$d^{E-D}(\mathcal{T})$	PEP–based diversity of code $\mathcal{T}$ with respect to estimation-detection rule

Riassunto

Questa tesi raccoglie parte dei risultati ottenuti durante il mio dottorato di ricerca, che ho svolto nell'ambito di un accordo di cotutela tra l'Università di Padova e l'École Nationale Supérieure des Télécommunications (E.N.S.T.) di Parigi a partire dal mese di gennaio 2001 fino a dicembre 2004. A Padova sono stato inserito nell'equipe del Prof. Gianfranco Cariolaro del Dipartimento d'Ingegneria dell'Informazione (DEI), mentre a Parigi la ricerca è stata supervisionata dal Prof. Georges Rodriguez Guisantes all'interno del Dipartemento Communications et Electronique (ComElec).

Gli enormi progressi delle tecnologie della comunicazione negli ultimi quindici anni hanno permesso lo sviluppo di nuovi modi di comunicare e di lavorare; pensiamo ad Internet, agli enormi flussi di dati che transitano sulla rete ogni secondo, ai servizi integrati multimediali sempre più accessibili, grazie anche all'affidabilità delle fibre ottiche e ai progressi fatti nello sfruttamento del doppino (ADSL). Ultimamente, una certa filosofia vorrebbe rendere tali servizi disponibili agli utenti là dove si trovano, integrando la tecnologia necessaria nei computer portatili e nei telefoni cellulari. Per far questo, bisogna abbandonare la "sicurezza" rappresentata dalle trasmissioni via cavo, per passare alle trasmissioni via radio. Purtroppo, il canale radio è un mezzo trasmissivo tra i meno affidabili, è soggetto ad interferenze e pone grossi problemi di sicurezza.

Ci concentreremo su un aspetto: come fornire su un canale radio una velocità di trasmissione sufficientemente elevata ed un tasso di errore abbastanza basso da garantire i flussi di dati e la qualità necessaria ai servizi multimediali? Una proposta tra le tante fatte è quella di dotare il trasmettitore ed il ricevitore di una schiera di antenne, cioè di aumentare la cosiddetta diversità spaziale del sistema di comunicazione. L'idea è semplice: se si dispongono le antenne sufficientemente lontane le une dalle altre in maniera tale che i diversi canali non siano correlati tra loro, la probabilità che tutti i cammini radio siamo fortemente perturbati è via via più bassa man mano che il numero delle antenne aumenta.

Alla fine degli anni novanta, i lavori di Telatar e, parallelamente, di Foschini e Gans hanno dimostrato che con questa tecnica si possono teoricamente raggiungere velocità di trasmissione elevate. Negli stessi anni Tarokh e altri ricercatori hanno fornito delle strategie per organizzare in maniera conveniente i dati sulle diverse antenne in trasmissione, riuscendo a sfruttare a pieno la diversità spaziale offerta dal canale e ottenendo un guadagno di codifica. Nascevano dunque i cosiddetti *codici spazio–tempo*.

Da allora un numero crescente di ricercatori si è dedicato a questo promettente

filone di ricerca, sviluppando le idee originali, proponendone altre e adattandole a diversi scenari. Questa tesi sviluppa soprattutto uno di questi scenari, tutt'ora oggetto di ricerca, in cui il ricevitore ed il trasmettitore non siano a conoscenza del canale, al contrario di quanto accade nella maggior parte dei lavori su questo tema, dove si suppone una conoscenza perfetta del canale al ricevitore e/o al trasmettitore.

Il principale argomento di questo lavoro, trattato nei primi 4 capitoli, è dunque uno studio della codifica e decodifica dei cosiddetti codici Spazio–Tempo a Blocco (STB) non coerenti. Lo scenario è costituito da una comunicazione punto–punto e singolo utente in cui né il trasmettitore né il ricevitore abbiano una conoscenza dello sfasamento e dell'attenuazione introdotta dal canale (sistemi non–coerenti). Quest'ultimo viene simulato secondo delle ipotesi semplificate universalmente accettate nella letteratura e formulate ad–hoc per la progettazione degli algoritmi di codifica e decodifica. Contemporaneamente, il modello di canale utilizzato in questa tesi è sufficientemente generale da poter coprire le problematiche fondamentali di tali sistemi: il canale a più ingressi e più uscite (Multiple Input Multiple Output – MIMO) può avere delle attenuazioni profonde (Rayleigh fading channel), ma non sono presi in conto né l'effetto Doppler (flat fading), né canali a cammini multipli (il canale si suppone a banda stretta).

I sistemi non coerenti non sono molto diffusi nell'ambito della ricerca perché di solito si preferisce cercare di stimare il canale al ricevitore per migliorare le prestazioni. Comunque, quando il canale varia troppo rapidamente o quando considerazioni di costo lo impongano, la stima di canale può essere troppo onerosa o addirittura impossibile da implementare. Potrebbe essere il caso, per esempio, di canali con tempi di coerenza di pochi periodi di simbolo, o di sistemi ad accesso multiplo in cui brevi intervalli temporali e/o frequenziali non contigui siano assegnati a diversi utenti. Il modello utilizzato per rappresentare tali canali suppone i loro coefficienti costanti su un intervallo di tempo T (chiamato "blocco"). Ad ogni blocco i coefficienti vengono rinnovati secondo un processo stocastico tempo invariante a simboli indipendenti (block fading channel). La durata del blocco T in periodi di simbolo è dell'ordine del numero di antenne in emissione M. Per tali valori di T, stimare il canale attraverso delle sequenze di simboli pilota può diventare sconveniente. In questi casi anche i metodi differenziali sono poco efficienti spettralmente e l'alternativa dei codici spazio–tempo non coerenti può diventare interessante.

Il Capitolo 2 introduce formalmente il modello di canale precedentemente descritto e rivisita tutti i concetti necessari per la comprensione dei codici spazio–tempo non coerenti, sia da un punto di vista matematico che da un punto di vista più prettamente ingegneristico (capacità del sistema, probabilità di errore, diversità). Tali considerazioni ci hanno permesso di giustificare la scelta dei parameteri fondameltali del sistema, cioè la durata della parola di codice e la struttura geometrica del codice. In seguito sono riportate le proposte più importanti della letterature specializzata, con un breve riassunto dei loro vantaggi e svantaggi.

La tecnica proposta in questa tesi viene approfondita nel Capitolo 3: le parole di codice sono delle matrici unitarie $T \times M$, dove T è il numero di periodi di simbolo del blocco in cui il canale resta costante e M è il numero di antenne all'emissione.

L'informazione viene in realtà codificata sui *sottospazi vettoriali* generati dalle colonne delle parole di codice, si dimostra infatti che questa strategia è ottima nel caso ergodico ed a rapporti segnale su rumore (SNR) elevati. Ora, l'insieme dei sottospazi vettoriali di $\mathbb{C}^T$ di dimensione M è una varietà differenziale, detta Grassmanniana $G_{T,M}$. Il metodo di codifica proposto consiste nel localizzare le parole di codice (sottospazi) sulla Grassmanniana a partire dallo spazio tangente ad un punto di riferimento di $G_{T,M}$. Dettagliando un po' meglio, ogni parola di codice in $G_{T,M}$ è in corrispondenza biunivoca con un punto dello spazio tangente attraverso una mappa non lineare detta mappa esponenziale. L'idea è di scegliere intelligentemente i punti sullo spazio tangente in modo da mapparli poi sulla Grassmanniana e ottenere un buon codice spazio–tempo non coerente. Il metodo proposto è di utilizzare nello spazio tangente un codice spazio–tempo a blocco (STB) *coerente*, ossia progettato per sistemi di comunicazione coerenti. Questa scelta nasce dal fatto che molto lavoro è stato sviluppato per i codici STB coerenti, di cui si conoscono molte proprietà. Vorremmo dunque sfruttare le conoscenze accumulate per creare buoni codici non coerenti a partire dai codici coerenti. Nel Capitolo 3 tutto ciò è spiegato in maggiore dettaglio, introducendo il formalismo matematico minimo per descrivere e manipolare questi oggetti. Abbiamo approfondito le relazioni tra i codici STB non coerenti e i correspondenti codici coerenti, un compito non facile data la non linearità della mappa esponenziale. Dopo aver formulato opportunamente il problema, abbiamo ottenuto risultati originali sui legami tra la diversità del codice STB non coerente e quella del suo codice coerente corrispondente. Infine, abbiamo riportato diversi esempi di codici.

Nel Capitolo 4 abbiamo trattato del problema della decodifica di tali codici nel caso in cui il ricevitore ed il trasmettitore abbiano solo un'antenna ciascuno (Single Input Single Output – SISO). La regola di decisione adottata al ricevitore è il GLRT (Generalized Likelihood Ratio Test). Calcolare tutte le metriche richieste dal GLRT per ogni segnale ricevuto può essere proibitivo soprattutto ad elevate efficienze spettrali. È dunque necessario trovare degli algoritmi di decodifica semplificati che abbiano possibilmente delle prestazioni comparabili a quelle del GLRT. Basandoci sull'interpretazione geometrica della procedura di codifica decritta nel Capitolo 3, abbiamo proposto un nuovo algoritmo subottimo che permette di ottenere performance indistinguibili da quelle GLRT, per lo meno nei casi in cui è stato possibile simulare le prestazioni GLRT. Questo metodo è poi stato adattato per ricevitori con più antenne (Single Input Multiple Output – SIMO) grazie ad un semplice algoritmo di stima della direzione di un sottospazio. Alla fine del capitolo sono riportati diverse curve di probabilità d'errore e dei confronti con altre proposte.

Nel Capitolo 5 abbiamo affrontato il caso generale di sistema con più antenne in emissione ed in ricezione (MIMO). L'analisi del GLRT si è rivelata impraticabile ed allora abbiamo tentato di semplificare il problema linearizzando localmente la Grassmanniana. L'intento consisteva nell'approssimare la Grassmanniana con un suo spazio tangente, per riportarsi al codice STB coerente in modo da poter sfruttare le tecniche di decodifica già disponibili. Abbiamo verificato che linearizzare la Grassmanniana intorno al segnale ricevuto è equivalente ad operare una trasformanzione non lineare sulle parole del codice STB coerente corrispondente, il che rende impossibile adottare gli

algoritmi semplificati già disponibili. Per contro, é possile linearizzare la Grassmanniana intorno allo sottospazio di riferimento utilizzato nel processo di codifica. Tuttavia, questa semplificazione introduce una distorsione non lineare tanto più marcata quanto più le parole di codice si allontanano dal sottospazio di riferimento. Un algoritmo di decodifica semplificato è stato proposto in questo caso e attraverso simulazione abbiamo mostrato quali parametri controllano l'effetto della distorsione. Anche in questo caso abbiamo simulato diverse curve di performance e paragonato la nostra proposta con quelle più promettenti della letteratura.

Il Capitolo 6 tratta della modulazione a fase continua (CPM), un formato che viene utilizzato in sistemi coerenti e non coerenti in cui ci siano vincoli stringenti sulla banda e/o sulla potenza. La modulazione CPM è particolarmente indicata per trasmettitori che utilizzino amplificatori non lineari, in quanto il segnale ha inviluppo costante. Il modulatore, sebbene sia abbastanza semplice da implementare, introduce un'operazione non lineare ed produce un segnale con memoria, ossia dipendente anche da dati forniti in istanti passati. Queste due caratteristiche fanno sí che il ricevitore ottimo possa essere molto complesso. Negli anni ottanta e novanta (e anche recentemente) sono state proposte diverse scomposizioni del segnale CPM in implusi PAM (Pulse Amplitude Modulation). Ciò equivale a dire che si può descrivere linearmente il segnale CPM, la non linearità essendo stata spostata alla definizione dei pseudo–simboli corrispondenti agli impulsi PAM. A partire da quel momento, la scomposizione PAM é stata sfruttata per semplificare il ricevitore CPM ottimo, per proporre nuovi algoritmi di sincronizzazione, per progettare codici spazio–tempo, ecc.. In questo capitolo proponiamo un'altra scomposizione PAM, valida per segnali cha hanno una certa simmetria nella risposta di fase. Il metodo per ottenere la nuova scomposizione è originale e permette di dimostrare che essa ha cardinalità minima: per questo tipo di segnali CPM non esistono scomposizioni PAM ottenute con meno impulsi. Vari esempi numerici e analitici sono forniti.

Résumé

Cette thèse rassemble une partie des résultats obtenus au cours de mon doctorat de recherche réalisé entre le mois de janvier 2001 et la fin du mois de décembre 2004. Le travail s'est déroulé dans le cadre d'un accord de cotutelle entre l'Université de Padoue et l'École Nationale Supérieur des Télécommunications (E.N.S.T.) de Paris. A Padoue j'ai été intégré dans l'équipe du Prof. Gianfranco Cariolaro du Département d'Ingénierie de l'Information (DEI), alors qu'à Paris la recherche a été supervisée par le Prof. Georges Rodriguez Guisantes au sein du Département Communications et Electronique (ComElec). Une partie de cette thèse, celle qui traite des codes espace-temps, s'inscrit à la suite d'un sujet de recherche déjà existant à l'E.N.S.T., étudié notamment par le Prof. Jean-Claude Belfiore et le Dr. Inès Kammoun.

Les importants progrès de la technologie de la communication lors des quinze dernières années ont permis le développement de nouveaux modes de communication et de travail; on peut penser à Internet, aux flux importants de données qui transitent sur le réseau chaque seconde et aux services multimédias intégrés toujours plus accessibles grâce à la fiabilité des fibres optiques et aux progrès réalisés dans l'exploitation des paires cuivrées (ADSL). Dernièrement une certaine philosophie voudrait rendre accessibles ces services aux utilisateurs là où ils se trouvent, en intégrant la technologie nécessaire dans les ordinateurs et téléphones portables. Pour ceci il faut abandonner la « sécurité » que représente la transmission par câble, et passer à la transmission radio. Malheureusement, le canal radio est un des moyens de transmission les moins fiables, est propice aux interférences, et pose d'importants problèmes de sécurité.

Nous nous intéresserons à un aspect du problème: comment munir un canal radio d'une vitesse de transmission suffisamment élevée et d'un taux d'erreur assez bas pour garantir les flux de données et la qualité nécessaire aux services multimédias? Une proposition parmi d'autres est de doter l'émetteur et le récepteur d'un réseau d'antennes, c'est-à-dire d'augmenter la diversité spatiale du système de communication. L'idée est simple: si l'on implante les antennes suffisamment éloignées les unes des autres, de manière à ce que les différents canaux ne soient pas corrélés entre eux, la probalité que tous les trajets du canal radio soient fortement perturbés est de plus en plus réduite à mesure que le nombre d'antennes croît.

A la fin des années quatre-vingt-dix, les travaux de Telatar et, parallèlement ceux de Foschini et Gans, ont démontré que cette technique permettait théoriquement d'atteindre un débit de transmission élevé. Au cours de ces mêmes années Tarokh et d'autres chercheurs ont fourni des stratégies pour organiser de manière convenable les données

sur les différentes antennes en émission, réussissant ainsi à exploiter pleinement la diversité spatiale offerte par le canal et à obtenir un gain de codage. Naissaient donc les *codes espace-temps*.

Depuis lors un nombre croissant de chercheurs s'est consacré à ce filon de recherche prometteur, en développant l'idée de départ, en proposant d'autres et en l'adaptant à divers cas. Cette thèse développe surtout un de ces cas , aujourd'hui objet de recherche, dans lequel le récepteur et l'émetteur n'ont pas connaissance du canal, à la différence de ce qui se passe dans la majorité des travaux sur ce sujet, au sein desquels l'on suppose une connaissance parfaite du canal par l'émetteur et/ou le récepteur.

Le principal sujet de ce travail, traité dans les 4 premiers chapitres, est donc une étude du codage et du décodage des codes Espace-Temps en Blocs (STB) non cohérents. Nous avons considéré une communication point à point dans laquelle ni l'émetteur ni le récepteur ont connaissance du déphasage et de l'atténuation introduite dans le canal (système non cohérent). Ce dernier est simulé selon des hypothèses simplifiées acceptées unanimement dans la littérature et formulées pour réaliser plus aisément les algorithmes de codage et de décodage. Conjointement, le modèle de canal utilisé dans cette thèse est suffisamment général pour pouvoir couvrir la problématique fondamentale de tels systèmes: le canal à plusieurs entrées et plusieurs sorties (Multiple Input Multiple Output – MIMO) peut avoir des atténuations profondes (Rayleigh fading channel), mais n'y sont pris en compte ni l'effet Doppler (flat fading), ni les canaux à plusieurs rayons (le canal est supposé à bande étroite).

Les systèmes non cohérents sont peu diffusés dans le milieu de la recherche car l'on essaie généralement d'évaluer le canal au récepteur pour améliorer les performances. Quoi qu'il en soit, quand le canal varie trop rapidement ou quand des considérations concernant le coût l'imposent, l'estimation peut être trop onéreuse ou vraiment impossible à mettre en oeuvre. Cela pourrait être le cas par exemple de canaux avec des temps de cohérence égaux à un petit nombre de temps de symbole, ou des systèmes à accès multiple dans lesquels de brefs intervalles temporels et/ou fréquentiels non contigus sont alloués aux utilisateurs. Le modèle utilisé pour représenter ces canaux considère les coefficients des canaux constants sur un intervalle de temps T (appelé « bloc x»). Les coefficients de chaque bloc sont générés selon un processus stochastique invariant dans le temps et à symboles indépendants. La durée T du bloc, en temps symbole, est du même ordre de grandeur que le nombre d'antennes en émission M. Pour ces valeurs de T, l'estimation du canal par une séquence pilote peut être désavantageuse. Même les méthodes différentielles ont une faible efficacité spectrale, les méthodes non cohérentes peuvent alors devenir une alternative intéressante.

Le chapitre 2 introduit formellement le modèle du canal décrit ci-dessus. Les concepts de base de la théorie des codes espace-temps non cohérents sont rappelés par la suite (capacité du système, taux d'erreur, diversité). Ces observations nous ont permis de choisir les paramètres fondamentaux du système: la durée T et la structure géométrique du code. Sont ensuite rappelées les propositions les plus importantes de la littérature, accompagnées d'un bref résumé de leurs avantages et inconvénients.

La technique que nous proposons est approfondie dans le chapitre 3: les mots de code sont des matrices unitaires $T \times M$, où T est le nombre de temps de symbole

du bloc dans lequel le canal reste constant, et M est le nombre d'antennes en émission. L'information est en réalité codée sur les *sous-espaces vectoriels* générés par les colonnes des mots de code. En effet, on peut démontrer que celle-ci est la stratégie optimale dans le cas ergodique avec un rapport signal à bruit (SNR) élevé. Or, l'ensemble des sous-espaces vectoriels de $\mathbb{C}^T$ de dimension T est une variété différentielle appelée Grassmannien $G_{T,M}$. La méthode de codage proposée consiste à localiser les mots de code sur $G_{T,M}$ en partant de l'espace tangent à un point de référence du Grassmannien-même. En fait, chaque mot de code en $G_{T,M}$ est en correspondance biunivoque avec un point de l'espace tangent à travers une fonction non-linéaire dite «exponentielle». L'idée est de choisir judicieusement les points sur l'espace tangent de manière à obtenir sur le Grassmannien un bon code espace-temps non cohérent à travers la fonction exponentielle. La méthode proposée est d'utiliser sur l'espace tangent un code espace-temps à blocs (STB) *cohérent*, c'est-à-dire conçu pour les systèmes cohérents. Ce choix naît du fait que les codes STB cohérents ont été très étudiés et que par conséquent on en connaît les propriétés. On souhaiterait exploiter ces connaissances dans l'étude et la création des codes STB non cohérents. Dans le chapitre 3 tout cela est plus amplement détaillé avec le formalisme mathématique approprié. Les relations entre codes STB cohérents et non cohérents ont été approfondies par la suite, tâche difficile du fait de la non linéarité de la fonction exponentielle. Après avoir formalisé la théorie du problème, nous avons obtenu des résultats concernant la relation entre la diversité des codes STB non cohérents et celle de leurs correspondants cohérents. Enfin, nous avons présenté différents exemples de codes.

Le chapitre 4 traite du problème du décodage de ces codes dans le cas où le récepteur et l'émetteur ont seulement une antenne chacun (Single Input Single Output – SISO). La règle de décision adoptée pour le récepteur est le GLRT (Generalized Likelihood Ratio Test). Calculer toutes les métriques requises par le critère de détection pour chaque signal reçu peut être très coûteux surtout à efficacité spectrale élevée. Il est donc nécessaire de trouver des algorithmes de décodage simplifiés donnant des performances les plus proches possibles de celles du GLRT. En s'appuyant sur l'interprétation géométrique de la procédure de codage décrite dans le chapitre 3, nous avons proposé un nouvel algorithme simplifié qui permet d'obtenir des performances indistinguables de celles du GLRT, au moins dans les cas où il a été possible de simuler les performances GLRT. Cette méthode a été ensuite adaptée aux récepteurs avec plusieurs antennes (Single Input Multiple Output – SIMO) grâce à un algorithme simple d'estimation de la direction d'un sous-espace. En fin de chapitre sont présentées plusieurs courbes de probabilité d'erreur et différentes comparaisons avec d'autres propositions.

Dans le chapitre 5 nous avons abordé le cas général du système à plusieurs antennes à l'émission et à la réception (MIMO). L'analyse du critère de détection GLRT s'est avérée impraticable et nous avons tenté de simplifier le problème en linéarisant localement le Grassmanien. Le but est d'approximer le Grassmannien avec un de ses espaces tangents afin de se reporter au code STB cohérent et d'ainsi exploiter une technique de décodage déjà disponible. Malheureusement nous avons démontré que cette linéarisation autour du signal reçu revenait à appliquer une transformation non linéaire aux

mots du code STB cohérent correspondant, ce qui rend impossible l'adoption des algorithmes simplifiés déjà disponibles. Il est par contre possible de linéariser le Grassmanien autour du sous-espace de référence utilisé dans le processus de codage. Néanmoins cette simplification introduit une distorsion non linéaire de plus en plus importante à mesure que l'on s'éloigne du sous-espace de référence. Un algorithme de décodage simplifié a été proposé dans ce cas et à travers des simulations nous avons montré quels sont les paramètres qui contrôlent l'effet de la distorsion. Nous avons également dans ce cas simulé plusieurs courbes de performances, et comparé notre proposition aux plus prometteuses de la littérature.

Le chapitre 6 traite de la modulation à phase continue (CPM), une technique qui est utilisée dans les systèmes cohérents et non cohérents avec des contraintes sur la bande et/ou la puissance. La modulation CPM est particulièrement indiquée pour les émetteurs qui utilisent des amplificateurs non linéaires car le signal a une enveloppe constante. Le modulateur, bien qu'il soit assez simple à implanter, introduit une opération non linéaire et produit un signal avec mémoire, c'est-à-dire qu'il dépend aussi des données fournies aux instants passés. Ces deux caractéristiques font que le récepteur optimal puisse être extrêmement complexe. Dans les années quatre-vingts et quatre-vingt-dix (et récemment) les chercheurs ont proposé plusieurs décompositions du signal CPM en impulsions PAM (Pulse Amplitude Modulation). Ceci équivaut à dire que l'on peut décrire linéairement le signal CPM, la non linéarité étant alors reléguée à la définition des pseudo-symboles correspondants aux impulsions PAM. Dès lors, les décompositions PAM ont été exploitées pour simplifier le récepteur CPM optimal, proposer des algorithmes de synchronisation, projeter des codes espace-temps, etc.. Dans ce chapitre nous proposons une autre décomposition PAM valide pour les signaux qui ont une certaine symétrie dans la réponse de phase. La méthode pour obtenir la nouvelle décomposition est inédite et permet de démontrer que celle-ci a une cardinalité minimale: pour ce type de signaux CPM il n'existe pas de décomposition PAM obtenue avec moins d'impulsions. Différents exemples numériques et analytiques sont présentés.

Introduction

This thesis collects part of the results I obtained during my Ph.D. program, period I spent in Padova at the Information Engineer Department of the University of Padova and in Paris at Communications and Electronics Department of the Ecole Nationale Supérieure des Télécommunications (E.N.S.T. Paris). In the first months, I was involved in the study of quantum communications with particular attention to quantum cryptography. Encouraged by my tutor in Padova, prof. Gianfranco Cariolaro, I have redirected my interest to space–time coding for Multiple Input Multiple Output (MIMO) non–coherent wireless system, which constitutes the main body of this work. For these channels, in fact, information is coded on subspaces, as in certain error correcting codes for quantum systems. With prof. Cariolaro I also investigated some signal processing topics on multidimensional multirate systems and CPM signal analysis. We report here results on the latter topic only, since they can find valuable application in narrow–band non–coherent system. Research about space–time codes has been carried out at E.N.S.T. under the supervision of M. Georges Rodriguez Guisantes and the collaboration of prof. Jean–Claude Belfiore.

General interest on space–time codes was generated by the information theoretical works of Telatar, Foschini and Gans and by the works of Tarokh and collaborators at the end of the nineties. Multiple antenna wireless links finally seemed to assure sufficient rate and reliability to the critical wireless channel, an important step toward the deployment of wireless networks able to support advanced multimedia services. Since then, the research community has spent a lot of resources on the promises preconized by these pioneering investigations. Research mainly focused on systems in which channel realizations are perfectly estimated at the receiver. Different space–time trellis and block codes have been proposed for coherent wireless links.

In this thesis, we focused on space–time block coding and decoding for systems in which no channel knowledge is available at the receiver and at the transmitter. Coding for these non–coherent communications links received less attention than their coherent counterpart. In our opinion, two main reasons can be given: such non–coherent systems are less common in practice and their coding and decoding design problems are quite hard. These codes are commonly referred to as “non–coherent space–time codes”, even if in a proper sense system can be “non–coherent” but not codes themselves. Anyway, we will use this widely spread notation, as well. Moreover, throughout this whole work, the word “code” must not be understood in the sense of classic error correcting codes. Space–time codes we dealt with here are space–time block codes. They opportunely transform blocks of symbols coming from “standard” con-

stellations, like PSK or QAM, and then distribute them on the different active trasmit antennas throughout the whole frame. This operation has a double aim: to fully exploit channel diversity and to increase the coding gain of the system, to allows power saving, for instance. At the receiver side, an algorithm should be implemented able to exploit the code advantages and at the same time to minimize the computational burden. Codes make sense only in respect of the particular channel used to communicate. The communication channel, in fact, can raise some communications problems but also can offer some good qualities to be exploited. A good code is able to exploit channel characteristics to assure a good link, according to a desired and previously specified criterion. In this work a simplified MIMO channel model was adopted, in order to focus on the coding design and decoding algorithm. The channel model is the so called quasi–static block fading channel, which assures spatial diversity since the paths among trasmit and receive antennas are independent.

In Chapter 2 we introduce the channel model considered throughout the whole work and we justify the choice of some basic system parameters. Basic mathematical tools to deal with non–coherent space–time codes are also provided. We recall known results on error probability and diversity, as well as the advantages and disadvantages of many propositions in the literature. In Chapter 3 an in–depth investigation of non–coherent space–time codes obtained via the exponential map is carried out. Codes obtained with this method are called also EP codes and are the main object of our work. We explain the geometrical interpretation of this coding procedure and we solve some open problems on code design. In Chapter 4 we propose a new simplified decoder for the case of one transmit antenna and many receive antennas. To find this decoder, the geometrical interpretation of the coding process is related to the decision function. Discussion on the expected complexity and parameters of the decoder are detailed, as well as simulations and comparisons with other propositions. In Chapter 5 we cope with the general MIMO case, we propose two simplified decoders, based on once again on the geometrical interpretation of the coding process. As in the previous case, discussion about the expected complexity and about decoders parameters is provided. Simulations and comparisons conclude this chapter. Chapter 6 deals with CPM signal decompositions in PAM pulses. CPM is a non–linear modulation, while signal decomposition as a linear combination of waveforms can simplify the code and receiver design both for coherent and non–coherent systems. A final conclusion is reported in the last chapter.

Chapitre 1

Algorithmes de décodage pour des codes espace-temps non cohérents

1.1 Etat de l'art

En cette section on établira le modèle de canal utilisé dans ce travail, en suite on introduira les propositions les plus importantes de la littérature.

1.1.1 Modèle de Canal

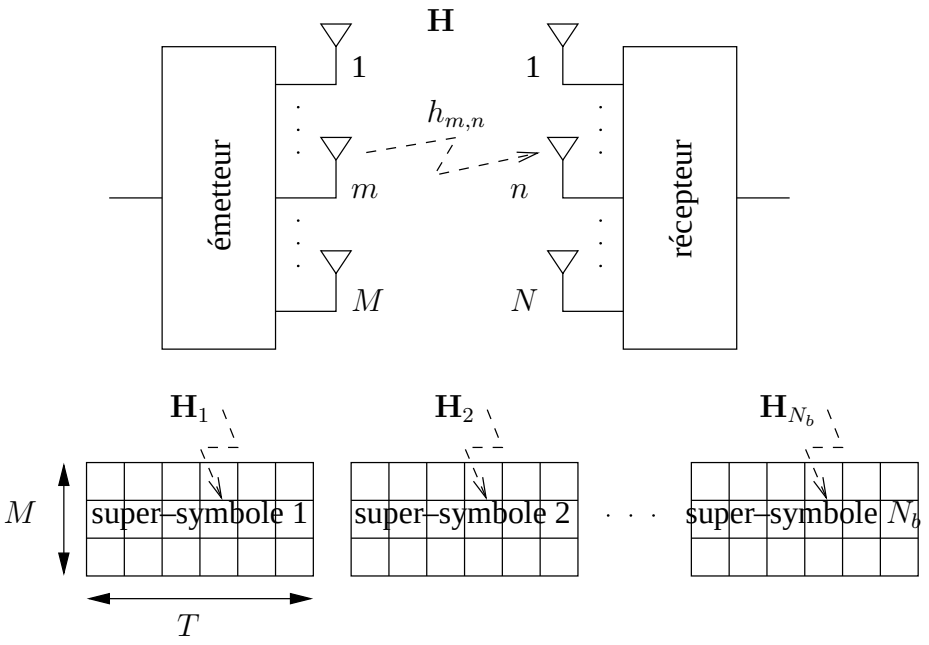

Figure 1.1: Canal MIMO et un mot de code de N_b super-symboles bruités par un canal à évanouissement par blocs.

Le modèle du canal sans fils utilisé dans cette thèse est le canal à évanouissement par blocs (block fading channel) [1], [2], qui doit son nom au fait que les coefficients du canal sont constant pendant T périodes de symbole T_s (T est entier). On considère des canaux à entrées et sorties multiples : M et N sont respectivement le nombre d'antennes à l'émemission et à la réception (voir Fig. 1.1).

Sous l'hypothèse d'une modulation à bande étroite, sans interférence entre symboles, le modèle équivalent en bande de base est

$$\mathbf{Y}_k = \alpha\,\mathbf{X}_k\mathbf{H}_k + \sigma\,\mathbf{W}_k\,, \qquad k = 1, 2, \ldots\,. \tag{1.1}$$

L'indice k indique le bloc (ou paquet), $\mathbf{Y}_k$ est la matrice $T \times N$ du signal reçu, $\mathbf{X}_k$ est la matrice $T \times M$ du signal envoyé, $\mathbf{H}_k$ est la matrice $M \times N$ qui collecte les coefficients du canal et $\mathbf{W}_k$ est la matrice $T \times N$ du bruit additif gaussien et blanc. Les nombre réels positifs α et σ sont utilisés pour normaliser la puissance du signal utile et la variance du bruit.

Les coefficients de $\mathbf{H}$ et $\mathbf{W}$ sont des variables gaussiennes complexes, à symétrie circulaire, indépendant et identiquement distribués (i.i.d.) avec une espérance nulle et une variance égal à 1 ($\mathcal{CN}(0,1)$). Le signal complexe envoyé est indépendant des coefficients du canal et du bruit additif. Lors de cette étude, les coefficients du canal sont considérés inconnus à l'émetteur et au récepteur. Un tel système de communications est dit non cohérent et, en suivant une notation imprécise mais très répandue en littérature, on nommera les codes utilisés pour ces systèmes codes (espace-temps) non cohérents. L'étude est menée en considérant T du même ordre de grandeur que M (en particulier $T \geq 2M$), de manière à rendre peu rentable l'utilisation de longues séquences d'apprentissage pour l'estimation du canal.

Le modèle (1.1) peut être mis sous la forme

$$\mathbf{y} = \alpha\,\overline{\mathbf{X}}\,\mathbf{h} + \sigma\,\mathbf{w}\,, \qquad \overline{\mathbf{X}} = \mathbf{I}_N \otimes \mathbf{X} \tag{1.2}$$

où $\otimes$ indique le produit de Kronecker et $\mathbf{y} = \mathrm{vec}(\mathbf{Y})$ est le vecteur colonne obtenu en enchaînant les colonnes de $\mathbf{Y}$ l'une après l'autre; de même pour $\mathbf{w} = \mathrm{vec}(\mathbf{W})$ et $\mathbf{h} = \mathrm{vec}(\mathbf{H})$ (cf. annexe A).

Le rapport signal à bruit moyen (SNR) ρ par antenne en réception est donné par :

$$\rho = \frac{\frac{1}{N}\,\mathrm{tr}(\mathrm{E}\,[\mathbf{Y}\,\mathbf{Y}^\dagger]_{\mathbf{W}=\mathbf{0}})}{\frac{1}{N}\mathrm{tr}(\mathrm{E}\,[\mathbf{W}\,\mathbf{W}^\dagger])} = \frac{\alpha^2\,\mathrm{tr}(\mathrm{E}\,[\mathbf{X}\,\mathbf{X}^\dagger])}{\sigma^2 T}\,. \tag{1.3}$$

Pour plus de détails, nous renvoyons le lecteur à l'annexe B.

1.1.2 Introduction aux Représentations des Sous-espaces

Du point de vue de la théorie de l'information, il a été démontré que dans les systèmes non cohérent à haut SNR l'information est portée principalement par les sous-espaces vectoriels générés par les colonnes des matrices représentantes les mot de codes (cf. Sect. 2.2.2). En conséquence, nous introduirons la notation de base sur les sous-espaces vectoriels.

Soit $\Omega_{\mathbf{X}}$ un sous-espace vectoriel M-dimensionnel de $\mathbb{C}^T$, où $T > M$. Soit $\mathbf{X}$ une base de $\Omega_{\mathbf{X}}$, alors nous pouvons écrire

$$\Omega_{\mathbf{X}} = \text{span}[\mathbf{x}_1 \ \dots \mathbf{x}_M] = \text{span}(\mathbf{X}) \quad \text{avec} \quad \text{rang}(\mathbf{X}) = M \,. \tag{1.4}$$

Nous introduisons l'ensemble des sous-espaces vectoriels dans la définition suivante :

Définition 1 *L'ensemble des sous-espaces vectoriels de $\mathbb{C}^T$ ayant une dimension M, avec $T > M$, est appelé Grassmannien ou variété de Grassmann et est noté par $G_{T,M}$.*

Le Grassmannien est une variété différentielle et sera rapidement introduit dans la prochaine section. Pour plus de détails le lecteur est renvoyé à la Sect. 3.2.

Les concepts de bases bi-orthogonales et d'angles principaux sont très importants pour caractériser la distance entre deux sous-espaces [3, pag. 603].

Définition 2 *Soient $\Omega_{\mathbf{X}}, \Omega_{\mathbf{Y}} \in G_{T,M}$ deux sous-espaces. Leur bases $\mathbf{X}$ et $\mathbf{Y}$ sont dites bi-orthogonales si les vecteurs sont orthonormaux et*

$$\mathbf{x}_m^\dagger \mathbf{y}_{m'} = 0 \text{ pour tous } m \neq m' \,, \qquad \mathbf{x}_m^\dagger \mathbf{y}_m = c_m \text{ avec } 0 < c_m \leq 1 \tag{1.5}$$

c'est-à-dire pour tous $m = 1, \dots, M$, le $m^{\text{ème}}$ vecteur de la première base est orthogonal à tous les vecteurs de l'autre base excepté le $m^{\text{ème}}$.

Les bases bi-orthogonales peuvent être obtenues à partir de deux bases orthonormales quelconques à travers la décomposition à valeurs principales (SVD). La procédure est la suivante : une fois calculé

$$\mathbf{X}^\dagger \mathbf{Y} = \mathbf{U}_X \mathbf{C} \mathbf{U}_Y^\dagger \,, \qquad \mathbf{U}_X, \mathbf{U}_Y \in \mathcal{U}_M \,, \ \mathbf{C} = \text{diag}([c_1, \dots, c_M]) \tag{1.6}$$

où $0 < c_m \leq 1$ pour tout m, les bases orthonormals sont les suivantes :$\mathbf{X}\,\mathbf{U}_X$ et $\mathbf{Y}\,\mathbf{U}_Y$.

Définition 3 *A partir de deux bases bi-orthogonales des sous-espaces $\Omega_{\mathbf{X}}, \Omega_{\mathbf{Y}} \in G_{T,M}$, les produits scalaires $c_m \geq 0$ sont déterminés uniquement par :*

$$c_m = \cos\theta_m \,, \ \theta_m \in [0, \pi/2] \,, \qquad m = 1, \dots, M \,. \tag{1.7}$$

Les $\theta_1, \dots, \theta_M$ sont appelés angles principaux entre $\Omega_{\mathbf{X}}$ et $\Omega_{\mathbf{Y}}$.

Plusieurs distances sur le Grassmannien peuvent être définies grâce aux angles principaux [4], [5]. Nous en introduirons une qui est utilisé pour définir le gain de codage des codes espace-temps par bloc étudiés dans cette thèse :

Définition 4 *Soient $\mathbf{X}$ et $\mathbf{Y}$ deux bases orthonormales et soit $\mathbf{X}^\dagger\mathbf{Y} = \mathbf{U}_X\mathbf{C}\mathbf{U}_Y^\dagger$ la SVD définie dans (1.6) avec $\mathbf{C} = \cos\boldsymbol{\Theta}$. La pseudo-distance appelée distance produit est définie :*

$$d_p(\Omega_{\mathbf{X}}, \Omega_{\mathbf{Y}}) = \left(\prod_{m=1}^{M} \sin\theta_m \right)^{1/M} = \left(\det \left\{ \begin{bmatrix} \mathbf{X}^\dagger \\ \mathbf{Y}^\dagger \end{bmatrix} [\mathbf{X}\ \mathbf{Y}] \right\} \right)^{\frac{1}{2M}} \tag{1.8}$$

Pour la suite nous noterons la pseudo-distance appelée distance produit $d_p(\Omega_{\mathbf{X}}, \Omega_{\mathbf{Y}})$ ou $d_p(\mathbf{X}, \mathbf{Y})$.

1.1.3 Critères de détection

Le critère de détection optimale, dans le cas où au récepteur l'unique information connue sur le canal est sa statistique, est appelé maximum de vraisemblance non cohérent (non-coherent Maximum Likelihood : nc-ML) et il s'écrit de la forme suivante :

$$\hat{\mathbf{X}}_{ML} = \arg \max_{\mathbf{X}_\ell \in \mathcal{C}} p(\mathbf{Y}|\mathbf{X}_\ell) = \arg \max_{\ell=1,\dots,L} p(\mathbf{Y}|\mathbf{X}_\ell)\,, \tag{1.9}$$

où $p(\mathbf{Y}|\mathbf{X}_\ell)$ est la densité de probabilité de $\mathbf{Y}$ sous la condition d'avoir envoyé le mot de code $\mathbf{X}_\ell \in \mathcal{C}$ et L est la taille de $\mathcal{C}$.

Sous les hypothèses du modèle de canal (2.2), l'expression (1.9) dévient :

$$\hat{\mathbf{X}}_{ML} = \arg \min_{\ell=1,\dots,L} \left[-\mathbf{y}^\dagger \mathbf{F}_\ell \mathbf{y} + c_\ell\right], \tag{1.10}$$

où

$$\mathbf{F}_\ell = \frac{1}{\sigma^2}\overline{\mathbf{X}}_\ell\left(\frac{\sigma^2}{\alpha^2}\mathbf{I}_{NM} + \overline{\mathbf{X}}_\ell^\dagger \overline{\mathbf{X}}_\ell\right)^{-1}\overline{\mathbf{X}}_\ell^\dagger\,, \quad c_\ell = \ln\left|\frac{\sigma^2}{\alpha^2}\mathbf{I}_{NM} + \overline{\mathbf{X}}_\ell^\dagger \overline{\mathbf{X}}_\ell\right|\,. \tag{1.11}$$

plus de détails sont donnes dans l'annexe C du chapitre 2.

Dans le cas où le récepteur ne connait ni les coefficients du canal, ni leur statistique, le critère de détection optimale est le Generalized Likelihood Ratio Test (GLRT) [6], [7] qui s'écrit dans la forme suivante :

$$\hat{\mathbf{X}}_{GLRT} = \arg \max_{\ell=1,\dots,L} \sup_{\mathbf{H}} p(\mathbf{Y}|\mathbf{X}_\ell, \mathbf{H})\,. \tag{1.12}$$

Dans le cas d'un bruit additif blanc gaussien (AWGN, comme dans (1.2)) le GLRT se simplifie ainsi :

$$\hat{\mathbf{X}}_{GLRT} = \arg \max_{\ell=1,\dots,L} \operatorname{tr}\left[\mathbf{Y}^\dagger \mathbf{X}_\ell (\mathbf{X}_\ell^\dagger \mathbf{X}_\ell)^{-1} \mathbf{X}_\ell^\dagger \mathbf{Y}\right]. \tag{1.13}$$

Cette expression nous suggère que le GLRT sélectionne le mot de code qui a la norme de sa projection sur le sous-espace généré par le signal reçu $\mathbf{Y}$ la plus importante, ou, également, le mot de code qui génère le sous-espace le plus proche à celui généré par $\mathbf{Y}$.

Dans le cas d'évanouissement i.i.d. et de code unitaire (dont les mots de code ont des vecteurs colonne orthonormaux entre eux), les critères nc-ML et GLRT coïncident

$$\hat{\mathbf{X}} = \arg \max_{\ell=1,\dots,L} \operatorname{tr}(\mathbf{Y}^\dagger \mathbf{X}_\ell \mathbf{X}_\ell^\dagger \mathbf{Y}) = \arg \max_{\ell=1,\dots,L} \|\mathbf{Y}^\dagger \mathbf{X}_\ell\|_F^2\,. \tag{1.14}$$

Si le récepteur connaît la réalisation des coefficients du canal, alors il est possible d'utiliser le critère du maximum de vraisemblance cohérent (coherent Maximum Likelihood : co-ML)

$$\hat{\mathbf{X}}_{co-ML} = \arg \max_{\ell=1,\dots,L} p(\mathbf{Y}|\mathbf{X}_\ell, \mathbf{H}) \tag{1.15}$$

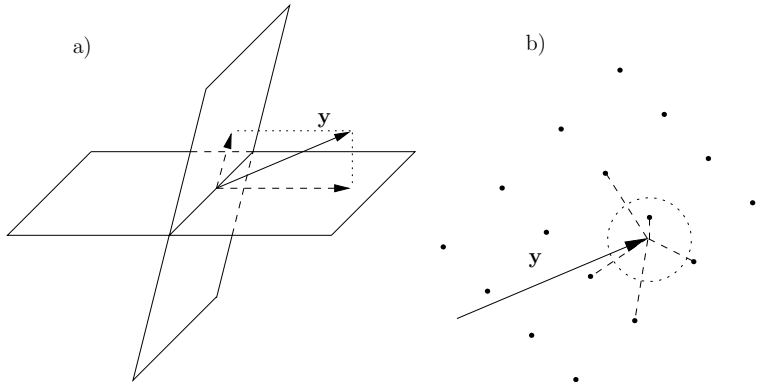

Figure 1.2: a) Le GLRT sélectionne le mot de code correspondant au sous-espace le plus proche à $\mathbf{y}$ (dont la projection sur $\mathbf{y}$ est la plus importante). b) Le ML cohérent sélectionne le point le plus proche.

Selon les hypothèses du modèle (1.2), le critère devient

$$\hat{\mathbf{X}}_{co-ML} = \arg \min_{\ell=1,\dots,L} \|\mathbf{Y} - \mathbf{X}_\ell \mathbf{H}\|_F^2 = \arg \min_{\ell=1,\dots,L} \|\mathbf{y} - (\mathbf{H}^t \otimes \mathbf{I}_T)\mathbf{x}_\ell\|^2 \qquad (1.16)$$

où $\mathbf{x}_\ell = \mathrm{vec}(\mathbf{X}_\ell)$. Le co-ML sélectionne le mot de code dont la distance (définie par le canal) est la plus faible. (cf. Fig. 1.2). Ce critère peut être utilisé même quand la connaissance du canal n'est pas parfaite, et que seule une estimation des coefficients du canal est disponible au récepteur. Dans ce cas le critère n'est plus appelé co-ML, mais est nommé critère estimation-détection (E-D). Finalement nous notons que lorsque les mots de code sont issus d'un réseau de points généré par la matrice $\mathbf{L}$, la solution donnée par (1.16) revient à chercher le point du réseau de points modifié $(\mathbf{H}^t \otimes \mathbf{I}_T)\mathbf{L}$ le plus proche à $\mathbf{y}$. Cette recherche peut être conduite efficacement grâce à l'algorithme nommé détecteur à sphère (sphere decoder).

1.1.4 Probabilités d'erreur

La borne de l'union sur la probabilité d'erreur de super-symbole est [8]

$$P_e \leq P_e^{UB} = \frac{1}{L} \sum_{\ell=1}^{L} \sum_{j \neq \ell} P_{\ell j} = \frac{1}{L} \sum_{\ell=1}^{L-1} \sum_{j=\ell+1}^{L} (P_{\ell j} + P_{j\ell}) \qquad (1.17)$$

où L est la taille du code et $P_{\ell j}$ est la probabilité d'erreur par paire (PEP)

$$P_{\ell j} = \mathrm{P}\left[\hat{\mathbf{X}} = \mathbf{X}_j | \mathbf{X}_{sent} = \mathbf{X}_\ell\right]. \qquad (1.18)$$

Dans le cas de codes unitaires, la PEP $P_{\ell j}$ dépend des angle principaux entre $\Omega_{\mathbf{X}_\ell}$ and $\Omega_{\mathbf{X}_j}$ [9]. La borne de Chernoff de la PEP s'ècrit de la manière suivante (cf. [10],

[9]) :

$$P_{\ell j}^{CB} = \frac{1}{2}\prod_{m=1}^{M}\left[1+\frac{(\rho T/M)^2\sin^2\theta_{m,\ell j}}{4(1+\rho T/M)}\right]^{-N} \underset{\rho\to\infty}{\simeq} \frac{1}{2}\left[\frac{M}{\rho T}\right]^{N m_{d,\ell j}}\left[\prod_{m=1}^{m_{d,\ell j}}\frac{4}{\sin^2\theta_{m,\ell j}}\right]^{N} \tag{1.19}$$

où $\theta_{1,\ell j},\ldots,\theta_{m_{d,\ell j},\ell,j}$ sont les angles principaux différents de zéro entre $\Omega_{\mathbf{X}_\ell}$ et $\Omega_{\mathbf{X}_j}$. Si tous les angle principaux sont différents de zéro, la expression asymptotique suivante, à haut SNR, de la PEP est valable [11] :

$$P_{\ell j}^{\infty} = \left[\frac{M}{T\rho}\right]^{NM}\binom{2MN-1}{MN}\frac{1}{|\sin^2\boldsymbol{\Theta}_{j\ell}|^N} = \left[\frac{M}{T\rho}\right]^{NM}\binom{2MN-1}{MN} d_p^{-2NM}(\Omega_{\mathbf{X}_\ell},\Omega_{\mathbf{X}_j})\,. \tag{1.20}$$

Dans le cas de codes non-unitaires ou d'évanouissements corrélés, le critère ML et le GLRT ne coïncident pas. Une expression asymptotique a été trouvé également dans le deux cas par Breheler *et al.* [11].

1.1.5 Diversité

La diversité est une mesure du nombre de coefficients statistiquement indépendants du canal qui affectent le même signal. Nous allons donner la définition de la diversité qui sera utilisée dans la suite de ce travail, et qui représente la définition classique, basée sur la PEP (cela revient à la donner sur la probabilité d'erreur moyenne) :

Définition 5 (Définition basée sur la PEP) *Soit $P_{\ell j}(\rho)$ La PEP entre les mots de code $\mathbf{X}_\ell$ et $\mathbf{X}_j$ en fonction du SNR ρ. $\mathbf{X}_\ell$ et $\mathbf{X}_j$ appartiennent au code $\mathcal{C}$ de taille L. Le code $\mathcal{C}$ a un gain de diversité d (ou plus brièvement diversité d) si :*

$$\min_{\ell,j:\ell\neq j}\lim_{\rho\to\infty}\frac{\ln P_{\ell j}(\rho)}{\ln\rho} = -d\,. \tag{1.21}$$

La diversité de $\mathcal{C}$ sera indiquée par $d(\mathcal{C})$.

Nous soulignons que la diversité donnée dans la définition 5 dépend du code mais aussi du critère de détection, puisque la PEP en dépend elle aussi. Dans le cas où le critère ML cohérent est utilisé au récepteur, on parlera de « code cohérent » et dans le cas de code par bloc sa diversité est donnée par la définition suivante (voir aussi [12]) :

Définition 6 (Diversité du code cohérent) *Soit $\mathcal{B}$ un code espace-temps cohérent par blocs et soit le ML cohérent le critère de détection utilisé (voir (1.15) et (1.16)). La diversité basée sur la PEP est :*

$$d^{co-ML}(\mathcal{B}) = \min_{k\neq\ell}\operatorname{rank}(\mathbf{B}_k-\mathbf{B}_\ell)\,. \tag{1.22}$$

Dans le cas des codes espace-temps unitaires $\mathcal{C}$ pour les systèmes non cohérents avec GLRT au récepteur, la diversité basée sur la PEP est introduite par Hochwald *et al.* [9]. Nous la reportons ci-dessous :

Définition 7 (Diversité du code non-cohérent) *Soit $\mathcal{C}$ un code espace-temps unitaire par blocs, dont les mots de code $\mathbf{X}_k$ génèrent des sous-espaces de dimension M constante. Alors, la diversité basée sur la PEP du code $\mathcal{C}$, par rapport au GLRT, est :*

$$d^{GLRT}(\mathcal{C}) = M - \max_{k \neq \ell} \dim(\Omega_{\mathbf{X}_k} \cap \Omega_{\mathbf{X}_\ell}) \,. \tag{1.23}$$

Il est facile de démontrer que :

$$d^{GLRT}(\mathcal{C}) = \min_{k \neq \ell} \left\{ \mathrm{rank}([\mathbf{X}_k \; \mathbf{X}_\ell]) \right\} - M \,. \tag{1.24}$$

La proposition suivante a été établie par Brehler *et al.* [11], elle est valide pour les codes unitaires et pour ceux qui ne le sont pas :

Proposition 1 *Sous les hypothèses du modèle (1.1), si pour toutes les couples de mots de code $\mathbf{X}_\ell$ et $\mathbf{X}_j$ appartenant à $\mathcal{C}$, les matrices :*

$$\begin{bmatrix} \mathbf{X}_\ell^\dagger \\ \mathbf{X}_j^\dagger \end{bmatrix} \begin{bmatrix} \mathbf{X}_\ell & \mathbf{X}_j \end{bmatrix} = \begin{bmatrix} \mathbf{R}_{\ell\ell} & \mathbf{R}_{\ell j} \\ \mathbf{R}_{j\ell} & \mathbf{R}_{jj} \end{bmatrix} \tag{1.25}$$

ont rang plein, alors $\mathcal{C}$ a diversité pleine selon le GLRT et le critère ML non cohérent

$$d^{GLRT}(\mathcal{C}) = d^{nc-ML}(\mathcal{C}) = M \,. \tag{1.26}$$

Une condition nécessaire est que $T \geq 2M$.

Brièvement, si $T = 2M - m_1 < 2M$ (ce qui revient à dire $m_1 > 0$), chaque couple de sous-espaces M-dimensionnels de $\mathbb{C}^T$ ont une intersection au moins de dimension $m_1 > 0$, et la PEP entre ces deux mots de code ne peut donc pas atteindre l'allure descendante la plus rapide (ρ^{-NM}).

1.1.6 Propositions de la littérature

Des arguments de théorie de l'information à propos des canaux ergodiques et des critères de minimisation de la probabilité d'erreur (cf. Sect. 2.5) démontrent qu'à SNR élévé les signaux optimaux peuvent être représentés par des matrices avec des colonnes orthonormales. C'est pour cela que notre recherche s'est consacrée à des codes ayant cette propriété. Néanmoins, différentes propositions, conçues avec divers critères, sont présentées dans la littérature. Les plus importantes sont :

- Codes obtenus par minimisation d'une fonction coût donné : cette dernière peut être liée aux distances définies sur le Grassmannien [9, 13, 14], à la borne de l'union de la probabilité de super-symbole/bit [15, 16], ou encore à la distance de Kullback-Leibler [17].

- Codes obtenus par paramétrisation de l'ensemble des matrices unitaires via une certaine fonction : par exemple la transformée de Cayley comme donnée dans [18, 19, 20], ou par paramétrisation du Grassmannien à travers la fonction exponentielle, comme dans cette thèse et les travaux précédents sur ce sujet [21, 22].
- Codes issus des constructions algébriques ad-hoc pour des cas particulaires [23, 24, 25].
- Codes conçus en s'inspirant de systèmes avec séquence d'apprentissage : la première partie du mot de code contient la séquence d'apprentissage, tandis que la deuxième contient l'information codée (ou modulée) selon un code espace-temps pour des systèmes cohérents. Au récepteur la première partie du signal reçu sert à avoir une estimation du canal qui est ensuite utilisée pour décoder l'information [16, 26, 27, 28, 29].

Dans le tableau 1.1 sont résumées les principales caractéristiques des propositions mentionnées.

1.2 Les codes EP : codes unitaires obtenus via la fonction exponentielle

Dans cette section nous introduirons rapidement le Grassmannien, en décrivant sa structure mathématique. Nous décrirons ensuite la méthode utilisée pour construire les codes unitaires qui sont l'objet de cette étude : leurs mots de code peuvent être vus comme des points du Grassmannien. Nous appellerons ces codes « codes EP » parce qu'ils sont obtenus à partir des codes espace-temps cohérents à travers une fonction non linéaire : la fonction exponentielle. Nous décrirons les propriétés des codes EP et la relation qui existe avec les codes cohérents qui les génèrent. Nous terminerons par quelques exemples.

1.2.1 Le Grassmannien $G_{T,M}$

Nous utilisons ici la définition de Grassmannien donné par [4] :

Définition 8 *Soit $\mathcal{U}_n$ le groupe unitaire. Soient $T, M \in \mathbb{N}$ et $T > M$, le Grassmannien $G_{T,M} = \mathcal{U}_T/(\mathcal{U}_M \times \mathcal{U}_{T-M})$.*

Un point du Grassmannien, c'est-à-dire un sous-espace Ω, est décrit par la classe d'équivalence :

$$\Omega = \left\{ \mathbf{Q} \begin{bmatrix} \mathbf{Q}_M & \mathbf{0} \\ \mathbf{0} & \mathbf{Q}_{T-M} \end{bmatrix} : \mathbf{Q} \in \mathcal{U}_T \, , \, \mathbf{Q}_M \in \mathcal{U}_M \, , \, \mathbf{Q}_{T-M} \in \mathcal{Q}_{T-M} \right\} . \qquad (1.27)$$

En séparant les premières M colonnes, on obtient :

$$\mathbf{Q} = [\mathbf{X} \; \mathbf{X}^{\perp}] \, , \qquad \mathbf{X}^{\dagger}\mathbf{X} = \mathbf{I}_M \, , \; (\mathbf{X}^{\perp})^{\dagger}\mathbf{X}^{\perp} = \mathbf{I}_{T-M} \, , \; \mathbf{X}^{\dagger}\mathbf{X}^{\perp} = \mathbf{0} \, . \qquad (1.28)$$

Référence	type[a]	méthode de conception	code co.[b]	diversité	dec. simplifié[c]	complexité dec.
[13]	U	min. num. $d_c^2(\mathcal{C})$	non	pas de controle	non	$O(2^{RT})$
[14]	U	min. num. $d_{cF}^2(\mathcal{C})$	non	pas de contrôle	S	GLRT locale
[15]/[16]	U	min. num. $P_e/P_{e,bit}$	non	pleine	non	$O(2^{RT})$
[17]	N/U	min. num.	non	pas de contrôle	non[e]	$O(2^{RT})$
[18]	U	rotations successives	non	pas de contrôle	non	$O(2^{RT})$
[19, 20]	U	parametrisation de Cayley	non	pas de contrôle	S	dec. à sphère
[22]	U	parametrisation exponentielle	oui	pleine	S	GLRT locale
[23]	U	algébrique/apprentissage	oui[d]	pleine	O	$O(MN)$/$O(M^2N)$
[24]	U	algébrique/apprentissage	oui	pleine	O	$O(2^{TR/2})$
[25]	N/U	algébrique	non	pleine	non	$O(2^{TR})$
[16, 26, 27, 28]	N/U	apprentissage	oui	pleine	S	dec . à sphère

[a] Type de code non cohérent: U = unitaire, N/U = non unitaire et unitaire.

[b] Est-ce que le code non cohérent est obtenu à partir d'un code cohérent ?

[c] S = décodage simplifié sous-optimal, O = décodage simplifié optimal
(par rapport aux performances ML).

[d] Une proposition qui n'est pas construite sur un code cohérent est également présentée.

[e] Des constellations unitaires qui ont un algorithme de décodage simplifié peuvent être utilisées, mais ce n'est pas le cas général.

Tableau 1.1: Résumé des proposition les plus citées dans la littérature.

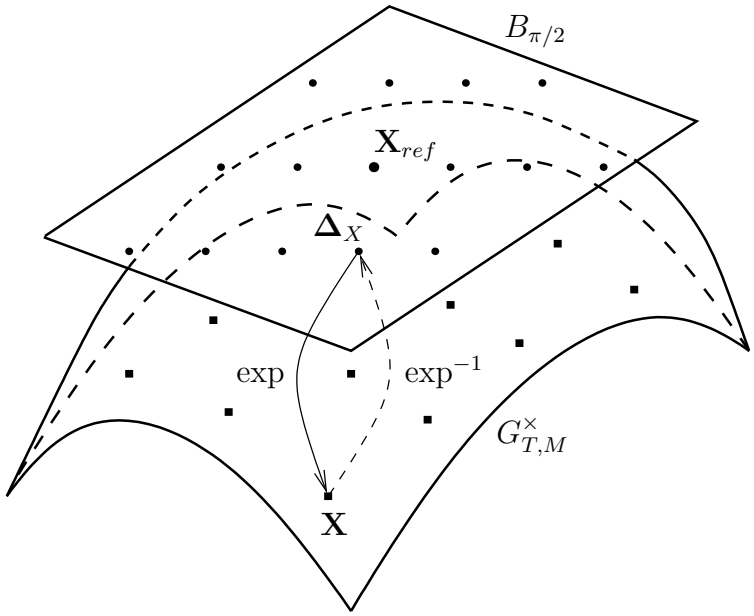

Figure 1.3: La fonction exponentielle envoie des points de l'espace tangent sur le Grassmannien. Un ensemble de points sur l'espace tangent génère donc un ensemble de points sur le Grassmannien, qui est ainsi un code seulement si la fonction exponentielle est inversible.

Le sous-espace Ω en (1.27) coïncide avec le sous-espace généré par les colonnes de $\mathbf{X}$.

L'opération de quotient sur $\mathcal{U}_M \times \mathcal{U}_{T-M}$ décrit le fait que des rotations arbitraires des bases de $\mathbf{X}$ et séparément de $\mathbf{X}^{\perp}$, ne changent pas le sous-espace. Au contraire, une rotation en $\mathbb{C}^T$, représentée par une multiplication à gauche par une matrice unitaire, génère un sous-espace différent.

Puisque $\mathcal{U}_T$ et $\mathcal{U}_M \times \mathcal{U}_{T-M}$ sont des groupes de Lie fermés, le Grassmannien est une variété différentielle C^{∞} homogène. Le Grassmannien peut être vu comme une surface de dimension (réelle) $2M(T-M)$ plongée dans un espace vectoriel de dimension plus grande (par exemple $\mathbb{C}^{TM}$) [30].

Il est possible d'associer un espace tangent à chaque point du Grassmannien [4]. Par convention, nous considérerons l'espace tangent $t\pi_{ref}$ à un sous-espace fixé par référence (dit « sous-espace de référence ») qui s'exprime de la manière suivante :

$$\mathbf{Q}_{ref} = [\mathbf{X}_{ref}\ \mathbf{X}_{ref}^{\perp}] = \mathbf{I}_T\,, \qquad \mathbf{X}_{ref} = \begin{bmatrix} \mathbf{I}_M \\ \mathbf{0}_{T-M,M} \end{bmatrix} = \mathbf{I}_{T,M}\,. \tag{1.29}$$

Ce choix nous aidera à simplifier la notation et les calculs. Chaque point de $t\pi_{ref}$ est représenté par :

$$\mathbf{\Delta}_X = \begin{bmatrix} \mathbf{0} & -\mathbf{B}_X^{\dagger} \\ \mathbf{B}_X & \mathbf{0} \end{bmatrix}, \qquad \mathbf{B}_X \in \mathbb{C}^{(T-M)\times M}\,. \tag{1.30}$$

La dimension (réelle) de $t\pi_{ref}$ est $2M(T-M)$. Elle est identique à celle du Grassmannien.

La fonction exponentielle est utilisée afin d'obtenir des points du Grassmannien à partir des points de l'espace tangent (cf. Fig. 1.3) :

$$\mathbf{X} = \exp \begin{bmatrix} \mathbf{0}_M & -\mathbf{B}_X^\dagger \\ \mathbf{B}_X & \mathbf{0}_{T-M} \end{bmatrix} \begin{bmatrix} \mathbf{I}_M \\ \mathbf{0}_{T-M,M} \end{bmatrix} = \exp(\mathbf{\Delta}_X)\mathbf{I}_{T,M} \,. \tag{1.31}$$

La formule précédente peut être mise sous une forme particulière appelée forme Cosinus-Sinus (CS) obtenue à partir de la décomposition à valeurs singulières de la matrice $\mathbf{B}_X$ (Thin Singular Value Decomposition - TSVD [3, pag. 72]) :

$$\mathbf{B}_X = \mathbf{V}\,\mathbf{\Theta}\,\mathbf{U}^\dagger\,, \qquad \mathbf{V} \in \mathcal{U}_{T,M},\ \mathbf{U} \in \mathcal{U}_M,\ \mathbf{\Theta} = \mathrm{diag}([\theta_1\ \ldots\ \theta_{\mathrm{M}}]) \tag{1.32}$$

où nous ordonnons les valeurs singulières par ordre croissant : $0 \leq \theta_1 \leq \theta_2 \leq \ldots \leq \theta_M$. La forme CS de la formule (1.31) est alors donnée par :

$$\mathbf{Y} = \begin{bmatrix} \mathbf{UC} \\ \mathbf{VS} \end{bmatrix} \mathbf{U}^\dagger\,, \qquad \mathbf{C} = \cos\mathbf{\Theta}\,,\ \mathbf{S} = \sin\mathbf{\Theta} \tag{1.33}$$

Les valeurs singulières de $\mathbf{B}_X$, rassemblées en $\mathbf{\Theta}$, sont les angles principaux entre $\Omega_{\mathbf{X}}$ et le sous-espace de référence Ω_{ref}.

1.2.2 Structure des codes EP

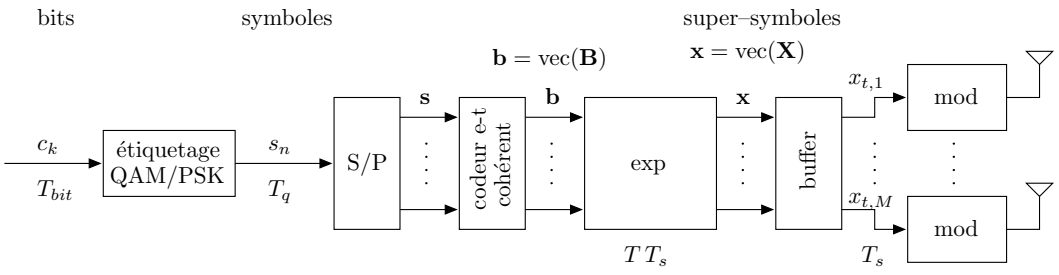

Figure 1.4: Schéma de la chaîne de transmission.

L'idée que nous suivrons dans cette étude est d'obtenir des codes espace-temps unitaires à partir des codes espace-temps par blocs utilisés dans les systèmes cohérents. Le code cohérent, que nous noterons $\mathcal{B}$, est disposé sur l'espace tangent $t\pi_{ref}$ et le code unitaire $\mathcal{C}$ est obtenu à travers la fonction exponentielle, il est appelé plus simplement « code EP ». Le schéma par bloc du codeur est dessiné sur la Fig. 1.4. Le code $\mathcal{B}$ n'est pas construit ad-hoc mais il est choisi parmi les codes espace-temps cohérents par blocs, parce que les propriétés des ces codes sont déjà assez bien connues et qu'il est donc possible d'exploiter leur structure afin d'obtenir une procédure efficace de décodage.

Or, comme la fonction exponentielle est non-linéaire, elle n'est pas toujours inversible. Il faut d'abord trouver sous quelles conditions il est possible de réobtenir le code $\mathcal{B}$ à partir du code $\mathcal{C}$ (indiqué aussi avec $\mathcal{C}_\mathcal{B}$), pour avoir une définition bien formée de code EP. La réponse à cette question est donnée par la proposition suivante :

Proposition 2 *Soit $B_{\pi/2}$ le sous-ensemble ouvert de $t\pi_{ref}$ défini par (cf. aussi Fig. 1.3) :*

$$B_{\pi/2} = \left\{ \mathbf{\Delta} = \begin{bmatrix} \mathbf{0} & -\mathbf{B}^\dagger \\ \mathbf{B} & \mathbf{0} \end{bmatrix} \in t\pi_{ref} : \max_{m=1,\ldots,M}(\theta_m) < \frac{\pi}{2} \right\} \tag{1.34}$$

où θ_m sont les valeurs singulières de $\mathbf{B}$. Soit $G_{T,M}^{\times}$ le sous-ensemble ouvert du Grassmannien défini comme

$$G_{T,M}^{\times} = \{\Omega_{\mathbf{X}} \in G_{T,M} : \Omega_{\mathbf{X}} \cap \Omega_{ref}^{\perp} = \{0\}\}\,. \tag{1.35}$$

Alors

$$\exp : B_{\pi/2} \subset t\pi_{ref} \longrightarrow G_{T,M}^{\times} \subset G_{T,M} \tag{1.36}$$

est une fonction bijective.

En cette démonstration est donnée la méthode pour inverser la fonction exponentielle à partir d'une base orthonormale quelconque d'un point de $G_{T,M}^{\times}$. Soit donc $\tilde{\mathbf{X}}$ une base (pas nécessairement en forme CS) $\Omega_{\mathbf{X}} \in G_{T,M}^{\times}$:

$$\tilde{\mathbf{X}} = \begin{bmatrix} \tilde{\mathbf{X}}_1 \\ \tilde{\mathbf{X}}_2 \end{bmatrix}, \qquad \tilde{\mathbf{X}}_1 \in \mathbb{C}^{M\times M}, \;\; \tilde{\mathbf{X}}_2 \in \mathbb{C}^{(T-M)\times M}\,. \tag{1.37}$$

Le point $\mathbf{B}_X$ correspondant sur l'espace tangent est obtenu en appliquant l'algorithme suivant :

1. Calculer la SVD de $\tilde{\mathbf{X}}_1$: $\tilde{\mathbf{X}}_1 = \mathbf{U}\mathbf{C}\tilde{\mathbf{U}}^\dagger$
2. Calculer $\mathbf{X} = \tilde{\mathbf{X}}\tilde{\mathbf{U}}\mathbf{U}^\dagger$ qui est maintenant en forme CS.
3. Diviser $\mathbf{X}$ en deux sous-blocs comme en (1.37): $\mathbf{X}^\dagger = [\mathbf{X}_1^\dagger \;\; \mathbf{X}_2^\dagger]$ et calculer la TSVD de $\mathbf{X}_2$: $\mathbf{X}_2 = \mathbf{V}\mathbf{S}\mathbf{U}^\dagger$.
4. Calculer $\mathbf{\Theta} = \sin^{-1}(\mathbf{S})$.
5. Construire la matrice $\mathbf{B} = \mathbf{V}\,\mathbf{\Theta}\,\mathbf{U}^\dagger$.

Un fois choisi un code cohérent $\mathcal{B}'$, pour satisfaire la condition d'inversibilité (1.34) on fixera un nombre réel positif α, appelé facteur homothétique, qui multiplie tous les mots de code en obtenant un autre code :

$$\mathcal{B} = \alpha\mathcal{B}' = \{\mathbf{B} = \alpha\mathbf{B}',\, \forall\, \mathbf{B}' \in \mathcal{B}'\}$$

dont les mots de codes appartiennent à $B_{\pi/2}$. Le facteur homothétique influence linéairement les valeurs principales des matrices $\mathcal{B}'$, et n'influence pas les matrices de rotation de la SVD.

Une fois choisi le bon facteur homothétique et obtenu le code $\mathcal{B}$, on peut se demander s'il existe un lien entre les propriétés du code $\mathcal{B}$ et du code $\mathcal{C}_{\mathcal{B}}$, en particulier pour ce qui est de la diversité en transmission assurée par ce type de code. Une réponse est donnée par le théorème suivant :

Théorème 1 *Soit $\mathcal{C}_{\mathcal{B}}$ le code EP obtenu par le code cohérent $\mathcal{B} = \alpha\mathcal{B}'$. Soit $d^{co-ML}(\mathcal{B}') = d$ la diversité de $\mathcal{B}'$. Alors*

$$d^{GLRT}(\mathcal{C}_{\mathcal{B}}) \geq d^{co-ML}(\mathcal{B}) = d^{co-ML}(\mathcal{B}')\,. \tag{1.38}$$

sous la condition que le facteur homothétique appartienne à l'intervalle

$$0 < \alpha < \bar{\alpha}\,, \qquad \bar{\alpha} = \min\left\{\frac{\pi}{2\,\theta'_{max}}, \hat{\alpha}_d\right\}\,, \qquad \hat{\alpha}_d = \min_{k\neq l}\alpha_d(k,l) \tag{1.39}$$

où $\theta'_{max} = \max_k \|\mathbf{B}'_k\|_2 = \max_k \theta'_{k,1}$ et

$$\alpha_d(k,l) \text{ est solution de } \tan(\alpha\theta'_{k,1}) + \tan(\alpha\theta'_{l,1}) - \alpha(\theta'_{k,1} + \theta'_{l,1}) = \alpha\sigma'_d(k,l) \tag{1.40}$$

où $\sigma_d(k,l)$ est le $d^{ème}$ valeur singulière (en ordre décroissant) de $\mathbf{B}'_k - \mathbf{B}'_l$ avec $k \neq l$.

Ce théorème, bien qu'il assure la pleine diversité du code EP si le code de départ a pleine diversité aussi, donne des valeurs très petites du facteur homothétique. Si α est très petit, les performances du code seront mauvaises parce que les mots du code $\mathcal{B}$ sont toutes près du sous-espace de référence. Néanmoins il est possible de trouver des facteurs homothétiques, hors de l'intervalle fixé par le théorème, qui gardent la diversité du code EP. Ceci a été vérifié par simulation.

1.2.3 Exemples de codes EP

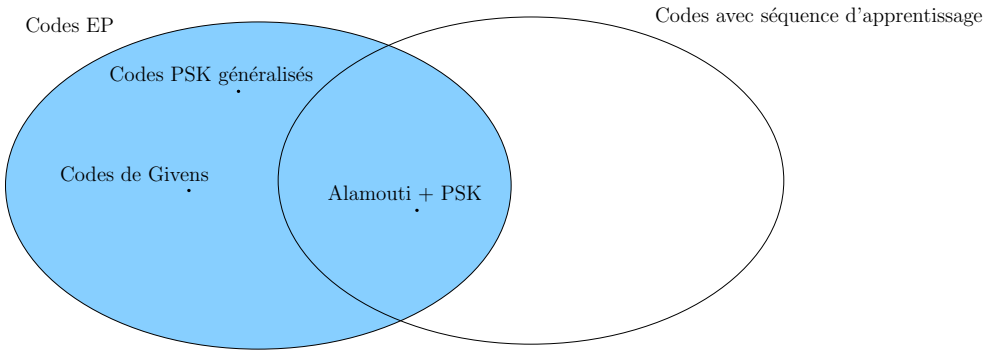

Figure 1.5: Les codes PSK généralisés et les codes de Givens sont des codes EP. Aussi, certains codes avec des séquence d'apprentissage (notamment ceux présentés dans [23]) peuvent être vus comme des codes EP.

Il existe une famille de codes EP pour laquelle nous peuvons étudier plus en détail la relation entre les mots du code cohérent et du code EP. Cette famille est formée par les codes qui satisfont la propriété suivante :

$$\begin{cases} \mathbf{B}_k^\dagger\mathbf{B}_\ell = \mathbf{B}_\ell^\dagger\mathbf{B}_k \\ \mathbf{B}_k\mathbf{B}_\ell^\dagger = \mathbf{B}_\ell\mathbf{B}_k^\dagger \end{cases}, \qquad \text{pour chaque } k \neq \ell\,. \tag{1.41}$$

Sous cette condition très stricte, toutes les pairs de matrices $\mathbf{\Delta}_k$ et $\mathbf{\Delta}_\ell$ dans l'espace tangent commutent. Dans ce cas, grâce aux propriétés de l'exponentiel, on peut facilement démontrer que si $\mathbf{X}_k, \mathbf{X}_\ell \in \mathcal{C}$

$$\mathbf{X}_\ell^\dagger \mathbf{X}_k = \mathbf{I}_{T,M}^\dagger \exp\left\{ \begin{bmatrix} \mathbf{0}_M & -(\mathbf{B}_k - \mathbf{B}_\ell)^\dagger \\ (\mathbf{B}_k - \mathbf{B}_\ell) & \mathbf{0}_{T-M} \end{bmatrix} \right\} \mathbf{I}_{T,M} \,. \tag{1.42}$$

Grâce à cette relation nous pouvons finalement démontrer la proposition suivante :

Proposition 3 *Soit $\mathcal{B}$ un code dont les matrices satisfont (1.41). Alors $\mathcal{B}$ et le code EP correspondant $\mathcal{C}_\mathcal{B}$ ont la même diversité (selon le critère de réception associé). De plus, la distance produit peut être bornée comme il suit :*

$$\frac{2}{\pi} |(\mathbf{B}_k - \mathbf{B}_\ell)^\dagger (\mathbf{B}_k - \mathbf{B}_\ell)|^{\frac{1}{2M}} \leq d_p(\mathbf{X}_k, \mathbf{X}_\ell) \leq |(\mathbf{B}_k - \mathbf{B}_\ell)^\dagger (\mathbf{B}_k - \mathbf{B}_\ell)|^{\frac{1}{2M}} \tag{1.43}$$

Les codes PSK généralisés sont en effet des codes EP qui satisfont les conditions (3.58). Toutefois, ces conditions contraignantes n'ont pas permi de trouver d'autres codes qui les satisfont. De plus, les codes PSK généralisés n'utilisent pas tous les dégrés de liberté disponibles, à cause de leur structure qui emploie plusieurs dégrées de liberté.

La Fig. 1.5 montre d'autres propositions déjà existantes dans la littérature, qui peuvent être vues comme des codes EP.

1.3 Décodage Simplifié des Codes EP en $G_{T,1}$

Dans cette section nous introduirons les codes EP pour les systèmes à une antenne en transmission ($M = 1$), définis sur le Grassmannien $G_{T,1}$. Ensuite nous décrirons un algorithme sous optimal pour le décodage de ces codes, qui arrive à suivre les performances GLRT.

1.3.1 Forme et propriétés des codes EP en $G_{T,1}$

Le Grassmannien $G_{T,1}$ peut être vu comme l'ensemble des lignes complexes dans l'espace $\mathbb{C}^T$. Le sous-espace de référence est fixé ainsi :

$$\mathbf{x}_{ref} = \begin{bmatrix} 1 & 0 & \dots & 0 \end{bmatrix}^\dagger = \mathbf{e}_1 \tag{1.44}$$

et la forme CS du mot de code EP est :

$$\mathbf{x} = \begin{bmatrix} \cos \|\mathbf{b}\| \\ \dfrac{\sin \|\mathbf{b}\|}{\|\mathbf{b}\|} \mathbf{b} \end{bmatrix} = \begin{bmatrix} \cos \rho_b \\ \dfrac{\sin \rho_b}{\rho_b} \mathbf{b} \end{bmatrix} \,, \qquad \rho_b = \|\mathbf{b}\| \,, \tag{1.45}$$

où ρ_b est l'angle principal entre le sous-espace de référence et le sous-espace généré par $\mathbf{x}$. La condition pour inverser la fonction exponentielle est

$$\mathbf{b} \in B_{\pi/2} + \{\mathbf{b} \in \mathbb{C}^{T-1} : \rho_b = \|\mathbf{b}\| < \pi/2\} \,. \tag{1.46}$$

Sous cette condition l'image de la fonction exponentielle est

$$G_{T,1}^{\times} = \{\mathbf{x} \in \mathbb{U}^T : x_1 > 0\} \quad \text{where} \quad \mathbf{x}^t = \begin{bmatrix} x_1 & x_2 & \dots & x_T \end{bmatrix} . \tag{1.47}$$

où $(\cdot)^t$ indique la transposition et $\mathbb{U}^T$ indique (avec abus de notation) la sphère complexe de dimension T. On remarque que dans le cas où $M = 1$, le représentant de la classe d'équivalence en forme CS (1.45) est unique. Si $\mathbf{x} \in G_{T,1}^{\times}$ alors il est possible d'inverser la fonction exponentielle à partir de la forme CS en (1.45). Nommé

$$\hat{\mathbf{x}} = [x_2 \ \dots \ x_M]^t , \tag{1.48}$$

le vecteur $\mathbf{b} \in B_{\pi/2}$ est calculé ainsi :

$$\mathbf{b} = \exp^{-1}(\mathbf{x}) = \frac{\rho_b}{\sqrt{1 - x_1^2}} \hat{\mathbf{x}} , \qquad \rho_b = \arccos x_1 . \tag{1.49}$$

L'opération d'arccos est bien définie parce que $x_1 \in (0, 1]$.

La distance produit entre deux sous-espaces (lignes) $\mathbf{x}_k, \mathbf{x}_\ell \in G_{T,1}$ est très simple : $d_p(\mathbf{x}_k, \mathbf{x}_\ell) = \sin\theta_{k,l} = \sqrt{1 - |\mathbf{x}_k^\dagger \mathbf{x}_\ell|^2}$. Il est possible de démontrer la proposition suivante :

Proposition 4 *Soient $\mathbf{x}_k, \mathbf{x}_\ell \in \mathcal{C}$ obtenus de $\mathbf{b}_k, \mathbf{b}_\ell \in \mathcal{B}$, avec $\rho_k = \|\mathbf{b}_k\|$. Alors la borne inférieure suivante vaut :*

$$d_p(\mathbf{x}_k, \mathbf{x}_\ell) = \sin\theta_{k,l} \geq \begin{cases} \frac{\sin(2\rho_b)}{2\rho_b} \|\mathbf{b}_k - \mathbf{b}_\ell\| & , \text{si } \|\mathbf{b}_k\| = \|\mathbf{b}_\ell\| = \rho_b \\ \frac{2}{\pi} |\|\mathbf{b}_k\| - \|\mathbf{b}_\ell\|| & , \text{si } \|\mathbf{b}_k\| \neq \|\mathbf{b}_\ell\| \end{cases} \tag{1.50}$$

A partir de la proposition précédente il est possible de calculer de bons facteurs homothétiques. Soit la constellation Q-QAM :

$$Q\text{-QAM} = \{q_1 d + i q_2 d, \ q_1 = \pm 1, \dots \pm(Q_1 - 1), \ q_2 = \pm 1, \dots \pm(Q_2 - 1), \ Q = Q_1 Q_2\} \tag{1.51}$$

pour des constellations carrées les entiers Q_1 et Q_2 sont égaux $Q = Q_1^2$. Il est possible de prouver que, dans les cas de constellations carrées, un bon facteur homothétique est donné par :

$$\alpha = (\pi/2)[1 + \sqrt{2(T-1)}(\sqrt{Q} - 1)]^{-1} \tag{1.52}$$

et pour des constellations rectangulaires il est donné par :

$$\alpha = (\pi/2)\{1 + \sqrt{(T-1)[(Q_1 - 1)^2 + (Q_2 - 1)^2]}\}^{-1} . \tag{1.53}$$

1.3.2 Géométrie du GLRT

L'idée du décodeur est la suivante : puisqu'aucune méthode efficace pour le calcul du GLRT n'est connue, on veut localiser un sous-ensemble de mots de code sur lesquels calculer et comparer les métriques GLRT. On appellera cette approche « GLRT locale ».

Pour ce faire, nous avons tout d'abord étudié la forme des ensembles de points sur le Grassmannien qui ont le même valeur de la métrique GLRT par rapport au point reçu. Le GLRT dans ce cas est :

$$\psi(\mathbf{x}) = |\mathbf{y}^\dagger \mathbf{x}| \quad \text{en supposant que } \mathbf{x}, \mathbf{y} \in \mathbb{U}^T \,, \tag{1.54}$$

et on cherche la forme des ensembles $S_c = \{\mathbf{x} \in G_{T,1} : \psi(\mathbf{x}) = c\}$, où c peut être écrit comme un cosinus $c = \cos\theta_r$, puisque $c \in (0, 1]$. Naturellement, si θ_r est bien choisi, un certain nombre de mots du code EP $\mathcal{C}$ se situera à l'intérieur de l'ensemble $S_c = S_{\cos\theta_r}$. Celui-ci est le sous-ensemble sur lequel nous voulons calculer les métriques GLRT. Il existe un autre problème : il n'existe pas une méthode efficace pour énumérer les mots de code dans $S_{\cos\theta_r}$. La solution que nous proposons est la suivante : en utilisant la fonction inverse de l'exponentielle (cf. (1.49)), nous obtenons l'image réciproque $S^{-1}_{\cos\theta_r} = \exp^{-1}(S_{\cos\theta_r})$ dans l'espace tangent. Puisque l'espace tangent n'est pas courbe, et que nous supposons que le code $\mathcal{B}$ est tiré d'un réseau de points, des méthodes de recherche efficaces existent, sous la condition que cette recherche soit effectuée à l'intérieur d'une sphère (ou d'un hyper-cube). Or, comme la fonction exponentielle est non linéaire, les images réciproques dans l'espace tangent ne ressemblent pas à des sphères (voir la Fig. 1.6). Néanmoins on a réussi à couvrir l'image réciproque avec trois sphères. Ceci nous permet d'utiliser des algorithmes efficaces pour chercher les mots du code $\mathcal{B}$ dans l'espace tangent à l'intérieur de $S^{-1}_{\cos\theta_r}$. Ces mots de codes sont ensuite donnés en entrée à la fonction exponentielle pour obtenir la liste cherchée de mots du code EP $\mathcal{C}$ sur laquelle calculer les métriques GLRT.

Un autre effet dû à la définition même de Grassmannien et à la représentation que nous avons choisi pour chaque sous-espace (le vecteur en forme CS) est le suivant. Supposons qu'un mot du code EP $\mathcal{C}$ quasi-orthogonal au sous-espace de référence soit envoyé (point $\mathbf{x}_1$ en Fig. 1.7). Supposons aussi que le bruit du canal perturbe le mot de code d'une façon telle que le signal reçu représente un sous-espace de l'autre coté du Grassmannien par rapport au sous-espace vectoriel orthogonal au sous-espace de référence (point $\mathbf{x}_3$ en Fig. 1.7). Alors le vecteur en forme CS qui représente le même sous-espace peut être très loin, même opposé, du premier (point $\mathbf{x}_2$ en Fig. 1.7). On a appelé cet effet, effet modulo $\mathbb{U}$, parce que il est dû au quotient par $\mathbb{U}$ dans la définition du Grassmannien.

Dans une représentation du type de la Fig. 1.6, l'effet modulo $\mathbb{U}$ donne des courbes comme celles sur la Fig. 1.8. Dans ce cas la, il est impossible de couvrir efficacement l'image réciproque avec un faible nombre de sphères. Pour limiter la complexité du décodeur nous proposons d'utiliser toujours trois sphères, placées différemment, et de choisir le paramètre θ_r d'une façon telle que l'effet modulo $\mathbb{U}$ soit le moins significatif possible par rapport à son influence sur les performances du code.

1.3.3 Proposition de décodeur

Nous rappellons un décodeur simplifié déjà proposé par Kammoun et Belfiore [31] et que nous appellerons ici décodeur ML cohérent sur l'espace tangent (co-ML-tg), sim-

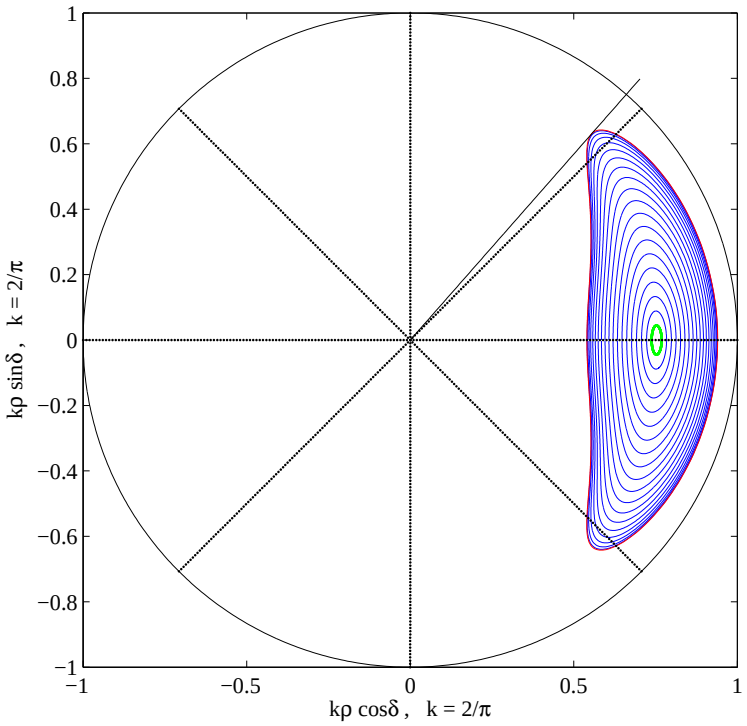

Figure 1.6: Représentation en coordonnées polaires de $\rho = \|\mathbf{b}\|$ et de la phase commune δ des vecteurs $\mathbf{b} \in S^{-1}_{\cos\theta_r}$ dans l'espace tangent, où θ_r assume différentes valeurs. Sur ce plan des sphères devraient donner des circonférences. Donc Nous pouvons remarquer la déformation due à la non linéarité de la fonction exponentielle.

plement parce que sa métrique est définie sur l'espace tangent et sur le code cohérent $\mathcal{B}$. Le décodeur peut être implementé selon les points suivants :

1. Mettre le signal reçu $\mathbf{y}$ en forme CS et calculer à l'aide de la formule (1.49) le point correspondant $\mathbf{b}_y$ dans l'espace tangent.

2. Calculer
$$\mathbf{b}^{co-ML-tg} = \min_{\mathbf{b}\in\mathcal{B}} \|\mathbf{b}_y - \mathbf{b}\| \,. \tag{1.55}$$

Naturellement cette métrique n'est pas optimale, elle ne correspond à la métrique GLRT sur le Grassmannien que pour les mots de code très proches du sous-espace de référence. Si le code $\mathcal{B}$ est simplement une constellation QAM multidimensionnelle, le calcul de (1.55) est simple. Si $\mathcal{B}$ est un sous-ensemble d'un réseau de points plus complexe, il faut utiliser un décodeur à sphère. Dans ce cas une approximation de la complexité du décodeur est :

$$O(8(T-1)^3) + 10T\text{(mult. réelles)} + 3T\text{(add. réelles)} + 2\text{(sqrt)} + 2\text{(look-up table)} \tag{1.56}$$

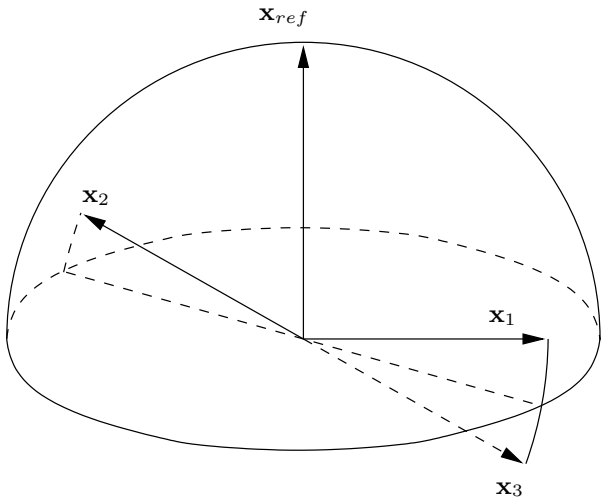

Figure 1.7: Le Grassmannien réel pour $T = 3$ peut être représenté par une hémisphère. Chaque point de l'hémisphère « nord » est en forme CS. Le point opposé dans l'autre hémisphère représente naturellement le même sous-espace, mais il n'est pas dans la forme CS.

Le décodeur que l'on propose ici pour la première fois est le GLRT locale. Puisqu'il utilise trois recherches dans des sphères, ce décodeur utilise certains paramètres qui servent à placer les sphères, décider du rayon ou s'apercevoir quand l'effet modulo $\mathbb{U}$ dévient très probable. L'algorithme est le suivant :

1. Choisir le paramètre θ_{nl} qui mesure l'angle par rapport du sous-espace de référence à partir duquel l'effet de la non linéarité devient important. Habituellement $\theta_{nl} = \pi/5, \pi/6$.

2. Choisir le paramètre θ_r, qui est lié à la taille du sous-ensemble du Grassmannien autour du point correspondant au signal reçu, là où il faut chercher les mots de code.

3. Soit $\mathbf{y}$ le vecteur en forme CS qui correspond au signal reçu. Calculer $\theta_1 = \arccos(y_1)$, qui est l'angle principal entre $\mathbf{y}$ et $\mathbf{x}_{ref} = \mathbf{e}_1$.

4. Si $\theta_1 \leq \theta_{nl}$, utiliser le décodeur co-ML-tg (1.55) (non linéarité négligeable).

5. Si $\theta_{nl} < \theta_1 \leq \pi/2 - \theta_r$, calculer $\mathbf{b}_y$, le correspondant dans l'espace tangent de $\mathbf{y}$. Ensuite, effectuer trois recherches dans l'espace tangent avec un rayon :

$$r_{max} = (\theta_1 + \theta_r) \sin\theta_r / \sin(\theta_1 + \theta_r) \tag{1.57}$$

et des centres :

$$\mathbf{o}_{1,2,3} = o\, e^{i\delta_{1,2,3}} \hat{\mathbf{u}}_y \,; \quad o = \frac{\rho_0}{\sin\rho_0} \cos\theta_r \sin\theta_1 \,; \quad \rho_0 = \arccos(\cos\theta_r \cos\theta_1) \tag{1.58}$$

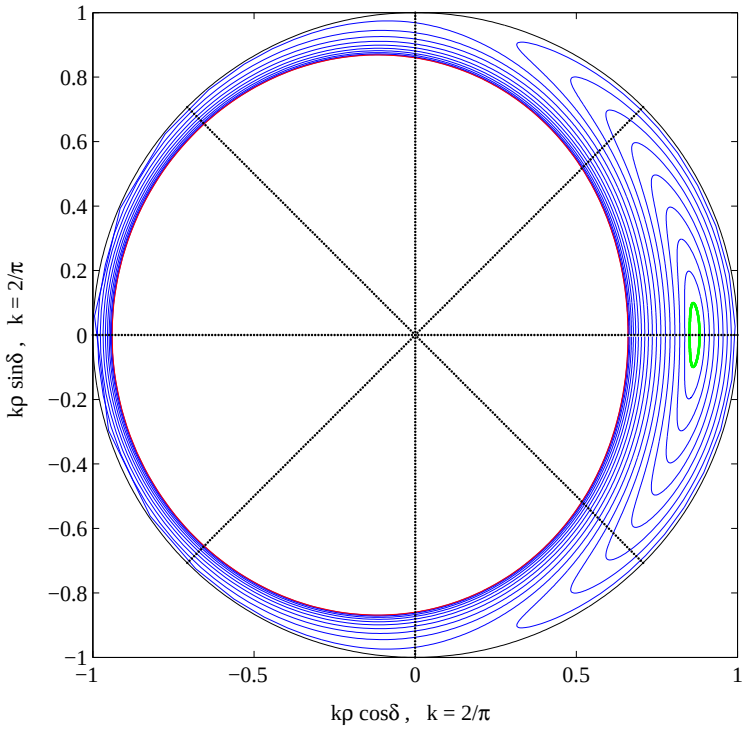

Figure 1.8: Représentation en coordonnées polaires de $\rho = \|\mathbf{b}\|$ et de la phase commune δ des vecteur $\mathbf{b} \in S^{-1}_{\cos\theta_r}$ dans l'espace tangent, où θ_r assume différentes valeurs. A partir d'une certaine valeur de θ_r les courbes ont des points aussi dans la partie gauche du plan, ce qu signifie que des petites perturbations des sous-espaces peuvent donner des très grandes perturbations des représentants en forme CS.

où

$$\delta_1 = 0\,, \qquad \delta_{2,3} = \pm \arcsin(\tan\theta_r \tan\theta_1)/\delta_F \tag{1.59}$$

et le facteur $\delta_F > 1$ est optimisé pour minimiser la performance. On obtient une liste de mots du code $\mathcal{B}$. Cette liste est dite « liste de mots candidats » $\mathcal{L}_\mathcal{B} = \{\mathbf{b}_{l_1}, \ldots, \mathbf{b}_{l_L}\}$. A partir de cette liste on calcule la liste correspondant au code EP: $\mathcal{L}_\mathcal{C} = \{\mathbf{x}_{l_1}, \ldots, \mathbf{x}_{l_L}\}$. Le mot de code choisi est celui qui satisfait la condition suivante :

$$\hat{\mathbf{x}} = \min_{\mathbf{x}\in\mathcal{L}_\mathcal{C}} |\mathbf{y}^\dagger \mathbf{x}| \tag{1.60}$$

6. Si $\theta_1 > \pi/2 - \theta_r$, l'effet modulo-$\mathbb{U}$ est présent. On utilise les mêmes paramètres que dans le cas suivant, mais on adapte la position des sphères en choisissant $\delta_{2,3}$ différemment

$$\delta_{2,3} = \arccos\left[1 - \frac{1}{2}\left(\frac{kr_{max}}{o}\right)^2\right] \tag{1.61}$$

où k est choisi entre 1 et 2.

Le choix numérique des paramètres est justifié dans la Sect. 4.4.4. La complexité du décodeur GLRT locale est bien sûr plus grande que celle du décodeur co-ML-tg, cela est dû au fait qu'il faut calculer les mots du code EP et les métriques GLRT. De plus, ces calcules donnent un terme de complexité linéaire en T et en la longueur de la liste des mots candidats L. Si L devient trop grand, ce terme peut gagner sur la complexité de la recherche à l'intérieur des sphères.

1.3.4 Simulations

Des simulations on été effectuées dans un canal AWGN et dans un canal de Rayleigh qui démontrent que le décodeur local atteint les performances GLRT.

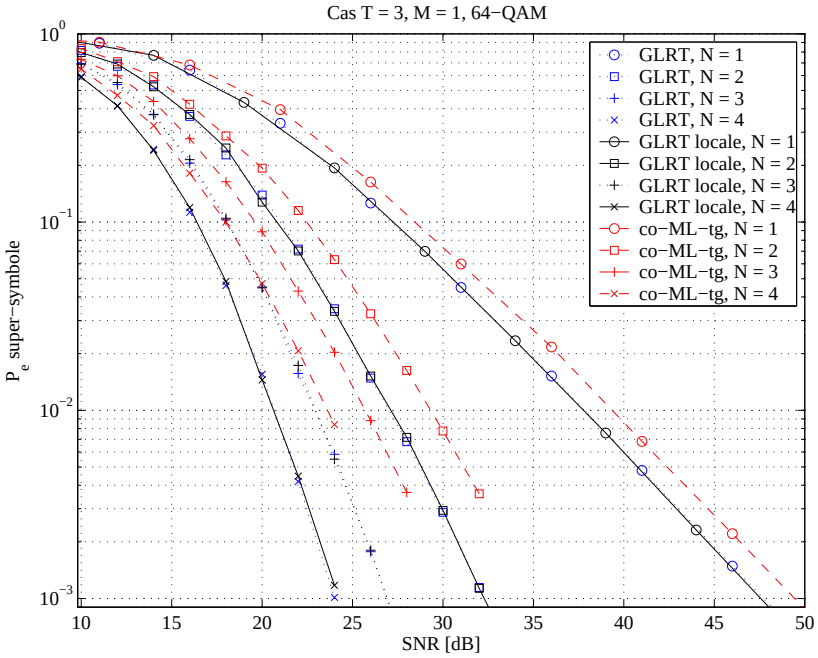

Figure 1.9: Performances des codes EP générés à partir du code cohérent $(64\text{-QAM})^2$ ($T = 3$), pour $N = 1, 2, 3, 4$. Les paramètres du décodeur sont : $\cos\theta_r = 0.97, \delta_F = 2, \theta_{nl} = \pi/6$. La simulation est arrêtée avec au moins 500 erreurs sur les super-symboles.

Les performances du code EP obtenues à partir du code $\mathcal{B}$ =$(64\text{-QAM})^2$ ($T = 3$) sont montrées en Fig. 1.9, avec plusieurs antennes en réception. Le décodeur GLRT local donne des performances pratiquement indiscernables de celles du décodeur qui calcule toutes les métriques GLRT. A taux d'erreur fixé, le décodeur co-ML-tg montre une perte croissante de SNR par rapport au GLRT local, lorsque le nombre d'antennes en réception augmente.

Des comparaisons avec des propositions de la littérature [26], [16], [23] sont proposées en Fig. 1.10. La comparaison se porte sur l'efficacité spectrale η des différents

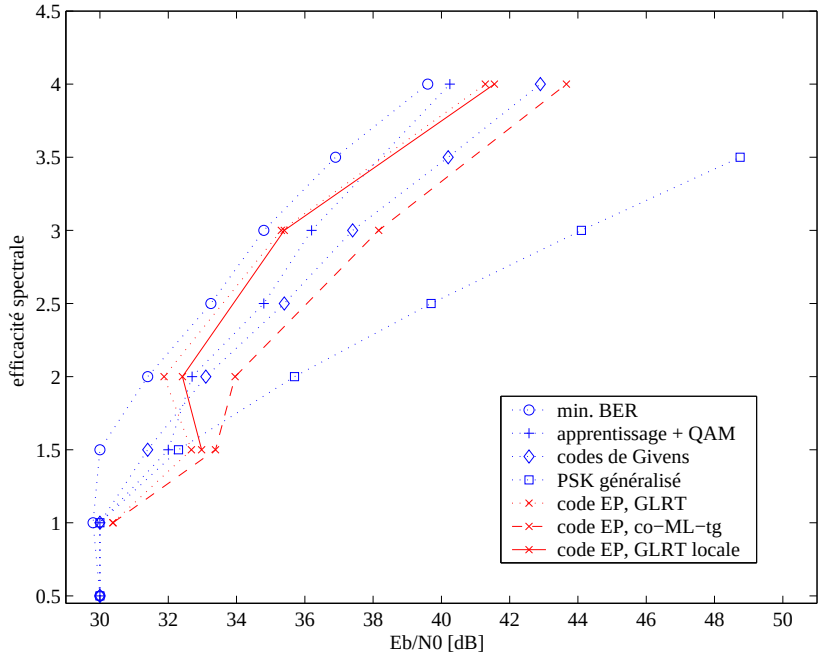

Figure 1.10: Efficacité spectrale à 10^{-3} de taux d'erreur par bit (BER) pour des codes proposés dans la littérature, avec $T = 2$ et $N = 1$.

codes en fonction du E_b/N_0 à un niveau de taux d'erreur sur bit fixé à 10^{-3}, avec $T = 2$ et $N = 1$. Pour $\eta = 1.5$ bits/s/Hz, le code EP n'a pas une bonne performance à cause de la forme rectangulaire de la constellation 8-QAM. Le problème peut être dépassé en choisissant une constellation avec une forme différente, ayant un meilleur facteur de forme. Les codes EP proposés sont très proches des codes optimaux, dessinés par optimisation numérique en minimisant la probabilité d'erreur sur le bit. Naturellement, l'opération de codage des codes EP et de décodage est bien plus simple que pour les codes optimaux. Par rapport aux codes avec séquence d'apprentissage, les performances sont meilleures dans le cas des codes EP au moins pour certains niveaux d'efficacité spectrale. Par contre la complexité de calcul est à la faveur des codes avec séquence d'apprentissage.

1.4 Décodage Simplifié des Codes EP dans le cas de $G_{T,M}$

Dans cette section nous étudierons les codes EP pour les systèmes avec $M > 1$ antennes en transmission et $N \geq M$ antennes en réception, définis sur le Grassmannien $G_{T,M}$. Ensuite, nous décrirons un algorithme sous optimal pour le décodage basé sur l'approche GLRT locale.

1.4.1 Propriétés des codes EP en $G_{T,M}$

La forme de la fonction de codage est celle déjà décrite dans la formule (1.31) et illustrée par la Fig. 1.4. Pour ce qui est des propriétés du code, nous n'avons pas réussi à trouver un lien analytique précis entre le gain de codage du code cohérent $\mathcal{B}$, défini comme $\Lambda(\mathcal{B}) = \min_{k\neq\ell} \Lambda(\mathbf{B}_k, \mathbf{B}_\ell)$ où

$$\Lambda(\mathbf{B}_k, \mathbf{B}_\ell) = \det[(\mathbf{B}_\ell - \mathbf{B}_k)^\dagger(\mathbf{B}_\ell - \mathbf{B}_k)] = |\det(\mathbf{B}_\ell - \mathbf{B}_k)|^2 \tag{1.62}$$

et la distance produit minimale du code EP $d_p(\mathcal{C}) = \min_{k\neq\ell} d_p(\mathbf{X}_k, \mathbf{X}_\ell)$. Dans deux cas particuliers, nous avons trouvé un lien entre ce deux quantités

Proposition 5 *Considérons un code EP $\mathcal{C}_\mathcal{B}$ obtenu à partir du code cohérent $\mathcal{B}$. Si le facteur homothétique tend à zéro, $\alpha \to 0$, et $T = 2M$, en définissant*

$$\beta = \left(1 - \frac{2}{\pi} \min_{\mathbf{B}\in\mathcal{B}}\{\|\mathbf{B}\|_2\}\right)^2 < 1\,,$$

alors

$$\beta\,\Lambda(\mathcal{B}) \leq d_p(\mathcal{C}_\mathcal{B}) \leq \Lambda(\mathcal{B})$$

Un autre résultat dérive directement de la proposition 3

Proposition 6 *Soit $\mathcal{B}$ un code dont les matrices satisfont (1.41). Alors $\mathcal{B}$ et le code EP correspondant $\mathcal{C}_\mathcal{B}$ satisfont*

$$\frac{2}{\pi}\Lambda(\mathcal{B}) \leq d_p(\mathbf{X}_k, \mathbf{X}_\ell) \leq \Lambda(\mathcal{B})\,.$$

Néanmoins des résultats plus généraux qui pourraient nous aider à choisir un bon facteur homothétique (bon dans le sens de la performance) sont très difficiles à trouver par calcul analytique, donc un tel facteur sera fixé par simulation, en minimisant le taux d'erreur par trame (Frame Error Rate – FER).

1.4.2 Proposition de décodeur

Pour ce cas général l'analyse mathématique de la métrique GLRT s'est avérée très difficile, mais, pour trouver un algorithme de décodage simplifié, nous avons toujours besoin de ramener le problème au code cohérent $\mathcal{B}$. L'idée, dans ce cas, est de linéariser la métrique GLRT en considérant la région du Grassmannien près du sous-espace de référence ($\alpha \to 0$). Sous cette hypothèse, et si le bruit additif est assez faible, le mot du code EP et le signal reçu peuvent être approximes de la manière suivante :

$$\mathbf{X} \simeq \begin{bmatrix}\mathbf{I}_M \\ \mathbf{B}\end{bmatrix}\,, \qquad \mathbf{Y} \simeq \begin{bmatrix}\mathbf{I}_M \\ \mathbf{B}_Y\end{bmatrix}\mathbf{H}_e$$

où le facteur α est caché dans $\mathbf{B}$ et $\mathbf{B}_Y$. En insérant ces expressions approximées dans la métrique GLRT (1.14), on s'aperçoit que le terme $\mathrm{tr}(\mathbf{H}_e^\dagger\mathbf{H}_e)$ est constant et qu'il

n'a pas d'influence dans la maximisation. De plus, le terme $\mathrm{tr}(\mathbf{H}_e^\dagger \mathbf{B}_Y^\dagger \mathbf{B}\,\mathbf{B}^\dagger \mathbf{B}_Y \mathbf{H}_e)$ dépend de α^4 et il peut être négligé par rapport aux autres termes qui dépendent de α^2. Finalement, maximiser le GLRT est équivalent à résoudre $\max_{\ell=1,\ldots,L} 2\mathrm{Re}\,[\mathrm{tr}(\mathbf{H}_e^\dagger \mathbf{B}^\dagger \mathbf{B}_Y \mathbf{H}_e)]$. Par conséquent, nous pouvons démontrer que :

$$\max_{\ell=1,\ldots,L} \mathrm{tr}(\mathbf{Y}^\dagger \mathbf{X}_\ell \mathbf{X}_\ell^\dagger \mathbf{Y}) \simeq \min_{\ell=1,\ldots,L} \|(\mathbf{B}-\mathbf{B}_Y)\mathbf{H}_e\|_F^2 \,. \tag{1.63}$$

La métrique précédente est quadratique en fonction des mots du code $\mathbf{B}$ et peut être réalisée efficacement si le code $\mathbf{B}$ est tiré d'un réseau de points. Bien sûr, la métrique (1.63) est valide seulement pour α très petit ou pour les mots du code EP très proches du sous-espace de référence, ce qui la rend sous optimale quand elle est utilisée pour décoder tout signal reçu.

Un récepteur qui utilise (1.63) pour décoder un code EP avec $M > 1$ ne récupère pas la diversité en transmission. Pour compenser les effets de la non linéarité, nous proposons un décodeur GLRT local, que l'on décrit dans le cas $N = M$.

1. Calculer la forme CS $\mathbf{Y}_c$ du signal reçu $\mathbf{Y}$ et la matrice $\mathbf{H}_e = \mathbf{Y}_c^\dagger \mathbf{Y}$.
2. Calculer $\mathbf{B}_Y = \exp^{-1}(\mathbf{Y}_c)$.
3. Calculer une liste $\mathcal{L}_\mathcal{B}$ de mots du code $\mathcal{B}$ candidats, en utilisant la métrique $\|(\mathbf{B}-\mathbf{B}_Y)\mathbf{H}_e\|_F^2$ jusqu'à avoir au moins L_{min} mots de code dans la liste.
4. Calculer, via la fonction exponentielle, la liste correspondante $\mathcal{L}_\mathcal{C}$ des mots du code EP
5. Calculer les métriques GLRT sur $\mathcal{L}_\mathcal{C}$ et choisir le mot de code qui atteint le maximum.

Dans la Sect. 5.3 une analyse rapide de la complexité est reportée. Comme dans le cas SISO, il y a principalement deux termes, le premier dû au décodeur à sphère est cubique dans la dimension du réseau de points $O([2T(T-M)]^3)$ et l'autre dépend de la longueur moyenne $\hat{L}$ de la liste des mots de code candidats $O(\hat{L}TMN)$.

1.4.3 Simulations

Le codes cohérents utilisés dans les simulations sont reportés dans la Sect. 5.4.1. Le code $\mathcal{B}_1'$, appelé aussi code 1 dans les figures, est introduit par Damen *et al.* [32], le code $\mathcal{B}_2'$ appelé aussi code 2 ou «golden code» a été introduit par Belfiore et al. [33]. En fin le code $\mathcal{B}_3'$, pour le cas $G_{6,3}$, a été présenté dans [27, pag. 1109].

Au contraire du cas SISO, nous ne disposons pas toujours de bornes sur la distance produit minimale en fonction de la distance euclidienne minimale du code cohérent. Donc nous ne pouvons pas choisir un bon facteur homothétique pour les performances par voie analytique. Pour cette raison, nous avons décidé de choisir le α en minimisant la probabilité d'erreur par trame pour un certain niveau de SNR moyen à la réception. Naturellement la valeur optimale du facteur homothétique change en fonction du récepteur (GLRT ou GLRT locale) et aussi en fonction du SNR et des paramètres du

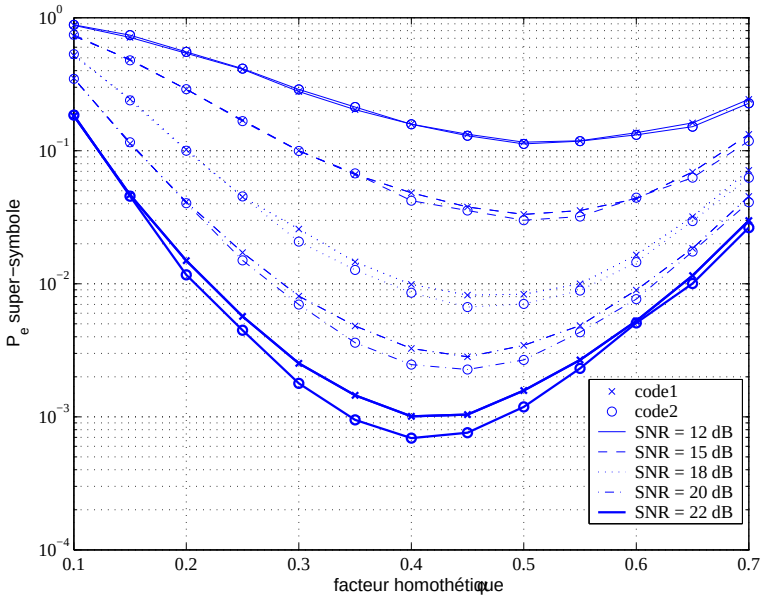

Figure 1.11: Probabilité d'erreur moyenne par trame (FER) du décodeur GLRT locale en fonction du facteur homothétique α pour des différents SNR. Les listes des mots de code candidats ont une longueur entre 10 et 30. L'efficacité spectrale est de 2 bits/s/Hz.

décodeur (par exemple, la longueur de la liste des mot candidats). Sur la Fig. 1.11 nous pouvons remarquer que, pour une valeur de SNR fixée, il existe une valeur optimale du facteur homothétique : si α est trop grand, la distance produit minimale du code augmente mais l'effet de la non linéarité est très important et les performances dégradent. Si α est trop petit, la non linéarité est moins importante mais, au delà d'un certainniveau, la distance produit minimale devient trop petite et la probabilité d'erreur augmente à cause du bruit additif. Nous pouvons aussi remarquer que le facteur homothétique optimal diminue lorsque le SNR augmente. Ceci signifie que pour faire face à la non linéarité il faut dégrader au fur et à mesure les performances (nous rappelons qu'en diminuant α la distance produit minimale diminue). Cet effet se produit puisque, à SNR élévé, l'influence de la non linéarité sur la probabilité d'erreur dévient de plus en plus importante et donc il faut agir surtout sur elle plutôt que sur la distance produit minimale du code.

Pour ce qui est de la longueur de la liste des mots de code candidats, nous avons vérifié par simulation que sa moyenne et son écart-type restent constants pour un grand intervalle de SNR (surtout à haut SNR) en choisissant comme rayon 1.1 fois le coefficient le plus petit sur la diagonale de la décomposition de Cholesky de la base du réseau de points (cette quantité correspond en gros à la plus petite norme des vecteurs de la base du réseau de points).

Sur la Fig. 1.12, nous pouvons voir des résultats de simulation dans le cas $T = 4$, $M = 2$. En choisissant bien le facteur homothétique pour les différents codes nous pouvons contrôler l'effet de la non linéarité et le décodeur GLRT locale arrive à suivre

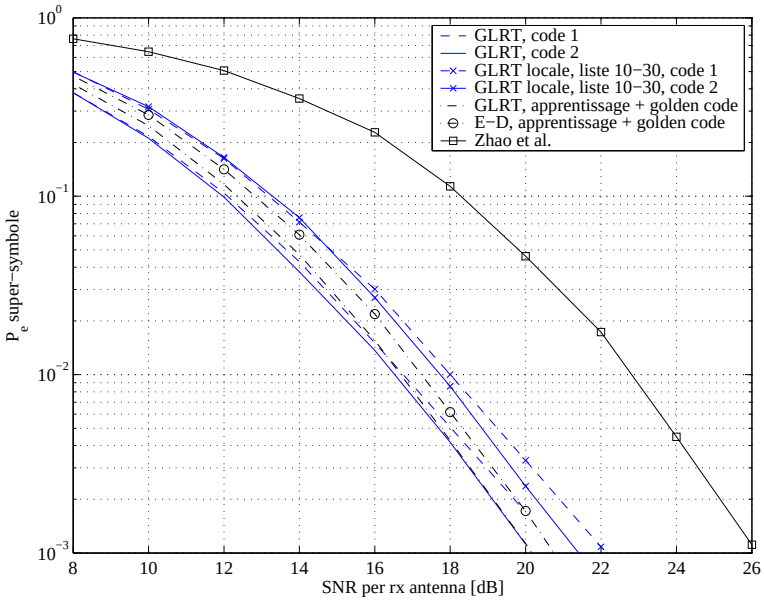

Figure 1.12: Des courbes de FER des codes EP $\mathcal{C}_1$ et $\mathcal{C}_2$ sont comparées aux codes avec des séquence d'apprentissage obtenus à partir du golden code $\mathcal{B}_2'$ et à la proposition de Zhao *et al.* [24]. La longueur de la liste de mots de code candidats du GLRT locale est comprise entre 10 et 30. Tous les codes ont une efficacité spectrale $\eta = 2$ bits/s/Hz.

le décodeur GLRT à moins de 1 dB de perte. Il faut aussi dire que à plus haut SNR, la courbe de FER du GLRT locale s'éloigne de celle du GLRT (perte de diversité). En effet, le facteur homothétique choisi pour les codes EP de Fig. 1.12 minimise le FER autour de 20 dB de SNR. Sur la même figure, nous peuvons aussi apprécier le fait que les codes EP ont des performances comparable à celles du code avec une séquence d'apprentissage (et bien meilleur que l'autre proposition avec récepteur simplifié). Néanmoins la complexité des codes avec une séquence d'apprentissage reste plus basse que la complexité de décodage du GLRT locale.

Nous terminons la section en disant que des résultats similaires sont obtenus quand T et M augmentent, mais l'effet de la non linéarité devient de plus en plus difficile à compenser, ce qui rend l'utilisation du décodeur GLRT local plus intéressante lorsque le nombre d'antennes à l'émission est $M = 2, 3$. (Cette dernière considération vaut pour le décodeur GLRT locale tel qu'il est formulé dans cette thèse. D'autres récepteurs simplifiés peuvent donner des conclusions différentes).

1.5 Décomposition Minimale des Signaux CPM en impulsions PAM

Cette section traite d'un sujet différent par rapport au reste de ce travail. Ici nous avons étudié une description mathématique des signaux issus d'une modulation à phase

continue (CPM). Cette modulation est particulièrement indiquée pour les émetteurs qui utilisent des amplificateurs non linéaires car le signal a une enveloppe constante. Le modulateur, bien qu'il soit assez simple à implanter, introduit une opération non linéaire et produit un signal avec une mémoire L (en périodes de symbole). Ces deux caractéristiques font que le récepteur optimal peut être extrêmement complexe. A cause de cela nombreux chercheurs se sont penchés sur le problème de décrire linéairement ces signaux, c'est-à-dire comme en somme d'un certain nombre d'impulsions. Plusieurs décompositions PAM des signaux CPM ont été proposées [34, 35, 36] et elles ont ensuite été appliquées pour proposer des récepteurs simplifiés [37, 38, 39, 40].

Ici, nous proposons une autre décomposition PAM valide pour les signaux qui ont une certaine symétrie dans la réponse de phase. La méthode pour obtenir la nouvelle décomposition est inédite et permet de démontrer que celle-ci a une cardinalité minimale : pour ce type de signaux CPM il n'existe pas de décomposition PAM obtenue avec moins d'impulsions.

1.5.1 Signaux CPM Séparables

L'enveloppe complexe d'un signal CPM générique peut s'écrire ainsi :

$$v(t) = \exp\left[j2\pi h\Big(\frac{1}{2}\theta_{n-L+1} + \sum_{i=0}^{L-1} a_{n-i}\,\varphi(t-nT+iT)\Big)\right], \qquad (1.64)$$

où h est *l'indice de modulation,* $\varphi(t)$ est *réponse de phase,* L est la mémoire du signal, a_n est la n-ème donnée en entrée et θ_{n-L+1} est *l'état de la phase* dans la période de symbole $n-L+1$. les données a_n appartiennent à un alphabet équilibré de taille M : $\mathcal{A}_M = \{\pm 1, \pm 3, \ldots, \pm(M-1)\}$ si M est pair ou $\mathcal{A}_M = \{0, \pm 2, \ldots, \pm(M-1)\}$ si M est impair.

La réponse de phase $\varphi(t)$ est une fonction croissante en $t \in [0, LT]$ et elle est égale à 0 pour $t \leq 0$ et à $\varphi(LT) = 1/2$ pour $t > LT$. Nous étudierons des signaux CPM dont la réponse de phase satisfait une propriété appelée « séparabilité » qui est la suivante:

$$\varphi(t+iT) = \varphi_0(t) + \frac{i}{2L}\,, \qquad i = 0, 1, \ldots, L-1,\ t \in [0, T)\,. \qquad (1.65)$$

Nous appélerons les signaux qui satisfont la proprieté (1.65) « signaux CPM séparables ». La fonction $\varphi_0(t)$ est appelée phase élémentaire et elle est croissante en $[0, T]$. Il vaut $\varphi_0(t) = 0$ pour $t \leq 0$ et $\varphi_0(t) = 1/(2L)$ pour $t \geq T$. Cette classe de signaux comprend les signaux L-REC (réponse de phase linéaire), donc aussi les signaux CPFSK et MSK et les signaux à *réponse pleine* (des signaux CPM avec une mémoire $L = 1$ et une réponse de phase arbitraire).

En introduisant la condition (1.65) dans l'expression du signal CPM on obtient :

$$v(t) = \exp\left[j2\pi h\Big(\frac{1}{2L}\Theta_n + A_n\,\varphi_0(t-nT)\Big)\right], \qquad t \in \mathcal{I}_n\,. \qquad (1.66)$$

où

$$A_n = \sum_{i=0}^{L-1} a_{n-i} \tag{1.67}$$

représentent les symboles « compacts », obtenus à partir de L symboles consécutifs $a_{n-L+1}, \ldots, a_n$ et $\Theta_n = L\,\theta_{n-L+1} + \sum_{i=0}^{L-1} i\,a_{n-i}$ est l'état de phase « compacte ». L'alphabet de A_n est $\mathcal{A}_M$ même pour $L = 1$, $\mathcal{A}_M + \mathcal{A}_M = \{a_{n-1} + a_n \,|\, a_{n-1} \in \mathcal{A}_M,\, a_n \in \mathcal{A}_M\} = \mathcal{A}_{2M-1}$ pour $L = 2$, en général $\mathcal{A}_N$ où $N = L(M-1)+1$. Il est possible de démontrer le principe d'équivalence suivant :

Proposition 7 *Soit $\mu_L(M)$ un modulateur CPM séparable défini par les paramètres M, L, h et $\varphi(t)$, où $\varphi(t)$ est généré par une phase élémentaire arbitraire $\varphi_0(t)$. Alors, $\mu_L(M)$ est équivalent à un modulateur CPM $\mu_1(N)$ défini par les paramètres : $M_1 = N = L(M-1)+1, L_1 = 1, h_1 = h/L$, et $\varphi_1(t) = L\,\varphi_0(t)$. Les données $A_n \in \mathcal{A}_N$ en entré de $\mu_1(N)$ sont obtenues à partir des $a_n \in \mathcal{A}_M$ de $\mu_L(M)$ par l'opération (1.67).* □

En utilisant la proposition 7 il est possible de démontrer que l'espace du signal CPM séparable V dans une période de symbole générique (par exemple $[0, T)$) peut être décrit par la base suivante : $\left\{ f_\gamma(t) = e^{j\,2\pi\,h\gamma\,\varphi_0(t)} \,|\gamma \in \mathcal{A}_N \right\}$. Puisque les fonctions $\{ f_\gamma(t) \,|\gamma \in \mathcal{A}_N \}$ forment une base, la dimension de l'espace V coïncide avec le nombre de ces fonctions : $\dim(V) = N = L(M-1)+1$.

1.5.2 Formulation des Nouvelles Décompositions PAM

Un signal CPM séparable peut être exprimé linéairement en fonction d'une base de l'espace du signal. Nous re-écrivons (1.66) ainsi : $v(t) = S_n\, e^{j\,2\pi\,h\,A_n\varphi_0(t)}$, $t \in \mathcal{I}_n$ où $A_n \in \mathcal{A}_N$ sont définis dans la formule (1.67) et l'état S_n est renouvelé selon la loi suivante :

$$S_{n+1} = S_n\, Z^{A_n} \quad \text{with} \quad Z = e^{j\,\pi\frac{h}{L}}\,. \tag{1.68}$$

Alors, soit $\gamma \in \mathcal{A}_N = \{\gamma_1, \ldots, \gamma_N\}$ et

$$e_n(\gamma) = S_n\,\delta_{A_n,\gamma}\,, \qquad f_\gamma(t) = \eta(t)\, e^{j\,2\pi\,h\,\gamma\,\varphi_0(t)} \tag{1.69}$$

où

$$\delta_{A_n,\gamma} = \begin{cases} 1 & , A_n = \gamma \\ 0 & , \text{autrement} \end{cases}\,, \qquad \eta(t) = \begin{cases} 1 & , t \in [0, T) \\ 0 & , \text{autrement} \end{cases}\,.$$

Nous obtenons ainsi une décomposition que nous appelons la décomposition compacte (CD) du signal CPM :

$$\boxed{v(t) = \sum_n \mathbf{e}'_n\, \mathbf{f}(t - nT)\,,} \tag{1.70}$$

$\mathbf{e}_n$ et $\mathbf{f}(t)$ sont des vecteurs colonne de taille N, dont les éléments sont respectivement les $e_n(\gamma)$ et les fonctions de la base $f_\gamma(t)$. L'apostrophe « $'$ » désigne la transposition.

La CD a cardinalité minimale de $N = L(M-1)+1$, puisque les impulsions PAM coïncident avec les fonctions de la base du signal en $[0, T)$.

La décomposition minimale (MD) peut être obtenue à partir de la CD comme suit : 1) nous générons une autre base de V à travers une transformation linéaire inversible (matrice $N \times N$) $\mathbf{P} = [p_{\gamma,k}]$, $\gamma \in \mathcal{A}_N$, $k \in \mathcal{K}_N = \{0, 1, \ldots, N-1\}$; 2) nous choisissons une matrice $\mathbf{P}$ qui permet d'établir des récurrences parmi les symboles et finalement de regrouper ensemble des impulsions PAM en réduisant la cardinalité de la décomposition.

Soit $\mathbf{R} = \mathbf{P}^{-1} = [r_{k,\gamma}]$. En insérant $\mathbf{I}_N = \mathbf{P}\,\mathbf{R}$ en (1.70) on obtient $v(t) = \sum_n \mathbf{e}'_n\,\mathbf{P}\,\mathbf{R}\mathbf{f}(t-nT) = \sum_n \mathbf{c}'_n\,\mathbf{g}(t-nT)$ et par la (1.69), les symboles modifiés sont dérivés ainsi :

$$c_n(k) = S_n\, p_{A_n,k}\,, \qquad k \in \mathcal{K}_N\,. \tag{1.71}$$

Naturellement toutes ces décompositions sont équivalentes à la CD et ont la même cardinalité N.

Nous illustrons au moyen d'un exemple l'idée des récurrences. Fixons $N = 4$, le signal CPM est $v(t) = v_0(t) + v_1(t) + v_2(t) + v_3(t)$, où $v_k(t) = \sum_n c_n(k)\, g_k(t - nT)$. Or, si la récursion $c_n(3) = c_{n-1}(0)$ est valide pour tous n, les impulsions $v_0(t)$ et $v_3(t)$ peuvent être combinées ensemble $v_0(t) + v_3(t) = \sum_n c_n(0)\, h_0(t-nT)$ et exprimées par une unique impulsion $h_0(t) = g_0(t) + g_3(t-T)$ de durée double. Donc, la cardinalité de la décomposition passe de $N = 4$ à $N_c = 3$.

Il est possible de démontrer qu'en général avec la méthode des récurrences on peut au maximum diminuer la cardinalité de la décomposition de 1, comme dans l'exemple précédent. La matrice $\mathbf{P}$ qui permet cette opération doit avoir la structure suivante :

$$\mathbf{P} = \begin{bmatrix} Z^{-N+1} & p_{0,1} & \cdots & p_{0,N-2} & 1 \\ Z^{-N+3} & p_{1,1} & \cdots & p_{1,N-2} & 1 \\ \vdots & \vdots & \ddots & \vdots & \vdots \\ Z^{N-1} & p_{N-1,1} & \cdots & p_{N-1,N-2} & 1 \end{bmatrix} \tag{1.72}$$

où les colonnes à l'intérieur de la matrice peuvent être choisies arbitrairement sous la contrainte d'inversibilité de la matrice. La MD prend donc la forme suivante :

$$\boxed{v(t) = \sum_n \mathbf{d}'_n\,\mathbf{h}(t-nT)} \tag{1.73}$$

où $\mathbf{d}'_n$ est obtenu de $\mathbf{c}_n$ en laissant tomber le dernier symbole $c_n(N-1)$ et

$$h_k(t) = \begin{cases} g_0(t) + g_{N-1}(t-T), & k = 0 \\ g_k(t), & k = 1, \ldots, N-2 \end{cases} \tag{1.74}$$

Le support de $h_0(t)$ est $[0, 2T)$ alors que celui des autres impulsions $h_k(t)$ reste $[0, T)$. Pour toute matrice $\mathbf{P}$ inversible, il est possible de vérifier que les impulsions de la MD sont des fonctions continues de t. Finalement il est aussi possible de démontrer que la MD est la décomposition PAM des signaux CPM séparables avec la cardinalité minimale.

$M = 4$, réponse de phase séparable			
cardinalité de la décomp.	LMMD $M^L - M^{L-1}$	CD, mCD $L(M-1)+1$	MD $L(M-1)$
$L = 1$	3	4	3
$L = 2$	12	7	6
$L = 3$	48	9	8
$L = 4$	208	13	12
$L = 5$	768	16	15

Tableau 1.2: Cardinalité de différentes décompositions des signaux CPM séparables en fonction de la mémoire L du signal, pour $M = 4$.

$L = 1$, réponse de phase arbitraire			
cardinalité de la décomp.	LMMD $2^{\lceil \log_2 M \rceil} - 1$	CD, mCD M	MD $M-1$
$M = 2$	1	2	1
$M = 4$	3	4	3
$M = 6$	7	6	5
$M = 8$	7	8	7
$M = 10$	15	10	9

Tableau 1.3: Cardinalité de différentes décompositions des signaux CPM à réponse pleine ($L = 1$, aucune contrainte sur la réponse de phase) en fonction de la taille M de l'alphabet.

Dans le Tableau 1.2, les cardinalités des nouvelles décompositions PAM des signaux CPM séparables sont comparées avec la cardinalité de la décomposition de Laurent-Mengali-Morelli (LMMD) [34, 35] en fonction de la mémoire L du signal. Dans le cas de la CD et MD, la cardinalité augmente seulement linéairement en fonction de L, alors que pour la LMMD l'augmentation est exponentielle. Dans le cas de signaux à réponse pleine ($L = 1$), avec réponse de phase arbitraire, les décompositions ici proposées sont encore capables d'achever une réduction de la cardinalité, comme il est montré dans le Tableau 1.3. Cette réduction dans le nombre d'impulsions nécessaires pour décrire las signaux CPM peuvent ouvrir la route à des nouveaux récepteurs simplifiés.

1.6 Conclusion

Cette thèse à été consacré à deux sujets distingués, le premier concernant les codes espace-temps pour des systèmes sans fils sans estimation du canal ni à l'émetteur ni au récepteur, le deuxième concernant la décomposition linéaire des signaux à phase continue (CPM).

Les contributions originales vont de l'analyse des codes espace-temps obtenus par paramétrisation exponentielle à la proposition des décodeurs simplifiés pour cette classe de codes et à la caractérisation de leur performances. Pour ce qui est des signaux

CPM, des nouvelles décompositions ont été dérivées avec une démarche innovante du point de vue de la formulation du problème.

La recherche peut se poursuivre sur les codes espace-temps d'un coté en cherchant à approfondir encore plus la thématique du décodage simplifié, d'autre part en essayant d'optimiser les critères de construction pour différents type de canaux plus proches de cas pratiques, tout en comprenant les avantages des autres propositions de la littérature et leur éventuels liens avec les codes EP. Pour la partie sur les signaux CPM, la recherche peut se poursuivre en appliquant les nouvelles décompositions à la recherche de récepteurs simplifiés pour voir si effectivement ces nouvelles descriptions du signal CPM peuvent donner une valeur ajoutée par rapport aux récepteurs déjà présents dans la littérature.

Chapter 2

Non–Coherent Space–Time Codes: State of the Art

In this chapter we introduce the fundamental frame of this work (channel assumptions, basic code parameters and definitions, mathematical basics) and the state of the art of current non–coherent space–time codes propositions.

In the first section channel models are introduced which will be used throughout all this work. In the second subsection, results on information theory are reported to justify the choice of some fundametal system parameters, like the duration of the fading block and its relation to the number of transmit and receive antennas. Besides, this information theory summary helps us understand under which channel assumptions the proposed non–coherent codes are optimal. The importance of letting information be on subspaces spanned by codewords columns emerges from the previous discussion. Hence, in the third section, basics on subspaces, sets of subspaces and distances between subspaces are introduced. In the fourth section detection rules, both for coherent and non–coherent Multiple Input Multiple Output (MIMO) systems, are recalled. The fifth section contains a summary of the known expression of Pairwise Error Probability (PEP) and its bounds for different kinds of non–coherent space–time codes, under different criteria. The following section deals with diversity, another fundamental parameter of space–time codes, strictly linked with error performance and the geometrical structure of the non–coherent codes. The seventh section collects most of current propositions on this topic and briefly describes code design criterion as well as code characteristics, advantages and disadvantages. The eigth section is dedicated to one particular proposition called “training–based approach”, since in our opinion it is one of the best competitors. In the final section, an example drawn from previous propositions of the literature illustrates some previously introduced concepts.

2.1 The channel model

The channel model we use throughout this thesis is the so–called *block fading* channel model [1], [2]. In this model the channel coefficients are constant during a block of T

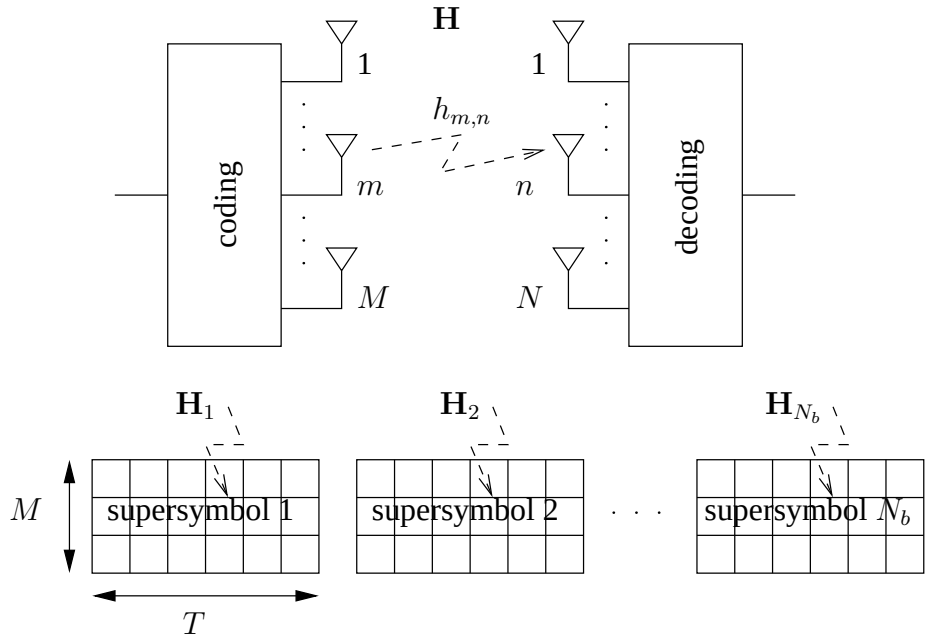

Figure 2.1: The MIMO channel and a codeword of N_b supersymbols affected by a block fading channel.

symbol periods T_s (we consider T integer). For each block the channel coefficients are generated independently from the previous blocks, according to a certain probability distribution. The block fading channel model is applicable when the channel is substantially time-invariant for a duration $T\,T_s$ and then it changes abruptly. This occurs, for example, when the blocks are separated in time or frequency or both, e.g. in system where the access to time and band resources are managed dynamically.

We generally consider a multiple–input multiple output (MIMO) channel where M and N are the number of antennas respectively at the transmitter and receiver as in Fig. 2.1. Under the assumption of a ideal band-limited modulation scheme, without inter-symbol interference, the discrete–time baseband equivalent channel model is

$$\mathbf{Y}_k = \alpha\,\mathbf{X}_k\mathbf{H}_k + \sigma\,\mathbf{W}_k \quad \text{with} \quad k = 1, 2, \ldots \tag{2.1}$$

where the subscript k refers to the k–th block, $\mathbf{Y}_k$ is the $T \times N$ complex matrix of the received signal, $\mathbf{X}_k$ is $T \times M$ sent signal, $\mathbf{H}_k$ is $M \times N$ and $\mathbf{W}_k$ is the $T \times N$ additive noise matrix. The real scalars α and σ are used to normalize transmit power and noise variance. If not otherwise stated, the entries of $\mathbf{H}$ and $\mathbf{W}$ are i.i.d. mean–zero, unit-variance, circularly symmetric, complex Gaussian variables $\mathcal{CN}(0, 1)$ and the complex–valued signal at the transmitter is independent of the channel and the Gaussian noise. In the following we do not explicitly write the block index k because coding among different blocks is not considered and, since all the random variables are independent from one block to another, all blocks are statistically equivalent (there is no memory in the system).

In this work we assume that the channel realization $\mathbf{H}$ is *unknown* to the receiver. This assumption is usually justified by the fact that in future generation MIMO wireless systems with high mobility requirements, the coherence time of the channel [8] is very short. For example, at a vehicle speed of 100 km/h a mobile operating at 1.9 GHz has a fading coherence interval of about 5.7 ms, which corresponds to an uncorrelated fading each 200-300 symbols at a symbol transmission rate of 50 kbaud. At the same symbol rate and vehicle speed, but for an operating frequency of 30 GHz, the fading is uncorrelated after only 10-20 symbols. Hence, to estimate the channel can be a more and more computationally demanding task as the number of the antennas grows up, or it can unacceptably decrease the throughput of the system, especially if only short data or control packets must be sent.

We prevent the reader that the above rough argumentations do not necessarily justify the use of space–time codes designed for non-coherent detection. Another important practical problem is the existence of simple and efficient decoding algorithms for such codes and the analysis of the trade-off between performance benefits and complexity costs. However, the previous short reasoning indicates that such codes can become interesting when the duration of the block T is comparable with the number of transmit and receive antennas, otherwise a good estimation can be performed at the receiver. Hence, in the following we will make the assumption that T is comparable $\max(M, N)$.

2.1.1 Other forms and power normalization

This model can be reformulated in vector form

$$\mathbf{y} = \alpha\, \overline{\mathbf{X}}\, \mathbf{h} + \sigma\, \mathbf{w}\,, \qquad \overline{\mathbf{X}} = \mathbf{I}_N \otimes \mathbf{X} \tag{2.2}$$

where $\otimes$ is the Kronecker product and $\mathbf{y} = \mathrm{vec}(\mathbf{Y})$ is the column vector obtained concatenating the columns of the matrix $\mathbf{Y}$, analogously $\mathbf{w} = \mathrm{vec}(\mathbf{W})$ and $\mathbf{h} = \mathrm{vec}(\mathbf{H})$ (see Appendix A). $\mathbf{y}$ and $\mathbf{w}$ are column vectors of length TN, $\mathbf{h}$ has length NM while $\overline{\mathbf{X}}$ is a $(TM) \times (NM)$ block–diagonal matrix.

The average received Signal to Noise Ratio (SNR) ρ per receiver antenna is (see Appendix B)

$$\rho = \frac{\frac{1}{N}\,\mathrm{tr}(\mathrm{E}\,[\mathbf{Y}\,\mathbf{Y}^\dagger]_{\mathbf{W}=\mathbf{0}})}{\frac{1}{N}\mathrm{tr}(\mathrm{E}\,[\mathbf{W}\,\mathbf{W}^\dagger])} = \frac{\alpha^2\,\mathrm{tr}(\mathrm{E}\,[\mathbf{X}\,\mathbf{X}^\dagger])}{\sigma^2 T}\,. \tag{2.3}$$

In literature we can find many different ways to normalize the transmit power. We will mostly deal with codebooks whose codewords have orthonormal columns, being called *unitary space–time codebooks*, for which it holds $\mathbf{X}^\dagger\mathbf{X} = \mathbf{I}_M$. Under this assumption, supposing i.i.d. sent supersymbols $\mathbf{X}$, we set the power constraint as

$$\alpha^2\,\mathrm{tr}(\mathrm{E}\,[\mathbf{X}\,\mathbf{X}^\dagger]) = M \quad \Longrightarrow \quad \alpha = 1 \tag{2.4}$$

which means in fact that the total power for a supersymbol (a frame) must be M (for every T). Then, $\sigma^2 = M/(T\rho)$. We generally leave α and σ explicitly expressed when we want to switch from different normalizations. For example, normalization in [41] is obtained by letting $\alpha = \sqrt{T}$.

2.2 Results from Information Theory

We recall here some fundamental results about the capacity of MIMO block fading channels when the channel is unknown both to the receiver and to the transmitter. We are focusing on the ergodic capacity, which makes sense when the transmission duration is much longer that the coherence time of the channel [1]. Each codeword is formed by N_b supersymbols and the capacity study is asymptotically valid as N_b goes to infinity. In this case the classic Shannon formulation holds [42]

$$C = \max_{p_{\mathbf{X}}(\cdot)} I(\mathbf{X}; \mathbf{Y}) \tag{2.5}$$

where $p_{\mathbf{X}}(\cdot)$ is the probability distribution of the input signal. Usually there is some constraint on the power of $\mathbf{X}$.

It is well–known that when it is not possible to code among different blocks or when a delay constraint is imposed, then the ergodic capacity cannot be applied and the concept of *outage capacity* or *outage probability* is more appropriate [43], [44], [2]. The outage capacity is a well–defined concept when a perfect Channel State Information (CSI) is available to the receiver. However, in the case of no CSI there are some difficulties arise to define it. As far as we know, the only proposal for an outage capacity definition is in [45]. Since some results for the optimal signal structure are the same that in the ergodic case, we prefer to investigate this latter case only.

2.2.1 General Results

The power–constrained ergodic capacity in the Single Input Single Output (SISO) case ($M = N = 1$) and fast fading $T = 1$ was studied by [46], [47] (see also references therein). The first investigations of the general MIMO case is due to [41], [9] and [48]. We report the following fundamental results.

1. **The power constraint.** Constraining the average power of the single antenna symbol $\mathrm{E}[x_{tm}] = 1$, of the symbols emitted in one symbol period from all the M antennas $\sum_{m=1}^{M} \mathrm{E}[|x_{tm}|^2] = M$, of the symbols emitted from each antenna during all the block $\sum_{t=1}^{T} \mathrm{E}[|x_{tm}|^2] = T$ or of the whole supersymbols $\mathrm{tr}(\mathrm{E}[\mathbf{X}\,\mathbf{X}^{\dagger}]) = TM$ does not affect capacity, provided that the supersymbol total average power is the same. If not, only a simple scaling of the SNR ρ is required.

2. **Capacity Dependence on T.** For any block length T, any number of receiver antennas N and any SNR ρ, the capacity obtained with $M > T$ and $M = T$ are equal. This is substantially different from the coherent case (perfect CSI available to the receiver) where the capacity is independent of T [44].

3. **Optimal signal structure.** For every SNR ρ, the capacity–achieving signal matrix can be written as

$$\mathbf{X} = \mathbf{\Phi}\,\mathbf{\Lambda}\,, \qquad \mathbf{\Phi} \in \mathcal{U}_{T,M} \text{ i.e. } \mathbf{\Phi}^{\dagger}\mathbf{\Phi} = \mathbf{I}_M\,, \qquad \mathbf{\Lambda} = \begin{bmatrix} \lambda_1 & 0 & \cdots & 0 \\ 0 & \lambda_2 & \cdots & 0 \\ \vdots & & \ddots & \vdots \\ 0 & 0 & \cdots & \lambda_M \end{bmatrix} \tag{2.6}$$

where $\mathbf{\Phi}$ is a $T \times M$ isotropically distributed unitary matrix[1] and $\mathbf{\Lambda}$ is an independent $M \times M$ real, nonnegative, diagonal matrix. In other words, the optimal signal is formed by M *orthogonal vectors whose norms are* $\lambda_m \geq 0$, $m = 1, \ldots, M$. The general analytical form of the joint density of $[\lambda_1, \ldots, \lambda_M]$ is still unknown.

4. **Asymptotic capacity for** $T \to \infty$**.** When $T \to \infty$ the capacity approaches the capacity of the coherent case with perfect CSI available to the receiver. Moreover, all the density distributions $p(\lambda_m)$ converge to a Dirac delta centered in $\sqrt{T}$, showing that *the information is carried by the direction of the vectors* and not by their norms (see also [6]).

2.2.2 Asymptotic Results at high SNR

An investigation about the ergodic capacity in the high SNR regime can be found in [30], where the following results are proved.

1. **Optimal signal structure.** For high SNR ρ, the random variables λ_m converge to the deterministic constant $\sqrt{T}$, as in the case of $T \gg 1$. Once again the optimal signal structure is a matrix whose columns are isotropically distributed orthogonal vectors

$$\mathbf{X} = [\mathbf{x}_1 \ \ldots \ \mathbf{x}_M] = \sqrt{T}\,\mathbf{\Phi}\,, \qquad \mathbf{\Phi} \in \mathcal{U}_{T,M}\,. \tag{2.7}$$

2. **The information is carried by subspaces.** Indeed, (2.7) states that a good codebook should put information in the directions of the vectors $\mathbf{x}_m$, $m = 1, \ldots, M$. However, [30] shows that the information is not in the single directions $\text{span}(\mathbf{x}_1), \ldots, \text{span}(\mathbf{x}_M)$, but in the *subspace*

$$\Omega_{\mathbf{X}} = \text{span}(\mathbf{x}_1, \ldots, \mathbf{x}_M) = \text{span}(\mathbf{X})\,. \tag{2.8}$$

In other words, at high SNR and for $\mathbf{H}, \mathbf{W}$ with i.i.d. circularly symmetric Gaussian variables, the mutual information in the capacity definition (2.5) is $I(\mathbf{X}; \mathbf{Y}) = I(\Omega_{\mathbf{X}}; \mathbf{Y})$. An intuitive explication is that, at high SNR, we can write

$$\mathbf{Y} = \alpha \mathbf{X}\,\mathbf{H} + \sigma \mathbf{W} \simeq \alpha \mathbf{X}\,\mathbf{H} \tag{2.9}$$

[1] An isotropically distributed unitary matrix has a probability density function which is invariant under left–multiplication of deterministic unitary matrices.

and we see that the channel stretches and rotates the basis $\mathbf{X}$ of $\Omega_{\mathbf{X}}$. Since the channel is unknown, the receiver cannot recover the particular basis $\mathbf{X}$, but the subspace $\Omega_{\mathbf{X}}$ is unchanged.

3. **Capacity and degrees of freedom.** The asymptotic capacity (in bit/s/Hz) is

$$C = K_{nc} \log_2 \rho + c_{M,N} + o(1) \tag{2.10}$$

where $o(1)$ is a quantity which goes to zero at high SNR and $c_{M,N}$ is a constant which depends on M, N and T (for more details see [30]).

$$K_{nc} = M^*(1 - M^*/T) \quad \text{with} \quad M^* = \min(M, N, \lfloor T/2 \rfloor) \tag{2.11}$$

is called the number of *degrees of freedom* or *multiplexing gain* of the noncoherent MIMO channel [45]. Since $\log_2(\rho)$ is the high SNR behavior of a classical AWGN SISO channel, K_{nc} can be interpreted as the number of parallel spatial channels that can be used at the same time [49]. M^* is the optimal number of transmit antennas that should be used to communicate. Using more that M^* transmit antennas does not yield any benefit (in terms of capacity!).

We notice that, as recalled in the previous section, the capacity depends on T, while for coherent systems the degrees of freedom are $K_{co} = \min(M, N)$, independent from T [44], [49],[50].

We can draw some useful conclusions from the previous observations. Since K_{nc} is the leading coefficient and a 3 dB SNR increase means an increase of K_{nc} bit/s/Hz in the capacity, the number of degrees of freedom should be maximized. This means that M^* should be $T/2$ or as close to this value as possible. Moreover, it should be

$$\boxed{T \geq 2M, 2N} \tag{2.12}$$

otherwise the additional antennas will be not useful (from a capacity perspective).

2.2.3 Asymptotic results for low SNR

In the low SNR regime, results are quite different. In fact, generally, if $\rho \to 0$, the coherent and noncoherent capacities are asymptotically equal and their limit is [30]

$$\lim_{\rho \to 0} C(\rho)/\rho = N \log_2 e\,, \qquad \text{bit/s/Hz}\,, \tag{2.13}$$

so that the relationship with the number of degrees of freedom disappears. Only an augmentation of the number of receive antennas can be profitable to collect the small signal power. Moreover, even if T and M are greater than one, the optimal strategy consists in allocating all the transmit power to only one antenna during one symbol period.

2.3 Introduction to Subspace Representations

As we said in Sect. 2.2.2, the information is principally carried by subspaces in systems with unknown channel and high SNR. We will recall here some basic definitions on subspaces.

2.3.1 Basics on Subspaces

Let $\Omega_{\mathbf{X}}$ be an M–dimensional (vector) subspace of $\mathbb{C}^T$, with $T > M$. Given one of its bases $\mathbf{X}$, we recall (2.8)

$$\Omega_{\mathbf{X}} = \text{span}[\mathbf{x}_1 \ldots \mathbf{x}_M] = \text{span}(\mathbf{X}) \quad \text{with} \quad \text{rank}(\mathbf{X}) = M\,. \tag{2.14}$$

The basis $\mathbf{X}$ is not unique, in fact given any invertible $M \times M$ complex matrix $\mathbf{A}$, another valid basis of the same subspace is $\mathbf{X}\,\mathbf{A}$. The Thin Singular Value Decomposition[2] (TSVD) [3, pag. 72] gives interesting insights into the structure of a generic basis

$$\mathbf{X} = \mathbf{V}\,\mathbf{\Lambda}\,\mathbf{U}^\dagger\,, \qquad \mathbf{V} \in \mathcal{U}_{T,M},\ \mathbf{U} \in \mathcal{U}_M,\ \mathbf{\Lambda} = \text{diag}([\lambda_1 \ \ldots \ \lambda_{\text{M}}]) \tag{2.15}$$

where $\mathcal{U}_{T,M}$ is the set of the $T \times M$ complex matrices with orthonormal columns, $\mathcal{U}_M$ is the group of unitary $M \times M$ matrices and $\mathbf{\Lambda}$ is a diagonal matrix whose entries are positive and ordered in decreasing order. Resuming

$$\mathbf{V}^\dagger\mathbf{V} = \mathbf{I}_M\,, \qquad \mathbf{U}^\dagger\mathbf{U} = \mathbf{I}_M\,, \qquad \lambda_1 \geq \lambda_2 \geq \ldots \geq \lambda_M\,. \tag{2.16}$$

The TSVD (2.15) has an interesting geometrical interpretation: $\mathbf{V}$ is an orthonormal basis of the same subspace $\Omega_{\mathbf{X}}$. The basis $\mathbf{X}$ is obtained from $\mathbf{V}$ by means of $\mathbf{\Lambda}\,\mathbf{U}^\dagger$ which first stretches the basis vector $\mathbf{v}_m$ according to the positive constant λ_m and then rotates it according $\mathbf{U}^\dagger$.

While the basis of a subspace is not unique, its projector, i.e. the linear operator which projects a vector on the subspace, is unique. Given a generic basis $\mathbf{X}$ of $\Omega_{\mathbf{X}}$, the projector $\mathbf{P}_{\Omega_{\mathbf{X}}}$ is defined as

$$\mathbf{P}_{\Omega_{\mathbf{X}}} = \mathbf{X}(\mathbf{X}^\dagger\mathbf{X})^{-1}\mathbf{X}^\dagger \tag{2.17}$$

while if $\mathbf{X} \in \mathcal{U}_{M,T}$, the previous definition trivially simplifies in

$$\mathbf{P}_{\Omega_{\mathbf{X}}} = \mathbf{X}\mathbf{X}^\dagger\,. \tag{2.18}$$

The projector has the following properties

$$\mathbf{P}_{\Omega_{\mathbf{X}}} = \mathbf{P}^\dagger_{\Omega_{\mathbf{X}}}\,, \qquad \mathbf{P}^2_{\Omega_{\mathbf{X}}} = \mathbf{P}_{\Omega_{\mathbf{X}}}\,, \qquad \mathbf{P}_{\Omega_{\mathbf{X}}}\mathbf{X} = \mathbf{X}\,. \tag{2.19}$$

[2] When $T = M$, the thin Singular Value Decomposition becomes the common Singular Value Decomposition, where all matrices in (2.15) are square.

2.3.2 Basics on the Grassmann Manifold

We give the following basic definitions:

Definition 1 *The set of the M–dimensional complex (real) vector subspaces $\Omega_{\mathbf{X}}$ of $\mathbb{C}^T$ ($\mathbb{R}^T$), with $T > M$ is called Grassmann manifold or Grassmannian, denoted by $G_{T,M}$.*

The concept of differentiable manifold will be recalled in Sect. 3.2.

The concept of biorthogonal bases and of principal angles is very important to characterize a couple of subspaces [3, pag. 603].

Definition 2 *Given two subspaces $\Omega_{\mathbf{X}}, \Omega_{\mathbf{Y}} \in G_{T,M}$, two corresponding bases $\mathbf{X}$ and $\mathbf{Y}$ are said to be biorthogonal if they are orthonormal and*

$$\mathbf{x}_m^\dagger \mathbf{y}_{m'} = 0 \text{ for all } m \neq m' , \qquad \mathbf{x}_m^\dagger \mathbf{y}_m = c_m \text{ with } 0 < c_m \leq 1 \tag{2.20}$$

i.e. for all $m = 1, \ldots, M$, the m–th vector of the first basis is orthogonal to all the vectors of the other basis except of the m–th one.

A pair of biorthogonal bases can be obtained by any two *orthonormal* bases by means of the SVD decomposition. Let $\mathbf{X}, \mathbf{Y}$ be two orthonormal but not necessarily biorthogonal bases of $\Omega_{\mathbf{X}}, \Omega_{\mathbf{Y}}$ and let

$$\mathbf{X}^\dagger \mathbf{Y} = \mathbf{U}_X \mathbf{C} \mathbf{U}_Y^\dagger , \qquad \mathbf{U}_X, \mathbf{U}_Y \in \mathcal{U}_M , \ \mathbf{C} = \mathrm{diag}([c_1, \ldots, c_M]) \tag{2.21}$$

where $0 < c_m \leq 1$ for all m. Then two biorthogonal basis are $\mathbf{X}\,\mathbf{U}_X$ and $\mathbf{Y}\,\mathbf{U}_Y$. From (2.21) we can also see that the squared cosines of the principal angles are the eigenvalues of the matrix $\mathbf{X}^\dagger \mathbf{Y} \mathbf{Y}^\dagger \mathbf{X}$ or equivalently of $\mathbf{Y}^\dagger \mathbf{X} \mathbf{X}^\dagger \mathbf{Y}$.

Definition 3 *Given two biorthogonal bases of the subspaces $\Omega_{\mathbf{X}}, \Omega_{\mathbf{Y}} \in G_{T,M}$, the real positive inner products c_m can be uniquely written in the following form*

$$c_m = \cos \theta_m , \ \theta_m \in [0, \pi/2) , \qquad m = 1, \ldots, M . \tag{2.22}$$

$\theta_1, \ldots, \theta_M$ are called the principal angles between subspaces $\Omega_{\mathbf{X}}$ and $\Omega_{\mathbf{Y}}$.

From (2.21) we see that given two orthonormal bases, their principal angles are the inverse cosine of singular values of the matrix $\mathbf{X}^\dagger \mathbf{Y}$. Equivalently, letting $\boldsymbol{\theta} = [\theta_1 \ \ldots \ \theta_M]^t$ be the principal angles ordered in decreasing order, from (2.21) and (2.22) we can write

$$\mathbf{C} = \cos \boldsymbol{\Theta} , \qquad \boldsymbol{\Theta} = \mathrm{diag}(\boldsymbol{\theta}) . \tag{2.23}$$

The principal angles are unique, while the biorthogonal bases are not (for example a common permutation of two biorthogonal bases gives again two valid biorthogonal bases).

Definition 4 *Two subspaces $\Omega_{\mathbf{X}}, \Omega_{\mathbf{Y}} \in G_{T,M}$ are called intersecting subspaces if the dimension of their intersection is greater than zero, i.e. $\dim(\Omega_{\mathbf{X}} \cap \Omega_{\mathbf{Y}}) > 0$. Otherwise they are called non–intersecting.*

When two M–dimensional subspaces are intersecting the dimension of their intersection coincides with the number of principal angles equal to zero (and vice versa). In this case some vectors of the two biorthogonal bases coincide: they span the intersection [3, pag. 604].

Several distances between subspaces can be defined over the Grassmannian [4], [5]. We recall here the mostly used ones.

Definition 5 *Let* $\mathbf{X}$ *and* $\mathbf{Y}$ *two orthonormal bases of two different subspaces and let* $\mathbf{X}^\dagger\mathbf{Y} = \mathbf{U}_X\mathbf{C}\mathbf{U}_Y^\dagger$ *the SVD as in (2.21) with* $\mathbf{C} = \cos\boldsymbol{\Theta}$*. Then we can define the following distances*

1. *The geodesic distance*

$$d_{arc}(\Omega_{\mathbf{X}}, \Omega_{\mathbf{Y}}) = \|\boldsymbol{\theta}\| = \left(\sum_{m=1}^{M} \theta_m^2\right)^{1/2} \tag{2.24}$$

2. *The chordal distance*

$$d_c(\Omega_{\mathbf{X}}, \Omega_{\mathbf{Y}}) = \frac{1}{\sqrt{2}}\|\mathbf{P}_{\Omega_{\mathbf{X}}} - \mathbf{P}_{\Omega_{\mathbf{Y}}}\|_F = \|\sin\boldsymbol{\theta}\| = \left(\sum_{m=1}^{M} \sin^2\theta_m\right)^{1/2} \tag{2.25}$$

   where $\mathbf{P}_{\Omega_{\mathbf{X}}}$ *and* $\mathbf{P}_{\Omega_{\mathbf{Y}}}$ *are the projectors defined as in (2.18) and* $\|\mathbf{A}\|_F$ *is matrix Frobenius norm (see Appendix A).*

Another pseudo–distance called product distance -which actually is not a true distance but it is often used in literature- is

$$d_p(\Omega_{\mathbf{X}}, \Omega_{\mathbf{Y}}) = \left(\prod_{m=1}^{M} \sin\theta_m\right)^{\frac{1}{M}} = \left(\det\left\{\begin{bmatrix}\mathbf{X}^\dagger \\ \mathbf{Y}^\dagger\end{bmatrix}[\mathbf{X}\ \mathbf{Y}]\right\}\right)^{\frac{1}{2M}} \tag{2.26}$$

In the following we will use sometimes the notation $d(\mathbf{X}, \mathbf{Y})$ meaning $d(\Omega_{\mathbf{X}}, \Omega_{\mathbf{Y}})$.

2.4 Detection Criteria

2.4.1 The Non–Coherent Maximum Likelihood Criterion

When the channel statistics of the fading and noise are known to the receiver (not its realization), the Maximum–Likelihood (ML) criterion can be used for non–coherent detection [8]. The ML rule is

$$\hat{\mathbf{X}}_{ML} = \arg\max_{\mathbf{X}_\ell \in \mathcal{C}} p(\mathbf{Y}|\mathbf{X}_\ell) = \arg\max_{\ell=1,\dots,L} p(\mathbf{Y}|\mathbf{X}_\ell)\,, \tag{2.27}$$

where $p(\mathbf{Y}|\mathbf{X}_\ell)$ is the conditional probability distribution of $\mathbf{Y}$ knowing that $\mathbf{X}_\ell$ has been sent and $\mathbf{X}_\ell$ is the ℓ–th codeword of the codebook $\mathcal{C}$, whose cardinality is $|\mathcal{C}| = L$.

In the hypotheses of channel model (2.2) (i.i.d. Gaussian fading and noise), the received signal $\mathbf{y}$ is a complex Gaussian vector with zero mean and covariance $\mathbf{K}_{\mathbf{y}|\mathbf{X}_\ell} = \alpha^2 \overline{\mathbf{X}}_\ell \overline{\mathbf{X}}_\ell^\dagger + \sigma^2 \mathbf{I}_{NT}$, $\overline{\mathbf{X}}_\ell$ as in (2.2). Hence

$$p(\mathbf{Y}|\mathbf{X}_\ell) = \frac{\exp\{-\mathrm{tr}([\sigma^2 \mathbf{I}_T + \alpha^2 \mathbf{X}_\ell \mathbf{X}_\ell^\dagger]^{-1} \mathbf{Y}\,\mathbf{Y}^\dagger)\}}{\pi^{TN} \det^N [\sigma^2 \mathbf{I}_T + \alpha^2 \mathbf{X}_\ell \mathbf{X}_\ell^\dagger]} \tag{2.28}$$

In this hypothesis the ML is a quadratic receiver and can be stated as

$$\hat{\mathbf{X}}_{ML} = \arg \min_{\ell=1,\dots,L} \left[-\mathbf{y}^\dagger \mathbf{F}_\ell \mathbf{y} + c_\ell \right], \tag{2.29}$$

where the dependence on the signal is in $\mathbf{F}_\ell$:

$$\mathbf{F}_\ell = \frac{1}{\sigma^2} \overline{\mathbf{X}}_\ell \left(\frac{\sigma^2}{\alpha^2} \mathbf{I}_{NM} + \overline{\mathbf{X}}_\ell^\dagger \overline{\mathbf{X}}_\ell \right)^{-1} \overline{\mathbf{X}}_\ell^\dagger, \quad c_\ell = \ln \left| \frac{\sigma^2}{\alpha^2} \mathbf{I}_{NM} + \overline{\mathbf{X}}_\ell^\dagger \overline{\mathbf{X}}_\ell \right|. \tag{2.30}$$

See Appendix C for the derivation of the non–coherent ML criterion.

2.4.2 The Generalized Likelihood Ratio Test

The Generalized Likelihood Ratio Test (GLRT) does not require the knowledge of the fading and noise statistics, nor the knowledge of its realization (see [6], [7] and references therein). It is defined as

$$\hat{\mathbf{X}}_{GLRT} = \arg \max_{\ell=1,\dots,L} \sup_{\mathbf{H}} p(\mathbf{Y}|\mathbf{X}_\ell, \mathbf{H}) \tag{2.31}$$

where $\mathbf{y}$ given $\mathbf{X}_\ell, \mathbf{H}$ is a complex Gaussian variable $\mathbf{y} \sim \mathcal{CN}(\alpha \overline{\mathbf{X}_\ell} \mathbf{h}, \mathbf{I}_{NT})$ in the case AWGN noise (as in model (2.2)). The criterion simplifies in

$$\hat{\mathbf{X}}_{GLRT} = \arg \max_{\ell=1,\dots,L} \mathbf{y}^\dagger \overline{\mathbf{X}}_\ell (\overline{\mathbf{X}}_\ell^\dagger \overline{\mathbf{X}}_\ell)^{-1} \overline{\mathbf{X}}_\ell^\dagger \mathbf{y}. \tag{2.32}$$

or equivalently

$$\hat{\mathbf{X}}_{GLRT} = \arg \max_{\ell=1,\dots,L} \mathrm{tr}\left[\mathbf{Y}^\dagger \mathbf{X}_\ell (\mathbf{X}_\ell^\dagger \mathbf{X}_\ell)^{-1} \mathbf{X}_\ell^\dagger \mathbf{Y} \right]. \tag{2.33}$$

From (2.32) or (2.33) we see that the GLRT applies a projection operation of the received signal $\mathbf{Y}$ on the different subspaces $\Omega_{\mathbf{X}_\ell}$ (see (2.17) and then calculates their norms and chooses the "closest" subspace.

From the perspective of the average supersymbol error probability minimization, the GLRT generally supplies a suboptimal estimation with respect to the ML criterion. However, the GLRT independence of every kind of fading information makes it an excellent candidate–detection rule when the receiver cannot estimate the channel correlations or when the channel has variable statistics.

In the case of i.i.d. fading and unitary codebook, the ML and the GLRT criteria are equivalent (it trivially comes from (2.30)). In this case the decision is made according

$$\hat{\mathbf{X}} = \arg \max_{\ell=1,\dots,L} \mathrm{tr}(\mathbf{Y}^\dagger \mathbf{X}_\ell \mathbf{X}_\ell^\dagger \mathbf{Y}) = \arg \max_{\ell=1,\dots,L} \|\mathbf{Y}^\dagger \mathbf{X}_\ell\|_F^2 \tag{2.34}$$

regarding which the remarks of (2.34) are valid too.

The equivalence of the GLRT and non–coherent ML criterion holds under slightly looser assumptions of i.i.d. circularly complex Gaussian fadings and correlated additive noise $\mathbf{w} \sim \mathcal{CN}(\mathbf{0}, \overline{\mathbf{K}}_{\mathbf{w}})$, where the covariance matrix is separable in space and time, and uncorrelated in space i.e. $\overline{\mathbf{K}}_{\mathbf{w}} = \mathbf{I}_N \otimes \mathbf{K}_{\mathbf{w}t}$ [10]. See Appendix C for general calculations and proofs.

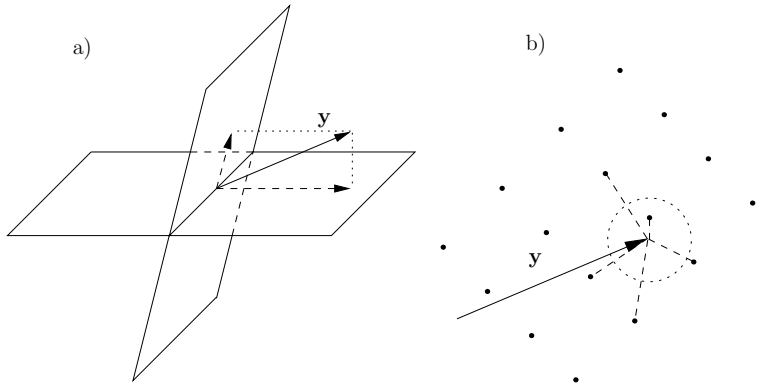

Figure 2.2: a) The GLRT chooses the subspace with greatest projection. b) the coherent ML chooses the closest point.

2.4.3 The Coherent ML Criterion

When the receiver exactly knows the channel realization the ML criterion is

$$\hat{\mathbf{X}}_{co-ML} = \arg \max_{\ell=1,\dots,L} p(\mathbf{Y}|\mathbf{X}_\ell, \mathbf{H}) \tag{2.35}$$

Since $\mathbf{y}$ given $\mathbf{X}_\ell$ and $\mathbf{H}$ is a Gaussian random variable as in the GLRT case, (2.35) is equivalent to minimize the exponent of its probability distribution, which in the AWGN case is

$$\hat{\mathbf{X}}_{co-ML} = \arg \min_{\ell=1,\dots,L} \|\mathbf{Y} - \mathbf{X}_\ell \mathbf{H}\|_F^2 = \arg \min_{\ell=1,\dots,L} \|\mathbf{y} - (\mathbf{H}^t \otimes \mathbf{I}_T)\mathbf{x}_\ell\|^2 \tag{2.36}$$

where $\mathbf{x}_\ell = \mathrm{vec}(\mathbf{X}_\ell)$. The ML choice is the vector $\mathbf{x}_{co-ML}$ that minimize the distance between the vector $\mathbf{y}$ and the vectors $(\mathbf{H}^t \otimes \mathbf{I}_T)\mathbf{x}_\ell$. While the GLRT maximizes a projection onto different subspaces, the coherent ML criterion searches for the closest point (see Fig. 2.2). When the codewords come from a lattice with generator matrix $\mathbf{L}$, the solution of (2.36) comes to find the closest point in the modified lattice $(\mathbf{H}^t \otimes \mathbf{I}_T)\mathbf{L}$.

2.5 Error Probability Bounds

The average error probability of the received supersymbol can be upper bounded by the classical union bound [8]

$$P_e \leq P_e^{UB} = \frac{1}{L}\sum_{\ell=1}^{L}\sum_{j\neq\ell} P_{\ell j} = \frac{1}{L}\sum_{\ell=1}^{L-1}\sum_{j=\ell+1}^{L}(P_{\ell j} + P_{ji}) \tag{2.37}$$

where L is the size of the codebook. $P_{\ell j}$ is the Pairwise Error Probability (PEP) between $\mathbf{X}_\ell$ and $\mathbf{X}_j$, with $\ell \neq j$ and $\ell, j = 1, \ldots, L$, which is the probability of deciding $\mathbf{X}_j$ when $\mathbf{X}_\ell$ is sent and the codebook is formed by just these two supersymbols, i.e.

$$P_{\ell j} = \mathrm{P}\left[\hat{\mathbf{X}} = \mathbf{X}_j | \mathbf{X}_{sent} = \mathbf{X}_\ell\right]. \tag{2.38}$$

2.5.1 Unitary Codebooks

In the case of unitary codebooks under the assumptions of channel model (2.1), (for which the ML criterion and GLRT are equivalent) an exact closed–form analytical expression of the PEP $P_{\ell j}$ was found in [9]. The PEP $P_{\ell j}$ depends only on the principal angles between $\Omega_{\mathbf{X}_\ell}$ and $\Omega_{\mathbf{X}_j}$. However, we do not report it since it is based on the evaluation of the residue of an analytical complex function, which gives not particular insights. The Chernoff Bound on the PEP (see [10] or [9] for a definition) is reported too in [9]

$$\begin{aligned} P_{\ell j}^{CB} &= \frac{1}{2}\prod_{m=1}^{M}\left[1 + \frac{(\rho T/M)^2 \sin^2\theta_{m,\ell j}}{4(1+\rho T/M)}\right]^{-N} \\ &\underset{\rho\to\infty}{\simeq} \frac{1}{2}\left[\frac{M}{\rho T}\right]^{N m_{d,\ell j}}\left[\prod_{m=1}^{m_{d,\ell j}}\frac{4}{\sin^2\theta_{m,\ell j}}\right]^{N} \end{aligned} \tag{2.39}$$

where $\theta_{1,\ell j}, \ldots, \theta_{m_{d,\ell j},\ell,j}$ are the non–zero principal angles between $\Omega_{\mathbf{X}_\ell}$ and $\Omega_{\mathbf{X}_j}$ (they correspond to the singular values of $\mathbf{R}_{\ell j} = \mathbf{X}_\ell^\dagger \mathbf{X}_j$ different from 1). As it can be appreciated from (2.39), the choice that minimizes the Chernoff bound is $\theta_m = \pi/2$ for all m, which geometrically states the orthogonality of the two subspaces.

An asymptotic expression (at high SNR) of the PEP was found in [11], which is tighter than the Chernoff bound (2.39). This asymptotic expression is valid only for the case of non–intersecting subspaces (see Definition 4), i.e. $\theta_{m,\ell j} \neq 0,\ \forall\, m$

$$\begin{aligned} P_{\ell j}^{\infty} &= \left[\frac{M}{T\rho}\right]^{NM}\binom{2MN-1}{MN}\frac{1}{|\sin^2\boldsymbol{\Theta}_{j\ell}|^N} \\ &= \left[\frac{M}{T\rho}\right]^{NM}\binom{2MN-1}{MN} d_p^{-2NM}(\Omega_{\mathbf{X}_\ell}, \Omega_{\mathbf{X}_j}). \end{aligned} \tag{2.40}$$

2.5.2 Non–Unitary Codebooks

In the case of non–unitary codebooks or correlated fading the non–coherent ML criterion and the GLRT do not coincide.

In the case of the **ML detection**, from (2.38), the PEP is defined as

$$P_{\ell j,ML} = \mathrm{P}\left[\mathbf{y}^{\dagger}\mathbf{F}_{\ell j}\mathbf{y} < c_{\ell j}\right]$$

where $\mathbf{F}_{\ell j} = \mathbf{F}_{\ell} - \mathbf{F}_{j}$ and $c_{\ell j} = c_{\ell} - c_{j}$ (see (2.30)). The pairwise error probability can be expressed in analytical form as a function of the eigenvalues of $\mathbf{K}_{\mathbf{y}|\mathbf{X}_{\ell}}\mathbf{F}_{\ell j}$. Many works reported this fundamental expression, usually with the help of residue theory (see for example [51], [11] and references therein). Since the expressions are usually complicated and never insightful nor suitable for numerical evaluation, we report the asymptotic expression at high SNR as in [11]. Assuming

$$\begin{bmatrix}\mathbf{X}_{\ell}^{\dagger}\\ \mathbf{X}_{j}^{\dagger}\end{bmatrix}\begin{bmatrix}\mathbf{X}_{\ell} & \mathbf{X}_{j}\end{bmatrix} = \begin{bmatrix}\mathbf{R}_{\ell\ell} & \mathbf{R}_{\ell j}\\ \mathbf{R}_{j\ell} & \mathbf{R}_{jj}\end{bmatrix}, \qquad \hat{c}_{\ell j} = N\ln\frac{|\mathbf{R}_{\ell\ell}|}{|\mathbf{R}_{jj}|} \tag{2.41}$$

and supposing that the matrix in (2.41) has full rank, hence ($T \geq 2M$), the asymptotic expression is

$$P_{\ell j,ML}^{\infty} + P_{j\ell,ML}^{\infty} = \left[\frac{M}{T\rho}\right]^{NM} \frac{\displaystyle\sum_{k=0}^{MN-1}\binom{2MN-k}{MN}\frac{\hat{c}_{\ell j}^{k}}{k!}}{|\mathbf{R}_{\ell\ell} - \mathbf{R}_{\ell j}\mathbf{R}_{jj}^{-1}\mathbf{R}_{j\ell}|^{N}} \tag{2.42}$$

for $\hat{c}_{\ell j} \geq 0$, signals can always be renumbered to satisfy this condition.

In the case of i.i.d. Gaussian additive noise, the asymptotic PEP for the **GLRT** can be written [11]

$$P_{\ell j,GLRT}^{\infty} + P_{j\ell,GLRT}^{\infty} = \left[\frac{M}{T\rho}\right]^{NM}\binom{2MN-1}{MN}\frac{\left(1+\frac{|\mathbf{R}_{\ell\ell}|}{|\mathbf{R}_{jj}|}\right)}{|\mathbf{R}_{\ell\ell} - \mathbf{R}_{\ell j}\mathbf{R}_{jj}^{-1}\mathbf{R}_{j\ell}|^{N}} \tag{2.43}$$

[11] showed that if the fadings are correlated $\mathbf{h} \sim \mathcal{CN}(\mathbf{0}, \mathbf{K}_{\mathbf{h}})$, expressions (2.42) and (2.43) must be multiplied by a scalar factor of $1/|\mathbf{K}_{\mathbf{h}}|$. Hence, even in the case of correlated fadings, for unitary codebooks the two asymptotic PEPs (2.42) and (2.43) coincide, even if the GLRT and non–coherent ML do not!

The deduction of the asymptotic PEP (in the ML and GLRT case) of [11] can be easily generalized in the case of correlated additive zero–mean Gaussian noise, when its covariance matrix takes the form $\overline{\mathbf{K}}_{\mathbf{w}} = \mathbf{I}_N \otimes \mathbf{K}_{\mathbf{w}t}$. The proofs of the propositions in [11] are the same, provided that $\mathbf{R}_{\ell j}$ is replaced by $\mathbf{X}_{\ell}^{\dagger}\mathbf{K}_{\mathbf{w}s}^{-1}\mathbf{X}_{j}$.

Under the assumption of equal–energy codewords ($\mathrm{tr}(\mathbf{X}_{\ell}^{\dagger}\mathbf{X}_{\ell}) = P,\ \forall\,\ell = 1,\ldots,L$), the codewords which minimize the ML asymptotic PEP (and hence the asymptotic union bound) have orthogonal columns [11]. In other words, if the equal–energy constraint is imposed, unitary codebooks are optimal from an asymptotic PEP minimization perspective. Hence *at high SNR the same signal structure is optimal from the perspective of capacity and performance*.

2.6 Diversity

Diversity roughly measures the number of independent channel paths through which the signal passes. Using the statistical independence of these paths, it is more probable to recover the correct information as long as one path is strong enough [52], [53]. There are many kinds of diversity: temporal diversity (codes exploit channel temporal uncorrelation), frequency diversity (codes exploit for instance the uncorrelation among channel frequency responses at different frequencies), and so on. MIMO channels offer spatial diversity thanks to the presence of multiple antennas, which of course must be correctly spaced far apart to assure the statistical independence of the fadings. The physical environment around the antennas is very important as well [54], [53]. When the correlation among antennas can be controlled, beam-forming systems and smart antennas can be used (see [55] and references therein).

There are three different definitions of diversity for non–coherent MIMO block–fading systems in literature. The most widespread and classical definition of diversity is based on the asymptotic Pairwise Error Probability (PEP) or on its Chernoff Bound or on the average error probability. This diversity denoted by PEP–based diversity (or simply diversity) is used for coherent system too [12]. Another definition relates diversity (as a mesure of the average error probability) to multiplexing gain (an information theoretical concept, see Sect. 2.2.2) [49], [45]. This definition is given for families of codes whose rate scales logarithmically with the SNR and it enables clear diversity–multiplexing gain trade–off analysis. This is not the central topic of our investigation, so we just report the reference and recall that it contains Definition 6 as a special case. Eventually, algebraic diversity is another definition based only on codewords algebraic properties [28].

2.6.1 Pairwise Error Probability–based Diversity

Definition 6 (PEP–based Definition) *Let $P_{\ell k}(\rho)$ be the Pairwise Error Probability ($P_{\ell k}^{CB}(\rho)$ be the Chernoff Bound) between the codewords $\mathbf{X}_\ell$ and $\mathbf{X}_k$, as a function of the SNR ρ. Let $\mathbf{X}_\ell$ and $\mathbf{X}_k$ belong to a codebook $\mathcal{C}$ of size L. The codebook $\mathcal{C}$ is said to achieve the diversity gain d (or briefly to have diversity d) if*

$$\min_{\ell,k:\ell\neq k} \lim_{\rho\to\infty} \frac{\ln P_{\ell k}(\rho)}{\ln \rho} = -d\,, \qquad \left(\min_{\ell,k:\ell\neq k} \lim_{\rho\to\infty} \frac{\ln P_{\ell k}^{CB}(\rho)}{\ln \rho} = -d\right). \tag{2.44}$$

The diversity of the codebook $\mathcal{C}$ will be denoted by $d(\mathcal{C})$.

In other words, $\mathcal{C}$ has diversity d if the minimum slope among all the PEP curves (in a log-log scale) at high SNR is $-d$. Another equivalent explication is that, at high SNR we can write $P_{\ell k}(\rho) \propto \rho^{-n}$ with $n \geq d$ for all $\ell, k, \ell \neq k$. To underline the importance of diversity in increasing the performance of a code, we notice that to divide the PEP by 10 an increase $[\Delta\rho]_{\mathrm{dB}} = 10/d$ in SNR is required (see Table 2.1)

diversity d	1	2	3	4	5	6
$[\Delta\rho]_{\mathrm{dB}}$ [dB]	10	5	3.4	2.5	2	1.7

Table 2.1: SNR increase $[\Delta\rho]$ to lower of a factor 10 the asymptotic PEP of codebooks with diversity d, at high SNR.

For unitary codebooks, the Chernoff Bound is given in (2.39). Since the exponent of the SNR is $Nm_{d,\ell k}$ we can state that

$$N \leq d = N\, m_d \leq MN\,, \qquad m_d = \min_{\ell,k:\ell\neq k} m_{d,\ell k} \tag{2.45}$$

where $m_{d,\ell k}$ is the number of zero principal angles between subspaces $\Omega_{\mathbf{X}_\ell}$ and $\Omega_{\mathbf{X}_k}$. When the subspaces are not intersecting then d reaches its maximum NM and the codebook is called *full–diversity* code. The worst case is when only receiver diversity is provided. This happens when there are two subspaces whose intersection has dimension $M-1$. Obviously, the diversity cannot be zero; in fact in that case the two subspaces would coincide and the codebook is not correctly designed, because the map between information bits and codewords would not be bijective.

The *average error probability* slope at high SNR is related to diversity, but do not necessarily coincide with $-d$. In fact, the average error probability P_e is upper bounded by the union bound (2.37), while we can write the following lower bound [56]

$$\frac{1}{L}P_{\ell k} \leq \frac{1}{L}\sum_{\ell=1}^{L} P_{\ell k} \leq P_e \leq P_e^{UB}\,, \qquad k\neq\ell,\,\forall\,\ell \tag{2.46}$$

where the PEP $P_{\ell k}$ can be chosen arbitrarily. For example, if a codebook do not achieve full–diversity and has L_1 couples of non–intersecting subspaces, and the others L_2 couples have an intersection with dimension 1, then the asymptotic slope of P_e will be between $-NM$ and $-N(M-1)$ depending on the statistics of the codewords. On the contrary, if the intersections of all the couples of subspaces have the same dimension, then the asymptotic slope of P_e really coincides with $-d$, as directly comes from (2.46).

We stress that *the PEP–based diversity of Definition 6 does not depend only on the codebook, but also on the detection criterion*. In fact, the PEP depends on the detection criterion. We formulate therefore For instance, two devinition of diversities which are more precise and which we will use in the following. First of all, we introduce the compact expression "coherent code" to refer to a code designed for coherent systems. For this kind of codes, the following difinition of diversity was formulated in [12]

Definition 7 (Coherent Code Diversity) *Let $\mathcal{B}$ a coherent code, being detected with the coherent ML criterion (see (2.35) and (2.36)). The PEP–based diversity gain is*

$$d^{co-ML}(\mathcal{B}) = \min_{k\neq\ell} \mathrm{rank}(\mathbf{B}_k - \mathbf{B}_\ell)\,. \tag{2.47}$$

In the following, when we write "coherent code diversity", if not otherwise stated, we refer to the code PEP–based diversity corresponding to the coherent ML criterion as defined in (2.47). Definition 7 is not a real definition because it was in fact proved in [12]. But this result is so widely known that we prefer to state it in form of definition.

In the case of a *unitary* codebook $\mathcal{C}$ for non–coherent systems with GLRT detection, the PEP–based diversity from (2.39) (see also [9]) is defined as follows

Definition 8 (Non–Coherent Code Diversity) *Let $\mathcal{C}$ be a unitary codebook, whose codewords $\mathbf{X}_k$ span subspaces of constant dimension M. Then the PEP–based diversity of code $\mathcal{C}$, with respect to the GLRT criterion, is*

$$d^{GLRT}(\mathcal{C}) = M - \max_{k \neq \ell} \dim(\Omega_{\mathbf{X}_k} \cap \Omega_{\mathbf{X}_\ell})\,. \tag{2.48}$$

In the following when we refer to $\mathcal{C}$ as a "non–coherent code", we mean that the GLRT is the detection criterion which defines its PEP–based diversity. We can rewrite $\dim(\Omega_{\mathbf{X}_k} \cap \Omega_{\mathbf{X}_\ell}) = \dim[\mathrm{null}([\mathbf{X}_k \ \mathbf{X}_\ell])]$, where $\mathrm{null}(\mathbf{A})$ is the vector space of the vectors $\mathbf{x}$ satisfying the condition $\mathbf{A}\,\mathbf{x} = \mathbf{0}$. Besides, let $\mathbf{A}$ be a linear transformation $\mathbf{A} : \mathbb{C}^m \longrightarrow \mathbb{C}^n$, with $m \leq n$, it is well–known that $\dim[\mathrm{span}(\mathbf{A})] + \dim[\mathrm{null}(\mathbf{A})] = m$. Combining these facts and $\dim[\mathrm{span}(\mathbf{A})] = \mathrm{rank}(\mathbf{A})$, we have the equivalent expressions of (2.48)

$$\begin{aligned} d^{GLRT}(\mathcal{C}) &= M - \max_{k \neq \ell} \dim[\mathrm{null}([\mathbf{X}_k \ \mathbf{X}_\ell])] \\ &= M - \max_{k \neq \ell} \left\{2M - \mathrm{rank}([\mathbf{X}_k \ \mathbf{X}_\ell])\right\} \\ &= \min_{k \neq \ell} \left\{\mathrm{rank}([\mathbf{X}_k \ \mathbf{X}_\ell])\right\} - M\,. \end{aligned} \tag{2.49}$$

When $\mathcal{C}$ is a unitary codebook and the fadings are i.i.d. we have:

$$d^{GLRT}(\mathcal{C}) = d^{nc-ML}(\mathcal{C})\,, \tag{2.50}$$

since the two detection criteria coincide.

The following proposition is valid both for unitary and non–unitary codebooks [11].

Proposition 1 *Under the hypotheses of channel model (2.1), if for all the couples of codewords $\mathbf{X}_\ell$ and $\mathbf{X}_k$ belonging to $\mathcal{C}$, the matrices*

$$\begin{bmatrix} \mathbf{X}_\ell^\dagger \\ \mathbf{X}_k^\dagger \end{bmatrix} \begin{bmatrix} \mathbf{X}_\ell & \mathbf{X}_k \end{bmatrix} = \begin{bmatrix} \mathbf{R}_{\ell\ell} & \mathbf{R}_{\ell k} \\ \mathbf{R}_{k\ell} & \mathbf{R}_{kk} \end{bmatrix} \tag{2.51}$$

have full rank, then the codebook $\mathcal{C}$ achieves full PEP–based diversity, both for the GLRT and the non–coherent ML criterion, i.e.

$$d^{GLRT}(\mathcal{C}) = d^{nc-ML}(\mathcal{C}) = M\,. \tag{2.52}$$

Moreover it is necessary that $T \geq 2M$.

Intuitively, the condition $T \geq 2M$ is necessary for, in unitary codebooks when $T = 2M - m_1 < 2M$ ($m_1 \in \mathbb{N}$), every two M-dimensional subspaces of $\mathbb{C}^T$ have an intersection of dimension $m_1 > 0$, so the Chernoff Bound cannot have a slope of $-NM$. In fact condition (2.51) exactly states that all subspaces are not intersecting.

2.6.2 Algebraic Diversity

A definition based on some algebraic properties of the codebooks is introduced in [28]. We state it in the particular case of no coding between different fading blocks and we give a slightly different but equivalent definition. Let's suppose that the receiver has one antenna (when $N > 1$ just multiply each diversity by N) and that no additive noise is present on the channel. Let's define the subspace of channel realizations $\mathcal{H}_{nc}(\ell, k)$ which makes the GLRT unable to differentiate between two possible transmitted symbols $\mathbf{X}_\ell$ and $\mathbf{X}_k$ as

$$\mathcal{H}_{nc}(\ell, k) = \{\mathbf{h} \in \mathbb{C}^M : \exists\, \mathbf{h}_1 \in \mathbb{C}^M,\, \mathbf{X}_\ell \mathbf{h} = \mathbf{X}_k \mathbf{h}_1\} \tag{2.53}$$

$$= \{\mathbf{h} \in \mathbb{C}^M : \exists\, \tilde{\mathbf{h}} \in \Omega_{\mathbf{X}_\ell} \cap \Omega_{\mathbf{X}_k},\ \text{where } \tilde{\mathbf{h}} = \mathbf{X}_\ell \mathbf{h}\} \tag{2.54}$$

Definition 9 (Algebraic Diversity Gain) *The codebook $\mathcal{C}$ is said to achieve the algebraic diversity gain d if*

$$d = N[M - \max_{\ell,k:\ell\neq k} \dim\, \mathcal{H}_{nc}(\ell, k)] = N \min_{\ell,k:\ell\neq k} [\dim(\Omega_{\mathbf{X}_\ell} + \Omega_{\mathbf{X}_k}) - \dim\, \Omega_{\mathbf{X}_k}] \tag{2.55}$$

The algebraic diversity if $\mathcal{C}$ will be denote by $d^{alg}(\mathcal{C})$.

What is important here is that, since Definition 9 is not based on the PEP, but only on algebraic properties of the codewords, *the algebraic diversity is independent from the detection criterion*.

There is no formal proof of the equivalence of the classical PEP–based diversity and the algebraic diversity, for generic codebooks. However, it has been proved in [29] the following

Proposition 2 *If the codebook $\mathcal{C}$ is unitary, it holds*

$$d^{alg}(\mathcal{C}) = d^{GLRT}(\mathcal{C}) \tag{2.56}$$

that is, the algebraic diversity and the PEP–based diversity (with GLRT detection) are equivalent.

It is also clear that when codebook has full algebraic diversity, then it has also full PEP–based diversity, because in this hypothesis the matrices in (2.51) have full rank and Proposition 1 can be applied.

2.7 Code Design Criteria and Propositions

Both information theoretical criteria (see (2.7)) and error probability criteria (Sect. 2.5) show that, at high SNR, the optimal signals are matrices with orthonormal columns, most research concentrated on codes of this kind. However many propositions are actually present in literature, both for unitary and non–unitary codebooks. These propositions differ in code design methods and criteria and hence in decoding methods. The principal propositions are

- Codebooks designed by numerical minimization of a cost function related to the distances defined in Definition 5 [9, 13, 14] or by numerical minimization of the union bound on the supersymbol/bit error probability [15, 16] or on the Kullback–Leibler distance [17].
- Codebooks obtained by some parameterization of unitary matrices [18, 19, 20] or of the Grassmannian (it is also the case of this thesis) [21, 22].
- Codebooks obtained by algebraic construction for some particular cases [23, 24, 25].
- Codebooks which follow the so–called training–based format, i.e. which estimate the channels in the first part of the supersymbols and use the second part to send information by means of a space–time code designed for coherent detection [16, 26, 27, 28, 29].

In the following we will report briefly the various propositions with advantages and disadvantages. Some characteristics of these codes are resumed in Tab. 2.2.

2.7.1 Numerical Optimization Designs

These propositions differ in cost functions and in (often suboptimal) minimization methods. They suffer from common shortcomings:

1. only low size constellations can be constructed, because of the increasing complexity in the design process;
2. the codebook of size $L = 2^{RT}$ has to be stored in the transmitter and receiver equipment and so the memory required is exponential in RT. (R is the transmit rate in bit per symbol period);
3. in general no simplified decoding algorithm is available, so that the GLRT or ML rule must be evaluated for all codewords. Hence, the decoding complexity is in general exponential in RT.

Small ($L \leq 64$) unitary space–time constellations were designed in [9]. In [13] the minimum chordal distance is used as cost function

$$d_c^2(\mathcal{C}) = \min_{1 \leq l < l' \leq L} d_c^2(\Omega_{\mathbf{X}_l}, \Omega_{\mathbf{X}_{l'}}) = \min_{1 \leq l < l' \leq L} \sum_{m=1}^{M} \sin^2 \theta_{m,ll'} \tag{2.57}$$

where $\theta_{m,ll'}$ are the M principal angles between the two subspaces generated by $\mathbf{X}_l$ and $\mathbf{X}_{l'}$ belonging to $\mathcal{C}$ (see (2.25)). The minimum chordal distance can be related to the worst case upper bound of the Chernoff Bound on the PEP, a quite loose approximation of the PEP. Moreover, $d_c^2(\mathcal{C})$ is a good approximation of the product distance (2.26) only when all the subspaces are quasi–orthogonal [18], assumption which is not true even for small–size codebook, when T is comparable to M. The optimization

Reference	code type[a]	design method	co. code[b]	diversity	simplified dec.[c]	dec. compl.
[13]	U	num. min. $d_c^2(\mathcal{C})$	no	no control	no	$O(2^{RT})$
[14]	U	num. min. $d_{cF}^2(\mathcal{C})$	no	no control	S	local GLRT
[15]/[16]	U	num. min. $P_e/P_{e,bit}$	no	full	no	$O(2^{RT})$
[17]	N/U	num. min.	no	no control	no[e]	$O(2^{RT})$
[18]	U	successive rotations	no	no control	no	$O(2^{RT})$
[19, 20]	U	Cayley map	no	no control	S	sphere dec.
[22]	U	exponential map	yes	full	S	local GLRT
[23]	U	algebraic/training	yes[d]	full	O	$O(MN)$/$O(M^2N)$
[24]	U	algebraic/training	yes	full	O	$O(2^{TR/2})$
[25]	N/U	algebraic	no	full	no	$O(2^{TR})$
[16, 26, 27, 28]	N/U	training	yes	full	S	sphere dec.

[a] Non–Coherent code type: U = unitary codebooks, N/U = all kind of codebooks.

[b] Is the non–coherent code built from a coherent code?

[c] There exists a simplified decoding? S = yes, but is it sub–optimal, O = yes and it is optimal
(it matches non–coherent ML performances).

[d] A proposition not based on coherent codes is presented as well.

[e] Unitary constellations with simplified decoding can be used, however its not the general case.

Table 2.2: Resume of the most quoted propositions in the literature.

technique used in [13] is called relaxation method and it generalized from [57] where it was used for real Grassmannians.

[14] uses another metric, the so–called chordal Frobenius distance [4]

$$d_{cF}^2(\Omega_{\mathbf{X}_l}, \Omega_{\mathbf{X}_{l'}}) = 4 \sum_{m=1}^{M} \sin^2(\theta_{m,ll'}/2) < d_c^2(\Omega_{\mathbf{X}_l}, \Omega_{\mathbf{X}_{l'}})$$

looser than the chordal distance. A simplified decoding method is proposed which, from some reference point on the Grassmannian, locates a list of candidate points over which the GLRT is calculated (local GLRT). This procedure allow not to calculate the GLRT metric for all the codewords, however tables with the coordinates of all codewords must be saved in the memory as well as the codebook, which has no algebraic structure.

Codebooks created with these methods sometimes cannot achieve full diversity. In fact, even if $d_{c,min}$ is maximized, one or more terms in the sum can be zero ($\theta_{m,ll'} = 0$ for some m), decreasing the diversity order. As an example, in [14, Fig. 1], the code is designed for $M = N = 2$ antennas and so its maximal diversity gain is 4, while the slope of the error probability at high SNR reveals an average diversity gain of about 2.

In [15] and [16] constellations are obtained through numerical search minimizing the asymptotic union bound on the supersymbol error rate (also called FER – Frame Error Rate) and the asymptotic union bound on the bit error rate (BER). While the common disadvantages persist the advantage of this method is that, being based on the PEP, it guarantees full order diversity of the constellations, when $T \geq 2M$.

Motivated by the fact that unitary codebooks are not optimal at low SNR or for T comparable to M, in [17] non–unitary codebooks designed with the Kullback–Leibler distance[3] are proposed. This method has been proposed due to the intractability of the PEP–based design criterion, when the assumption of being unitary (constant power) is loosened. The proposed codewords have orthogonal columns but they have not the same norm, so they are not unitary. The proposed criterion is equivalent to the maximization of $d_c(\mathcal{C})$ when the codewords are constrained to be unitary and it is equivalent to the minimization of the maximum PEP of the ML criterion in the case $T = 1, M = 1$. In the other cases it is related to the ML criterion when the number of receiving antennas is high or when a quite redundant outer code is used. In any case a sub-optimal optimization algorithm is proposed to find multilevel unitary codebooks. The decoding algorithm can be simplified choosing the unitary matrices of each level to belong to codes with simple decoding algorithms. However, the optimal code does not scale linearly with the SNR. This means that for each value of SNR the transmitter and

[3]The Kullback–Leibler distance between two distributions $p_1(x)$ and $p_2(x)$ is defined as [58]

$$D(p_1 \| p_2) = \int_x p_1(x)(\ln p_1(x) - \ln p_2(x)) \mathrm{d}x \,.$$

receiver must store a different constellation. This could be a problem in environment with variable SNR and the performance degradation of an incorrect estimation of the SNR are not yet evaluated. Only small size codes are proposed.

2.7.2 Parameterization Designs

The coding method we study in this thesis belongs to this class. In fact, these methods are quite heterogeneous. The first one uses random method. The second one is not random and uses a non–linear transformation called Cayley map, to obtain non–coherent codes from codes which are opportunely and more simply designed. The third one is investigated in more detail in this thesis. This coding method too is not random and it uses a non–linear transformation, called exponential map, to obtain non–coherent codes from coherent codes (space–time codes used for receivers which known channel realization).

A more structured approach was used in [18], where an initial matrix generates the whole code by successive rotations[4]. The parameters of the codebook $\mathcal{C}$ are chosen by a random search to maximize the minimal chordal distance $d_c(\mathcal{C})$ as in (2.57). However no simplified decoding algorithm is reported.

In [19], a method to build unitary codebooks is described. The codeword $\mathbf{X}$ is obtained via the Cayley Transform

$$\mathbf{X} = (\mathbf{I}_T + j\mathbf{A})^{-1}(\mathbf{I}_T - j\mathbf{A}) \begin{bmatrix} \mathbf{I}_M \\ \mathbf{0} \end{bmatrix} \tag{2.58}$$

where the Hermitian matrix $\mathbf{A}$ is obtained from a set of fixed Hermitian matrices as $\mathbf{A} = \sum_{q=1}^{Q} \alpha_q \mathbf{A}_q$. To assure the orthogonality of $\mathbf{X}$, the coefficients α_q are real scalars belonging to a discrete set $\mathcal{A}$ whose cardinality is r. Even if (2.58) is invertible (for all Hermitian matrices $\mathbf{A}$ with no eigenvalue equal to -1), the Cayley Transform is non–linear. The authors constrain some entries of the set of matrices $\{\mathbf{A}_q\}$, the scalar Q (related to the rate of the system $R = Q\log_2(r)/T$ and make an approximation of the ML rule to resort to a simplified suboptimal decoding criteria which can be solved via the sphere decoder algorithm [60]. Many variables involved in the design of the code are found by numerical optimization, for example the set of matrices $\{\mathbf{A}_q\}$. One open issue is that the maximization criterion of $\{\mathbf{A}_q\}$ does not a priori guarantees full diversity of Cayley unitary codebooks for non–coherent systems, even if it has been shown in [61] that the same criterion guarantees the diversity of differentially encoded unitary codebooks. Successively, in [20] other optimization methods to find the codes are proposed in order to ameliorate performances.

In this thesis we further investigate a method based on the exponential parameterization, proposed in [22], [21]. The unitary code is obtained via the exponential map from a subset of skew-Hermitian matrices ($\mathbf{A} = -\mathbf{A}^\dagger$).

$$\mathbf{X} = \exp(\mathbf{A})\mathbf{I}_{T,M} = \exp\left\{ \begin{bmatrix} \mathbf{0}_M & -\mathbf{B}^\dagger \\ \mathbf{B} & \mathbf{0}_{T-M} \end{bmatrix} \right\} \begin{bmatrix} \mathbf{I}_M \\ \mathbf{0} \end{bmatrix} \tag{2.59}$$

[4] In [59] codes with better statistical properties and spectral efficiencies are constructed. However, the current absence of a simplified decoder prevents researchers from verifying their performances.

where the matrices $\mathbf{B}$ must satisfy some conditions which we investigate in the next chapter. In fact matrices $\mathbf{B}$ are codewords of a code for coherent systems, and are linearly scaled by a positive real factor α also called *homothetic factor*. The homothetic factor is the only parameter to optimize for fixed codebook. The diversity of the unitary codebook is not simple to link with the diversity of the coherent code, a conjecture about this relationship is proposed in [21]. We managed to give, under some assumptions, a positive responses to this conjecture (see Chapter 3). These codes can reach high spectral efficiencies just choosing the appropriate coherent code, only the homothetic factor must be optimized and not an increasing number of parameter as in [19] or [15]. In this thesis we will also provide some simplified decoding algorithms.

2.7.3 Algebraic Designs

These codes are quite different and could be also classified under other categories (which we will notice in case). They share a common quality: it is possible to control code parameters thanks to a quite constraining and powerful algebraic structure.

In [23] two code constructions are presented. The first code is called *generalized PSK constellation* and it can be constructed for $T = 2M$:

$$\mathbf{X}_l = \begin{bmatrix} \cos(\phi_l)\mathbf{I}_M \\ \sin(\phi_l)\mathbf{I}_M \end{bmatrix}, \qquad \phi_l = l\pi/L, \;\; l = 0, 1, \ldots, L-1\,. \tag{2.60}$$

where L is the size of the code. An ML decoder exists whose complexity is only $O(MN)$, independent from the duration T of the frame and the rate $R = \log_2(L)/T$. However, this is achieved by imposing a strong structure (2.60), which only exploits M real degrees of freedom out of $2M(T-M)$. The principal angles between two given codewords $\mathbf{X}_k$ and $\mathbf{X}_l$ are all the same and equal to $\pi(k-l)/2^{TR}$. Even if the constellation has full diversity, the minimal product distance (2.26) is $d_{p,min} = \sin(\pi/L) = \sin(\pi/2^{TR})$ and exponentially decreases according to the rate or the duration so that this method is efficient for low spectral efficiencies. A generalization called complex Givens codes was proposed in [26] which exploits $2M$ degrees of freedom out of $2M(T-M)$ and only doubles the decoding complexity of the generalized PSK codes. These codes can also be obtained through the exponential parameterization. The second proposition in [23] is based on the coherent space–time orthogonal designs [62] and can be described in the framework of the training–based codes [26]. The generic constellation matrix is $\mathbf{X}_k^\dagger = [\mathbf{I}_M \;\; \mathbf{C}_k^\dagger]$, where $M = 1, 2, 4, 8$. Since the authors want to build a unitary code, some constraints are imposed on the constellation choice (e.g. only for $M = 2$ a PSK constellation can be used in $\mathbf{C}_k$ and BPSK in the other cases). As in the previous case, not all the degrees of freedom are exploited but the ML detection can be implemented by an algorithm with low complexity $O(M^2N)$, independent from the rate.

Some unitary codes derived from the orthogonal designs were presented in [24]; these codes can be described as training–based codes. A simplified decoder is presented to perform the ML detection with complexity $O(2^{RT/2})$, instead of $O(2^{RT})$. We are detailing one of these codes in Sect. 2.9.

Eventually in [25] we can find an investigation about the maximum number of non intersecting subspaces, on condition that the codewords entries belong to fixed small constellations. The problem is solved when these constellations coincide with Galois Field $GF(q)$, where q is a power of a prime integer; in this case the maximum number of non–intersecting subspaces is $(q^T-1)/(q^M-1)$. An upper and lower bound are given in the case of PSK constellations, when the number of transmit antenna is $M = 2$. A simplified decoding has not been proposed yet.

2.8 Training Based Schemes

Recently research community growing interest is going to the so–called training based schemes [16], [26], [27], [28]. This section is entirely dedicated to these schemes, since it is actually one of the best available propositions.

In this approach each block fading is divided into two parts, respectively of T_t and T_d symbol periods (channel uses) ($T_t + T_d = T$). In the first T_t symbol periods, a pilot signal, known to the transmitter and to the receiver, is sent to obtain a rough estimation of the channel (training phase). The following T_d symbols periods are used to send information, usually encoded via some coherent space–time code $\mathcal{B}$. Codeword typically assume this form

$$\mathbf{X} = \begin{bmatrix} \sqrt{\tau}\mathbf{T} \\ \sqrt{1-\tau}\mathbf{B} \end{bmatrix}, \qquad \mathbf{T} \text{ is the pilot } T_t \times M \text{ matrix, } \mathbf{B} \in \mathcal{B} \text{ is } T_d \times M \tag{2.61}$$

where $\tau \in (0, 1)$ is scalar to assign different ratios of the transmit power to the training. The codeword can extend to several blocks of the fading channel (see for example [28]). We will write $\mathcal{T}_{\mathcal{B}}$ in order to indicate that the training code $\mathcal{T}$ exploits the coherent code $\mathcal{B}$.

The channel estimation performed in the training phase is quite unusual in estimation practice. As a matter of fact, in this kind of non–coherent systems, channel estimation is performed without having different estimates of the channel coefficients, but one. This is due to statistical independence of channel coefficients from one block to another. Moreover, the block length is so short that to repeate the estimation within the same block would cause an unacceptable decrease of the spectral efficiency. In the specialized literature, training for these systems has been ignored for some years (as remarked by [26]), probably because of the previous reasons.

However, since their introduction, training based codes seem to be one of the best competitors. The advantages of this approach are:

- the theoretical and design knowledge on space–time codes for the coherent channel (called also coherent ST codes) can be re–used;

- simplified decoding techniques of coherent space–time codes can be used to decode training based codes (whenever these algorithm exist);

- training based codes as in (2.61) achieve the diversity (in the PEP sense) of the underlying coherent space code $\mathcal{B}$, when $\mathbf{T}$ is full–rank and the fadings are i.i.d. Gaussian random variables [26].

In the next subsections results on information theory are reported to justify the choice of the optimal training phase duration. Then, a suboptimal decoding rule is introduced which gives another PEP–diversity definition. In Appendix B SNR normalizations used in simulations are calculated.

2.8.1 Information Theoretical Considerations

In case of ergodic capacity, [63] showed that the optimal number of symbol period T_t dedicated to the training is equal to M, the number of the transmit antennas, when it is possible to control the training power. Similar conclusions are presented also in [30]. So that in our examples we will always set

$$T_t = M \tag{2.62}$$

(if $T_t < M$ no meaningful channel estimation is possible because the number of unknown variables is greater than the number of equations). Moreover, when a linear MMSE estimation is performed, the optimal training symbol is a unitary matrix (it minimizes the total expected estimation error) [63]

$$\mathbf{T}^\dagger \mathbf{T} = \mathbf{I}_M / M \, . \tag{2.63}$$

In *low* SNR regime or when the coherence interval T is slightly larger than M and all the transmit antennas are used, the training based approach seems to be suboptimal, from an (ergodic) capacity perspective [63]. At *high* SNR, activating M^* transmit antennas (as in (2.11)), the training based system can be optimal (see [30] and [63] for other details). Anyway, if the codeword length is limited to a finite number of blocks, the optimal choice of the active transmit antennas can differ from M^*, also according to the SNR value [27].

2.8.2 Simplified Decoding

Let the channel model be

$$\mathbf{Y} = \begin{bmatrix} \mathbf{Y}_t \\ \mathbf{Y}_d \end{bmatrix} = \begin{bmatrix} \sqrt{\tau}\mathbf{T} \\ \sqrt{1-\tau}\mathbf{B} \end{bmatrix} \mathbf{H} + \begin{bmatrix} \mathbf{W}_t \\ \mathbf{W}_d \end{bmatrix} \, . \tag{2.64}$$

where the channel coefficients are i.i.d. $\mathcal{CN}(0,1)$ and each complex component of the additive noise is $\mathcal{CN}(0,\sigma^2)$.

The simplified receiver for training based symbols performs two operations

1. the receiver estimates the channel coefficients via an MMSE (Minimum Mean Square Error) estimator [63] from signal received during the first M symbol periods
$$\widehat{\mathbf{H}} = \sqrt{\tau}(\sigma^2 \mathbf{I}_M + \tau \mathbf{T}^\dagger \mathbf{T})^{-1} \mathbf{T}^\dagger \mathbf{Y}_t \, . \tag{2.65}$$

2. the receiver treats channel estimate as if it was perfect and decodes the signal received in the following $T - M$ symbol periods through the coherent ML rule (2.36)

$$\widehat{\mathbf{B}} = \arg \min_{l=1,\ldots,L} \|\mathbf{Y}_d - \mathbf{B}_l \widehat{\mathbf{H}}\|_F^2 \tag{2.66}$$

The rule (2.66) corresponds to finding the closest point to a given point vec$(\mathbf{Y}_d)$ of $\mathbb{C}^{M(T-M)}$. This problem can be efficiently solved via the so–called sphere decoder algorithm [64]. There are different search strategies (see [60] and references therein). The Pohst strategy scans the points inside an hypersphere of fixed radius and decreases the radius as soon as it finds a point. The Schnorr–Euchner strategy searches in an hypersphere too but scans the points in a different order (i.e. it searches first for points in the nearest hyperplanes inside the sphere).

The complexity of the sphere decoding algorithm is a current research topic and we do not investigate it in this thesis (see for example [60], [65], [66], [67]). Complexity depends on a host of parameters: the lattice itself, the particular lattice basis, the choice of the radius, the visiting strategy, etc.. Resuming, given an n–dimensional lattice (in real dimension, e.g. in (2.66) we have $n = 2M(T - M)$), the worst case complexity is exponential in n [64], [60]. In communications problems with AWGN, it makes more sense the notion of expected complexity, because the worst case has very low probability [67]. Extensive search has shown that for a large range of the parameters, the expected complexity is polynomial in n, in particular is $O(n^3)$ [65].

2.8.3 Diversity

The PEP–based diversity for a training code is generally calculated with respect to the new detector (2.66). We denote this diversity by $d^{E-D}(\mathcal{T}_\mathcal{B})$ and when we talk about the diversity of a training code, we implicitly refer to the PEP found by detector (2.66), if not stated otherwise. A recent interesting result of [26], which relates the diversity of the training code $\mathcal{T}$ with the diversity of the correspondent coherent code $\mathcal{B}$, is

Proposition 3 *Let $\mathcal{T}$ be a training code of the form (2.61), obtained from a coherent code $\mathcal{B}$, where $\mathbf{T}^\dagger\mathbf{T} = \mathbf{I}_M/M$ and with i.i.d, Gaussian fadings and AWGN. Then,*

$$d^{E-D}(\mathcal{T}_\mathcal{B}) = d^{co-ML}(\mathcal{B})\,. \tag{2.67}$$

In [29] it is shown that

Proposition 4 *Let $\mathcal{T}$ be a training code of the form (2.61), obtained from a coherent code $\mathcal{B}$. If the range of the training matrix $\mathbf{T}$ contains the range of all the codewords of $\mathcal{B}$, then the algebraic diversity $\mathcal{T}$ coincides with the diversity of $\mathcal{B}$, i.e.*

$$d^{alg}(\mathcal{T}_\mathcal{B}) = d^{co-ML}(\mathcal{B})\,. \tag{2.68}$$

If $\mathbf{T}^\dagger\mathbf{T} = \mathbf{I}_M/M$, rank$(\mathbf{T}) = M$ is maximum. Hence, from Proposition 3 and Proposition 4, we have that $d^{alg}(\mathcal{T}_\mathcal{B}) = d^{E-D}(\mathcal{T}_\mathcal{B})$, i.e. *for training codes of the kind (2.61), the algebraic and PEP–based diversities coincide (under the detection criterion (2.66))*.

2.9 Example

In this section we describe a particular example, to better understand code parameters.

Let's take the code for $M = 2$ transmit antennas and $T = 4$ symbol periods described in [24]. This is a unitary code, built according to the training based approach from the 2×2 Alamouti code [54]. It is one of the the rare codes that allows to calculate the different distances among subspaces, which is not possible for a generic training based code. This code $\mathcal{C}_z$ has codewords

$$\mathbf{X}_{k,l} = \begin{bmatrix} \mathbf{T}_z \\ \mathbf{B}_{k,l} \end{bmatrix}, \qquad \mathbf{T}_z = \begin{bmatrix} 1 & 1 \\ -1 & 1 \end{bmatrix}, \quad \mathbf{B}_{k,l} = \begin{bmatrix} s_k & s_l \\ -s_l^* & s_k^* \end{bmatrix} \tag{2.69}$$

where the symbols s_k, s_l belong to a Q–PSK constellation to assure the orthogonality of $\mathbf{X}_{k,l}$

$$s_k = e^{j\frac{2\pi}{Q}k}, \qquad k = 0, \ldots, Q-1\,. \tag{2.70}$$

and then the codebook $\mathcal{C}_z$ has size $L = Q^2$. Since the Alamouti code is an orthogonal design, i.e. $\mathbf{B}_{k,l}^\dagger \mathbf{B}_{k,l} = 2\mathbf{I}_2$, we have $\mathbf{X}_{k,l}^\dagger \mathbf{X}_{k,l} = 4\mathbf{I}_2$. To calculate the principal angles between all the subspaces $\Omega_{\mathbf{X}_{k,l}}$ we need their orthonormal bases, e.g. $\frac{1}{2}\mathbf{X}_{k,l}$, as described in Sect. 2.3.2. The squared cosine of the principal angles between two subspaces represented by $\mathbf{X}_{k,l}$ and $\mathbf{X}_{k',l'}$ are given by the eigenvalues of the matrix (see (2.21)) [24]

$$\mathbf{R}_{kl,k'l'}\mathbf{R}_{kl,k'l'}^\dagger, \qquad \mathbf{R}_{kl,k'l'} = \frac{1}{4}\mathbf{X}_{k,l}\mathbf{X}_{k',l'}^\dagger$$

and following calculations in [24] we have that the two principal angles are equal to a value $\theta_{kl,k'l'}$ and its cosine is

$$\cos^2(\theta_{kl,k'l'}) = \frac{1}{4}\big[2 + \cos(2\pi(k-k')/Q) + \cos(2\pi(l-l')/Q)\big]\,.$$

which show that if two codewords are different (i.e. at least one of the two inequality holds: $k \neq k'$, $l \neq l'$) the subspaces are non–intersecting and hence the code has full diversity. The minimal product distance can be calculated

$$d_p(\mathcal{C}_z) = \sin(\pi/Q)/\sqrt{2}\,.$$

In literature we can find another independent proposition based on the Alamouti code [23]. In this code, denoted by $\mathcal{C}_t$, the structure is like in (2.69), but this case the training matrix is $\mathbf{T}_t = \mathbf{I}_2$. As pointed out by [26], the two codes are equivalent. As before in fact, we can calculate the squared cosine of the principal angles of the code $\mathcal{C}_t$. We have

$$\mathbf{R}_{kl,k'l'}\mathbf{R}_{kl,k'l'}^\dagger = \frac{5}{9} + \frac{2}{9}\big[2 + \cos(2\pi(k-k')/Q) + \cos(2\pi(l-l')/Q)\big]\mathbf{I}_2$$

hence the principal angle are equal and from the expression of their squared cosines (above) we can calculate the minimum product distance which is $d_p(\mathcal{C}_t) = \sin(\pi/Q)$ $\sqrt{2/3}$, that is $2/\sqrt{3}$ times greater than $d_p(\mathcal{C}_z)$.

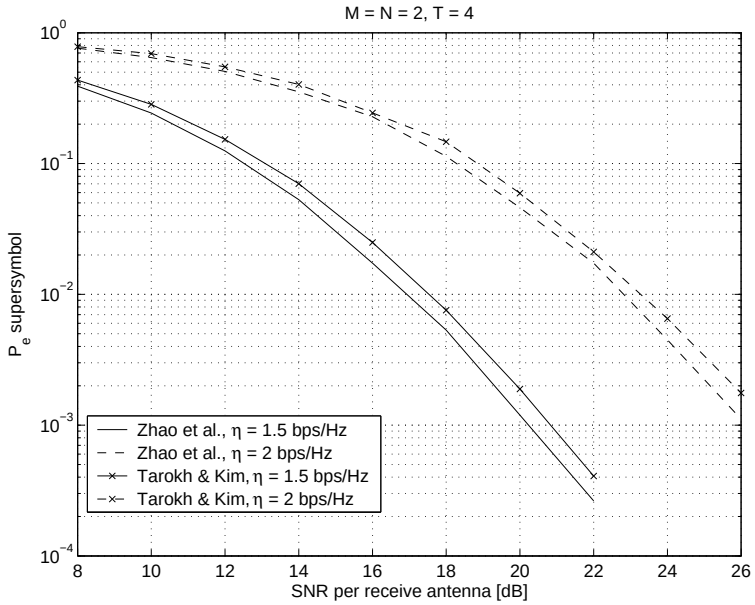

Figure 2.3: The two codes proposed by Zhao et al. [24] and Tarokh, Kim [23] have in the end the same structure, but a non–optimal allocation of the energy in [23] causes a loss of about 0.5 dB (in the figure the case of spectral efficiencies $\eta = 1.5, 2$ bps/Hz).

This difference in the product distance is not due to training matrix $\mathbf{T}$, but to power distribution between the training and the data. While in code $\mathcal{C}_z$ equal power is allocated to the two phases (this strategy has proved to be optimal in our working hypotheses [26]), in the case of $\mathcal{C}_t$ the ratio between the training and the data power is $1/2$. This results in a performance degradation, as shown in Fig. 2.3. On the contrary, if the power in code $\mathcal{C}_t$ is well distributed, for example by fixing $\mathbf{T}_t = \sqrt{2}\mathbf{I}_2$, the two codes become equivalent in the sense that the distribution of product distances of the two codes coincides.

Codes being equivalent, the decoding algorithm proposed in [23] has lower complexity than the one proposed in [24]. Eventually, the two codes does not exploit all the available complex degrees of freedom (4 in this case).

A Summary of Some Matrix Properties

We recall that $(\cdot)^t$, $(\cdot)^*$ and $(\cdot)^\dagger$ respectively denote the transpose, conjugate and transpose conjugate matrix. We consider complex matrices.

Kronecker product. If $\mathbf{A}$ is a $M \times N$ complex matrix and $\mathbf{B}$ is a $K \times L$ matrix, the Kronocker matrix product $\mathbf{C} = \mathbf{A} \otimes \mathbf{B}$ is defied as

$$\mathbf{C} = \begin{bmatrix} a_{1,1}\mathbf{B} & \dots & a_{1,N}\mathbf{B} \\ \vdots & \ddots & \vdots \\ a_{M,1}\mathbf{B} & \dots & a_{M,N}\mathbf{B} \end{bmatrix} .$$

The following identity holds

$$\mathrm{vec}(\mathbf{A}\,\mathbf{B}\,\mathbf{C}) = (\mathbf{C}^t \otimes \mathbf{A})\mathrm{vec}(\mathbf{B}) \tag{2.71}$$

where vec$(\mathbf{B})$ is the vector formed by the columns of $\mathbf{B}$ and all the matrices can be rectangular with proper dimensions. From (2.71) comes

$$\mathrm{vec}(\mathbf{A}\,\mathbf{B}) = (\mathbf{I} \otimes \mathbf{A})\mathrm{vec}(\mathbf{B})\,. \tag{2.72}$$

Other properties

1. $(\mathbf{A} \otimes \mathbf{B})^\dagger = \mathbf{A}^\dagger \otimes \mathbf{B}^\dagger$;
2. $(\mathbf{A} \otimes \mathbf{B})(\mathbf{C} \otimes \mathbf{D}) = (\mathbf{AC}) \otimes (\mathbf{BD})$;
3. $(\mathbf{A} \otimes \mathbf{B})^{-1} = \mathbf{A}^{-1} \otimes \mathbf{B}^{-1}$.

Trace properties. Matrices can be rectangular

1. $\mathrm{tr}(\mathbf{A}\,\mathbf{B}) = \mathrm{tr}(\mathbf{B}\,\mathbf{A})$, when the two products make sense;
2. $\mathrm{tr}(\mathbf{U}^\dagger\mathbf{A}\,\mathbf{U}) = \mathrm{tr}(\mathbf{A})$, if at least one of the following conditions holds $\mathbf{U}^\dagger\mathbf{U} = \mathbf{I}$ or $\mathbf{U}\,\mathbf{U}^\dagger = \mathbf{I}$;
3. $\mathrm{tr}(\mathbf{A}^\dagger) = \mathrm{tr}(\mathbf{A}^*) = [\mathrm{tr}(\mathbf{A})]^* = [\mathrm{tr}(\mathbf{A}^\mathbf{T})]^*$, from 1);
4. $\mathrm{tr}(\mathbf{A}^\dagger\mathbf{B}^\dagger) = [\mathrm{tr}(\mathbf{A}\,\mathbf{B})]^*$, in fact $\mathrm{tr}(\mathbf{A}^\dagger\mathbf{B}^\dagger) = [\mathrm{tr}(\mathbf{B}\,\mathbf{A})]^* = [\mathrm{tr}(\mathbf{A}\,\mathbf{B})]^*$.

Matrix norms. The matrix Frobenius norm is defined for a generic $T \times M$ complex matrix as

$$\|\mathbf{X}\|_F = \sqrt{\mathrm{tr}(\mathbf{X}^\dagger\mathbf{X})} = \sqrt{\mathrm{tr}(\mathbf{X}\mathbf{X}^\dagger)} = (\textstyle\sum_{m,t}|x_{tm}|^2)^{1/2}$$

and the spectral norm is defined as [68, pag. 295]

$$\|\mathbf{X}\|_2 = \max\{\sqrt{\lambda},\ \lambda \text{ is eigenvalue of } \mathbf{X}^\dagger\mathbf{X}\}\,. \tag{2.73}$$

Suppose $T \geq M$, let $\mathbf{X} = \mathbf{V}\mathbf{\Sigma}\mathbf{U}^\dagger$ be the Thin Singular Value Decomposition (TSVD), where $\sigma_1 \geq \sigma_2 \geq \ldots \geq \sigma_1 \geq 0$, [3, pag. 72], then we have

$$\|\mathbf{X}\|_F = \sqrt{\sigma_1^2 + \ldots + \sigma_M^2}\,, \qquad \|\mathbf{X}\|_2 = \sigma_1 \tag{2.74}$$

Determinantal formula. We reporte the useful determinantal formula in [68, pag. 22]. Let $\mathbf{A}$ be a square complex matrix, partitioned as

$$\mathbf{A} = \begin{bmatrix} \mathbf{A}_{11} & \mathbf{A}_{12} \\ \mathbf{A}_{21} & \mathbf{A}_{22} \end{bmatrix} \tag{2.75}$$

then

$$\det \mathbf{A} = \det \mathbf{A}_{11} \, \det(\mathbf{A}_{22} - \mathbf{A}_{21}\mathbf{A}_{11}^{-1}\mathbf{A}_{12}) \, . \tag{2.76}$$

B Signal Normalization Calculation

With respect to the channel model (2.1), the transmit supersymbol is $\alpha\mathbf{X}$. Its statistical power averaged over the M transmit antennas is

$$\alpha^2 \frac{1}{M} \sum_{m=1}^{M} \mathrm{E}\left[||\mathbf{x}_m||^2\right] = \alpha^2 \frac{1}{M} \mathrm{E}\left[\mathrm{tr}(\mathbf{X}^\dagger\mathbf{X})\right] = \frac{E_{ss}}{M} \tag{2.77}$$

Suppose equally probable (correlated) supersymbols $\mathbf{X}$ and impose the following normalization [11][5]

$$\mathrm{E}\left[\mathrm{tr}(\mathbf{X}^\dagger\mathbf{X})\right] = \frac{1}{L} \sum_{i=1}^{L} \mathrm{tr}(\mathbf{X}_i^\dagger\mathbf{X}_i) = M \tag{2.78}$$

where L is the size of the codebook. Normalization (2.78) states that the statistical power of the supersymbol $\mathbf{X}$ is globally M.

The signal model (2.1) column–wise reads

$$\mathbf{y}_n = \alpha \, \mathbf{X}\mathbf{h}_n + \sigma\mathbf{w}_n \, , \qquad n = 1, \ldots, N \tag{2.79}$$

If the noise samples $z_{t,n} \sim \mathcal{CN}(0, \sigma_z^2)$ are i.i.d., the noise average statistical power per receive antenna is

$$\frac{1}{N} \sum_{n=1}^{N} \sigma^2 \mathrm{E}\left[||\mathbf{w}_n||^2\right] = \sigma^2 TN/N = \sigma^2 T \, . \tag{2.80}$$

The useful (no noise) average statistical signal power per receive antenna is

$$\frac{1}{N} \sum_{n=1}^{N} \mathrm{E}\left[||\mathbf{y}_n||^2\right] = \frac{\alpha^2}{N} \mathrm{E}\left[\mathbf{h}_n^\dagger \mathbf{X}^\dagger \mathbf{X} \mathbf{h}_n\right] = \frac{\alpha^2}{N} \mathrm{E}\left[\mathrm{tr}(\mathbf{X}^\dagger\mathbf{X} \, \mathbf{h}_n\mathbf{h}_n^\dagger)\right] \tag{2.81}$$

Now, the expectation must be considered in the supersymbol and channel. If the supersymbols are independent of the channel and the fadings are spatially uncorrelated $\mathbf{h}_n \sim \mathcal{CN}(\mathbf{0}, \mathbf{K_h})$ for all n, we have

$$\frac{1}{N} \sum_{n=1}^{N} \mathrm{E}\left[||\mathbf{y}_n||^2\right] = \frac{\alpha^2}{N} \sum_{n=1}^{N} \mathrm{tr}\big(\mathrm{E}\left[\mathbf{X}^\dagger\mathbf{X}\right]\mathbf{K_h}\big) = \alpha^2 \, \mathrm{tr}\big(\mathbf{K_h}\mathrm{E}\left[\mathbf{X}^\dagger\mathbf{X}\right]\big)$$

[5] With notation of [11], the SNR per receive antenna is $\bar{\gamma}/T$.

If $\mathbf{K_h} = \mathbf{I}_M$ (temporal uncorrelation of the channel), we obtain (2.3). For a more general treatment, when the channel has spatial and temporal correlation see [11].

It is interesting to express results as a function of the energy per information bit over the noise spectral density variance E_b/N_0. Let $N_{bit/ss}$ be the number of information bits per supersymbol, and let the complex baseband noise have a variance of $\sigma^2/2 = N_0/2$ per real dimension [69, pp. 549, 613]. From (2.77) we have that $E_{ss} = E_b N_{bit/ss}$ and from (2.3) we obtain

$$\frac{E_b}{N_0} = \frac{\rho\, T}{N_{bit/ss}}\,, \qquad \left(\frac{E_b}{N_0}\right)_{dB} = (\rho)_{dB} + 10\log_{10}(T) - 10\log_{10}(N_{bit/ss})\,. \quad (2.82)$$

B.1 SNR Normalization of Training–Based Codes

Let $\mathbf{X} \in \mathcal{T}_{\mathcal{B}}$ be a training code as in (2.61), we normalize the codeword in the following way

$$\mathrm{tr}(\mathrm{E}\,[\mathbf{X}^\dagger\mathbf{X}]) = 1 \quad \Longrightarrow \quad \tau\,\mathrm{tr}(\mathrm{E}\,[\mathbf{T}^\dagger\mathbf{T}]) + (1-\tau)\mathrm{tr}(\mathrm{E}\,[\mathbf{B}^\dagger\mathbf{B}]) \quad (2.83)$$

supposing (2.62) and (2.63), the energy spent in training is $E_t = \tau$ and the energy spent for data transmission must be $E_d = (1-\tau)$ in order to satisfy condition (2.83). Hence,

$$\mathrm{tr}(\mathrm{E}\,[\mathbf{B}^\dagger\mathbf{B}]) = \mathrm{E}\,[\|\mathbf{B}\|_F^2] = 1\,. \quad (2.84)$$

Let $(T-M)M \times 1$ vector $\mathbf{b} = \mathrm{vec}(\mathbf{B})$ be calculated as $\mathbf{b} = \mathbf{\Phi s}$ where $\mathbf{\Phi}$ is unitary and $\mathbf{s}$ belongs to a constellation $\mathcal{A}^{M(T-M)}$ (e.g. QAM, PSK). Denote by $E_{s,av}$ the average statistical power of the constellation $\mathcal{A}$, then (2.84) becomes

$$\mathrm{E}\,[\|\mathbf{B}\|_F^2] = M(T-M)E_{s,av} = 1 \quad \Longrightarrow \quad E_{s,av} = \frac{1}{M(T-M)}\,. \quad (2.85)$$

Under these condition the (global, for training and data) SNR per receiver antenna is $\rho = 1/(T\sigma^2)$, where σ^2 is the additive noise variance and fading are considered i.i.d. as usual.

C Derivation of the ML and GLRT

Let introduce in channel model (2.2) spatial and temporal correlation in the fading and noise: $\mathbf{h} \sim \mathcal{CN}(\mathbf{0}, \mathbf{K_h})$ and $\sigma\mathbf{w} \sim \mathcal{CN}(\mathbf{0}, \overline{\mathbf{K}}_\mathbf{w})$, then the received signal $\mathbf{y} = \mathrm{vec}(\mathbf{Y})$, having been sent $\mathbf{X}$, is a complex Gaussian vector with zero mean and covariance $\mathbf{K_{y|X}} = \alpha^2\,\overline{\mathbf{X}}\mathbf{K_h}\overline{\mathbf{X}}^\dagger + \overline{\mathbf{K}}_\mathbf{w}$. We follow the proofs in [11], and we prove a slightly general results.

The non–coherent **ML criterion** for Gaussian vectors $\mathbf{y} \sim \mathcal{CN}(\mathbf{0}, \mathbf{K}_y)$, where the covariance matrix depends on the sent symbol $\mathbf{X}$ and assumes the form

$$\mathbf{K_y} = \alpha^2(\overline{\mathbf{X}}\,\mathbf{K_h}\overline{\mathbf{X}}^\dagger) + \overline{\mathbf{K}}_\mathbf{w} \quad (2.86)$$

can be simplified.

$$\begin{aligned}\max_{\mathbf{X}} p(\mathbf{y}|\mathbf{X}) &= \min \mathbf{y}^\dagger {\mathbf{K_y}}^{-1}\mathbf{y} + \ln|\mathbf{K_y}| \\ &\overset{(a)}{=} \min\left[-\mathbf{y}^\dagger\overline{\mathbf{K}}_\mathbf{w}^{-1}\overline{\mathbf{X}}(\frac{1}{\alpha^2}{\mathbf{K_h}}^{-1}+\overline{\mathbf{X}}^\dagger\overline{\mathbf{K}}_\mathbf{w}^{-1}\overline{\mathbf{X}})^{-1}\overline{\mathbf{X}}^\dagger\overline{\mathbf{K}}_\mathbf{w}^{-1}\mathbf{y}+\ln|\mathbf{K_y}|\right] \\ &\overset{(b)}{=} \min\left[-\mathbf{y}^\dagger\mathbf{F}\,\mathbf{y}+\ln|{\mathbf{K_h}}^{-1}/\alpha^2+\overline{\mathbf{X}}^\dagger\overline{\mathbf{X}}|\right]\end{aligned}$$

where (a) follows from the identity (when matrices are non–singular) $\mathbf{B} = \mathbf{A} + \mathbf{X}\,\mathbf{R}\,\mathbf{Y} \Rightarrow \mathbf{B}^{-1} = \mathbf{A}^{-1} - \mathbf{A}^{-1}\mathbf{X}(\mathbf{R}^{-1} + \mathbf{Y}\,\mathbf{A}^{-1}\mathbf{X})^{-1}\mathbf{Y}\mathbf{A}^{-1}$ [68, pag. 19] applied to (2.86) and being ignored the constant term $\mathbf{y}^\dagger\overline{\mathbf{K}}_\mathbf{w}^{-1}\mathbf{y}$. the logarithmic part in (b) follows by applying twice the determinantal formula in (2.76) to the composite matrix

$$\mathbf{A} = \begin{bmatrix} \frac{1}{\alpha^2}{\mathbf{K_h}}^{-1}+\overline{\mathbf{X}}^\dagger\overline{\mathbf{K}}_\mathbf{w}^{-1}\overline{\mathbf{X}} & \overline{\mathbf{X}}^\dagger\overline{\mathbf{K}}_\mathbf{w}^{-1} \\ \overline{\mathbf{K}}_\mathbf{w}^{-1}\overline{\mathbf{X}} & \overline{\mathbf{K}}_\mathbf{w}^{-1}\end{bmatrix}$$

so that we have

$$|\mathbf{A}| = \left|\frac{1}{\alpha^2}{\mathbf{K_h}}^{-1}+\overline{\mathbf{X}}^\dagger\overline{\mathbf{K}}_\mathbf{w}^{-1}\overline{\mathbf{X}}\right|\,|{\mathbf{K_y}}^{-1}| = \left|\overline{\mathbf{K}}_\mathbf{w}^{-1}\right|\,\left|\frac{1}{\alpha^2}{\mathbf{K_h}}^{-1}\right|$$

and it immediately follows

$$\ln|\mathbf{K_y}| = \ln\left|\frac{1}{\alpha^2}{\mathbf{K_h}}^{-1}+\overline{\mathbf{X}}^\dagger\overline{\mathbf{K}}_\mathbf{w}^{-1}\overline{\mathbf{X}}\right| + \ln\left(\left|\overline{\mathbf{K}}_\mathbf{w}\right|\left|\alpha^2\mathbf{K_h}\right|\right)$$

where the second part can be ignored in minimization since it gives a constant contribution. Thus, the ML criterion is

$$\max_{\mathbf{X}\in\mathcal{C}} p(\mathbf{y}|\mathbf{X}) = \min_{\mathbf{X}\in\mathcal{C}}\left[-\mathbf{y}^\dagger\mathbf{F}\,\mathbf{y}+c\right] \tag{2.87}$$

where

$$\mathbf{F} = \overline{\mathbf{K}}_\mathbf{w}^{-1}\overline{\mathbf{X}}(\frac{1}{\alpha^2}{\mathbf{K_h}}^{-1}+\overline{\mathbf{X}}^\dagger\overline{\mathbf{K}}_\mathbf{w}^{-1}\overline{\mathbf{X}})^{-1}\overline{\mathbf{X}}^\dagger\overline{\mathbf{K}}_\mathbf{w}^{-1}\,, \qquad c = \ln\left|\frac{1}{\alpha^2}{\mathbf{K_h}}^{-1}+\overline{\mathbf{X}}^\dagger\overline{\mathbf{K}}_\mathbf{w}^{-1}\overline{\mathbf{X}}\right|. \tag{2.88}$$

The **GLRT** requires the maximization of $p(\mathbf{Y}|\mathbf{X},\mathbf{H})$, i.e. of $p(\mathbf{y}|\overline{\mathbf{X}},\mathbf{h})$ (2.31). For correlated noise and fadings, $\mathbf{y}$ given $\mathbf{X},\mathbf{H}$ is a complex Gaussian variable $\mathbf{y}\sim\mathcal{CN}(\alpha\overline{\mathbf{X}}\mathbf{h},\overline{\mathbf{K}}_\mathbf{w})$, hence (2.31) can be written as

$$\hat{\mathbf{X}}_{GLRT} = \arg\min_{\mathbf{X}\in\mathcal{C}}\inf_{\mathbf{h}}(\mathbf{y}-\alpha\overline{\mathbf{X}}\mathbf{h})^\dagger\overline{\mathbf{K}}_\mathbf{w}^{-1}(\mathbf{y}-\alpha\overline{\mathbf{X}}\mathbf{h})$$

The matrix $\overline{\mathbf{K}}_\mathbf{w}^{-1}$ is definite positive (since it is the inverse of a covariance matrix, which we assume of full rank), from the eigenvalue decomposition we have: $\overline{\mathbf{K}}_\mathbf{w}^{-1} = \mathbf{U}^\dagger\mathbf{\Lambda}\mathbf{U} = \mathbf{B}^\dagger\mathbf{B}$, where $\mathbf{B} = \sqrt{\mathbf{\Lambda}}\mathbf{U}$.Letting $\mathbf{y}_B = \mathbf{B}\mathbf{y}$, $\overline{\mathbf{X}}_B = \mathbf{B}\overline{\mathbf{X}}$, we have

$$(\mathbf{y}-\alpha\overline{\mathbf{X}}\mathbf{h})^\dagger\overline{\mathbf{K}}_\mathbf{w}^{-1}(\mathbf{y}-\alpha\overline{\mathbf{X}}\mathbf{h}) = \|\mathbf{y}_B-\alpha\overline{\mathbf{X}}_B\mathbf{h}\|^2\,. \tag{2.89}$$

we must search for the channel $\mathbf{h} \in \mathbb{C}^{NM}$ which minimizes the above distance. We can describe the vector as $\mathbf{y}_B = \mathbf{y}_{B,\|} + \mathbf{y}_{B,\perp}$, where $\mathbf{y}_{B,\|}$ is the component of $\mathbf{y}_B$ which lies on span$(\overline{\mathbf{X}}_B)$ while $\mathbf{y}_{B,\perp}$ is the component orthogonal to the same subspace. The minimum of the distance (2.89) is obtained by annihilating the parallel component $\mathbf{y}_{B,\|}$. This is obtained when

$$\mathbf{h}_{inf} = \frac{1}{\alpha}(\overline{\mathbf{X}}_B^{\dagger}\overline{\mathbf{X}}_B)^{-1}\overline{\mathbf{X}}_B^{\dagger}\mathbf{y}_B = \frac{1}{\alpha}(\overline{\mathbf{X}}^{\dagger}\overline{\mathbf{K}}_{\mathbf{w}}^{-1}\overline{\mathbf{X}})^{-1}\overline{\mathbf{X}}^{\dagger}\overline{\mathbf{K}}_{\mathbf{w}}^{-1}\mathbf{y}$$

Through a substitution we obtain the result

$$\hat{\overline{\mathbf{X}}}_{GLRT} = \max_{\mathbf{X}\in\mathcal{C}} \mathbf{y}_B^{\dagger}\overline{\mathbf{X}}_B(\overline{\mathbf{X}}_B^{\dagger}\overline{\mathbf{X}}_B)^{-1}\overline{\mathbf{X}}_B^{\dagger}\mathbf{y}_B = \max_{\mathbf{X}\in\mathcal{C}} \mathbf{y}^{\dagger}\overline{\mathbf{K}}_{\mathbf{w}}^{-1}\overline{\mathbf{X}}(\overline{\mathbf{X}}^{\dagger}\overline{\mathbf{K}}_{\mathbf{w}}^{-1}\overline{\mathbf{X}})^{-1}\overline{\mathbf{X}}^{\dagger}\overline{\mathbf{K}}_{\mathbf{w}}^{-1}\mathbf{y}\,.$$

We can see that the original noise covariance matrix acts as a sort of distance. When the additive noise in only temporally correlated, so that $\overline{\mathbf{K}}_{\mathbf{w}} = \overline{\mathbf{K}}_{\mathbf{w}} = \mathbf{I}_N \otimes \mathbf{K}_{\mathbf{w}t}$, then we can write

$$\hat{\mathbf{X}}_{GLRT} = \max_{\mathbf{X}\in\mathcal{C}} \mathrm{tr}\big[\mathbf{Y}^{\dagger}\mathbf{K}_{\mathbf{w}t}{}^{-1}\mathbf{X}(\mathbf{X}^{\dagger}\mathbf{K}_{\mathbf{w}t}{}^{-1}\mathbf{X})^{-1}\mathbf{X}^{\dagger}\mathbf{K}_{\mathbf{w}t}{}^{-1}\mathbf{Y}\big]\,.$$

The GLRT and ML criteria are equivalent when $\mathbf{K}_{\mathbf{h}} = \mathbf{I}_{NM}$ and $\overline{\mathbf{X}}^{\dagger}\overline{\mathbf{K}}_{\mathbf{w}}^{-1}\overline{\mathbf{X}} = \mathbf{I}_{NT}$, i.e. when $\overline{\mathbf{X}}$ has orthogonal columns with respect to the metric given by $\overline{\mathbf{K}}_{\mathbf{w}}^{-1}$. Given the particular structure of $\overline{\mathbf{X}}$, the new orthogonality condition can be satisfied only if $\overline{\mathbf{K}}_{\mathbf{w}} = \mathbf{I}_N \otimes \mathbf{K}_{\mathbf{w}t}$, so that the orthogonality condition is separable and we must only satisfy $\mathbf{X}^{\dagger}\mathbf{K}_{\mathbf{w}t}{}^{-1}\mathbf{X} = \mathbf{I}_M$.

Chapter 3

Unitary Codes Obtained via the Exponential Map

In this chapter we propose codes for non–coherent MIMO systems. We introduce some basic mathematical tools on differential manifolds and Lie Groups. We explain that the Grassmannian $G_{T,M}$, i.e. the set of M–dimensional subspaces of $\mathbb{C}^T$, is a differential manifold. We introduce the concept of tangent space at a fixed point of the Grassmannian. The exponential map, which sends tangent space points to the Grassmannian, is presented too. We propose to build codes $\mathcal{C}$ over $G_{T,M}$ via the exponential map: the codewords of $\mathcal{C}$ are obtained from the codewords of another code $\mathcal{B}$, which is imbedded into the tangent space. Code $\mathcal{B}$ -usually designed for *coherent* MIMO systems- will be called coherent code, with a slight abuse of notation. Codes $\mathcal{C}$ will be called *EP codes*, since they are obtained via exponential parameterization.

We explain conditions under which the exponential map is invertible so that the described procedure makes sense. Some open problems about diversity of the EP codes are fixed, in particular we determined the relationship between the diversity of $\mathcal{C}$, calculated through GLRT, to the diversity of $\mathcal{B}$, calculated through the coherent ML detector. Relationships with training–based codes are examined. At the end of the chapter, some examples shows that certain non–coherent space–time codes can be seen as EP codes.

3.1 Differentiable Manifolds and Lie Groups

The Grassmannian $G_{T,M}$, i.e. the set of the M–dimensional complex vector subspaces, has a rich mathematical structure. Many algebraic and mathematical concepts are needed for a deep understanding of all its properties, namely the theory of Lie groups and algebras, the theory of manifolds and topology. For our purpose, we don't need to use and dominate all these mathematical concepts nor it would be possible to recall here the whole of their basic definitions. So we invite the interested reader to refer to some corner stone manuals as [70], [71], for instance. Anyway, we are sketching, when possible, in the most rapid and rigorous way, the framework of the main mathematical

concepts, in the hope that this can be helpfull to cope with the specialized literature.

3.1.1 Review of C^∞ Differentiable Manifolds

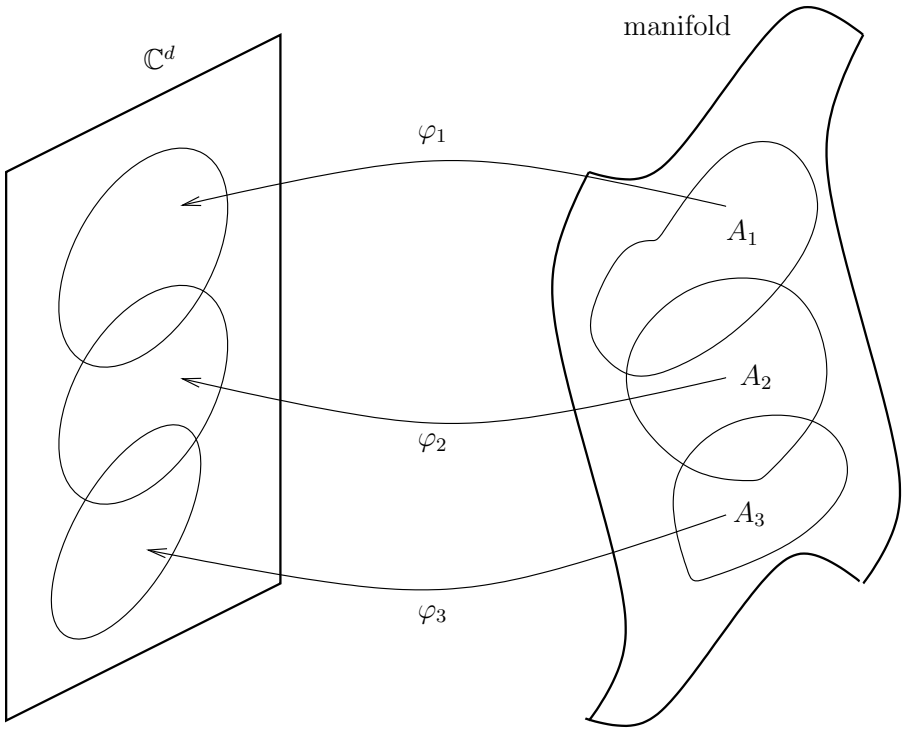

Figure 3.1: The coordinate maps φ_k associate connected open subsets of the manifold to open subsets of $\mathbb{C}^d$.

A C^∞ differentiable manifold (in our case $G_{T,M}$) is a topological space in which, for each connected open set A_k of $G_{T,M}$ there exists an homeomorphism[1] φ_k from A_k to an open subset of $\mathbb{C}^d$ (see Fig. 3.1). These homeomorphisms are infinitely differentiable functions (i.e. C^∞ functions)and are called coordinate maps. They enable the construction of local coordinate systems [71, pag. 576]. d is the complex dimension[2] of open set A_k [71, pag. 573].

When it is possible to cover the whole manifold with such A_k, all local charts grouped together form a C^∞ differentiable structure for the manifold [70, pag. 5]. A C^∞ differentiable manifold is said to be homogeneous when all the covering open sets have the same dimension d, which coincides with the manifold dimension [70, pag. 120].

A manifold can be imagined as a surface imbedded in a higher dimensional space [70]. For each point Ω of an infinitely differentiable manifold it is possible to associate

[1] A one–to–one continuous transformation between topological spaces, with continuous inverse map.

[2] One complex dimension corresponds to two real dimensions.

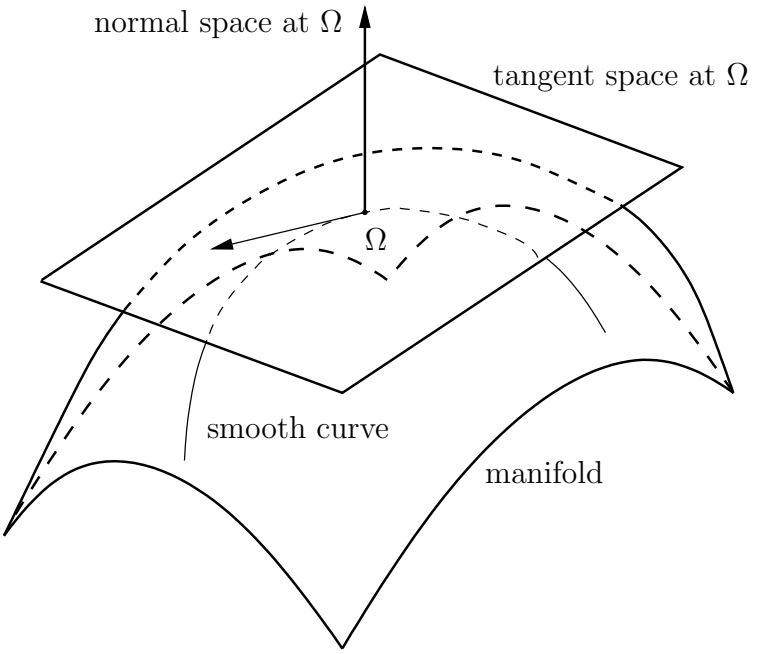

Figure 3.2: The geometrical interpretation of the tangent space and normal space in a 2–dimensional real manifold imbedded in $\mathbb{R}^3$. The direction of each smooth curve passing through Ω belongs to the tangent plane.

a *tangent space*, which is the tangent hyperplane to the manifold at that point [4] and which will be denoted by $t\pi_\Omega$ (here the notation differs from common use in order to be precise). The tangent space has the same dimension as the manifold [70, pag. 12]. Its orthogonal complement is called the normal space (at that point).

A smooth curve on the manifold, passing through Ω, has a tangent vector belonging to tangent space $t\pi_\Omega$ (see Fig. 3.2). Hence, $t\pi_\Omega$ can be seen as the collection of all directions or velocities that a point can take when it smoothly passes through Ω (see also [72] at the voice Tangent Space or Chart Tangent Space).

The tangent space is a vector space, and it can be seen as a special case of manifold.

3.1.2 Review of Lie Groups and Lie Algebras

Lie groups are a particular kind of differentiable manifolds obeying group properties and satisfying the additional condition that group operations are differentiable, see [70, pag. 82], [72].

Examples of Lie groups are the unitary group $\mathcal{U}_T$, the orthogonal group of real matrices (i.e. real matrices whose inverse coincides with the transpose), the general linear group $Gl(\mathbb{C}, T)$ of all $T \times T$ complex non–singular matrices, etc..

If a differentiable manifold is a Lie group G, then its tangent space is a Lie algebra[3]

[3]A Lie algebra is a vector space with a bilinear operator, called bracket $[\cdot, \cdot]$, satisfying two proper-

$\mathfrak{g}$. There always exists a map from a Lie algebra to its Lie group called *exponential map* [71, pag. 608].

Example. The complex unit circle $\mathbb{U} = \{c \in \mathbb{C} : |c| = 1\} \subset \mathbb{R}^2$ with the classical complex multiplication is a Lie group of dimension 1 (it is a curve). The tangent space at any point of $\mathbb{U}$ is a 1–dimensional real vector space, i.e. $\mathbb{R}$ with the common sum. Once fixed 1 to be the identity of $\mathbb{U}$, the exponential mapping from $\mathbb{R}$ to $\mathbb{U}$ is the classical $e^{j\theta}$, $\theta \in \mathbb{R}$.

Example. The unitary group $\mathcal{U}_T$ is a Lie group, its associated Lie algebra is denoted by $\mathfrak{u}_T$ and it is the set of the skew–Hermitian complex matrices

$$\mathfrak{u}_T = \{\mathbf{A} \in \mathbb{C}^{T\times T} : \ \mathbf{A}^\dagger = -\mathbf{A}\} \tag{3.1}$$

where $\mathbb{C}^{T\times T}$ is the set of the generic $T \times T$ complex matrices. Sum in $\mathfrak{u}_T$ is common matrix sum, while bracket operation is: $[\mathbf{A}_1, \mathbf{A}_2] = \mathbf{A}_1\mathbf{A}_2 - \mathbf{A}_2\mathbf{A}_1$ The exponential map is equal to the classical matrix exponential, defined as

$$e^{\mathbf{A}} = \exp \mathbf{A} = \sum_{n=0}^{\infty} \frac{\mathbf{A}^n}{n!}, \qquad \text{valid for all } \mathbf{A} \in \mathbb{C}^{T\times T} \tag{3.2}$$

and whose most important properties are

$$\exp(-\mathbf{A}) = (\exp \mathbf{A})^{-1} \tag{3.3}$$

$$\exp(\mathbf{A}^\dagger) = (\exp \mathbf{A})^\dagger \tag{3.4}$$

$$\exp(\mathbf{A}_1 + \mathbf{A}_2) = \exp(\mathbf{A}_1)\exp(\mathbf{A}_2) \iff \mathbf{A}_1\mathbf{A}_2 = \mathbf{A}_2\mathbf{A}_1 \tag{3.5}$$

From definition (3.1) and properties (3.3), (3.4) it comes that matrix exponential maps a skew–Hermitian matrix into a unitary matrix

$$\exp : \ \mathfrak{u}_T \ \longrightarrow \ \mathcal{U}_T \, . \tag{3.6}$$

Finally, we recall that if G is a Lie group and H a closed subgroup of G, then G/H has a unique manifold structure and is called homogeneous manifold [70, pag. 120].

3.2 The Grassmann Manifold $G_{T,M}$

3.2.1 The Grassmannian as a Quotient Group

There are many equivalent ways to describe a Grassmannian, one is [4]

Definition 10 *Let $\mathcal{U}_n$ be the unitary group , i.e. the group of the $n \times n$ unitary complex matrices under common matrix multiplication. Let $T > M$ integers, the Grassmannian $G_{T,M} = \mathcal{U}_T/(\mathcal{U}_M \times \mathcal{U}_{T-M})$, i.e. $G_{T,M}$ is the quotient group of $\mathcal{U}_T$ on its subgroup $\mathcal{U}_M \times \mathcal{U}_{T-M}$ and with the operation inherited from $\mathcal{U}_T$.*

ties: the anticommutativity ($[g_1, g_2] = -[g_2, g_1]$, $\forall\, g_1, g_2 \in \mathfrak{g}$) and the Jacobi identity ($[[g_1, g_2], g_3] + [[g_2, g_3], g_1] + [[g_3, g_1], g_2] = 0$, $\forall\, g_1, g_2, g_3 \in \mathfrak{g}$)[70, pag. 84]. Notice that the tangent space of a manifold is a vector space so that when the manifold is a Lie group its tangent space has two more properties.

The previous definition means that a point of the Grassmannian, i.e. a subspace Ω, can be seen as the equivalence class

$$\Omega = \left\{ \mathbf{Q} \begin{bmatrix} \mathbf{Q}_M & \mathbf{0} \\ \mathbf{0} & \mathbf{Q}_{T-M} \end{bmatrix} : \mathbf{Q} \in \mathcal{U}_T \, , \, \mathbf{Q}_M \in \mathcal{U}_M \, , \, \mathbf{Q}_{T-M} \in \mathcal{Q}_{T-M} \right\} . \tag{3.7}$$

Write $\mathbf{Q}$ in block form, separating the first M columns

$$\mathbf{Q} = [\mathbf{X} \; \mathbf{X}^{\perp}] \, , \qquad \mathbf{X}^{\dagger}\mathbf{X} = \mathbf{I}_M \, , \; (\mathbf{X}^{\perp})^{\dagger}\mathbf{X}^{\perp} = \mathbf{I}_{T-M} \, , \; \mathbf{X}^{\dagger}\mathbf{X}^{\perp} = \mathbf{0} \, . \tag{3.8}$$

The subspace Ω in (3.7) coincides with the subspace spanned by the columns of $\mathbf{X}$. The columns of $\mathbf{X}^{\perp}$ spans $\Omega^{\perp}$, the orthogonal complement of Ω, i.e. the *unique* subspace orthogonal to Ω completing vector space $\mathbb{C}^T$: $\Omega \oplus \Omega^{\perp} = \mathbb{C}^T$ ($\oplus$ is subspace direct sum) [72]. Because of this fact it is totally equivalent to represent a point $\Omega \in G_{T,M}$ with $\mathbf{Q}$, the subspace spanned by $\mathbf{X}$ or its orthogonal complement $\mathbf{X}^{\perp}$, if (3.8) is valid.

The quotient operation on $\mathcal{U}_M \times \mathcal{U}_{T-M}$ means that arbitrary rotations, internal to basis $\mathbf{X}$ and, separatetly, to $\mathbf{X}^{\perp}$, do not change the subspace and its orthogonal complement (see also the explication given in Sect. 2.3.1). These rotations are completely different from rotations in $\mathbb{C}^T$. Rotations in $\mathbb{C}^T$, represented by left unitary matrices, map a subspace to another and hence they obtain a different point of the Grassmannian.

3.2.2 The Grassmannian as a Differentiable Manifold

Since $\mathcal{U}_T$ and $\mathcal{U}_M \times \mathcal{U}_{T-M}$ are closed Lie groups, the Grassmannian is a *homogeneous C^{∞} differentiable manifold*. The Grassmannian $G_{T,M}$ can be imagined as a closed surface imbedded in a higher dimensional space, for example $\mathbb{C}^{T \times M}$, the vector space of $T \times M$ complex matrices, which is isomorphic to $\mathbb{C}^{TM}$ and has $2TM$ real dimensions. The Grassmannian is a compact manifold and has a finite volume [30].

The dimension of the Grassmannian $G_{T,M}$ is [30]

$$\dim G_{T,M} = M(T-M) \text{ complex dimensions } \iff 2M(T-M) \text{ real dimensions.} \tag{3.9}$$

This can be easily calculated by noticing that a $T \times M$ complex matrix $\mathbf{X}$ with orthogonal columns has $2TM - M^2$ real degrees of freedom (because condition $\mathbf{X}^{\dagger}\mathbf{X} = \mathbf{I}_M$ sets M^2 real constraints). Moreover, the quotient operation imposes a constraint over other M^2 real degrees of freeedom, so that (3.9) is obtained.

3.2.3 Tangent Spaces of $G_{T,M}$

We follow here the derivation in [4]. To define a tangent space, we need to consider the Grassmannian embedded in a higher dimensional space. We choose $\mathbb{C}^{TM}$ with its classical metric, even if other choices are possible [4], [14]. A point in $G_{T,M}$ is defined as an equivalence class (3.7) so that its representation through a unitary matrix is not unique.The representation in the tangent space is likewise not unique: there are many skew–Hermitian matrices which correspond to the same point in the Grassmannian. Skew–Hermitian matrices vector space $\mathfrak{u}_T$ can be split into two components, the

vertical space and the horizontal space (as called in [4]), respectively assuming the form

$$\begin{bmatrix} \mathbf{A}_{11} & \mathbf{0} \\ \mathbf{0} & \mathbf{A}_{22} \end{bmatrix},\ \mathbf{A}_{11} \in \mathfrak{u}_M,\ \mathbf{A}_{22} \in \mathfrak{u}_{T-M}\,, \qquad \begin{bmatrix} \mathbf{0}_M & -\mathbf{B}^\dagger \\ \mathbf{B} & \mathbf{0}_{T-M} \end{bmatrix},\ \mathbf{B} \in \mathbb{C}^{(T-M)\times M}\,.$$

Points in the vertical space correspond to different representatives of the same equivalence class on the Grassmannian, while points in the horizontal space correspond to different points on the Grassmannian. Hence, we will only consider the horizontal space and we will refer to it as the tangent space, in order to simplify the notation.

Fixed a point $\Omega_{\mathbf{X}} \in G_{T,M}$, represented by a unitary matrix $\mathbf{Q}_X$, as in (3.8), a point on the tangent space at $\mathbf{Q}_X$, denoted by $t\pi_{\mathbf{Q}_X}$ or $t\pi_{\Omega_{\mathbf{X}}}$, can be represented as [4]

$$\boldsymbol{\Delta}_Y = \mathbf{Q}_X \begin{bmatrix} \mathbf{0} & -\mathbf{B}_Y^\dagger \\ \mathbf{B}_Y & \mathbf{0} \end{bmatrix}, \qquad \mathbf{B}_Y \in \mathbb{C}^{(T-M)\times M}\,. \tag{3.10}$$

We observe that the real dimension of (3.10) is $2M(T-M)$, which coincides with the dimension of the Grassmannian, as it is supposed to be.

Fixed the tangent space at $\Omega_{\mathbf{X}}$, the *canonical metric* can be introduced [4]. According to this metric, the inner product of two points, defined as in (3.10), is

$$\langle \boldsymbol{\Delta}_1, \boldsymbol{\Delta}_2 \rangle = \frac{1}{2}\mathrm{tr}\{\boldsymbol{\Delta}_1^\dagger \boldsymbol{\Delta}_2\} = \frac{1}{2}\mathrm{tr}\left\{ \begin{bmatrix} \mathbf{B}_1\mathbf{B}_2^\dagger & \mathbf{0} \\ \mathbf{0} & \mathbf{B}_1^\dagger\mathbf{B}_2 \end{bmatrix} \right\} = \mathrm{Re}\left(\mathrm{tr}\{\mathbf{B}_1^\dagger\mathbf{B}_2\}\right) \tag{3.11}$$

which induces a norm proportional to the Frobenius norm of $\mathbf{B}$

$$\langle \boldsymbol{\Delta}, \boldsymbol{\Delta} \rangle = \frac{1}{2}\|\boldsymbol{\Delta}\|_F^2 = \|\mathbf{B}\|_F^2\,. \tag{3.12}$$

3.2.4 The Exponential Map

The exponential map $\exp : t\pi_{\Omega_X} \to G_{T,M}$ maps one point of the tangent space $t\pi_{\Omega_X}$ to a subspace in the following way [4]

$$\mathbf{Q}_Y = [\mathbf{Y}\ \mathbf{Y}^\perp] = \mathbf{Q}_X \exp \begin{bmatrix} \mathbf{0}_M & -\mathbf{B}_Y^\dagger \\ \mathbf{B}_Y & \mathbf{0}_{T-M} \end{bmatrix}, \qquad \mathbf{B}_Y \in \mathbb{C}^{(T-M)\times M} \tag{3.13}$$

which is a representative of $\Omega_{\mathbf{Y}} = \mathrm{span}(\mathbf{Y})$. We notice that if $\mathbf{B}_Y = \mathbf{0}$ in (3.13), then $\mathbf{Q}_Y = \mathbf{Q}_X$, i.e. the null matrix in the tangent space corresponds to the tangent point on $G_{T,M}$. This also corresponds to the physical intuition according to which a point passing through $\Omega_{\mathbf{X}}$ with a null velocity cannot leave the point. Moreover, the geodesic which starts from $\mathbf{Q}_X$ with velocity $\boldsymbol{\Delta}_Y$ is the curve [4]

$$\mathbf{Q}_Y(t) = \mathbf{Q}_X \exp\left\{ t \begin{bmatrix} \mathbf{0} & -\mathbf{B}^\dagger \\ \mathbf{B} & \mathbf{0} \end{bmatrix} \right\}. \tag{3.14}$$

Hence, the subspace $\Omega_{\mathbf{Y}}$ (3.13) can also be interpreted as the point of $G_{T,M}$ along the geodesic starting from $\Omega_{\mathbf{X}}$ reached at time $t = 1$ and having velocity $\boldsymbol{\Delta}_Y$ at $\Omega_{\mathbf{X}}$.

Representation (3.13) is redundant, we will also use matrix $\mathbf{Y}$, being given by the first M columns of (3.13)

$$\mathbf{Y} = \mathbf{Q}_X \exp \begin{bmatrix} \mathbf{0}_M & -\mathbf{B}_Y^\dagger \\ \mathbf{B}_Y & \mathbf{0}_{T-M} \end{bmatrix} \begin{bmatrix} \mathbf{I}_M \\ \mathbf{0}_{T-M,M} \end{bmatrix} = \mathbf{Q}_X \exp(\mathbf{\Delta}_Y) \mathbf{I}_{T,M} \,. \tag{3.15}$$

This representation is also used in our proposed codes.

In the following, we will fix a reference point of $G_{T,M}$, called *reference subspace* and we will consider the tangent space at that point. Our choice is

$$\mathbf{Q}_{ref} = [\mathbf{X}_{ref}\ \mathbf{X}_{ref}^\perp] = \mathbf{I}_T \,, \qquad \mathbf{X}_{ref} = \begin{bmatrix} \mathbf{I}_M \\ \mathbf{0}_{T-M,M} \end{bmatrix} = \mathbf{I}_{T,M} \,. \tag{3.16}$$

This choice is fully arbitrary and does not influence code properties, but the notation in many expression is simplified. The tangent space at the reference point will be called sometimes simply tangent space when no confusion can be made and will be denoted by $t\pi_{ref}$.

3.2.5 The Cosine–Sine (CS) Decomposition

In this subsection we present a particular decomposition which is very useful to understand the geometry of the exponential parametrization and to link parameters of the points on the tangent space to the parameters of the unitary matrices, which represent subspaces on the Grassmannian. Moreover, this decomposition supplies an efficient way to calculate the unitary matrices so that it is extremely useful for the practical implementation of the code.

Let us suppose that $T \geq 2M$. If this is not the case, i.e. if $M < T < 2M$, the following development can be done on the Grassmannian $G_{T,T-M}$. Take the TSVD of $\mathbf{B}$ as in (2.15), [3, pag. 72] which we restate for clearity

$$\mathbf{B} = \mathbf{V}\,\mathbf{\Theta}\,\mathbf{U}^\dagger \,, \qquad \mathbf{V} \in \mathcal{U}_{T,M},\ \mathbf{U} \in \mathcal{U}_M,\ \mathbf{\Theta} = \mathrm{diag}([\theta_1\ \ldots\ \theta_{\mathrm{M}}]) \tag{3.17}$$

with $0 \leq \theta_1 \leq \theta_2 \leq \ldots \leq \theta_M$ and let $\mathbf{V}_1$ an arbitrary $T \times (T-2M)$ matrix with orthonormal columns so that $[\mathbf{V}\ \mathbf{V}_1] \in \mathcal{U}_T$. Then we can write

$$\mathbf{\Delta}_Y = \mathbf{Q}_X \begin{bmatrix} \mathbf{0} & -\mathbf{B}^\dagger \\ \mathbf{B} & \mathbf{0} \end{bmatrix} = \mathbf{Q}_X \begin{bmatrix} \mathbf{U} & \mathbf{0} & \mathbf{0} \\ \mathbf{0} & \mathbf{V} & \mathbf{V}_1 \end{bmatrix} \begin{bmatrix} \mathbf{0} & -\mathbf{\Theta} & \mathbf{0} \\ \mathbf{\Theta} & \mathbf{0} & \mathbf{0} \\ \mathbf{0} & \mathbf{0} & \mathbf{0} \end{bmatrix} \begin{bmatrix} \mathbf{U}^\dagger & \mathbf{0} \\ \mathbf{0} & \mathbf{V}^\dagger \\ \mathbf{0} & \mathbf{V}_1^\dagger \end{bmatrix} \tag{3.18}$$

where some matrices can have zero size if $T = 2M$. Hence, by applying (3.2) we obtain

$$\begin{aligned} \mathbf{Q}_Y = [\mathbf{Y}\ \mathbf{Y}^\perp] &= \mathbf{Q}_X \exp \begin{bmatrix} \mathbf{0} & -\mathbf{B}^\dagger \\ \mathbf{B} & \mathbf{0} \end{bmatrix} \\ &= \mathbf{Q}_X \begin{bmatrix} \mathbf{U} & \mathbf{0} & \mathbf{0} \\ \mathbf{0} & \mathbf{V} & \mathbf{V}_1 \end{bmatrix} \begin{bmatrix} \mathbf{C} & -\mathbf{S} & \mathbf{0} \\ \mathbf{S} & \mathbf{C} & \mathbf{0} \\ \mathbf{0} & \mathbf{0} & \mathbf{I}_{T-2M} \end{bmatrix} \begin{bmatrix} \mathbf{U}^\dagger & \mathbf{0} \\ \mathbf{0} & \mathbf{V}^\dagger \\ \mathbf{0} & \mathbf{V}_1^\dagger \end{bmatrix} \end{aligned} \tag{3.19}$$

The above expression is the Cosine–Sine (CS) form of matrix $\mathbf{Q}_Y$, which represents a subspace with tangent vector $\mathbf{\Delta}_Y$ in tangent space $t\pi_{\Omega_\mathbf{X}}$ at point $\mathbf{Q}_Y$.

By taking the first M columns of (3.19), we obtain the CS form of (3.15)

$$\mathbf{Y} = \mathbf{Q}_X \begin{bmatrix} \mathbf{UC} \\ \mathbf{VS} \end{bmatrix} \mathbf{U}^\dagger \,, \qquad \mathbf{C} = \cos \mathbf{\Theta} \,,\ \mathbf{S} = \sin \mathbf{\Theta} \tag{3.20}$$

The singular values of $\mathbf{B}$*, collected in* $\mathbf{\Theta}$*, are the principal angles between* $\Omega_\mathbf{Y}$ *and* $\Omega_\mathbf{X}$. This can be easily verified by calculating $\mathbf{X}^\dagger\mathbf{Y}$ from (3.20) and by applying considerations of Sect. 2.3.2, namely (2.21).

3.3 Code Structure

In this section we investigate the structure of the coder we propose to build unitary non–coherent space–time (ST) codes for $T \geq 2M$ [22], [21].

The main idea is to obtain a non–coherent unitary (ST) code $\mathcal{C}$ from a coherent space–time block (STB) code $\mathcal{B}$. Let's imbeed $\mathcal{B}$ into the tangent space (of the reference point) and then map it to the Grassmannian $G_{T,M}$ via the exponential map (see Fig. 3.4). Codes $\mathcal{C}$ obtained via exponential parameterization are called EP codes in this work. An EP code $\mathcal{C}$ obtained from coherent code $\mathcal{B}$ is denoted by $\mathcal{C}_\mathcal{B}$. A block diagram of the coding and transmit chain si shown in Fig. 3.3. This approach has one point in common with the training–based approach [27], [26]: in both cases a coherent STB code is used to obtain a non–coherent code.

We hope that by choosing a good coherent STB code we can generate a good non–coherent STB code. Besides, if the parameters of the coherent STB code can be controlled (see for example [27], [32]), we hope to control the parameters of the non–coherent STB code, at least partially. Another important point is the decoding algorithm: the the coherent STB has sufficient algebric structure to have a simplified decoding algorithm, we would like to exploit the knowledge. However, before coping with this problem, many questions on the coding process must be answered: under what conditions the exponential mapping is well–defined and maps a coherent codebook to a non–coherent codebook? Is there a relationship among codeword distances of coherent and non–coherent codes? Is diversity maintained by the exponential map? and what kind of diversity?

In this section we use the reference subspace defined in (3.16).

3.3.1 Exponential Map Inverse

Generally the exponential map is not a bijective function, some constraints must be imposed to make it invertible. It is possible in fact to find a neighborhood[4] of $\mathbf{0}$ in $t\pi_{ref}$, and a corresponding neighborhood of Ω_{ref} over the Grassmannian between which the exponential map is invertible.

[4] An open set containing $\mathbf{0}$ in $t\pi_{ref}$.

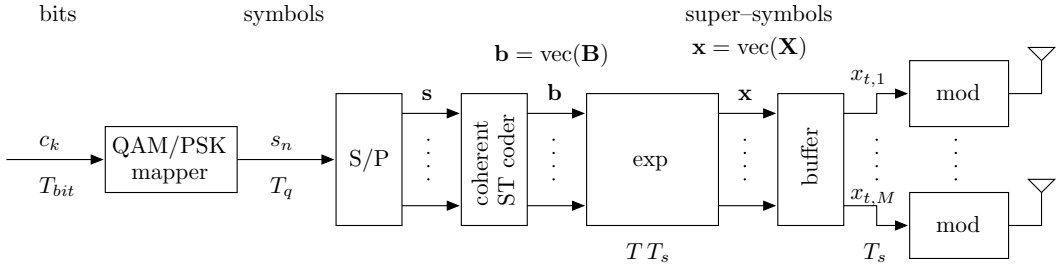

Figure 3.3: Block scheme of the transmit chain.

Proposition 5 *Let $B_{\pi/2}$ the open set of $t\pi_{ref}$ defined as*

$$B_{\pi/2} = \left\{ \mathbf{\Delta} = \begin{bmatrix} \mathbf{0} & -\mathbf{B}^\dagger \\ \mathbf{B} & \mathbf{0} \end{bmatrix} \in t\pi_{ref} : \max_{m=1,\ldots,M}(\theta_m) < \frac{\pi}{2} \right\} \tag{3.21}$$

where θ_m are the singular values of $\mathbf{B}$. Let $G^{\times}_{T,M}$ be the open set defined as

$$G^{\times}_{T,M} = \{\Omega_{\mathbf{X}} \in G_{T,M} : \mathbf{X}^\dagger_{ref}\mathbf{X} \textit{ is full rank}\}\,. \tag{3.22}$$

which is equivalent to state that there is no vectors of $\Omega_{\mathbf{X}} \in G^{\times}_{T,M}$ orthogonal to Ω_{ref}. Then

$$\exp : B_{\pi/2} \subset t\pi_{ref} \longrightarrow G^{\times}_{T,M} \subset G_{T,M} \tag{3.23}$$

is a bijective map.

Proof. This proof is important because it is constructive, we can understand how to invert the map.

We show that the exponential map is *injective*. We want to prove that if $\mathbf{\Delta}_1, \mathbf{\Delta}_2 \in B_{\pi/2}$ and $\exp \mathbf{\Delta}_1 = \exp \mathbf{\Delta}_2$, then $\mathbf{\Delta}_1 = \mathbf{\Delta}_2$, which is equivalent to $\mathbf{B}_1 = \mathbf{B}_2$. Let's write the TSVDs $\mathbf{B}_1 = \mathbf{V}_1\mathbf{\Theta}_1\mathbf{U}_1^\dagger$ and $\mathbf{B}_2 = \mathbf{V}_2\mathbf{\Theta}_2\mathbf{U}_2^\dagger$, with the singular values ordered from the smallest to the largest. From the CS decomposition (3.20) we have

$$\mathbf{X}_1 = \begin{bmatrix} \mathbf{U}_1\mathbf{C}_1 \\ \mathbf{V}_1\mathbf{S}_1 \end{bmatrix} \mathbf{U}_1^\dagger = \begin{bmatrix} \mathbf{U}_2\mathbf{C}_2 \\ \mathbf{V}_2\mathbf{S}_2 \end{bmatrix} \mathbf{U}_2^\dagger = \mathbf{X}_2\,. \tag{3.24}$$

Let's take the first M rows of (3.24)

$$\mathbf{C}_1 = \mathbf{U}\mathbf{C}_2\mathbf{U}^\dagger\,, \qquad \mathbf{U} = \mathbf{U}_1^\dagger\mathbf{U}_2\,.$$

This expression states that $\mathcal{C}_1$ and $\mathcal{C}_2$ are similar and hence they have the same eigenvalues. Hence $\mathbf{C}_1 = \mathbf{C}_2 = \mathbf{C}$, i.e.

$$\cos\theta_{1,m} = \cos\theta_{2,m} = \cos\theta_m \in (0,1] \quad \Longleftrightarrow \quad \theta_{1,m} = \theta_{2,m} = \theta_m \in [0, \pi/2)$$

for $m = 1, \ldots, M$, i.e. $\mathbf{\Theta}_1 = \mathbf{\Theta}_2 = \mathbf{\Theta}$. The above correspondence is one–to–one only if the cosine is constrained to the interval $[0, \pi/2)$, where the cosine is a bijective

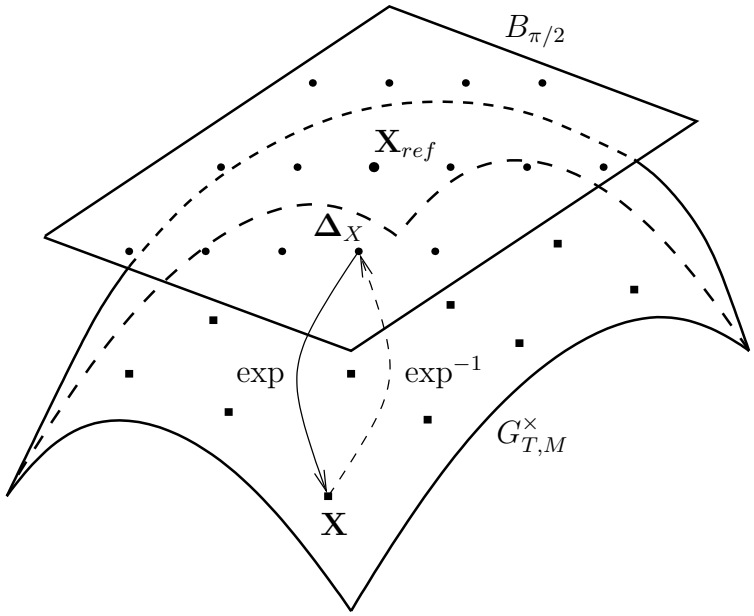

Figure 3.4: The concept of exponential parameterization: a code for coherent systems is imbedded into an open set of the tangent space, so that the exponential map is invertible.

function. For the same reason we can write $\mathbf{S}_1 = \mathbf{S}_2 = \mathbf{S}$. From (3.24), we can write $\mathbf{U}_1\mathbf{\Theta}\mathbf{U}_1^\dagger = \mathbf{U}_2\mathbf{\Theta}\mathbf{U}_2^\dagger$, which do *not* state that $\mathbf{U}_1$ is equal to $\mathbf{U}_2$. In fact, as explained in [68, Lemma 7.3.1], $\mathbf{U}_1 = \mathbf{U}_2\mathbf{D}$ where $\mathbf{D}$ is an block diagonal unitary matrix in which, if the singular value θ_m has multiplicity 1, then the corresponding block in $\mathbf{D}$ is an arbitrary phase factor $e^{i\delta_m}$, while if $\theta_m = \ldots = \theta_{m+r-1}$ has multiplicity r, then the corresponding block in $\mathbf{D}$ is an arbitrary $r \times r$ unitary matrix. To resume, $\mathbf{D}$ assumes the most generic block diagonal form satisfying

$$\mathbf{D}^\dagger\mathbf{\Theta}\mathbf{D} = \mathbf{\Theta}\,. \tag{3.25}$$

If we take care of these remarks, from the last $T - M$ rows of matrix identity (3.24) we have $\mathbf{V}_1\mathbf{S}\mathbf{U}_1^\dagger = \mathbf{V}_2\mathbf{S}\mathbf{D}\mathbf{U}_1^\dagger$. By applying (3.25) and if $\mathbf{S}$ has full rank, we have $\mathbf{V}_1 = \mathbf{V}_2\mathbf{D}$. If $\mathbf{S}$ has not full rank, for instance, the last r singular values are zero, then the last r columns of $\mathbf{V}_1$ and $\mathbf{V}_2$ can be chosen arbitrarily since they will be annihilated, so that we can set $\mathbf{V}_1 = \mathbf{V}_2\mathbf{D}$ in every case. Then, by building the original matrices through the TSVD

$$\mathbf{B}_1 = \mathbf{V}_1\mathbf{\Theta}_1\mathbf{U}_1^\dagger = \mathbf{V}_2\mathbf{D}\mathbf{\Theta}_2\mathbf{D}^\dagger\mathbf{U}_2^\dagger = \mathbf{B}_2$$

and we have proved the thesis.

We show that the exponential map is *surjective*. We must prove $\exp(B_{\pi/2}) = G^{\times}_{T,M}$. Let $\Omega_{\mathbf{X}}$ belong to $G^{\times}_{T,M}$ and let

$$\tilde{\mathbf{X}} = \begin{bmatrix}\tilde{\mathbf{X}}_1 \\ \tilde{\mathbf{X}}_2\end{bmatrix}\,, \qquad \tilde{\mathbf{X}}_1 \in \mathbb{C}^{M\times M}\,,\ \ \tilde{\mathbf{X}}_2 \in \mathbb{C}^{(T-M)\times M} \tag{3.26}$$

be one of its orthonormal bases. Let's apply the following algorithm

1. Calculate the SVD of $\tilde{\mathbf{X}}_1$: $\tilde{\mathbf{X}}_1 = \mathbf{U}\mathbf{C}\tilde{\mathbf{U}}^\dagger$
2. Calculate $\mathbf{X} = \tilde{\mathbf{X}}\tilde{\mathbf{U}}\mathbf{U}^\dagger$.

Since $\tilde{\mathbf{U}}\mathbf{U}^\dagger$ is a unitary matrix, $\mathbf{X}$ is another basis for $\Omega_{\mathbf{X}}$. Moreover $\mathbf{X}$ is a CS decomposition like in (3.20), because $\mathbf{X}_{ref} = \mathbf{I}_{T,M}$ and $\mathbf{C}$ has full rank since $\mathbf{X}_{ref}\tilde{\mathbf{X}} = \tilde{\mathbf{X}}_1$ is full rank by hypothesis. A point $\mathbf{\Delta} \in B_{\pi/2}$, in particular the associated matrix $\mathbf{B}$, can be built following next algorithm

1. Consider basis $\mathbf{X}^\dagger = [\mathbf{X}_1^\dagger\ \mathbf{X}_2^\dagger]$, where $\mathbf{X}_1$ is the upper $M \times M$ block and $\mathbf{X}_2$ is the lower $(T-M) \times M$ block.
2. Calculate the TSVD of $\mathbf{X}_2$, say $\mathbf{X}_2 = \mathbf{V}\mathbf{S}\mathbf{U}^\dagger$, the diagonal entries of the diagonal matrix $\mathbf{S}$ are non–negative (by definition of TSVD) and less than one (due to the fact $\mathbf{X}^\dagger\mathbf{X} = \mathbf{I}_M$).
3. Calculate $\mathbf{\Theta} = \sin^{-1}(\mathbf{S})$, the diagonal matrix $\mathbf{\Theta}$ has entries $\theta_m \in [0, \pi/2)$, for all $m = 1, \ldots, M$.
4. Build the matrix $\mathbf{B} = \mathbf{V}\,\mathbf{\Theta}\,\mathbf{U}^\dagger$.

The matrix $\mathbf{\Delta}$ built with this $\mathbf{B}$ satisfies (3.21) and it gives the basis $\mathbf{X}$ in $G^{\times}_{T,M}$. Hence, we have the thesis. □

Proposition 5 clearly sets a condition to assure an invertible exponential map (this condition was already present in [21], here we gave a formal proof). The inverse exponential map, denoted by $\exp^{-1}$, (see Fig. 3.4) can be operationally calculated with the algorithm presented in the proof of Proposition 5 and which can be summarized as the reduction into CS form of a generic orthonormal basis followed by the calculation of a TSVD on the lower part of this reduced matrix.

3.3.2 Relationships between Coherent Codes and their Corresponding EP Codes

Let $\mathcal{B}'$ a coherent code we use to build a non–coherent EP code $\mathcal{C}$, as in Fig. 3.4. Codewords of $\mathcal{B}'$ can generally generate directions $\mathbf{\Delta}$ lying outside the set $B_{\pi/2}$, in which the exponential map is invertible. To assure that the whole coherent code is contained inside $B_{\pi/2}$, we follow the approach of [22], where a positive homothetic factor α is used to scale the coherent code $\mathbf{B}'$ in order to obtain another coherent code

$$\mathcal{B} = \alpha\mathcal{B}' = \{\mathbf{B} = \alpha\mathbf{B}',\ \forall\, \mathbf{B}' \in \mathcal{B}'\} \tag{3.27}$$

whose codewords belong to $B_{\pi/2}$. We recall that if a matrix is multiplicated by a positive scalar, then the singular values of the product are simply scaled by the same factor: $\theta_m = \alpha\theta'_m$, where θ_m and θ'_m are the singular values of respectively $\mathbf{B}$ and $\mathbf{B}'$

(see [68, pag. 418]). Moreover a multiplication by a positive scalar does not change the range of the matrices, so that the diversity order of a coherent code is maintained

$$d^{co-ML}(\mathcal{B}) = d^{co-ML}(\mathcal{B}') \,. \tag{3.28}$$

In the following, if not otherwise stated, we suppose that the code $\mathcal{B}$ and $\mathcal{C}$ are well–defined, that is, the exponential map is invertible.

Let's consider a generic codeword $\mathbf{B} \in \mathcal{B}$ and the corresponding $\mathbf{X} \in \mathcal{C}$ obtained via exponential parameterization (3.20). If $\mathbf{B} = \mathbf{V}\,\mathbf{\Theta}\,\mathbf{U}^{\dagger}$, then, as recalled in Sect. 3.2.5 and [21], its singular values θ_m are the principal angles between the reference space $\mathbf{X}_{ref}$ and the subspace generated by $\mathbf{X}$. To scale the codewords by α multiplies by the same factor α all the principal angles. Summarizing

$$d_p(\mathbf{X}, \mathbf{X}_{ref}) = |\sin(\mathbf{\Theta})|^{\frac{1}{M}} = |\sin(\mathbf{B}^{\dagger}\mathbf{B})|^{\frac{1}{2M}} \tag{3.29}$$

and the relationship with the singular values of the codewords in $\mathbf{B}'$ is

$$d_p(\mathbf{X}, \mathbf{X}_{ref}) = \alpha|\sin(\mathbf{\Theta}')|^{\frac{1}{M}} = \alpha|\sin(\mathbf{B}'^{\dagger}\mathbf{B}')|^{\frac{1}{2M}} \,. \tag{3.30}$$

The dimension of the intersection between the reference space and $\mathbf{X}$ is given by $M - \mathrm{rank}(\mathbf{B})$, i.e. by the number of null principal angles. Eventually, we have a rich geometrical characterization of the non–coherent code with respect to the reference space.

Unfortunately, the above considerations do not completely characterize the non–coherent code $\mathcal{C}$ with respect to the code $\mathcal{B}$. What we are really interested in is, for example:

- The distribution of the principal angles between different codewords of $\mathcal{C}$ and the way to control them via the coherent code $\mathcal{B}$.
- The relationship between the diversity of $\mathcal{B}$ and the diversity of $\mathcal{C}$.

These points were not cleared up in [21], where a conjecture was formulated, which we restate in a more explicit form:

Conjecture 1 *If a coherent code $\mathcal{B}$ has fully diversity, then the corresponding non–coherent code $\mathcal{C}$ obtained via exponential parameterization, achieves the same diversity gain.*

We managed to find general assumptions under which this conjecture is true. We also get interesting insights into the relationship between training–based codes and EP codes obtained from the same coherent code $\mathcal{B}$. Further details can be found in the following subsection.

A first asymptotic argument (on small principal angles with respect to Ω_{ref}) let the reader understand the hidden relationship between training–based codes and EP codes.

Let homothetic factor α run to zero. Then, if $\mathbf{B} = \mathbf{V}(\alpha\mathbf{\Theta}')\mathbf{U}^{\dagger}$, we have

$$\mathbf{C} = \cos(\alpha\mathbf{\Theta}') \simeq \mathbf{I}_M \,, \qquad \mathbf{S} = \sin(\alpha\mathbf{\Theta}') \simeq \alpha\mathbf{\Theta}'$$

and hence the CS form (3.20) of the codewords $\mathbf{X}$ is

$$\mathbf{X} \simeq \begin{bmatrix} \mathbf{I}_M \\ \alpha \mathbf{B}' \end{bmatrix} , \tag{3.31}$$

which looks like a training–based code! Transmit power is almost completely allocated to the training phase. Anyway, through Proposition 3 we can see that EP code diversity is equal to $\mathcal{B}'$ diversity, *if the detection is made as in* (2.65), (2.66) (not with the non–coherent ML criterion or the GLRT) [26].

3.3.3 EP Code Diversity

We state the following

Theorem 1 *Let $\mathcal{C}_{\mathcal{B}}$ be an EP code obtained from the coherent code $\mathcal{B} = \alpha\mathcal{B}'$. Suppose that the diversity of $\mathcal{B}'$ is $d^{co-ML}(\mathcal{B}') = d$. Denote by $\theta'_{k,1} \geq \ldots \geq \theta'_{k,M} \geq 0$ the singular values of $\mathbf{B}'_k$ and define $\theta'_{max} = \max_k \|\mathbf{B}'\|_2 = \max_k \theta'_{k,1}$. Denote also by $\sigma_d(k,l)$ the d–th singular values (in decreasing order) of $\mathbf{B}'_k - \mathbf{B}'_l$ with $k \neq l$. Under the condition*

$$0 < \alpha < \bar{\alpha} , \qquad \bar{\alpha} = \min \left\{ \frac{\pi}{2\,\theta'_{max}}, \hat{\alpha}_d \right\} , \qquad \hat{\alpha}_d = \min_{k \neq l} \alpha_d(k,l) \tag{3.32}$$

where

$$\alpha_d(k,l) \text{ is the solution of } \tan(\alpha\theta'_{k,1}) + \tan(\alpha\theta'_{l,1}) - \alpha(\theta'_{k,1} + \theta'_{l,1}) = \alpha\sigma'_d(k,l) \tag{3.33}$$

we have

$$d^{GLRT}(\mathcal{C}_{\mathcal{B}}) \geq d^{co-ML}(\mathcal{B}) = d^{co-ML}(\mathcal{B}') . \tag{3.34}$$

Proof. Let us suppose that the codewords of $\mathcal{B} = \alpha\mathcal{B}'$ and $\mathcal{B}'$ have TSVD

$$\mathbf{B}_k = \mathbf{V}_k \mathbf{\Theta}_k \mathbf{U}_k^{\dagger} , \qquad \mathbf{B}'_k = \mathbf{V}_k \mathbf{\Theta}'_k \mathbf{U}_k^{\dagger} , \qquad \mathbf{\Theta}_k = \alpha \mathbf{\Theta'}_k \tag{3.35}$$

where $\theta_{k,1} \geq \theta_{k,2} \geq \ldots \geq \theta_{k,M} \geq 0$. Let $\mathbf{X}_k$, $\mathbf{X}_l \in \mathcal{C}_{\mathcal{B}} \subset G^{\times}_{T,M}$ be in the CS form (3.20). From the definition of diversity with GLRT detection (2.49)

$$\begin{aligned} d^{GLRT}(\mathcal{C}_{\mathcal{B}}) &= \min_{k \neq l} \left\{ \text{rank}([\mathbf{X}_k \; \mathbf{X}_l]) \right\} - M \\ &= \min_{k \neq l} \left\{ \text{rank} \left([\mathbf{X}_k \; \mathbf{X}_l] \begin{bmatrix} \mathbf{U}_k \mathbf{C}_k^{-1} \mathbf{U}_k^{\dagger} & \mathbf{0}_M \\ \mathbf{0}_M & \mathbf{U}_l \mathbf{C}_l^{-1} \mathbf{U}_l^{\dagger} \end{bmatrix} \right) \right\} - M \qquad (3.36) \\ &= \min_{k \neq l} \left\{ \text{rank} \begin{bmatrix} \mathbf{I}_M & \mathbf{I}_M \\ \mathbf{V}_k \mathbf{T}_k \mathbf{U}_k^{\dagger} & \mathbf{V}_l \mathbf{T}_l \mathbf{U}_l^{\dagger} \end{bmatrix} \right\} - M , \qquad (3.37) \end{aligned}$$

where (3.36) holds because the $(2M) \times (2M)$ right rotation in (3.36) is always full rank (even when $\mathbf{B}_k$ is not, provided that $\mathbf{B} \subset B_{\pi/2}$ and (3.37) follows from trivial calculations letting

$$\mathbf{T}_k = \tan(\mathbf{\Theta}_k) = \tan(\alpha \mathbf{\Theta}'_k) , \qquad \mathbf{T}_l = \tan(\mathbf{\Theta}_l) = \tan(\alpha \mathbf{\Theta}'_l) . \tag{3.38}$$

Let us define two new coherent codes $\tilde{\mathcal{B}}$ and $\tilde{\mathcal{B}}'$, whose codewords are defined as

$$\tilde{\mathbf{B}}_k = \mathbf{V}_k \mathbf{T}_k \mathbf{U}_k^\dagger \,, \qquad \tilde{\mathbf{B}}'_k = \mathbf{V}_k \tan(\mathbf{Theta}'_k) \mathbf{U}_k^\dagger \,. \tag{3.39}$$

We rewrite (3.37) introducing the new codewords

$$\begin{aligned} d^{GLRT}(\mathcal{C}_{\mathcal{B}}) &= \min_{k \neq l} \left\{ \operatorname{rank} \begin{bmatrix} \mathbf{I}_M & \mathbf{I}_M \\ \tilde{\mathbf{B}}_k & \tilde{\mathbf{B}}_l \end{bmatrix} \right\} - M \\ &= \min_{k \neq l} \left\{ \operatorname{rank}(\mathbf{I}_M) + \operatorname{rank}(\tilde{\mathbf{B}}_k - \tilde{\mathbf{B}}_l) \right\} - M \qquad (3.40) \\ &= \min_{k \neq l} \operatorname{rank}(\tilde{\mathbf{B}}_k - \tilde{\mathbf{B}}_l) = d^{co-ML}(\tilde{\mathcal{B}}) \,, \qquad (3.41) \end{aligned}$$

where (3.40) follows by basic rank identities (see for example [29]) and (3.41) by Definition 7.

To conclude our proof, we have to understand the relationship between the diversity of coherent codes $\mathcal{B}$ and $\tilde{\mathcal{B}}$. Let $\sigma_1(k,l) \geq \sigma_2(k,l) \geq \ldots \geq \sigma_M(k,l) \geq 0$ be the singular values of matrix $(\mathbf{B}_k - \mathbf{B}_l)$ and let $\tau_1(k,l) \geq \tau_2(k,l) \geq \ldots \geq \tau_M(k,l) \geq 0$ be the singular values of matrix $(\tilde{\mathbf{B}}_k - \tilde{\mathbf{B}}_l)$. Also recall that $\sigma_m(k,l) = \alpha \sigma'_m(k,l)$, where $\sigma'_m(k,l)$ is the generic singular value of $(\mathbf{B}'_k - \mathbf{B}'_l)$. From Corollary 7.3.8 in [68, pag. 419] about the perturbation of the singular values of a matrix, we have

$$|\tau_m(k,l) - \sigma_m(k,l)| \leq \|(\tilde{\mathbf{B}}_k - \tilde{\mathbf{B}}_l) - (\mathbf{B}_k - \mathbf{B}_l)\|_2 \,, \qquad m = 1, \ldots, M \tag{3.42}$$

Codewords of $\tilde{\mathcal{B}}$ have the same unitary matrices in the TSVD, therefore the spectral norm in (3.42) can be written as

$$\|\mathbf{V}_k (\tan \mathbf{\Theta}_k - \mathbf{\Theta}_k) \mathbf{U}_k^\dagger - \mathbf{V}_l (\tan \mathbf{\Theta}_l - \mathbf{\Theta}_l) \mathbf{U}_l^\dagger\|_2 \,. \tag{3.43}$$

Since function $f(x) = \tan x - x$ is non–negative and increasing in the range of interest $x \in [0, \pi/2)$, two TSVD are defined in (3.43). Hence

$$\begin{aligned} &\|\mathbf{V}_k f(\mathbf{\Theta}_k) \mathbf{U}_k^\dagger - \mathbf{V}_l f(\mathbf{\Theta}_l) \mathbf{U}_l^\dagger\|_2 \leq \\ &\qquad \leq \|\mathbf{V}_k f(\mathbf{\Theta}_k) \mathbf{U}_k^\dagger\|_2 + \|\mathbf{V}_l f(\mathbf{\Theta}_l) \mathbf{U}_l^\dagger\|_2 = f(\theta_{k,1}) + f(\theta_{l,1}) \,, \qquad (3.44) \end{aligned}$$

where the last passage comes from definition of spectral norm $\|\cdot\|_2$ in (2.74). Restate the inequality, by using (3.35) and writing the dependence of $\sigma_m(k,l)$ on α, we have

$$|\tau_m(k,l) - \alpha \sigma'_m(k,l)| \leq f(\theta_{k,1}) + f(\theta_{l,1}) = f(\alpha \theta'_{k,1}) + f(\alpha \theta'_{l,1}) \,. \tag{3.45}$$

To assure that the perturbation satisfies (3.45) we must impose (see Fig. 3.5)

$$\alpha \sigma'_m(k,l) > f(\alpha \theta'_{k,1}) + f(\alpha \theta'_{l,1}) \tag{3.46}$$

which is satisfied for all α

$$\alpha \in (0, \hat{\alpha}_m(k,l)) \,, \qquad \hat{\alpha}_m(k,l) : f(\alpha \theta'_{k,1}) + f(\alpha \theta'_{l,1}) - \alpha \sigma'_m(k,l) = 0 \tag{3.47}$$

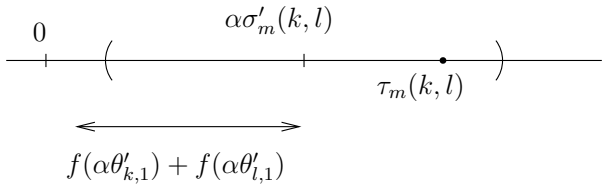

Figure 3.5: Graphical interpretation of condition (3.45).

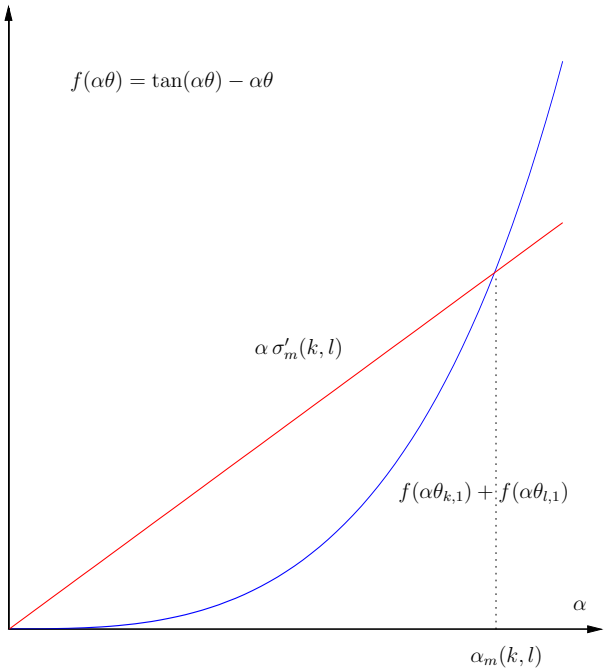

Figure 3.6: Graphical interpretation of equation (3.47).

We notice that the solution of equation in (3.47) always exists, is unique and different from 0 when $\sigma'_m(k,l) \neq 0$. This is because $f(\alpha\theta'_{k,1}) + f(\alpha\theta'_{l,1})$ is an increasing monotonic function with an asymptote at $\pi/(2\max\{\theta'_{k,1}, \theta'_{l,1}\})$ and a null derivate at zero (see Fig. 3.6).

Now, suppose that code $\mathcal{B}'$ has diversity d. This means that for all couples of codewords $\sigma'_1(k,l) \geq \ldots \geq \sigma'_{k,l} > 0$. If α is chosen to satisfy

$$0 < \alpha < \bar{\alpha}_d\,, \qquad \alpha_d = \min_{k \neq l} \alpha_d(k,l) \tag{3.48}$$

we are sure that $\tau_1(k,l) \geq \ldots \geq \tau_d(k,l) > 0$, for all $k \neq l$. Therefore diversity of $\tilde{\mathcal{B}}$ is equal to the diversity of $\mathcal{B}'$ at least, which coincides with the one of $\mathcal{B}$. α must be chosen also in order to satisfy $\mathcal{B} \subset B_{\pi/2}$, therefore conditions (3.32), (3.33) are found. This concludes the proof. □

From the previous theorem it immediately follows

Corollary 1 *With the same notation and hypotheses of Theorem 1 if $T \geq 2M$ and $\mathcal{B}$ has full diversity, $d^{co-ML}(\mathcal{B}) = M$, then EP code $\mathcal{C}_{\mathcal{B}}$ has full diversity.*

This proves Conjecture 1.

Remark 1. During the proof of Theorem 1, we showed that $d^{co-ML}(\tilde{\mathcal{B}}) \geq d^{co-ML}(\mathcal{B})$. Hence, training code $\mathcal{T}_{\tilde{\mathcal{B}}}$, built from $\tilde{\mathcal{B}}$, has at least equal diversity of training code $\mathcal{T}_{\mathcal{B}}$, built from $\mathcal{B}$ (see Proposition 3).

$$d^{co-ML}(\tilde{\mathcal{B}}) \geq d^{co-ML}(\mathcal{B}) \quad \Longrightarrow \quad d^{E-D}(\mathcal{T}_{\tilde{\mathcal{B}}}) \geq d^{E-D}(\mathcal{T}_{\mathcal{B}})\,.$$

Moreover, from (3.41) and Proposition 3 we can argue the following

Corollary 2 *Under the same hypothesis of Theorem 1*

$$d^{GLRT}(\mathcal{C}_{\mathcal{B}}) = d^{E-D}(\mathcal{T}_{\tilde{\mathcal{B}}}) \geq d^{E-D}(\mathcal{T}_{\mathcal{B}}) = d^{E-D}(\mathcal{T}_{\mathcal{B}'}) \tag{3.49}$$

This does not necessarily mean that EP codes have better performances than training–based codes, since code gain and distance distribution are not determined here.

Remark 2. About the fact: $d^{co-ML}(\tilde{\mathcal{B}}) \geq d^{co-ML}(\mathcal{B})$, under hypotheses of Theorem 1. Suppose for instance that $\sigma_M(k,l) = 0 = \sigma'_M(k,l)$. (3.45) claims simply that $|\tau_M(k,l)| \leq f(\theta_{k,1}) + f(\theta_{l,1}) = f(\alpha\theta'_{k,1}) + f(\alpha\theta'_{l,1})$, i.e. $\tau_M(k,l)$ is not forced to zero. On the contrary, since the perturbation depends in a complicate way on codeword entries, it is highly probable that $\tau_M(k,l) \neq 0$, for a fixed α. We have verified this phenomenon through simulations: from coherent codes without full diversity we obtained EP codes with full diversity, even if they have small minimum product distance.

Remark 3. From (3.36) and (2.43), the PEP of code $\mathcal{T}_{\tilde{\mathcal{B}}}$ can be obtained (with GLRT). By calling $\mathbf{R}_{\mathcal{T}}$ and $\mathbf{R}_{\mathcal{C}}$ the matrices (2.51) corresponding to codes $\mathcal{T}_{\tilde{\mathcal{B}}}$ and $\mathcal{C}_{\mathcal{B}}$, we have $|\mathbf{R}_{\mathcal{C}}| = |\mathbf{R}_{\mathcal{T}}||\mathbf{C}_k|^2|\mathbf{C}_l|^2$. Therefore, by using determinantal formula (2.76)

$$|\mathbf{R}_{ll,\mathcal{T}}|\,|\mathbf{R}_{kk,\mathcal{T}} - \mathbf{R}_{kl,\mathcal{T}}\mathbf{R}^{-1}_{ll,\mathcal{T}}\mathbf{R}_{lk,\mathcal{T}}|\,|\mathbf{C}_k|^2|\mathbf{C}_l|^2 = |\mathbf{R}_{ll,\mathcal{C}}|\,|\mathbf{R}_{kk,\mathcal{C}} - \mathbf{R}_{kl,\mathcal{C}}\mathbf{R}^{-1}_{ll,\mathcal{C}}\mathbf{R}_{lk,\mathcal{C}}|\,,$$

the identity $|\mathbf{R}_{ll,\mathcal{T}}| = |\mathbf{I}_M + \mathbf{U}_l\mathbf{T}_l^2\mathbf{U}_l^\dagger| = |\mathbf{C}_l|^{-2}$ and the property of $\mathcal{C}$ (unitary codewords), we conclude

$$|\mathbf{R}_{kk,\mathcal{T}} - \mathbf{R}_{kl,\mathcal{T}}\mathbf{R}^{-1}_{ll,\mathcal{T}}\mathbf{R}_{lk,\mathcal{T}}| = \frac{d_p^{2M}(\mathbf{X}_k,\mathbf{X}_l)}{|\mathbf{C}_k|^2}\,.$$

Therefore we can for example express the GLRT asymptotic PEP (2.43) of $\mathcal{T}_{\tilde{\mathcal{B}}}$ as a function of principal angles between the two codewords (rare thing for a training code!)

$$P^{\infty}_{ij,GLRT} + P^{\infty}_{ji,GLRT} = \left[\frac{M}{T\rho}\right]^{NM}\binom{2MN-1}{MN}|\mathbf{C}_k|^{2N}\frac{\left(1+\prod_{m=1}^{M}\frac{\tan^2(\theta_{k,m})}{\tan^2(\theta_{l,m})}\right)}{d_p^{2MN}(\mathbf{X}_k,\mathbf{X}_l)}$$

where $|\mathbf{T}_k| \geq |\mathbf{T}_l|$.

Remark 4. The above proof gives insights on the behaviour of EP codes and the exponential map non–linearity. However, the bigger the code size is, the more demanding the calculation of $\alpha_d(k,l)$ in (3.33) is[5]. Moreover, homothetic factor in (3.32) may be very small and may unnecessarily reduce product distances among codewords, and degrade EP code performance. Hence, since codeword dependence on singular values $\tau_m(k,l)$ is continuous but complicated, we conjecture that it is quite difficult to choose an homothetic factor annihilating some $\tau_m(k,l)$. Anyway, in numerical simulation a diversity gain decrease has never been reported. Therefore in the following we allow condition (3.32) not to be satisfied. We consider the proof of Conjecture 1 as a sort of existence proof and not as a mean to choose a practical value of homothetic factor α, which will be chosen (for big codebooks) via a numerical minimization of the error probability.

3.4 Examples of EP codes

We present in this section some particular cases of EP codes with a strong algebraic structure. Their rich structure always implies the loss of degrees of freedom so that these codes are never optimal from a capacity perspective. We also show that the generalized PSK codes [23] and the complex Givens code [26], which do not fit in the training based description, are EP codes.

3.4.1 EP Codes from Scaled Unitary Coherent Codes

Let the codewords of the coherent code $\mathcal{B}$ be scaled unitary matrices, i.e.

$$\mathbf{B}_k^\dagger \mathbf{B}_k = \beta_k^2 \, \mathbf{I}_M \,, \qquad \beta_k > 0 \,. \tag{3.50}$$

for all $k = 1, \ldots, L$ and where the coefficients β_k can be different. One valid TSVD of $\mathbf{B}_k$ is

$$\mathbf{B}_k = \mathbf{V}_k(\beta_k \, \mathbf{I}_M) \tag{3.51}$$

where $\mathbf{V}_k$ is implicitly defined. Then the corresponding EP codewords are

$$\mathbf{X}_k = \begin{bmatrix} \cos(\beta_k) \, \mathbf{I}_M \\ \sin(\beta_k) \, \mathbf{V}_k \end{bmatrix} = \begin{bmatrix} \cos(\beta_k) \, \mathbf{I}_M \\ \dfrac{\sin \beta_k}{\beta_k} \, \mathbf{B}_k \end{bmatrix} \tag{3.52}$$

which is similar to a training–based code but it is not!

In fact, if we let

$$\mathbf{B}_k = \beta_k \mathbf{I}_M \,, \quad \beta_k = \frac{\pi \, k}{Q} \,, \qquad k = 0, 1, \ldots, Q-1 \tag{3.53}$$

[5]Actually, it would be nice to use coherent codes $\mathcal{B}$ designed to maximize the minimum singular value of the difference of two arbitrary codewords. Unfortunately, current research on coherent codes deals with the optimization of $|(\mathbf{B}_k - \mathbf{B}_l)^\dagger (\mathbf{B}_k - \mathbf{B}_l)|$, i.e. the product of the singular values.

we obtain the generalized PSK codes of Tarokh–Kim [23] (see also (2.60) and that section for a discussion)

$$\mathbf{X}_k = \begin{bmatrix} \cos(\beta_k)\,\mathbf{I}_M \\ \sin(\beta_k)\,\mathbf{I}_M \end{bmatrix} . \tag{3.54}$$

It is possible to find the complex Givens codes [26] by defining the codewords of $\mathcal{B}$ as

$$\mathbf{B}_{k,l} = \beta_k e^{j\delta_\ell}\,\mathbf{I}_M \quad \Longrightarrow \quad \mathbf{X}_{k,l} = \begin{bmatrix} \cos(\beta_k)\,\mathbf{I}_M \\ \sin(\beta_k) e^{j\delta_\ell}\,\mathbf{I}_M \end{bmatrix}$$

where the alphabets of β_k and δ_ℓ are specified in [26].

EP codes of type (3.50) can also give some particular training–based codes. Let us assume that all the β_k in (3.50) are equal

$$\mathbf{B}_k^\dagger \mathbf{B}_k = \beta^2\,\mathbf{I}_M\,, \qquad \forall\,\mathbf{B}_k \in \mathcal{B}\,. \tag{3.55}$$

In this case the EP code $\mathcal{C}$ is

$$\mathbf{X} = \begin{bmatrix} \cos(\beta)\,\mathbf{I}_M \\ \dfrac{\sin\beta}{\beta}\,\mathbf{B}_k \end{bmatrix} . \tag{3.56}$$

The factor β is in common to all codewords, it plays therefore the role of an homothetic factor. For example, if we choose $\mathcal{B}'$ as the Alamouti coherent code with unitary energy PSK symbols for $M = 2$ (as in (2.69), (2.70) for propositions [24] and [23]), we have $\beta' = \sqrt{2}$. Letting $\mathbf{B} = \alpha\mathbf{B}'$ we have $\beta = \alpha\sqrt{2}$. Code (3.56) is a genuine training–based code. From Sect. 2.9, the correct choice for optimal performances is an equal distribution of power between the training and data phase, i.e.

$$2\cos^2(\alpha\sqrt{2}) = 2\sin^2(\alpha\sqrt{2}) \quad \Longrightarrow \quad \alpha = \pi/(4\sqrt{2})$$

which is a valid choice of the homothetic factor.

There exist training codes which do not directly fit into the EP codes, even if every training code can be associated to an EP code, as in the proof of Conjecture 1. Given the training matrix $\mathbf{T}$ (with $\mathbf{T}^\dagger\mathbf{T} = \mathbf{I}_M$) and the respective coherent code $\mathcal{B}_{train}$ with TSVDs $\mathbf{B}_{k,train} = \mathbf{V}_k\mathbf{\Lambda}_k\mathbf{U}_k^\dagger$, the coherent code $\mathcal{B}_{EP}$ over the tangent space producing an equivalent EP code over the Grassmannian is

$$\mathbf{B}_{k,EP} = \mathbf{V}_k \tan^{-1}(\mathbf{\Lambda}_k)\mathbf{U}_k^\dagger\mathbf{T}^\dagger\,. \tag{3.57}$$

In Fig. 3.7 we resume the considerations of this subsection in a graphical way.

3.4.2 EP Codes from Codes with Commuting Matrices

Let us suppose that codewords of coherent code $\mathcal{B}$ satisfy

$$\begin{cases} \mathbf{B}_k^\dagger\mathbf{B}_\ell = \mathbf{B}_\ell^\dagger\mathbf{B}_k \\ \mathbf{B}_k\mathbf{B}_\ell^\dagger = \mathbf{B}_\ell\mathbf{B}_k^\dagger \end{cases}, \qquad \text{for every } k \neq l\,. \tag{3.58}$$

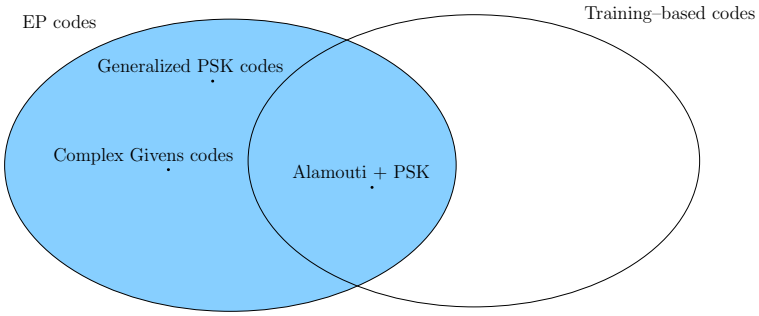

Figure 3.7: The generalized PSK and complex Givens codes fit in the EP code description, as well as the training codes described in [23].

Under this very strong condition, all couples of matrices $\mathbf{\Delta}_k$ and $\mathbf{\Delta}_\ell$ (3.21) in the tangent space commute, as well as $\mathbf{\Delta}_\ell^\dagger$ and $\mathbf{\Delta}_k$, for example. In this case, property (3.5) can be applied and the calculations performed over codewords of $\mathcal{C}$ can be reported to codewords of $\mathcal{B}$ on the tangent space. For each $\mathbf{X}_k, \mathbf{X}_\ell \in \mathcal{C}$, using (3.4) we have, for example

$$\mathbf{X}_\ell^\dagger \mathbf{X}_k = \mathbf{I}_{T,M}^\dagger \exp\left\{ \begin{bmatrix} \mathbf{0}_M & -(\mathbf{B}_k - \mathbf{B}_\ell)^\dagger \\ (\mathbf{B}_k - \mathbf{B}_\ell) & \mathbf{0}_{T-M} \end{bmatrix} \right\} \mathbf{I}_{T,M} \,. \tag{3.59}$$

Let the TSVD of $\mathbf{B}_k - \mathbf{B}_\ell$ be $\mathbf{B}_k - \mathbf{B}_\ell = \mathbf{V}_{k,l} \mathbf{\Sigma}_{k,l} \mathbf{U}_{k,l}^\dagger$, apply the CS decomposition as in (3.19), then (3.59) becomes

$$\mathbf{X}_\ell^\dagger \mathbf{X}_k = \mathbf{U}_{k,l} \cos(\mathbf{\Sigma}_{k,l}) \mathbf{U}_{k,l}^\dagger \,. \tag{3.60}$$

Hence, when the matrices $\mathbf{\Delta}_k$ on $t\pi_{ref}$ commute, principal angles between two subspaces spanned by $\mathbf{X}_k$ and $\mathbf{X}_\ell$ are the singular values of the difference of the respective codewords of $\mathbf{B}$, i.e. $\mathbf{B}_k - \mathbf{B}_\ell$. We have proved the following

Proposition 6 *Let $\mathcal{B}$ be such a coherent code that all the matrices $\mathbf{\Delta}_k$ mutually commute. Then $\mathcal{B}$ and the corresponding EP code $\mathcal{C}$ have equal diversity. The product distance can be bounded*

$$\frac{2}{\pi} |(\mathbf{B}_k - \mathbf{B}_\ell)^\dagger (\mathbf{B}_k - \mathbf{B}_\ell)|^{\frac{1}{2M}} \leq d_p(\mathbf{X}_k, \mathbf{X}_\ell) \leq |(\mathbf{B}_k - \mathbf{B}_\ell)^\dagger (\mathbf{B}_k - \mathbf{B}_\ell)|^{\frac{1}{2M}} \tag{3.61}$$

We notice that generalised PSK codes (3.54) satisfy conditions (3.58) and therefore have full diversity (because rank$[\cos(\beta_k)\mathbf{I}_M - \cos(\beta_\ell)\mathbf{I}_M] = M$ since $k \neq l$).

Unfortunately, condition (3.58) is so strong that we were not able to find interesting codes with this property.

3.5 Conclusion

In this chapter we have discussed conditions under which the exponential parameterization can be used to create a non–coherent unitary code. We also discussed the

relationships between the coherent code $\mathcal{B}$ and the non–coherent code $\mathcal{C}$ obtained via exponential map (EP code).

In Fig. 3.3, the transmit chain of an EP code is shown. The exponential map can be efficiently implemented according to the CS decomposition, starting from an TSVD of the codewords $\mathbf{B}_k$.

Chapter 4

Suboptimal Decoding of EP Codes over $G_{T,1}$

We investigate in this chapter EP code properties and decoding strategies when the transmitter has one antenna ($M = 1$). This case has been studied in [21], [31], where a partial characterization of EP code properties and a simplified decoding algorithm were proposed. We describe here another simplified suboptimal decoder, which has performances almost coincident to GLRT ones, but whose complexity is higher than the one of simplified decoder presented in [31]. We have investigated both the Single Input Single Output (SISO) case ($M = N = 1$) and the Single Input Multiple Output (SIMO) case ($M = 1$, $N > 1$), in order to understand how the different decoders behave.

In the first section we study the GLRT in the SISO case. Statistics of an important GLRT parameter are found and numerically evaluated. They gave some indications to choose the parameters of the simplified decoder we propose. In the SIMO case, a simple subspace estimation algorithm is briefly introduced, which gives a subspace estimation from the observations of N received signals. This allows to apply the simplified decoder introduced for the SISO case to SIMO systems .

In the second section, we detailed the properties of EP code for SISO channels. The particular structure of codes over $G_{T,1}$ permits to find close form relationships between the codewords distances of coherent code $\mathcal{B}$ and the codewords distances of the corresponding EP code $\mathcal{C}$. We then used this comprehension to determine a good choice of the homothetic factor, which maximizes the minimal Euclidean distance of the codewords of $\mathcal{C}$ and at the same time approximatively maximizes their minimal chordal distance.

A long geometrical study is presented in the third section. Its aim is to investigate the geometrical structure of the GLRT level sets over the Grassmannian $G_{T,1}$. In other words, we wanted to understand to which points of $G_{T,1}$ a certain value c of the GLRT corresponds, given the value of the received signal $\mathbf{y}$. This comprehension helps us to locate the region of the Grassmannian in which it is highly probable to find the correct sent codeword, so that the decoding process can be limited to this zone. However, we did not (and do not) know how to perform efficient numerical search in the Grassman-

nian, even inside bounded regions. On the other hand, mathematical tools to perform these searches are available for coherent STB codes. The idea is therefore to move the decoding problem to the tangent space, i.e. to the coherent code $\mathcal{B}$ corresponding to the EP code $\mathcal{C}$. To this end, we also studied the behaviour of GLRT level sets preimages in the tangent space. Their shape is warped by the exponential map non–linearity, nevertheless we succeeded in bounding these regions (where it is highly probable to find the coherent codewords corresponding to the sent non–coherent codeword).

In the fourth section, a new simplified decoder on the tangent space is proposed, thanks to the insights gained by previous geometrical investigations. The decoder complexity is roughly investigated. The choice of decoder parameters is discussed via simulations.

The final section is dedicated to simulations for both AWGN and Rayleigh channels in the SISO and SIMO case. Comparisons with other propositions are also presented.

4.1 Channel Model

AWGN channel with unknown channel phase is considered in the case of one receive antenna. We made this choice to better discriminate between performances of different decoders. However, also the Rayleigh channel is investigated in the single–input multiple–output (SIMO) case.

4.1.1 AWGN Channel with Unknown Phase

Suppose that the receiver has one antenna: $N = 1$. Let the codewords $\mathbf{x}$ be column vectors of length T with unit norm $\|\mathbf{x}\| = 1$. The channel introduces an unknown phase and an additive white Gaussian noise

$$\mathbf{y} = \mathbf{x}e^{i\varphi_h} + \mathbf{w} \tag{4.1}$$

where $w_t \sim \mathcal{CN}(0, \sigma^2)$ and φ_h is a uniform random variable in $[0, 2\pi)$. The GLRT is, in this case

$$\hat{\mathbf{x}} = \max_{\mathbf{x}\in\mathcal{C}} |\mathbf{x}^\dagger \mathbf{y}|^2 \tag{4.2}$$

In this particular case we notice that the GLRT is independent on the norm of the received codeword. The rule (4.2) is equivalent to maximize

$$c = \frac{|\mathbf{x}^\dagger \mathbf{y}|}{\|\mathbf{y}\|}\,. \tag{4.3}$$

which is the cosine of the principal angle between the subspaces spanned by $\mathbf{x}$ and $\mathbf{y}$.

If $\mathbf{x} = \mathbf{y}$, the value of GLRT metric c achieves its maximum. Its minimum value correspond to points orthogonal to $\mathbf{y}$, i.e. to the farthest points from the normalized received signal $\mathbf{y}/\|\mathbf{y}\|$. It is clear that the greatest is the channel additive noise, the less probable is to find the sent codeword close to the received signal (in the principal angle

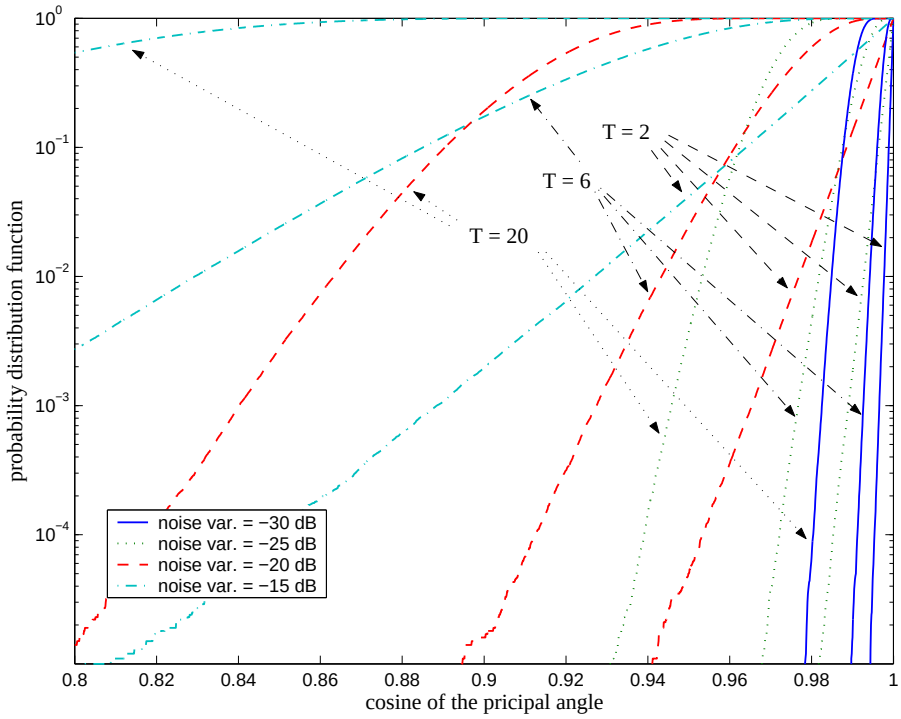

Figure 4.1: Probability distribution function of c, the cosine of the principal angle between the subspaces spanned by the received signal and the sent codeword.

sense). We are therefore interested in function (4.3) statistics, fixed sent codeword $\mathbf{x}$ and given channel phase φ_h, in order to relate the value of c to the noise variance.

We observe that the application of a unitary transformation $\mathbf{U} \in \mathcal{U}_T$ to all vectors does not change the value of (4.3) nor the statistics of $\mathbf{w}$ ($\mathbf{U}\,\mathbf{w} \sim \mathcal{CN}(0, \sigma^2)$). Hence, in order to simplify the study of the statistics of c, since $\mathbf{x}$ and φ_h are fixed, we choose a rotation so that after renaming terms and rewriting (4.1) we have

$$\mathbf{y} = \mathbf{e}_1 + \mathbf{w}\,, \qquad \mathbf{e}_1^\dagger = [1\ 0 \ldots 0]\,. \tag{4.4}$$

From (4.3)

$$c^2 = \frac{|1+z_1|^2}{1+2\Re(z_1)+\|\mathbf{z}\|^2} = \frac{(1+z_{1,R})^2+z_{1,I}^2}{(1+z_{1,R})^2+z_{1,I}^2+\sum_{t=2}^{T}(z_{t,R}^2+z_{t,I}^2)}\,. \tag{4.5}$$

Random variables $z_{t,R}, z_{t,I}$ are i.i.d. real Gaussian random variables $\mathcal{N}(0, \sigma^2/2)$. c^2 is a non-central beta random variable [73, pag. 944] (see also Appendix A.3). Since the probability distribution function of the cosine c in (4.3) cannot be obtained in a simple closed form, we used a Montecarlo method to obtain its statistics. Briefly we generate the random variable $\mathbf{y}$ in (4.4) by means of 10^6 realizations of noise vector $\mathbf{w}$.

In Fig. 4.1, probability distribution function F_c of c is plotted for different values of

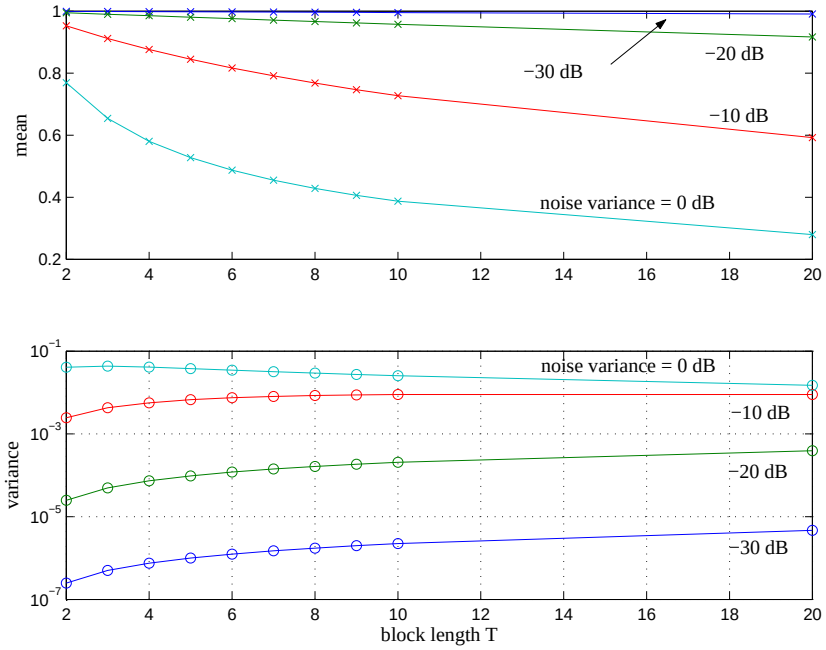

Figure 4.2: Mean and variance, as a function of the block length T, of the cosine of the principal angle between the subspaces spanned by the received signal and the sent codeword.

block length T and of noise variance[1] σ^2 (both real and complex parts). We can notice that, for a fixed noise variance, the smaller is the block length, the smaller is the support where the probability density function F_c assumes values significantly different from 0. Obviously, if the noise variance becomes smaller and smaller, the cosine in (4.3) converges to 1. In fact, if noise was absent the received vector would span the same subspace spanned by the sent codeword, channel phase factor having no influence. The curves are less regular around 10^{-5}, due to the number of realization used in the simulations (i.e. 10^6 as previously stated). In Fig. 4.2 we plot the mean and variance of c. For fixed noise variance σ^2, these parameters remain almost constant for a large interval of values of the block length T, especially at high SNR (small noise variance). For small values of T, the variance of c becomes smaller, as noticed above in Fig. 4.1.

These results indicates that the sent codeword has a negligible probability to have a principal angle less that 0.97 with respect to the received signal, at high SNR. So that, if we design a non–coherent system without outer code to have the acceptable error probability of 10^{-3} at 20 dB SNR per receive antenna, it does not make sense to search for the sent codeword farther than $\pi/13$ (in principal angle radians) from the received signal.

[1]In the figures we chose to represent the noise variance by the unusual notation in dB $(\sigma^2)_{\mathrm{dB}} = 10\log_{10}(\sigma^2)$. We adopted this notation because it is simple to calculate the corresponding average SNR per receive antenna in dB as $(\rho)_{\mathrm{dB}} = -(\sigma^2)_{\mathrm{dB}} - 10\log_{10} T$.

4.1.2 Rayleigh SIMO Channel

We consider a single–input multiple–output (SIMO) channel ($M = 1$, $N \geq 1$) with Gaussian fadings and additive white Gaussian noise

$$\mathbf{Y} = \mathbf{x}\mathbf{H} + \mathbf{W} \tag{4.6}$$

where the noise entries are i.i.d. $\mathcal{CN}(0, \sigma^2)$ and the fading entries are i.i.d. $\mathcal{CN}(0, 1)$. Matrices $\mathbf{Y}$ and $\mathbf{W}$ are $T \times N$, $\mathbf{H}$ is $1 \times N$ (a row vector), while $\mathbf{x} \in \mathcal{C}$ is a column vector $T \times 1$ with unit norm, as in the previous subsection. The GLRT in this case is

$$\hat{\mathbf{x}} = \max_{\mathbf{x} \in \mathcal{C}} \|\mathbf{x}^\dagger \mathbf{Y}\|^2 \,. \tag{4.7}$$

When $N = M = 1$, replacing $\mathbf{y}$ with $\mathbf{y}/\|\mathbf{y}\|$ does not change the GLRT estimation. When $M = 1$, $N > 1$, this is no longer possible and $\mathbf{Y}$ cannot be replaced in (4.7) by a matrix $\mathbf{Y}_u = \mathbf{Y}\mathbf{A}$ with $\mathbf{Y}_u^\dagger \mathbf{Y}_u = \mathbf{I}_M$. In fact, even if $\mathbf{Y}$ and $\mathbf{Y}_u$ span the same subspace the values of the metrics $\|\mathbf{x}^\dagger \mathbf{Y}\|^2$ and $\|\mathbf{x}^\dagger \mathbf{Y}_u\|^2$ are not scaled by the same constant!

In the following, we propose to apply the decoder for $M = N = 1$ to the SIMO case. To this end, we use the columns of the received matrix $\mathbf{Y}$ as independent noisy realizations of $\mathbf{x}$, from which we estimate the subspace direction $\mathbf{x}_e$ as the eigenvector corresponding to the maximum eigenvalue of the correlation matrix

$$\mathbf{x}_e \text{ eigenvector of max. eigenvalue of } \mathbf{R}_Y = \frac{1}{N} \sum_{n=1}^{N} \mathbf{y}_n \mathbf{y}_n^\dagger = \frac{1}{N} \mathbf{Y}\,\mathbf{Y}^\dagger \tag{4.8}$$

This estimation is unbiased. In fact, since

$$\mathbf{R}_Y = \frac{1}{N} [\mathbf{x}\,\mathbf{H}\,\mathbf{H}^\dagger \mathbf{x}^\dagger + \mathbf{x}\,\mathbf{H}\,\mathbf{W}^\dagger + \mathbf{W}\,\mathbf{H}^\dagger \mathbf{x}^\dagger + \mathbf{W}\,\mathbf{W}^\dagger]$$

once fixed the sent codeword $\mathbf{x}$ and being the fading and noise process independent, we have

$$\mathrm{E}\,[\mathbf{R}_Y] = \mathbf{x}\,\mathbf{x}^\dagger + \sigma^2 \mathbf{I}_T \,. \tag{4.9}$$

Reducing noise variance makes the estimation $\mathbf{x}_e$ converge in mean to the sent codeword $\mathbf{x}$.

Thanks to this estimation the SIMO system can be reduced to a SISO system, since we can use the estimated direction $\mathbf{x}_e$ as the received signal. This is equivalent to decode according to the suboptimal rule

$$\hat{\mathbf{x}}_{sub} = \max_{\mathbf{x} \in \mathcal{C}} (\|\mathbf{x}^\dagger \mathbf{x}_e\| / \|\mathbf{x}_e\|)^2 \,, \tag{4.10}$$

where $|\mathbf{x}^\dagger \mathbf{x}_e\|/\|\mathbf{x}_e\|$ is the cosine of the principal angle between the subspaces spanned by a generic codeword $\mathbf{x}$ and the estimated direction $\mathbf{x}_e$. This suboptimal criterion is well motivated, as a matter of fact the maximization term in (4.7) can be rewritten as

$$\|\mathbf{x}^\dagger \mathbf{Y}\|^2 = \mathbf{x}^\dagger \mathbf{Y}\,\mathbf{Y}^\dagger \mathbf{x} = N \mathbf{x}^\dagger \mathbf{R}_Y \mathbf{x} \,, \tag{4.11}$$

which coincides with $\|\mathbf{x}^\dagger \mathbf{x}_e\|^2$ for vanishing noise variance.

4.2 EP codes for $G_{T,1}$

In this section we specialize the results for the EP codes of Chapter 3 to the case $M = 1$. We introduce some properties of the EP codes and use them to determine a good choice of the homothetic factor.

4.2.1 The Exponential Map in the case $G_{T,1}$

Let us briefly recall the quotient geometry of $G_{T,1}$. From Definition 10 we have $G_{T,1} = \mathcal{U}_T/(\mathcal{U}_1 \times \mathcal{U}_{T-1})$, where $\mathcal{U}_1 = \{e^{j\varphi}\}$. An equivalent and economical description is

$$G_{T,1} = \mathbb{U}^T/\mathbb{U}\,, \qquad \mathbb{U}^n = \{\mathbf{v} \in \mathbb{C}^n : \|\mathbf{v}\| = 1\}\,. \tag{4.12}$$

In other words, the Grassmann manifold can be described as a point in the complex sphere $\mathbb{U}^T$ modulo a common phase, i.e. an arbitrary complex number with unit absolute value. We notice that the complex hypersphere $\mathbb{U}^n$ is isomorphic to the real hypersphere $\mathbb{S}^{2n} = \{\mathbf{a} \in \mathbb{R}^{2n} : \|\mathbf{a}\| = 1\}$, which has $2n - 1$ real dimensions. Hence, $G_{T,1}$ has dimension $2T - 1 - 1 = 2(T - 1)$, as claimed in (3.9).

Let $\mathbf{b} \in \mathbb{C}^{T-1}$, the matrices on the tangent space to the reference subspace (3.16)

$$\mathbf{x}_{ref} = \begin{bmatrix}1 & 0 & \dots & 0\end{bmatrix}^\dagger = \mathbf{e}_1 \tag{4.13}$$

are

$$\mathbf{\Delta} = \begin{bmatrix}0 & -\mathbf{b}^\dagger \\ \mathbf{b} & \mathbf{0}_{T-1}\end{bmatrix}$$

and therefore the exponential map in its CS form (3.20) can be written as

$$\mathbf{x} = \begin{bmatrix}\cos\|\mathbf{b}\| \\ \dfrac{\sin\|\mathbf{b}\|}{\|\mathbf{b}\|}\mathbf{b}\end{bmatrix} = \begin{bmatrix}\cos\rho_b \\ \dfrac{\sin\rho_b}{\rho_b}\mathbf{b}\end{bmatrix}\,, \qquad \rho_b = \|\mathbf{b}\|\,. \tag{4.14}$$

where ρ_b is the principal angle between the reference subspace and the subspace spanned by $\mathbf{x}$. The condition to invert the exponential map is

$$\mathbf{b} \in B_{\pi/2} + \{\mathbf{b} \in \mathbb{C}^{T-1} : \rho_b = \|\mathbf{b}\| < \pi/2\}\,. \tag{4.15}$$

Under condition (4.15), the image of the exponential map is

$$G_{T,1}^{\times} = \{\mathbf{x} \in \mathbb{U}^T : x_1 > 0\} \quad \text{where} \quad \mathbf{x}^t = \begin{bmatrix}x_1 & x_2 & \dots & x_T\end{bmatrix}\,. \tag{4.16}$$

where $(\cdot)^t$ denotes transposition.

We notice that a vector $\mathbf{x}$ belonging to $G_{T,1}^{\times}$ is the representative of the equivalence class given by the vectors $\{\mathbf{x}\, e^{j\varphi}, \varphi \in \mathbb{R}\}$. Indeed, $\mathbf{x}$ is the *unique* representative with the first element $x_1 > 0$. As a matter of fact, if another representative $\bar{\mathbf{x}}$ of the same subspace exists so that $\bar{x}_1 > 0$ and $\bar{\mathbf{x}} \neq \mathbf{x}$, we have that $\exists\, \bar{\varphi} \in [0, 2\pi)$ so that $\bar{\mathbf{x}} = \mathbf{x}e^{i\bar{\varphi}}$. But, since $\bar{x}_1 > 0$ and $x_1 > 0$ by construction, it must be $e^{j\bar{\varphi}} = 1$. Representation (4.14) is called *CS representation*. We can easily extend these considerations to the case where $x_1 = \ldots = x_m = 0$ considering the point as a representative of a subspace over $G_{T-m,1}$. We do not consider this case, since the set of points orthogonal to the reference space has zero measure with respect to the whole Grassmannian.

4.2.2 Properties of EP Codes over $G_{T,1}$

Let us consider two codewords $\mathbf{x}_k, \mathbf{x}_\ell \in \mathcal{C}$ and let use denote by $\theta_{k,l}$ the principal angle between $\Omega_{\mathbf{x}_k}$ and $\Omega_{\mathbf{x}_\ell}$ (which are two lines in $\mathbb{C}^T$), where

$$|\mathbf{x}_k^\dagger \mathbf{x}_\ell| = \cos\theta_{k,l}\,, \qquad \mathbf{x}_k^\dagger \mathbf{x}_\ell = \cos\theta_{k,l} e^{j\varphi_{k,l}}\,. \tag{4.17}$$

In [21], the following result for the case of *real* codebooks is reported

$$(2/\pi)^2 \|\mathbf{b}_k - \mathbf{b}_\ell\|^2 \le 4\sin^2(\theta_{k,l}/2)\,, \qquad \forall\, k \ne l\,. \tag{4.18}$$

This is no longer true where complex vectors are used. Let's consider for instance two codewords in the case $T = 3$ belonging to an EP code obtained from the parameterization of a $(64\text{–QAM})^2$ constellation in which each 64–QAM constellation $\{d(q_1 + jq_2), q_1, q_2 = \pm 1, \pm 3, \ldots, \pm 7\}$ has statistical power of $E_{av} \simeq 0.46$, so that $d = d_{min}/2 = 0.105$. Let's take

$$\mathbf{b}_1 = d\begin{bmatrix} 7+7j \\ 7+7j \end{bmatrix},\ \mathbf{b}_2 = d\begin{bmatrix} 7-7j \\ 7+7j \end{bmatrix} \quad \Longrightarrow$$
$$\mathbf{x}_1 = \begin{bmatrix} 0.105 \\ 0.497(1+j) \\ 0.497(1+j) \end{bmatrix},\ \mathbf{x}_2 = \begin{bmatrix} 0.105 \\ 0.497(1-j) \\ 0.497(1+j) \end{bmatrix}$$

then

$$\mathbf{x}^\dagger \mathbf{x}_2 = \cos(\pi/4) e^{-j\pi/4.06} \quad \Longrightarrow \quad (2/\pi)^2 \|\mathbf{b}_1 - \mathbf{b}_2\|^2 = 0.871 > 0.586 = 4\sin^2(\pi/8)\,.$$

The following proposition can be shown for complex vectors

Proposition 7 *Let $\mathbf{x}_k, \mathbf{x}_\ell \in \mathcal{C}$ obtained from the corresponding $\mathbf{b}_k, \mathbf{b}_\ell \in \mathcal{B}$, with $\rho_k = \|\mathbf{b}_k\|$. Then the following lower bounds on the product distance $d_p(\mathbf{x}_k, \mathbf{x}_\ell) = \sin\theta_{k,l}$ hold*

$$d_p(\mathbf{x}_k, \mathbf{x}_\ell) = \sin\theta_{k,l} \ge \begin{cases} \frac{\sin(2\rho_b)}{2\rho_b}\|\mathbf{b}_k - \mathbf{b}_\ell\| & \text{, if } \|\mathbf{b}_k\| = \|\mathbf{b}_\ell\| = \rho_b \\ \frac{2}{\pi}|\|\mathbf{b}_k\| - \|\mathbf{b}_\ell\|| & \text{, if } \|\mathbf{b}_k\| \ne \|\mathbf{b}_\ell\| \end{cases} \tag{4.19}$$

Proof. From (4.14)

$$\cos^2\theta_{k,l} = |\mathbf{x}_k^\dagger \mathbf{x}_\ell|^2 = |\cos\rho_k \cos\rho_\ell + \sin\rho_k \sin\rho_\ell \mathbf{b}_k^\dagger \mathbf{b}_\ell/(\rho_k\rho_\ell)|^2 \tag{4.20}$$

where $\mathbf{b}_k/\rho_k$ and $\mathbf{b}_\ell/\rho_\ell$ are two unit vectors. This fact implies that $\mathbf{b}_k^\dagger \mathbf{b}_\ell/(\rho_k\rho_\ell) = ae^{j\varphi}$, where $0 \le a \le 1$. Since $\cos\rho_k \cos\rho_\ell > 0$, it is easy to verify that (4.20) is upper bounded by

$$\cos^2\theta_{k,l} \le |\cos\rho_k \cos\rho_\ell + \sin\rho_k \sin\rho_\ell|^2 = \cos^2(\rho_k - \rho_\ell) \le \cos(\rho_k - \rho_\ell)\,. \tag{4.21}$$

Now, thanks to the inequality $\cos\rho_k \le 1 - (2/\pi)^2\rho_k^2$ if $\rho_k \in [0, \pi/2]$, we have

$$\cos^2\theta_{k,l} \le 1 - \frac{4}{\pi^2}(\|\mathbf{b}_k\| - \|\mathbf{b}_\ell\|)^2 \tag{4.22}$$

and the second inequality in (4.19) is easily obtained. For $\rho_k = \rho_\ell$ the bound (4.22) gives no information, while for $\rho_k \neq \rho_\ell$ it always holds $(\rho_k - \rho_\ell) < \pi/2$.

Let us suppose $\rho_k = \rho_\ell = \rho_b$, by developing (4.20) we obtain

$$\begin{aligned}\cos^2\theta_{k,l} &\leq \cos^4\rho_b + \sin^4\rho_b + 2\cos^2\rho_b \sin^2\rho_b \,\mathrm{Re}(\mathbf{b}_k^\dagger \mathbf{b}_\ell)/\rho_b^2 \\ &= 1 - \frac{\cos^2\rho_b \sin^2\rho_b}{\rho_b^2}[2\rho_b^2 - 2\mathrm{Re}(\mathbf{b}_k^\dagger \mathbf{b}_\ell)] \\ &= 1 - \frac{\cos^2\rho_b \sin^2\rho_b}{\rho_b^2}\|\mathbf{b}_k - \mathbf{b}_\ell\|^2\end{aligned}$$

where the first inequality follows from $|\mathbf{b}_k^\dagger \mathbf{b}_\ell/\rho_b^2| \leq 1$. And the first inequality in (4.19) immediately follows. □

To further simplify the dependence on ρ_b in (4.19), we simply observe that

$$\sin(2\rho_b)/(2\rho_b) \geq 1 - (2/\pi)\rho_b \quad \text{for} \quad \rho_b \in [0, \pi/2]\,.$$

The exponential map from $B_{\pi/2}$ to $G_{T,1}^\times$ is invertible. Let $\mathbf{x}$ belong to $G_{T,1}^\times$ and let $\hat{\mathbf{x}}$ be the vector of length $T-1$ obtained erasing the first entry of $\mathbf{x}$:

$$\hat{\mathbf{x}} = [x_2 \ \ldots \ x_M]^t\,. \tag{4.23}$$

If $\mathbf{x}$ is in CS representation (4.14), the corresponding $\mathbf{b} \in B_{\pi/2}$ is derived as [31]

$$\mathbf{b} = \exp^{-1}(\mathbf{x}) = \frac{\rho_b}{\sqrt{1-x_1^2}}\,\hat{\mathbf{x}}\,, \qquad \rho_b = \arccos x_1\,. \tag{4.24}$$

We notice that the arccos is uniquely defined because $x_1 \in (0, 1]$.

This latter expression will be useful to state the simplified decoders we will study in the follwing sections, while Proposition 7 is useful to choose the correct homothetic factor,i.e. to design a good EP code.

4.2.3 Choice of the Homothetic Factor

No outer code is considered in this work; codebooks are of type $\mathcal{B} = (Q\text{–QAM})^{T-1}$. In this subsection we show how to use previous results to choose a good homothetic factor, i.e. an homothetic factor which minimizes the distances of codewords in $G_{T,1}$.

Let a generic Q–QAM constellation be

$$Q\text{–QAM} = \{q_1 d + i q_2 d,\ q_1 = \pm 1, \ldots \pm(Q_1 - 1),\ q_2 = \pm 1, \ldots \pm(Q_2 - 1),\ Q = Q_1 Q_2\} \tag{4.25}$$

for square constellations, the integers Q_1 and Q_2 are equal $Q = Q_1^2$. For square constellations, the average energy and minimal distance are [69]

$$E_{av} = \frac{2}{3}(Q-1)d^2\,, \qquad d_{min}^2 = (2d)^2 = E_{av}\frac{6}{Q-1}\,.$$

In [31] the expression of optimal homothetic factor α was found for real codes by maximizing the minimal Euclidean distance. Even if the correct distance criterion is the distance product, this is of no importance for real codes, since the Euclidean distance and the product distance substantially coincide. In the complex case these two distances are no longer equivalent and the product distance should be chosen as the optimization criterion. Nevertheless, the Euclidean distance and the product distance give the same result, which coincide with the one for real codes. We first derive the optimal homothetic factor for complex codes with Euclidean distance, since the argument is simple. Then, we sketch the proof for the product distance.

If the Euclideand distance is used, the minimal distance of (Q–QAM)$^{T-1}$ coincides with the minimal distance of the single Q–QAM constellation. However, for codewords close to the boundary of $B_{\pi/2}$, we must also consider the distance with respect to their opposite, due to the modulo–$\mathbb{U}$ effect. Let $\mathbf{b}_1, \mathbf{b}_2$ be such two codewords so that $\mathbf{b}_2 = -\mathbf{b}_1$ and $\|\mathbf{b}_1\| = \|\mathbf{b}_2\| = \rho_{max} = \max_{\mathbf{b}\in\mathcal{B}} \|\mathbf{b}\|$. Their distance, keeping in mind the worst case modulo–$\mathbb{U}$ effect is, $2(\pi/2 - \rho_{max})$. Suppose that $d = 1$ in (4.25) and that all the codewords are multiplied by a common homothetic factor α. Since the minimal distance of(Q–QAM)$^{T-1}$ increases by increasing α but the distance $2(\pi/2 - \rho_{max})$ decreases, the optimal tradeoff is obtained by equating the two distances. For square constellations this condition yields:

$$\pi/2 - \alpha = \alpha\sqrt{2(T-1)}(\sqrt{Q}-1) \quad \Longrightarrow \quad \alpha = (\pi/2)[1+\sqrt{2(T-1)}(\sqrt{Q}-1)]^{-1} \tag{4.26}$$

while for rectangular constellations the homothetic factor is

$$\alpha = (\pi/2)\{1+\sqrt{(T-1)[(Q_1-1)^2+(Q_2-1)^2]}\}^{-1}\,. \tag{4.27}$$

The correct distance over $G_{T,1}$ is the product distance. Hence, to find the optimal homothetic factor, bounds in Proposition 7 must be used, and they lead to basically equal results, only their derivation is more complicated. Briefly, the second bound of (4.19) simply suggests that the homothetic factor must be chosen as high as possible, in order to maximize the minimal distance between groups of codewords with a constant norm. The first bound of (4.19) simplifies in $\|\mathbf{b}_1 - \mathbf{b}_2\|$, for codewords close to the origin ($\rho_b \to 0$ implies $\sin(2\rho_b)/(2\rho_b) \to 1$). In this case, the minimal product distance is lower bounded by $\|\mathbf{b}_1 - \mathbf{b}_2\| = 2\alpha$. Moreover, coefficient $\sin(2\|\mathbf{b}\|)/(2\|\mathbf{b}\|)$ annihilates at $2\|\mathbf{b}\| = \pi$. Then for opposite codewords with maximal norm ρ_{max} (worst case for modulo–$\mathbb{U}$ effect) the first bound in (4.19) can be simplified in $\sin(2\rho_{max}) = \sin(2\alpha\sqrt{2(T-1)}(\sqrt{Q}-1))$ (square constellations). If ρ_{max} is close to $\pi/2$, which is the case for EP codes which try to exploit the whole Grassmannian surface, $2\rho_{max}$ is greater than $\pi/2$. Hence $\sin(2\rho_{max})$ decreases when α increase. Therefore, for these codewords α must be minimized. The optimal tradeoff can be found by equating the two expressions of minimal distances (for codewords close to the origin and the ones close to the boundary)

$$2\alpha = \sin(2\alpha\sqrt{2(T-1)}(\sqrt{Q}-1)) \simeq \pi - 2\alpha\sqrt{2(T-1)}(\sqrt{Q}-1)\,.$$

In the previous expression we used the linearization $\sin x \simeq \pi - x$, valid for x sufficiently close to π, which holds true in our case if ρ_{max} is sufficiently close to $\pi/2$.

Homothetic factor (4.26) is then derived. We stress that previous considerations are not a complete formal proof: for instance, we also need to consider more carefully the second bound in (4.19) in order to draw general conclusions.

4.3 GLRT Geometry

At this point, as explained in the introduction of this chapter, it is very important to study some geometrical properties of the curves on the Grassmannian which have constant GLRT value, since they give insights about where to search for the sent codeword. These curves are called *level sets* of GLRT function. Since there exists no efficient method to maximize the GLRT even on a bounded subset of the Grassmannian, we restate the problem to the tangent space, which is not a manifold but just a linear vector space. In the tangent space, in fact, is located the coherent code corresponding to the EP code on the Grassmannian, and there exist mathematical tools to deal efficiently with codewords search. Anyway the shape of the level set in $G_{T,1}$ is not preserved because the inverse exponential map is non–linear! Hence, we studied the preimages of the level sets in the tangent space. The understanding of their shape allowed us to propose a suboptimal decoder in the tangent space. In this section we assume $M = N = 1$ (SISO system).

4.3.1 GLRT Level Sets on $\mathbb{U}^T$

As we saw in (4.2) and (4.3) the GLRT rule is equivalent to the cosine of the principal angle between the subspaces (lines!) spanned by the codeword $\mathbf{x}$ and the received signal $\mathbf{y}$, that is we let

$$\psi(\mathbf{x}) = |\mathbf{y}^\dagger \mathbf{x}| \quad \text{where we aussume } \mathbf{x}, \mathbf{y} \in \mathbb{U}^T . \tag{4.28}$$

We assume $\|\mathbf{y}\| = 1$ and we let $\mathbf{x}$ belong to $\mathbb{U}^T$ without forgetting that different $\mathbf{x}$ can represent the same point over the Grassmannian.

Obviously $\psi(\mathbf{x})$ takes its maximum value on the points $\mathbf{x}_{max} = \mathbf{y}e^{j\varphi}$, with $\varphi \in [-\pi, \pi)$, for which $\psi(\mathbf{x}_{max}) = 1$. The minimum value of the GLRT rule is zero.

Considering $\psi : \mathbb{U}^T \longrightarrow \mathbb{R}$, the level set of ψ corresponding to a real value c is defined as the subset of the domain $S_c = \{\mathbf{x} \in \mathbb{U}^T : \psi(\mathbf{x}) = c\}$ [72]. Since c is a cosine, the level set S_c is not empty when $c \in [0, 1]$. We set $c = \cos\theta_r$ where $\theta_r \in [0, \pi/2]$ is actually the principal angle between $\mathbf{x}$ and $\mathbf{y}$. The level sets $S_{\cos\theta_r}$ are

$$S_{\cos\theta_r} = \left\{\mathbf{x} \in \mathbb{U}^T : \mathbf{x} = \cos\theta_r e^{j\xi_r}\mathbf{y} + \sin\theta_r \mathbf{v},\ \forall\, \mathbf{v} \perp \mathbf{y},\ \|\mathbf{v}\| = 1,\ \xi_r \in [0, 2\pi)\right\} . \tag{4.29}$$

Expression (4.29) can be verified by substituting points of $S_{\cos\theta_r}$ in (4.28). We notice from (4.88) that the level set are hyperspheres with one fixed parameter θ_r, and they have therefore dimension $2T-2$ (see Appendix B.1 for more details and explications). Now, our codes are over the Grassmannian so that we must understand which vectors of $S_{\cos\theta_r}$ represent the same subspace, before inverting the map and trying to understand

how things work in the tangent space. To this end, we assume that the received signal is in CS representation (4.14)

$$\mathbf{y}^t = [\cos\theta_1 \ \cos\theta_2 e^{j\varphi_2} \ \dots \ \cos\theta_T e^{j\varphi_T}]\,, \qquad \theta_1 \in [0, \pi/2) \tag{4.30}$$

where θ_1 is the principal angle between $\Omega_{\mathbf{y}}$ and Ω_{ref}, represented as in (4.13) by $\mathbf{e}_1$. Since the level set (4.29) is an hypersphere, we apply the parameterization (4.94) given in Appendix B.1

$$S_{\cos\theta_r} : \ \mathbf{x} = e^{j\xi_r}(\cos\theta_r \mathbf{y} + \sin\theta_r \mathbf{v})\,. \tag{4.31}$$

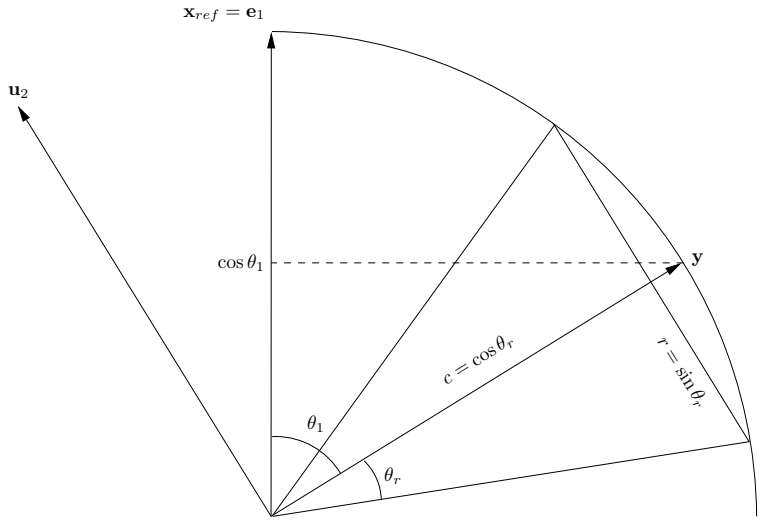

Figure 4.3: Basis vector for the parameterization of the level sets $S_{\cos\theta_r}$.

Since we want to express the points of $S_{\cos\theta_r}$ in CS representation, we choose basis vectors such as to simplify our calculation: the first one is $\mathbf{y}$ and the second one $\mathbf{u}_2$ defined as follows (see Fig. 4.3)

$$\mathbf{u}_2 \in \mathrm{span}(\mathbf{e}_1, \mathbf{y})\,, \qquad \mathbf{u}_2 \perp \mathbf{y}\,. \tag{4.32}$$

These conditions leave a degree in the choice of $\mathbf{u}_2$, which is fixed to have $\mathbf{u}_2$ in CS representation:

$$\mathbf{u}_2 = \frac{1}{\sin\theta_1}(\mathbf{e}_1 - \cos\theta_1 \mathbf{u}_y)\,, \qquad \theta_1 \neq 0, \pi/2\,. \tag{4.33}$$

where we suppose $\theta_1 \neq 0, \pi/2$, which is always verified with probability one when $\mathbf{y}$ is a received vector in a communication system. $\mathbf{u}_2$ is in CS representation because its first entry is $(1 - \cos^2\theta_1)/\sin\theta_1 = \sin\theta_1 > 0$. We rewrite the parameterization of the level set (4.31) according to (4.94)

$$\begin{aligned} &S_{\cos\theta_r} : \ \mathbf{x} = e^{i\xi_r}[\cos\theta_r \mathbf{y} + e^{i\xi_a}\sin\theta_r(\sin\theta_a \mathbf{u}_2 + \cos\theta_a \mathbf{v}_2)] \\ &\text{where } \mathbf{v}_2 \in \mathbb{U}_T^{T-2},\ \mathbf{v}_2 \perp \mathrm{span}(\mathbf{y}, \mathbf{u}_2)\,, \qquad \theta_a \in [0, \pi/2],\ \xi_r, \xi_a \in [0, 2\pi)\,. \end{aligned} \tag{4.34}$$

Orthogonality condition (4.34) eventually imposes a particular form to points $\mathbf{v}_2$

$$\begin{cases} \mathbf{y}^\dagger \mathbf{v}_2 = 0 \\ \mathbf{u}_2^\dagger \mathbf{v}_2 = 0 \end{cases} \overset{(4.33)}{\Longrightarrow} \mathbf{e}_1^\dagger \mathbf{v}_2 = 0 \Longrightarrow v_{2,1} = 0\,, \tag{4.35}$$

Let's use convention (4.23):

$$\mathbf{v}^t = [v_1 \ \hat{\mathbf{v}^t}]\,, \qquad \hat{\mathbf{v}}^t = [v_2 \ \dots \ v_t]\,, \tag{4.36}$$

then $\mathbf{v}_2$ in (4.34) takes the form

$$\mathbf{v}_2^t = [0 \ \hat{\mathbf{v}}_2^t] \quad \text{with} \quad \|\mathbf{v}_2\| = \|\hat{\mathbf{v}}_2\| = 1\,. \tag{4.37}$$

Injecting in (4.35), through convention (4.36) we have

$$\hat{\mathbf{y}}^\dagger \hat{\mathbf{v}}_2 = 0 \quad \Longleftrightarrow \quad \hat{\mathbf{y}} \perp \hat{\mathbf{v}}_2\,. \tag{4.38}$$

We have then obtained the parametric formula (with their corresponding conditions) which express the GLRT level sets on $\mathbb{U}^T$. We are ready for the next step, to translate this level sets on the Grassmannian by removing all the points which represent the same codeword.

4.3.2 GLRT Level Sets on $G_{T,1}^{\times}$

From parameterization (4.34), we can reduce the level sets from $\mathbb{U}^T$ on the Grassmannian, by imposing the CS representation (3.20) to their points. This is equivalent to let x_1, the first component of $\mathbf{x} \in S_{\cos\theta_r}$, be a positive real number (from (4.34), from definitions (4.30), (4.32) and from (4.37)):

$$x_1 = e^{i\xi_r}(\cos\theta_r \cos\theta_1 + e^{i\xi_a} \sin\theta_r \sin\theta_1 \sin\theta_a) > 0 \tag{4.39}$$

This can be obtained in the following way: let

$$\begin{aligned} a &= \cos\theta_r \cos\theta_1 \\ b_{max} &= \sin\theta_r \sin\theta_1 \\ b &= b_{max} \sin\theta_a \end{aligned} \tag{4.40}$$

and

$$\rho = \rho(\theta_a, \xi_a) = \arccos(|a + e^{i\xi_a} b|) = \arccos(|x_1|)\,, \quad \delta = \delta(\theta_a, \xi_a) = \angle(a + e^{i\xi_a} b) \tag{4.41}$$

we have to impose

$$\xi_r = -\delta(\theta_a, \xi_a) = \angle(\cos\theta_r \cos\theta_1 + e^{i\xi_a} \sin\theta_r \sin\theta_1 \sin\theta_a)\,. \tag{4.42}$$

Condition (4.42) fixes a degree of freedom and the dimension of the level set $S_{\cos\theta_r}$ over $G_{T,1}^{\times}$ is $2T-3$. To resume, the level set over the Grassmannian is

$$S_{\cos\theta_r} = \{\mathbf{x} = e^{i\xi_r}[\cos\theta_r \mathbf{y} + e^{i\xi_a} \sin\theta_r (\sin\theta_a \mathbf{u}_2 + \cos\theta_a \mathbf{v}_2)] : \text{(4.42) is satisfied}\}\,, \tag{4.43}$$

with $\theta_a \in [0, \pi/2]$, $\xi_a \in [0, 2\pi)$.

Expression (4.43) eventually gives the level set corresponding to $c = \cos\theta_r$ in the Grassmannian $G_{T,1}$. If we make θ_r run between 0 and a value $\theta_{r,max}$, we obtain a region of the Grassmannian. For example, if $T = 6$, the receive SNR is about 20 dB and $\theta_{r,max} = \pi/13$, there is a probability of about 10^{-5} that the sent codeword is out of this region (see Fig 4.1). Once we have the shape of the level sets on $G_{T,1}$ we must find their shape in the tangent space by mapping them back via the inverse exponential mapping. This is the successive step we described in the next subsection.

4.3.3 Preimage of the Level Sets in the Tangent Space

Operating a slight abuse, we decide here to call tangent space not imbedding space of the matrices $\mathbf{\Delta}$, but of vectors $\mathbf{b}$. These vectors are obtained by inverting the exponential map as in (4.24).

The vector $\mathbf{b}$ which corresponds to $\mathbf{x} \in S_{\cos\theta_r}$ via the exponential mapping is

$$\mathbf{b} = \frac{\rho\, e^{-i\delta}}{\sin\rho}\hat{\mathbf{x}} = \frac{\rho\, e^{-i\delta}}{\sin\rho}\left[\left(\cos\theta_r - \sin\theta_r \sin\theta_a e^{i\xi_a}\frac{\cos\theta_1}{\sin\theta_1}\right)\hat{\mathbf{y}} + \sin\theta_r\cos\theta_a e^{i\xi_a}\hat{\mathbf{v}}_2\right]$$

where we use convention (4.36) and definitions (4.41). Since $\|\hat{\mathbf{y}}\| = \sin\theta_1$, we define the unit vector $\hat{\mathbf{u}}_y = \hat{\mathbf{y}}/\sin\theta_1$, and including the phase factor $e^{i\xi_a}$ inside the hypersphere whose generic vector is $\hat{\mathbf{v}}_2$, we have

$$\mathbf{b} = \frac{\rho e^{-i\delta}}{\sin\rho}\left[(\cos\theta_r \sin\theta_1 - \sin\theta_r\cos\theta_1\sin\theta_a e^{i\xi_a})\hat{\mathbf{u}}_y + \sin\theta_r\cos\theta_a\,\hat{\mathbf{v}}_2\right] \qquad (4.44)$$

where $\hat{\mathbf{v}}_2 \perp \hat{\mathbf{u}}_y$ because of (4.38). Vectors like (4.44) are points of the preimage $S^{-1}_{\cos\theta_r}$ on the tangent–space. We notice that vectors $\mathbf{b}$ have length $T-1$ and, being $S^{-1}_{\cos\theta_r} \subset B_{\pi/2}$, they must have norm inferior to $\pi/2$ (see (4.15)). The dimension of the preimage of the level set is equal to that of the level set, that is $2T-3$. The free parameters in (4.44) are $\hat{\mathbf{v}}_2 \in \mathbb{U}^{T-2}_{T-1} \perp \hat{\mathbf{u}}_y$ and θ_a, ξ_a. θ_r is a fixed parameter which depends on the level set, while θ_1 is fixed by $\mathbf{y}$. Expression (4.44) needs some more comment

- *Effect of the non–linearity of the exponential map.* Vectors $\hat{\mathbf{v}}_2$ run over a $(2T-5)$–dimensional hypersphere in $\mathbb{C}^{T-1}$, which translates along the direction $\hat{\mathbf{u}}_y$. Even if (4.44) looks like the parameterization of an hypersphere, the surface $S^{-1}_{\cos\theta_r}$ is not an hypersphere, since its origin and radius depend on all the parameters. The warping of the surface is due to the non–linearity of the exponential map.

- *Effect of the modulo operation in the definition of Grassmannian.* This is a more subtle effect, due to the fact that the Grassmannian is defined as $\mathbb{U}^T/\mathbb{U}$, i.e. by means of a modulo operation (the quotient on $\mathbb{U}$). As previously recalled, the modulo–$\mathbb{U}$ operation means that several points on the hypersphere correspond to one point on the Grassmannian. This operation introduces discontinuity on the

representatives at the "equator" of the hypersphere, where $\mathbf{x} \perp \mathbf{x}_{ref} = \mathbf{e}_1$. This fact can be better visualized in the case of a real Grassmannian, whose points in CS representation all lie on the upper part of the hypersphere. For example, in Fig. 4.4, a real Grassmannian is represented for $T = 3$. Points $\mathbf{x}_2$ and $\mathbf{x}_3$ represent the same line, which indeed is close to the line represented by $\mathbf{x}_1$. But $\mathbf{x}_3$ is not in CS representation, while $\mathbf{x}_2$ is the correct representative, which is very far from $\mathbf{x}_1$ on the sphere. This situation is reproduced on the tangent space, where the corresponding vector $\mathbf{b}_2$ and $\mathbf{b}_1$ are opposite. The effect of the modulo–$\mathbb{U}$ operation on the complex Grassmannian $G_{T,M}$ is similar but it cannot be represented.

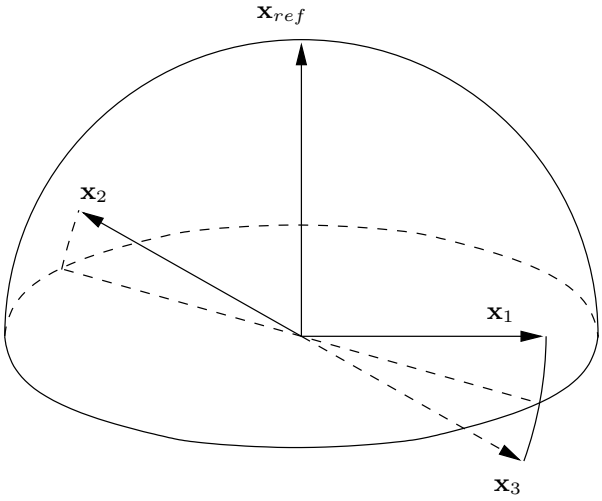

Figure 4.4: A real Grassmannian for $T = 3$ can be represented by an hemisphere. Each point of the "north" hemisphere is in CS representation and its opposite (in the other hemisphere) represents the same subspace.

The modulo–$\mathbb{U}$ effect is present only for those level sets $S_{\cos\theta_r}$ crossing the "equatorial plane" of $G_{T,M}$, i.e. the set of subspaces orthogonal to $\mathbf{x}_{ref}$. This happens if and only if

$$\pi/2 - \theta_r \leq \theta_1 < \pi/2\,. \tag{4.45}$$

We can better understand what happens in the complex case by plotting the behaviour of $\rho = \|\mathbf{b}\|$ and δ (common phase) as a function of ξ_a in polar coordinates. The parameter θ_a is fixed to $\pi/2$, to maximize the component of $\mathbf{x} \in S_{\cos\theta_r}$ which lies on $\text{span}(\mathbf{y}, \mathbf{u}_2)$. This component affects x_1 (the first entry of $\mathbf{x}$), which is responsible of the modulo–$\mathbb{U}$ effect.

Fig. 4.5 illustrates a case in which there is no modulo–$\mathbb{U}$ effect. In fact, the largest closed curve is given by $\theta_{r,max} = \pi/10$ and $\theta_1 = 0.9\,\pi/2 - 0.8\,\theta_{r,max}$, which is less than $\pi/2 - \theta_{r,max}$ so that (4.45) is not satisfied. The other closed curves are given varying θ_r toward 0 and keeping constant θ_1, so that points corresponding to a family

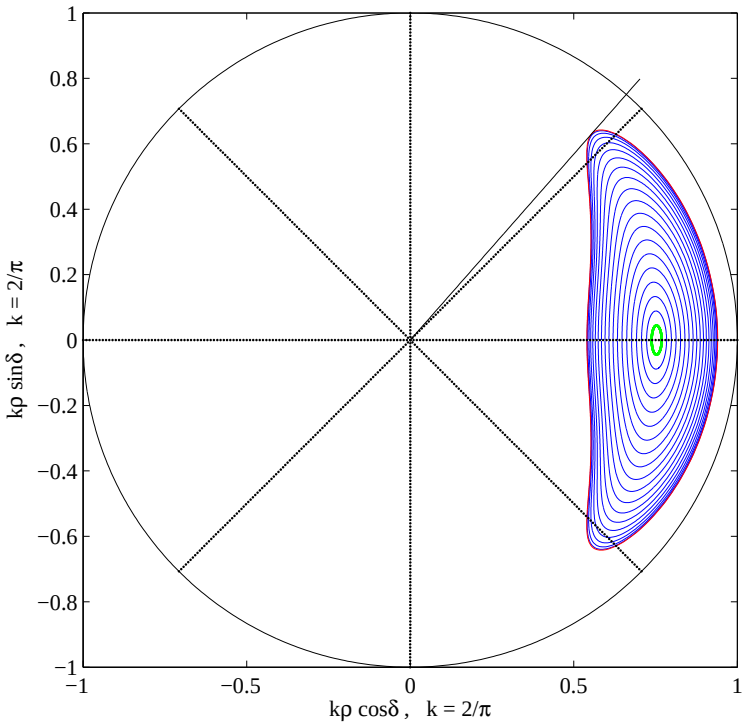

Figure 4.5: Representation of (normalized) $\rho = \|\mathbf{b}\|$ and the common phase δ as a function of ξ_a in polar coordinates. Different curves are obtained for different θ_r, decreasing its value from $\theta_{r,max} = \pi/10$. We set $\theta_1 = 0.9\pi/2 - 0.8\,\theta_{r,max}$. In this example there is no modulo–$\mathbb{U}$ effect, since for all θ_r it holds $\theta_1 < \pi/2 - \theta_r$.

of level sets are plotted. The maximal phase δ is (see Appendix B.2)

$$\bar{\delta} = \arcsin(\tan\theta_r \tan\theta_1) \text{ at } \xi_a = \pm(\pi/2 + \bar{\delta})\,. \tag{4.46}$$

When θ_1 goes to $\pi/2 - \theta_r$ the maximal phase $\bar{\delta}$ goes to $\pi/2$ and the curves become more and more warped. The effect of the non–linearity is the greater the farther $\mathbf{y}$ is from the reference point $\mathbf{x}_{ref}$ (or equivalently, the closer θ_1 is to $\pi/2$).

In Fig. 4.6 we plot an example were the modulo–$\mathbb{U}$ effect is present. In fact, this time $\theta_{r,max} = \pi/10$ and $\theta_1 = \pi/2 - 0.7\,\theta_{r,max}$ so that there are some θ_r for which $\theta_1 > \pi/2 - \theta_r$ (condition (4.45) satisfied). As in the case of Fig. 4.5, curves become more and more warped at growing θ_r. When θ_r becomes greater than $0.7\,\theta_{r,max}$ the curves suddenly pass to the right side of the plane too. On the Grassmannian this corresponds to level sets passing over the "equatorial plane" of the subspaces orthogonal to $\mathbf{x}_{ref}$.

We observe on Fig. 4.5 that subspaces inside the portion of Grassmannian delimited by a level set $S_{\cos\theta_r}$ correspond to preimage points *inside* the (ρ, δ) curve given by that θ_r. On the contrary consider the situation of Fig 4.6, in particular the curve given by $\theta_{r,max}$. Then, the modulo–$\mathbb{U}$ effect is present and the subspaces on the Grassmannian inside the level set $S_{\cos\theta_{r,max}}$ correspond to preimage points are *in between* the (ρ, δ)

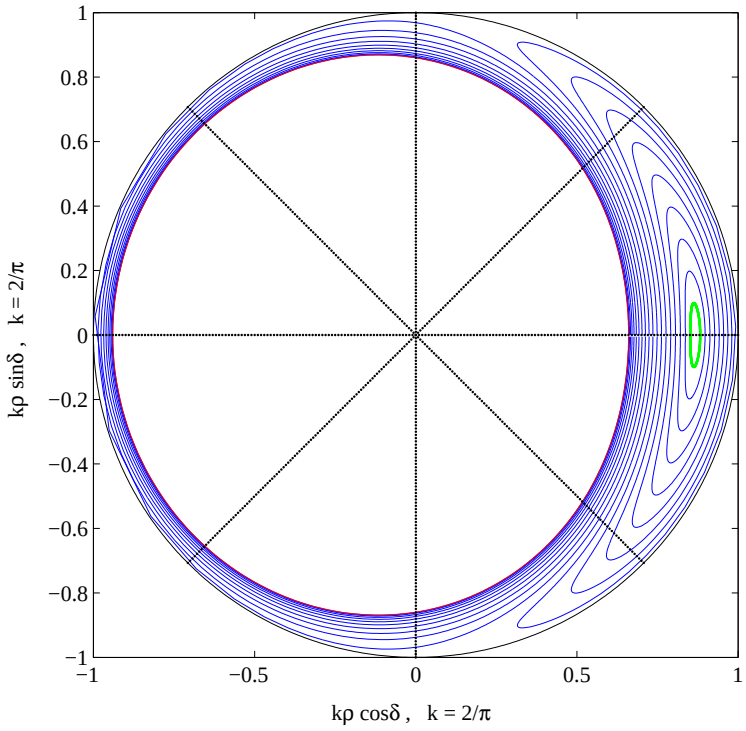

Figure 4.6: Representation of (normalized) $\rho = \|\mathbf{b}\|$ and the common phase δ as a function of ξ_a in polar coordinates. Different curves are obtained for different θ_r, decreasing its value from $\theta_{r,max} = \pi/10$. We set $\theta_1 = \pi/2 - 0.7\theta_{r,max}$. The modulo–$\mathbb{U}$ effect is present for $\theta_r \in (0.7\,\theta_{r,max}, \theta_{r,max}]$.

curve given by $\theta_{r,max}$ and the boundary of the domain $B_{\pi/2}$ (represented by a circle of radius $\pi/2$ in Fig. 4.5 and Fig. 4.6).

We eventually notice that when $\theta_a = \pi/2$ (4.44) reduces to

$$\mathbf{b} = \frac{\rho e^{-i\delta}}{\sin\rho}(\cos\theta_r \sin\theta_1 - \sin\theta_r \cos\theta_1 e^{i\xi_a})\hat{\mathbf{u}}_y \tag{4.47}$$

therefore the common phase factor of $\mathbf{b}$ should take into account the phase of the term $\cos\theta_r \sin\theta_1 - \sin\theta_r \cos\theta_1 e^{i\xi_a}$. It can be shown (see Appendix B.3) that this factor does not change substantially the behaviour of the point $\mathbf{b}$ in the tangent space, for example the condition to have the modulo–$\mathbb{U}$ effect is the same. So that here we preferred to avoid mathematical complication.

4.4 Decoders for EP codes over $G_{T,1}$

If $\mathbf{y}$ is the received signal and the parameter θ_r is properly chosen, the level set $S_{\cos\theta_r}$ of $\psi(\mathbf{x}) = \|\mathbf{y}^\dagger\mathbf{x}\|$ delimits a region of the Grassmannian where it is highly probable to find the sent codeword. However, a GLRT maximization algorithm for sets of discrete

point over the Grassmannian is not available, even if the search region is limited. Now, if the region of $G_{T,M}$ delimited by a level set contains the good sent codeword $\mathbf{X}$ (of the EP code $\mathcal{C}_\mathcal{B}$), the preimage of this region in the tangent space will contain the corresponding codeword $\mathbf{B}$ (of the coherent code $\mathcal{B}$), by continuity of the exponential map. Then, the idea is to perform the search on the tangent space (a linear vector space) where more standard tools are available to efficiently decode.

We therefore studied the preimage of GLRT level sets of the Grassmannian in the tangent space in order to understand their shape. We saw in the previous section that the preimages S_c^{-1} are warped by the non–linearity of the exponential map. Our idea is to approximatively cover these warped regions with a finite number of hyperspheres. The sphere decoder algorithm can then be used to search codewords of $\mathcal{B}$ inside these hyperspheres, under the hypothesis that $\mathcal{B}$ is carved from a lattice. We point out that we do not want to use the sphere decoding algorithm to decode the received codewords, since the sphere decoder solves a coherent ML maximization (2.36). We just exploit the geometrical meaning of a sphere decoder search to find a list of *candidate codewords*, for which the true GLRT metric will be calculated and compared. We call this procedure *local GLRT*, because we want to restrict exhaustive calculation of GLRT metrics to a subset of codebook $\mathcal{C}_\mathcal{B}$, i.e. the list of candidate codewords close to the received signal.

In this section, we show that our idea makes sense first, then we propose our decoder.

4.4.1 Covering the Preimages of the Level Sets with Hyperspheres

In this subsection we suppose that the modulo–$\mathbb{U}$ effect is not present

$$\theta_1 < \pi/2 - \theta_r \,. \tag{4.48}$$

This condition can never be satisfied with probability one during a communication. However, it is possible to control the probability of $\{\theta_1 > \pi/2 - \theta_r\}$ through a reduction of θ_r and/or of the maximum $\|\mathbf{b}\|$, $\mathbf{b} \in \mathcal{B}$ via the homothetic factor (see Sect. 4.4.4).

Points close to the Reference Subspace

Let us suppose that the sent subspace is near to the reference subspace, i.e. $\theta_1 \to 0$, so that $\sin\theta_1 \simeq \theta_1$ and $\cos\theta_1 \simeq 1$. Then $\delta \simeq \theta_1 \tan\theta_r \sin\theta_a$ and it goes to zero (null phase). In the same hypothesis $\rho \simeq \theta_r$. The preimage (4.44) becomes

$$\mathbf{b} \simeq \frac{\theta_r\,\theta_1}{\tan\theta_r}\hat{\mathbf{u}}_y + \theta_r(e^{i(\xi_a+\pi)}\sin\theta_a\hat{\mathbf{u}}_y + \cos\theta_a\hat{\mathbf{v}}_2)\,, \qquad \hat{\mathbf{v}}_2 \perp \hat{\mathbf{u}}_y\,,\ \|\hat{\mathbf{v}}_2\| = 1\,. \tag{4.49}$$

Expression (4.49) describes a complex hypersphere of radius θ_r centered at $\theta_r\,\theta_1/\tan\theta_r$ $\hat{\mathbf{u}}_y$, which is close to the origin of the tangent space. If also θ_r is small, we can approximate $\theta_r/\tan\theta_r \simeq 1$, so that the hypersphere in centered at $\theta_1\hat{\mathbf{u}}_y = \mathbf{b}_y = \exp^{-1}(\mathbf{y})$. We also remark that for $\theta_1 = 0$, the exact expression of preimages $S^{-1}_{\cos\theta_r}$ is $S^{-1}_{\cos\theta_r} = \{\mathbf{b} = \theta_r(e^{i(\xi_a+\pi)}\sin\theta_a\hat{\mathbf{u}}_y + \cos\theta_a\hat{\mathbf{v}}_2)\}$, i.e. hyperspheres for every valid value of θ_r.

The conclusion is that, *for received points close to the reference space*, the preimages are very well approximated by hyperspheres. Since curves with constant GLRT metric on $G_{T,1}$ have the same shape on the tangent space, *coherent ML detection on the tangent space is reasonably a good approximation of GLRT detection on the Grassmannian*.

Points far from the Reference Subspace

Let's define

$$r = \frac{\rho}{\sin\rho}\sin\theta_r\,, \qquad \mathbf{o} = \frac{\rho e^{-i\delta}}{\sin\rho}\cos\theta_r\sin\theta_1\,\hat{\mathbf{u}}_y\,. \tag{4.50}$$

We rewrite (4.44) in the following way

$$\mathbf{b} = \mathbf{o} + re^{-i\delta}(-\cos\theta_1\sin\theta_a e^{i\xi_a}\hat{\mathbf{u}}_y + \cos\theta_a\,\hat{\mathbf{v}}_2)\,. \tag{4.51}$$

The absolute value of the second addend of (4.51) is

$$\|re^{-i\delta}(-\cos\theta_1\sin\theta_a e^{i\xi_a}\hat{\mathbf{u}}_y + \cos\theta_a\,\hat{\mathbf{v}}_2)\|^2 = r^2(1-\sin^2\theta_1\sin^2\theta_a) \le r^2\,.$$

Hence, $S^{-1}_{\cos\theta_r}$ is contained inside the volume delimited by

$$\mathbf{b} = \mathbf{o} + r(\sin\theta_a e^{i\xi_a}\hat{\mathbf{u}}_y + \cos\theta_a\,\hat{\mathbf{v}}_2) \tag{4.52}$$

under the condition that *the modulo–$\mathbb{U}$ effect is not present*. The set spanned by (4.52) is a family of hyperspheres with center $\mathbf{o}$ and radius r continuously depending on $\theta_a \in [0,\pi/2]$ and $\xi_a \in [0,2\pi)$.

We upper bound the variable radius r in order to reduce and simplify the dependence on the different parameters. Maximizing r is equivalent to maximize ρ, because r is a monotonic increasing function for $\rho \in [0,\pi/2)$. However, ρ is an arc-cosine so that it reaches its maximum when its argument $|a + e^{i\xi_a}b|$ is minimum. Since there is no modulo–$\mathbb{U}$ effect, the minimum is achieved for $\xi_a = \pi$ and $\theta_a = \pi/2$, which gives $|a - b_{max}| = \cos(\theta_1+\theta_r)$ and finally

$$r \le r_{max} = (\theta_1+\theta_r)\sin\theta_r/\sin(\theta_1+\theta_r) \tag{4.53}$$

where $\theta_1+\theta_r < \pi/2$ in our hypothesis. When the maximum is reached $\delta = 0$.

Then, set $S^{-1}_{\cos\theta_r}$ is contained inside the volume delimited by

$$S = \{\mathbf{b}\in B_{\pi/2}\,:\,\mathbf{b}\in\{\mathbf{o}(\theta_a,\xi_a) + r_{max}\mathbb{U}^{T-1},\,\theta_a\in[0,\pi/2],\,\xi_a\in[0,2\pi)\}\,. \tag{4.54}$$

Now, only the center of the spheres depends on free parameters.

The center $\mathbf{o}$ always belongs to the subspace generated by $\hat{\mathbf{u}}_y$, but it has a changing absolute value and common phase. These two quantities have maximal excursion when $\theta_a = \pi/2$, i.e. when the component in the subspace of $\hat{\mathbf{v}}_2$ is absent

$$|\theta_1-\theta_r|\cos\theta_r\sin\theta_1/\sin(|\theta_1-\theta_r|) \le o = \|\mathbf{o}\| \le \theta_1+\theta_r\cos\theta_r\sin\theta_1/\sin(\theta_1+\theta_r)$$

if $\theta_r \leq \theta_1 < \pi/2 - \theta_r$. In these extremal values, since the component orthogonal to $\mathbf{u}_y$ is null, the volume contained by the set of points obtained for $\theta_a = 0$ is null in $\mathbb{C}^{T-1}$. Hence, in the following we fix the center at $\theta_a = 0$ where the component orthogonal to $\hat{\mathbf{u}}_y$ is maximized obtaining maximum volume and from (4.51) and (4.54)

$$\mathbf{b} = \mathbf{o} + r_{max}\hat{\mathbf{v}}_2\,, \qquad o = \|\mathbf{o}\| = \frac{\rho_0}{\sin\rho_0}\cos\theta_r \sin\theta_1\,, \qquad \rho_0 = \arccos(\cos\theta_r\cos\theta_1)\,. \tag{4.55}$$

To conclude, when the received point is far from the reference space, the preimages of the level sets are not hyperspheres, therefore GLRT and coherent ML criterion on the tangent space do not coincide. However, since the preimages of the level sets are contained inside a family of hyperspheres (4.54) with fixed radius and varying center, covering these sets with a finite number of hypersphere makes sense.

4.4.2 Decoder Proposal

The previous discussion leads us to a deep understanding of the effect of non–linearity and modulo–$\mathbb{U}$ operation on the level sets of the GLRT rule. However, we do not try to show how many hyperspheres are necessary to cover exactly (4.54) in the tangent space. We preferred to limit complexity by fixing the number of sphere search. Then we optimize sphere parameters to obtain a good covering, which means good performance.

The *local GLRT decoder* for $M = N = 1$ can be implementd by the following proposed algorithm

1. Choose a parameter θ_{nl} which measures when the non–linearity of the exponential map becomes negligible.

2. Choose a parameter θ_r which decides the maximal distance (as principal angle) between the received signal subspace and the codewords subspaces. The smallest θ_r, the fewer number of points in the list to be controlled during local GLRT. Values of θ_r and of θ_{nl} make sense if satisfy $\theta_{nl} \leq \pi/2 - \theta_r$.

3. Let $\mathbf{y}$ be the unit vector in CS representation which spans the subspace generated by the received signal. Let $\theta_1 = \arccos(y_1)$ be the principal angle between $\mathbf{y}$ and $\mathbf{x}_{ref} = \mathbf{e}_1$.

4. If $\theta_1 \leq \theta_{nl}$, we use the approximation for codewords close to the reference space. Let $\mathbf{b}_y = \exp^{-1}(\mathbf{y}) = \theta_1\hat{\mathbf{u}}_y$, use a sphere decoder to find the closest point to $\mathbf{b}_y$, i.e. the estimated $\mathbf{b}$ is

$$\mathbf{b}_{chosen} = \mathbf{x}^{co-ML-tg} = \min_{\mathbf{b}\in\mathcal{B}} \|\mathbf{b}_y - \mathbf{b}\|\,. \tag{4.56}$$

5. If $\theta_{nl} < \theta_1 \leq \pi/2 - \theta_r$, we substitute the search inside the preimage $S^{-1}_{\cos\theta_r}$ with three sphere searches, with radius (4.53)

$$r_{max} = (\theta_1 + \theta_r)\sin\theta_r / \sin(\theta_1 + \theta_r) \tag{4.57}$$

and centers

$$\mathbf{o}_{1,2,3} = o\, e^{i\delta_{1,2,3}} \hat{\mathbf{u}}_y \,, \qquad o = \frac{\rho_0}{\sin \rho_0} \cos\theta_r \sin\theta_1 \,, \qquad \rho_0 = \arccos(\cos\theta_r \cos\theta_1) \tag{4.58}$$

where

$$\delta_1 = 0 \,, \qquad \delta_{2,3} = \pm \arcsin(\tan\theta_r \tan\theta_1)/\delta_F \tag{4.59}$$

and scaling factor $\delta_F > 1$ can be optimized to minimize performance. The three searches give a list of candidate points $\mathcal{L}_{\mathcal{B}} = \{\mathbf{b}_{l_1}, \ldots, \mathbf{b}_{l_L}\}$, from which the corresponding list of $\mathcal{C}$ is constructed $\mathcal{L}_{\mathcal{C}} = \{\mathbf{x}_{l_1}, \ldots, \mathbf{x}_{l_L}\}$. The decoded point is

$$\mathbf{x}_{chosen} = \min_{\mathbf{x} \in \mathcal{L}_{\mathcal{C}}} |\mathbf{y}^\dagger \mathbf{x}| \tag{4.60}$$

6. If $\theta_1 > \pi/2 - \theta_r$, the modulo–$\mathbb{U}$ effect is present and the search should be performed in all the region close to the boundary of $B_{\pi/2}$. We prefer not increase the number of sphere searches, but to perform again three searches, with the same radius r_{max}, the same centers (4.58) but with different $\delta_{2,3}$ i.e.

$$\delta_{2,3} = \arccos\left[1 - \frac{1}{2}\left(\frac{k r_{max}}{o}\right)^2\right] \tag{4.61}$$

where k is chosen by optimization. To understand the choice (4.61) see Appendix B.4.

We rapidly explain the role of each parameter

- θ_{nl} divides the Grassmannian into two zones, the first one contains the referene space and the other does not. Points of the first zone have principal angle with $\mathbf{x}_{ref}$ less than θ_{nl}. Point of the second zone have principal angle with $\mathbf{x}_{ref}$ greater than θ_{nl}. For points in the first zone, we consider that non–linearity is negligible. This parameter influences the complexity of the decoder, since only one sphere search is needed (no local GLRT).

- θ_r fixes the "size" of the level set: the smaller θ_r, the closer the level set preimages are to $\mathbf{b}_y$. We also have that the smaller θ_r, the less probable the modulo–$\mathbb{U}$ effect is (because the received point $\mathbf{y}$ must be closer to the "equatorial plane" so that the level set crosses it). θ_r must not be chosen too small because, is noise is too strong, no point can be found inside the preimage (this is not a problem with big codebooks).

- δ_F. The sphere centers of the family S in (4.54) lie on the same direction $\mathbf{o}$, whose norm is reported in (4.58). The common phase of $\mathbf{o}$ is variable and its maximum value is $\arcsin(\tan\theta_r \tan\theta_1)$. We approximate family S with three hyperspheres: the first one has zero phase δ, the other two have opposite phases and their absolute value is in between zero and the maximum. Parameter δ_F permits to choose a particular δ in that interval ($\delta_F = 1$ corresponds to the maximum, $\delta_F = \infty$ corresponds to 0, see (4.59)).

- k in (4.61) controls the common phase of the hyperspheres with non–zero common phase, but in this case we have not a limit because of the modulo–$\mathbb{U}$ effect.

4.4.3 Complexity

We investigate the order of magnitude of the complexity of our decoder.

First of all, suppose to fix the parameter $\theta_{nl} = \pi/2$: the suboptimal coherent ML criterion on the tangent space (4.56) is used to decode all received signals. This correspond to the simplified decoder proposed in [31]. We denote this kind of decoder by *coherent ML on the tangent space* (co–ML–tg). The computational complexity of this decoder is

- to bring $\mathbf{y}$ in the CS representation we need: 1) $4T$ real multiplications, $T-1$ real additions and a square root operation (to normalize $\mathbf{y}$) 2) one phase estimation and T complex multiplications (to have the CS form) (one complex multiplication correspond to 4 real multiplications and 2 real additions).

- to invert the map and obtain $\mathbf{b}_y$: 1) one arc-cosine computation, 2 real multiplications, one real addition, and a square root computation (calculation of the scalar factor in (4.24)); 2) $2(T-1)$ real multiplications, (to finally calculate $\mathbf{b}_y$)

- to calculate the ML estimation (4.56) through a sphere decoder we have an expected complexity of $O([2(T-1)]^3)$ as explained in Sect. 2.8.

If we suppose to perform the nonlinear operation with a look–up table, the total complexity is

$$\begin{aligned}\text{co–ML-tg complexity:}\quad & O(8(T-1)^3) + 10T(\text{real mult.}) + 3T(\text{real add.}) \\ & + 2(\text{sqrt}) + 2(\text{look–up table})\end{aligned} \tag{4.62}$$

Notice that the expected complexity of the sphere search is pessimistic, because the lattice is known in (4.56) (no channel influence). Hence, low–complexity algorithms can be implemented for the particular lattice. For example, when the codebook is a Q–QAM^{T-1} a threshold detector can be implemented and multiplications are the most complex operation.

For the local GLRT decoder, the complexity analysis is not simple, so that we provide a raugh study. The derivation is the same as the co–ML–tg decoder, until the calculation of θ_1. Then

- choose the decoder to be applied in the following way:

  - if $\theta_1 \leq \theta_{nl}$ the co–ML–tg decoder is chosen. This happens only during a part of the total transmission duration. The duration percentage can be roughly estimated (at high SNR) by the ratio between the number L_{nl} of codewords for which $\|\mathbf{b}\| \leq \theta_{nl}$ and the code cardinality L.

- if $\theta_1 > \theta_{nl}$, three sphere searches are performed: 1) 6 real multiplications and 4 non–linear operations are performed (calculations of o and r_{max}; 2) 3 real multiplications, 1 non–linear operation and one comparison, $\theta_1 \leq \pi - \theta_r$ (calculation of $\delta_{2,3}$ in both cases of modulo–$\mathbb{U}$ effect or not); 3) nearly $6T$ real multiplication (calculation of the centers); 4) expected complexity $3O(8(T-1)^3)$ (three sphere searches), and $2(T-1)L_{av}$ memory cell (L_{av} is the average length of the candidate codewords list, which must be stocked).

- estimation of the sent codeword through (4.60): 1) $L_{av}(10T-3)$ real multiplications (to calculate metrics) and L_{av} memory cells (stock them) (calculation of the GLRT metrics); 2) L_{av} comparisons (to find the maximum).

The leading term of local GLRT complexity is clearly given by the sphere searches and by the calculation of GLRT metrics for candidate codewords. Summarizing

$$\begin{aligned} \text{local GLRT complexity:} \quad & 3O(8(T-1)^3) + (L_{av}(10T-3) + 18T + 9)(\text{real mult.}) \\ & + (L_{av}+2)(\text{comparisons}) + 5(\text{look–up table}) \end{aligned} \tag{4.63}$$

Since the length L_{av} of candidate lists is not a deterministic parameter, complexity (4.63) must be understood as a random variable. We will discuss later the average and standard deviation of L_{av}, through simulations. Real implementations of this algorithm must also cope with the memory size, which is variable too. The fact that the lattice is known can help to better control L_{av}, but it does not simplify the decoder complexity.

4.4.4 Choice of Decoder Parameters

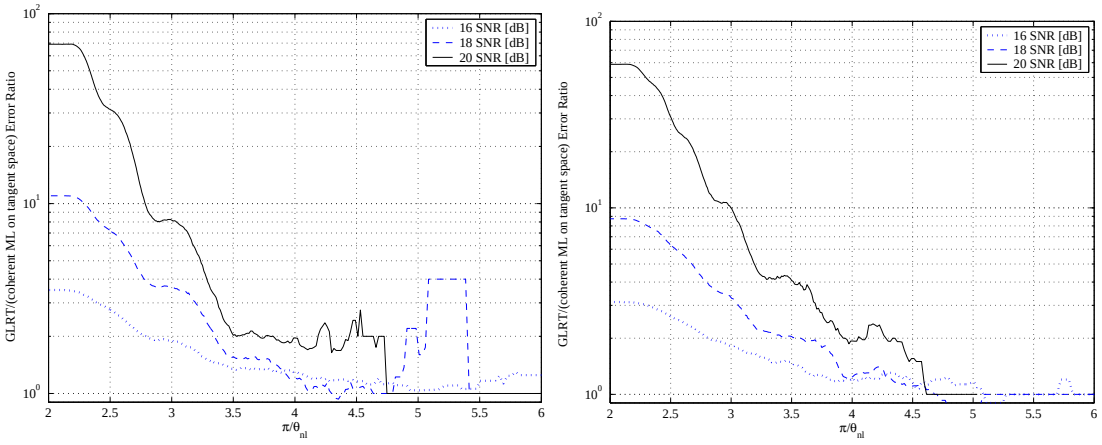

Figure 4.7: Effect of non–linearity in the decoding with the coherent ML decoder on the tangent space.Left plot: the codebook has 256 codewords. Right plot: the codebook has 4096 codewords.

The optimal choice of parameters presented in the previous subsection depends on codebook $\mathcal{C}$ (therefore on $\mathcal{B}$ and on homothetic factor α), on T and on the SNR. It also

depends on the optimization criterion: performance or complexity. In the following, we present some general guidelines for the choice of these parameters. In this section homothetic factor α was chosen as explained in Sect. 4.2.3.

The parameter θ_{nl} selects the zone of the Grassmannian around the reference subspace where we neglect the non–linearity on the exponential map. Each point of curves in Fig. 4.7 represents the ratio between errors made by the co–ML–tg decoder and the GLRT decoder, for θ_1 less than the abscissa of the curve, which represents a given θ_{nl} conveniently normalized. The examples reported in Fig. 4.7 come from two codebooks: $(16\text{–QAM})^2$ and $(16\text{–QAM})^3$ (see next section for details). The non–linearity effect is very important for $\theta_{nl} > \pi/4$. It is stressed increasing the received average SNR, because for low SNR the main source of error is the additive noise: only when the noise power is negligible the effect of non–linearity is recognizable. Simulations curves are not smooth due to the small number of error events for $\theta_{nl} < \pi/4$, because only a small fraction of codewords are located in that region. In the following θ_{nl} is fixed between $\pi/6$ and $\pi/4$, assuring best performance. The impact on complexity is negligible, because, for these values of θ_{nl}, the co–ML–tg decoder is used only during a small faction of the total communication duration.

The angle θ_r was chosen $\theta_r \leq \pi/13$, according to the particular communication system, so that $\cos\theta_r \leq 0.97$. In Fig. 4.1 we can see that this choice assures to find the sent codewords inside the level set $S_{\cos\theta_r}$ with a probability inferior to 10^{-5}, at high SNR (where non–linearity is the main source of errors). The exact choice of θ_r also depends on the code size. For large codebooks a too big θ_r gives big L_{av} and hence a complexity augmentation.

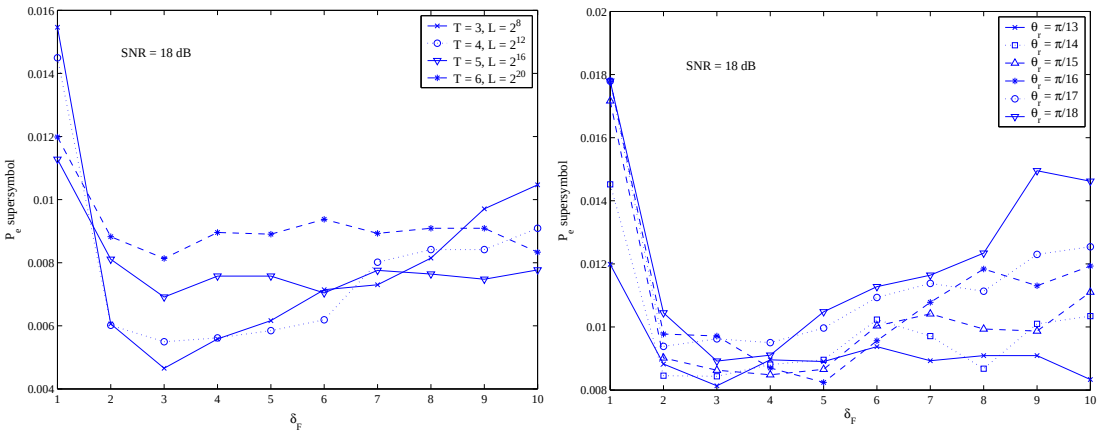

Figure 4.8: Left plot: the effect of δ_F for codebooks $(16\text{–QAM})^{T-1}$ with growing cardinality for $\cos\theta_r = 0.97$. Right plot: the effect of δ_F in the case of $(16\text{–QAM})^5$ with different θ_r.

The parameter δ_F was usually chosen equal to 2. We are reporting here some simulations for the codes $(16\text{–QAM})^{T-1}$, with $T = 3, 4, 5, 6$. Simulations are performed with $\theta_{nl} = \pi/5$, $k = 1.5$ at average receive SNR equal to 18 dB. The number of super-

symbols error are superior to 200 for each curve point. In Fig. 4.8 supersymbol average error probability is plotted with respect to δ_F for different codebooks $(16\text{–QAM})^{T-1}$, with growing cardinality. The second plot of Fig. 4.8 clearly shows that there is an interval of values of δ_F, approximatively from 2 to 5, which minimizes the error probability. The bigger the codebook size is, the larger this interval becomes. This can be explained by the fact that the denser the code is, the closer must be the solution to the received point, if a correct detection is performed (we recall that greater δ_F correspond to sphere closer to the received point in the tangent space). In Table 4.1 we report parameters and simulation results for communication system of Fig. 4.8. σ^2 is the noise complex variance as in Fig. 4.1 and L_{av} is the mean length of candidate codewords lists calculated for $\delta_F = 10$. The variation of L_{av} is in fact not significant in the range of variation of δ_F. We can see that L_{av} of lists used in local GLRT is multiplied only by 10 when the code size is respectively multiplied by 10^3. We point out that the θ_r used in this case is not optimized for big codebooks.

T	L	σ^2 [dB]	L_{av}	L_{av}/L
3	2^8	22.8	4.0	$0.15\,10^{-1}$
4	2^{12}	24.0	6.4	$0.16\,10^{-2}$
5	2^{16}	25.0	12.5	$0.2\,10^{-3}$
6	2^{20}	25.8	25.0	$0.2\,10^{-4}$

Table 4.1: Evolution of some decoder parameters for different $(16\text{–QAM})^{T-1}$ codes.

The second plot of Fig. 4.8 is obtained for fixed $T = 6$ and code $(16\text{–QAM})^5$ at 18 dB SNR. The curve for $\theta_r = \pi/13$ is in common with the firs plot. Parameter θ_r is decreased and supersymbol error probability (or FER) increases at $\delta_F > 5$, and its behaviour is similar to that of the curve for $T = 3$ in the first plot of Fig. 4.8. Hence, $\cos\theta_r = 0.97$ is a good choice for codes with low T, but introduces redundant complexity for codes with greater T. This can also be argued from Table 4.2, where the standard deviation σ_{av} of the length of candidate codeword lists is reported. From the second plot of Fig. 4.8 and Table 4.2, we can see that for code $(16\text{–QAM})^5$, θ_r can be decreased without loosing in performance by reducing the average length of the lists to some unities, like in the case of $T = 3$ in Table 4.2. This fact let us guess that, when an optimal θ_r is chosen for each codebook and δ_F is in between 2 and 5, L_{av} *is basically constant over a large range of codebook sizes* and lower than 10. Under this hypothesis, the leading term of expected complexity (4.63) is the $O(T^3)$ term if $T > 4$, while if $T = 2, 3$ the term with L_{av} becomes the most important. These considerations, which hold for these simulations, need more extensive simulations to be generalized.

Finally, let's consider the last parameter k, when modulo–$\mathbb{U}$ effect can be present. In Fig. 4.8 the average supersymbol error probability is plotted for code $(16\text{–QAM})^{T-1}$ with $T = 3, 6$, $\delta_F = 3$ and $\cos\theta_r = 0.97$ at 18 dB SNR. A proper choice of k is necessary not to degrade the performance, but the parameter is more sensible for small size codebooks. This behaviour can be explained by the choice of homothetic factor α. In fact, due to α, the maximum $\|\mathbf{b}\|$ of the code with $T = 3$ is about 1.35, while

θ_r	L_{av}	L_{av}/L	σ_{av}	σ_{av}/L
$\pi/13$	25.0	$0.24\,10^{-4}$	8.5	$0.81\,10^{-5}$
$\pi/14$	13.8	$0.13\,10^{-4}$	6.4	$0.60\,10^{-5}$
$\pi/15$	9.0	$0.09\,10^{-4}$	5.5	$0.53\,10^{-5}$
$\pi/16$	6.6	$0.06\,10^{-4}$	5.1	$0.48\,10^{-5}$
$\pi/17$	5.2	$0.05\,10^{-4}$	3.3	$0.32\,10^{-5}$
$\pi/18$	4.7	$0.04\,10^{-4}$	3.3	$0.32\,10^{-5}$

Table 4.2: Evolution of some decoder parameters for different θ_r fixed code (16–QAM)^5, ($T = 6$, $L = 2^{20}$), at 18 dB average (on supersymbols) receive SNR.

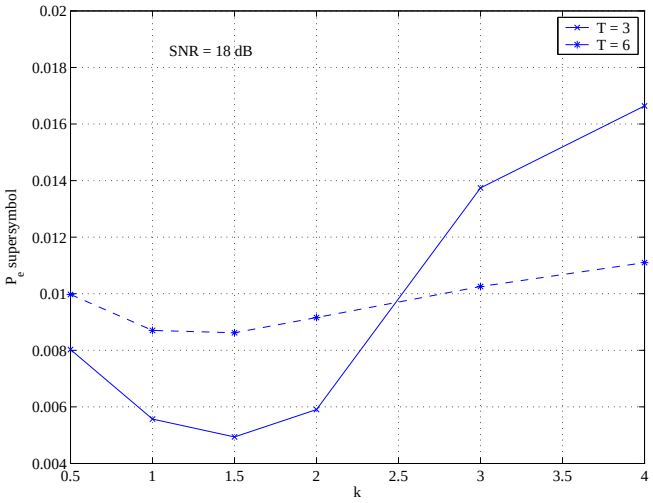

Figure 4.9: The effect of k for codebooks (16–QAM)$^{T-1}$ with $T = 3, 6$, with $\delta_F = 3$ and $\cos\theta_r = 0.97$ at 18 dB SNR.

for the code with $T = 6$ is 1.42. Generally, the modulo–$\mathbb{U}$ effect affects codewords of (16–QAM)^5 with higher probability than codewords (16–QAM)^2. In other words, when T increases, the correct codeword has higher probability to be located far from the received point ($k > 2$).

4.5 Simulations

We report in this section some simulations for the case $M = 1$ and $N = 1$ on AWGN channel with unknown phase, and for $M = 1$, $N \geq 1$ on the Rayleigh channel. No outer code is considered in these simulations. Codebooks are of type $\mathcal{B} = (Q$–QAM$)^{T-1}$. We recall that the co–ML–tg decoder is a simple threshold detector for this codebooks. Comparisons are performed with other propositions.

4.5.1 Simulations for AWGN with Unknown Channel Phase

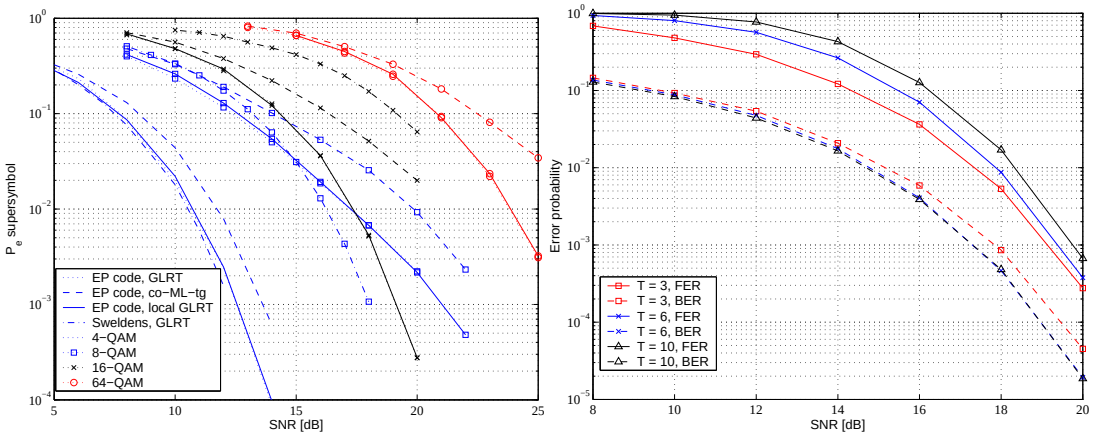

Figure 4.10: Left plot: performances of EP codes from coherent codes $(Q\text{–QAM})^{T-1}$ with $T = 3$ and $Q = 4, 8, 16, 64$. We set $\cos\theta_r = 0.97$ and $\delta_F = 3$, $\theta_{nl} = \pi/6$. Comparisons are also performed with proposal of Sweldens [74]. Right plot: Performances (average supersymbol error probability or FER and BER) of EP codes from $(16\text{–QAM})^{T-1}$ with $T = 3, 6, 10$.

The left plot of Fig. 4.10 represents performances (average supersymbol error or FER) of EP codes coming from coherent codes $(Q\text{–QAM})^2$ ($T = 3$), for $Q = 4, 8, 16, 64$. We used different decoding criteria: the GLRT (implemented by exhaustive search), the proposed local GLRT and the coherent ML criterion on tangent space (co–ML–tg). The channel model used is the AWGN with unknown phase, while simulation is stopped after 500 supersymbol errors at least. The proposed local GLRT follows closely the GLRT performances, while the co–ML–tg is close to the GLRT performances only when the size of the codebook is not large. Code $(8\text{–QAM})^2$ has very bad performance due to bad constellation shaping. In Fig. 4.10 a comparison with [74] is made. Sweldens proposed an efficient decoding algorithm of complexity $O(T \log T)$ for codes based on the Q–PSK constellation

$$\mathbf{x}^t = [1 \; e^{j2\pi k_1/Q} \; \dots \; e^{j2\pi k_{T-1}/Q}], \qquad k_1, \dots, k_{T-1} \in \{0, 1, \dots, Q-1\}. \quad (4.64)$$

For $Q = 4$, EP codes and codes of the kind (4.64) have equivalent performance. When $Q \geq 16$, EP codes outperform codes (4.64) because the minimal distance between codewords of Q–PSK is smaller than the one of Q–QAM (currently the simplified decoding exists only for codes (4.64) based on Q–PSK).

In the right plot of Fig. 4.10, we can see the performance of EP codes from $(16\text{–QAM})^{T-1}$ with $T = 3, 6, 10$ and AWGN noise with unknown channel phase. Decoding is done via local GLRT with the same parameters of previous case (except for $T = 10$, where $\theta_r = \pi/19$ is chosen to have small lists).

4.5.2 Simulations for Rayleigh SIMO Block Fading Channels

As mentioned in the first section of this chapter, we propose to use the same detector, in SIMO case. To this end, received signal $\mathbf{Y}$ provides an estimated direction via signal processing described in (4.8). Once the estimated direction is obtained, suboptimal criterion (4.10) is used instead of true GLRT (4.7), and the maximization problem is solved via local GLRT or co–ML–tg decoder. Nevertheless, our simulations show that GLRT performances are always matched.

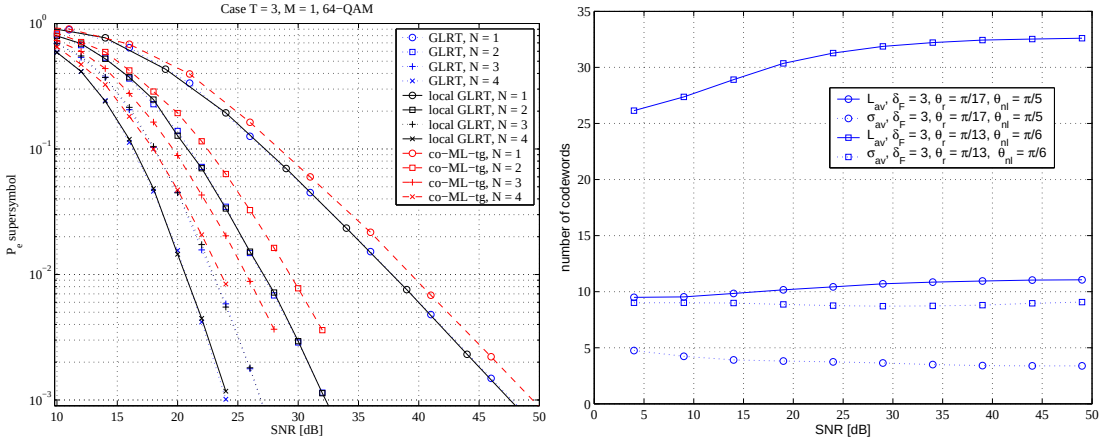

Figure 4.11: Left plot: performances of EP codes coming from $(64\text{–QAM})^2$ ($T = 3$), for $N = 1, 2, 3, 4$. Decoder parameters: $\cos\theta_r = 0.97, \delta_F = 2, \theta_{nl} = \pi/6$. Simulation stopped with more than 500 supersymbol errors. Right plot: behaviour of the mean and standard deviation of candidate lists length for local GLRT for the case $(64\text{–QAM})^2$ with one receive antenna ($N = 1$).

In the left plot of Fig. 4.11, performances of EP code from $(64\text{–QAM})^2$ ($T = 3$) are plotted in the case of different receive antennas. We notice that the local GLRT matches with the GLRT performances. We notice also that both simplified decoders (local GLRT and co–ML–tg) maintain full (receive) diversity. Nevertheless, the co–ML–tg decoder exhibits a growing SNR loss (for fixed error probability) as the number of receive antennas grows. In the right plot of Fig. 4.11, we show the behaviour of the mean and standard deviation of lengths of the candidate lists for local GLRT. We used the same code, with $N = 1$ in two different cases: one with parameters chosen in a conservative way and the other with better optimized parameters. We can see that in both cases, the mean and standard deviations substantially remain constant over a large interval of average received SNR.

At the left of Fig. 4.12 we see that the performances on Rayleigh channels converge to the ones on AWGN for growing N. This happens when the received SNR is normalized so that the total received power (from all receive antennas) is equal to transmit power (in our case channel complex fading have variance $1/N$). The right plot of Fig. 4.12 show performances for different codes $Q = 4, 8, 16, 64, 256$

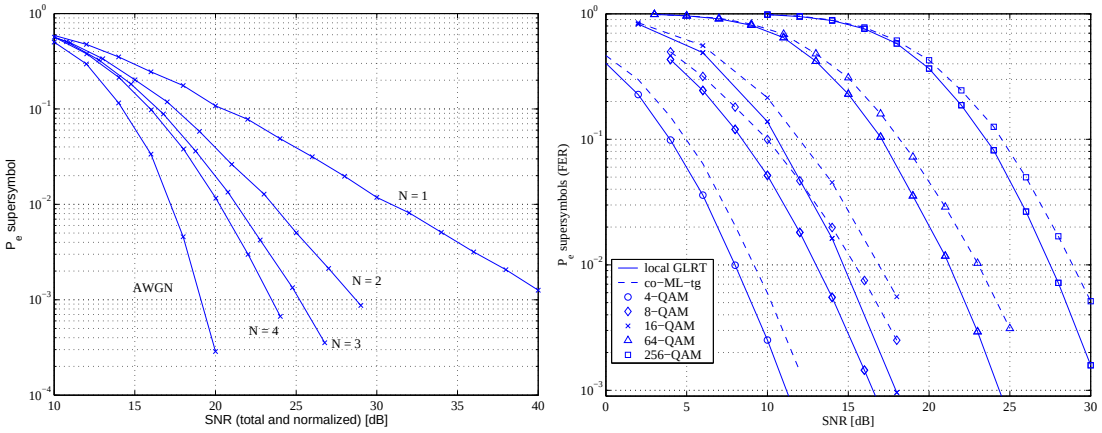

Figure 4.12: Left plot: performances of EP code from $(16\text{–QAM})^2$ ($T = 3$) on a Rayleigh block fading channel converge to performance on AWGN channel with unknown phase (if the SNR is properly normalized). Right plot: performances of different codes for $T = 4$ and $N = 4$.

and $N = 4$, with local GLRT and co–ML–tg. Spectral efficiencies are respectively $\eta = (\log_2 Q)(T-1)/T = 3/2, 9/4, 3, 9/2, 4$. EP code from 8–QAM works better than in AWGN case, due to the Rayleigh channel. We see that the local GLRT gain with respect to the co–ML–tg decoder goes from 1 to 2 dB at 10^{-2} FER (or supersymbol error probability), which is practically constant with respect to the SNR. The loss is greater for 8–QAM, 16–QAM and it decreases for lower or higher cardinality constellations.

In the left plot of Fig. 4.13, we measured SNR loss at 10^{-3} BER, due to decoding with co–ML–tg in stead of local GLRT. For fixed T, the loss increasess at a growing number of receive antennas. For fixed N, the loss decreases at growing N. As in the right plot of Fig. 4.12, loss is slightly greater in "medium size" constellations (8 and 16–QAM).

In the right plot of Fig. 4.13 comparisons with different propositions in the literature are performed [26], [16], [23]. We plot spectral efficiency versus E_b/N_0 at 10^{-3} BER, for $T = 2$, in order to compare with codebooks obtained by numerical optimization [16] (for greater T this benchmark is not available due to the numerical impossibility to perform such optimizations). For spectral efficiency 1.5 bits/s/Hz, EP codes are drawn from 8–QAM and have bad performance due to the rectangular shape of the constellation, as previously explained. This problem can be mitigated using constellations with different shapes. We can see that our proposition works better than every other one in certain cases (16 and 64 –QAM). However, for low and high spectral efficiencies, training based schemes work better. In this figure, training is performed sending a known first symbol (equal to 1) to extract the channel estimation. Data symbols, drawn from QAM constellations, follow. As a matter of fact, the advantage of training systems consists in their low decoding complexity: the estimation of the chan-

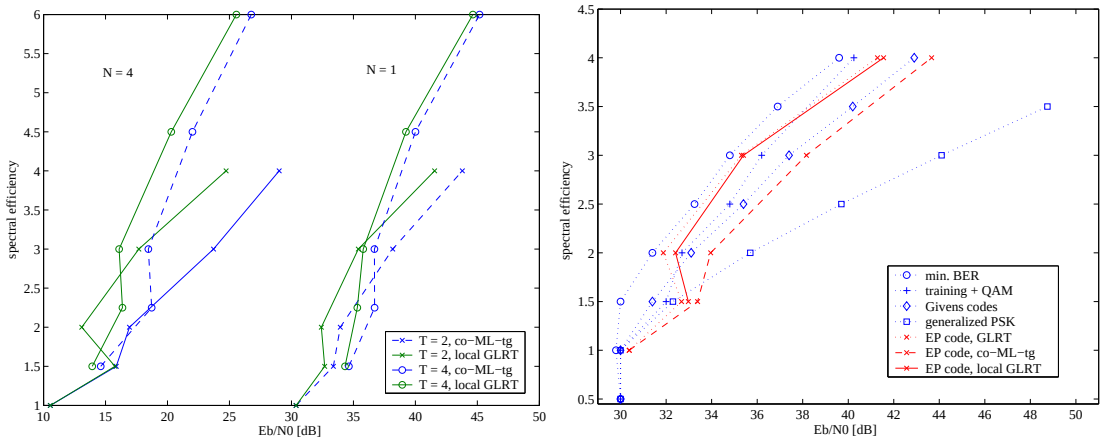

Figure 4.13: Left plot: spectral efficiency versus E_b/N_0 at 10^{-3} BER for $T = 2, 4$ and $N = 1, 4$. E_b/N_0 is calculated from transmit power; channel is normalized so that total received power is equal to total sent power (fading variances are $1/N$). Right plot: spectral efficiency versus E_b/N_0 at 10^{-3} BER for different code propositions are presented, for $T = 2$ and $N = 1$.

nel is immediate, since it is just the first received complex symbol. The decoder is just a simple threshold detector (complexity linear in T), which means that no sphere search must be performed.

4.6 Conclusions

After a presentation of the distance properties of EP codes for systems with one transmit antennas, we investigated the geometrical relationship of GLRT level sets on the Grassmannian and on the tangent space. This allowed us to find a decoding algorithm which closely follows GLRT performances under the assumption that decoder parameters are properly set. A rough complexity study was performed. Performance comparisons between EP codes and current best propositions (in particular training based codes) indicate that EP codes perform better than training based codes for intermediate spectral efficiencies. However, the performance–complexity trade–off is better optimized by training codes, which have very low decoding complexity.

A Class of Random Variables

A.1 Central and non–central Chi-Squared

The sum of ν squared i.i.d. gaussian variables $X_n \sim \mathcal{N}(0, \sigma^2)$ is a chi–squared random variable [8]

$$Y = \sum_{n=1}^{\nu} X_i^2 \,, \qquad Y \sim \chi^2_\nu(\sigma^2) \tag{4.65}$$

whose probability density function (pdf) is

$$p_Y(y) = \frac{1}{2^{\nu/2}\Gamma(\nu/2)\sigma^\nu} y^{\nu/2-1} e^{-y/(2\sigma^2)} 1(y) \,, \tag{4.66}$$

where $1(y) = 1$ for $y \geq 0$ and zero otherwise.

When the random variables X_n have non–zero mean and equal variance, $X_n \sim \mathcal{N}(m_n, \sigma^2)$, the sum of their squares is a non–central chi–squared with non centrality parameter

$$\lambda = \sum_{n=1}^{\nu} m_n^2 \tag{4.67}$$

and it is denoted by $Y \sim \chi'^2_\nu(\sigma^2, \lambda)$. Its pdf is given by [8]

$$p_Y(y) = \frac{1}{2\sigma^2} \left(\frac{y}{\lambda}\right)^{\frac{\nu-2}{4}} e^{(\lambda+y)/(2\sigma^2)} I_{\frac{\nu}{2}-1}\left(\frac{\sqrt{\lambda\, y}}{\sigma^2}\right) 1(y) \tag{4.68}$$

where $I_\alpha(u)$ is the modified Bessel funciton of the first kind of order α

$$I_\alpha(u) = \sum_{k=0}^{\infty} \frac{(u/2)^{2k+\alpha}}{k!\,\Gamma(\alpha + k + 1)} \,. \tag{4.69}$$

A.2 Central and non–central F

The (central) F random variable can be described as the ratio of two independent central chi–squared

$$Y = \frac{X_1/\nu_1}{X_2/\nu_2}, \quad \text{with} \quad X_1 \sim \chi^2_{\nu_1}(\sigma^2) \,,\; X_2 \sim \chi^2_{\nu_2}(\sigma^2) \tag{4.70}$$

then $Y \sim \mathcal{F}_{\nu_1,\nu_2}$. Indeed, the parameter σ^2 does not influence the pdf of an F rv, as it can be easily seen by multiplying at the numerator and denominator by the definition (4.70) (see also [75]). The pdf is given by

$$p_Y(y) = \frac{(\nu_1/\nu_2)^{\nu_1/2}}{B(\nu_1/2, \nu_2/2)} \frac{y^{\frac{\nu_1}{2}-1}}{\left(1 + \frac{\nu_1}{\nu_2} y\right)^{\frac{\nu_1+\nu_2}{2}}} 1(y) \tag{4.71}$$

where $B(u,v)$ is the Beta function defined as

$$B(u,v) = \frac{\Gamma(u)\Gamma(v)}{\Gamma(u+v)}\,. \tag{4.72}$$

Observe that if $X_2 \sim \chi^2_{\nu_2}(\sigma^2)$, then $X_2/\nu_2 \to 1$ if $\nu_2 \to \infty$. Hence if $Y \sim \mathcal{F}_{\nu_1,\nu_2}$, $Y \to X_1/\nu_1 \sim \chi^2_{\nu_1}(\sigma^2/\nu_1)$ if $\nu_2 \to \infty$ (see [76, pag. 28]).

The non–central F random variable can be described as the ratio of a non-central chi–squared $X_1 \sim \chi'^2_{\nu_1}(1,\lambda)$ and a central chi–squared $X_2 \in \chi^2_{\nu_2}(1)$

$$Y = \frac{X_1/\nu_1}{X_2/\nu_2}\,, \quad Y \sim \mathcal{F}_{\nu_1,\nu_2}(\lambda) \tag{4.73}$$

As a matter of fact, the non–central F depends on the parameter σ^2 of the chi–squared component. If $X_1 \sim \chi'^2_{\nu_1}(\sigma^2,\lambda)$ and $X_2 \sim \chi^2_{\nu_2}(\sigma^2)$, then $Y \sim \mathcal{F}_{\nu_1,\nu_2}(\lambda/\sigma^2)$ (the control is made developping y as a ratio of sums of squared Gaussian rvs $Z_n \sim \mathcal{N}(m_n,\sigma^2)$ and noticing that $Z_n/\sigma \sim \mathcal{N}(m_n/\sigma,1)$). The pdf of a $\mathcal{F}_{\nu_1,\nu_2}(\lambda)$ is

$$p_Y(y) = e^{-\frac{\lambda}{2}} \sum_{k=0}^{\infty} \frac{\left(\frac{\lambda}{2}\right)^k}{k!}\, p_{\mathcal{F}_{\nu_1+2k,\nu_2}}(y) \tag{4.74}$$

where $p_{\mathcal{F}_{\nu_1+2k,\nu_2}}(y)$ is the pdf of a $\mathcal{F}_{\nu_1+2k,\nu_2}$ given in (4.71). We observe that $\mathcal{F}_{\nu_1,\nu_2}(\lambda = 0) = \mathcal{F}_{\nu_1,\nu_2}$ and that if $Y \sim \mathcal{F}_{\nu_1,\nu_2}(\lambda)$ then $Y \to X_1/\nu_1$ with $X_1 \sim \chi'^2_{\nu_1}(1,\lambda)$ if $\nu_2 \to \infty$.

A.3 Central and non–central beta

A beta variable of parameters $\nu_1/2$ and $\nu_2/2$, $\beta_{\nu_1/2,\nu_2/2}$ can be generated as follows [73, pag. 944]

$$Y = \frac{X_1}{X_1+X_2}\,, \qquad X_1 \sim \chi^2_{\nu_1}(\sigma^2)\,,\ X_2 \sim \chi^2_{\nu_2}(\sigma^2) \tag{4.75}$$

where x_1 and x_2 are independent. We can write

$$Y = \frac{\frac{X_1}{X_2}}{1+\frac{X_1}{X_2}} = \frac{W}{1+W} \quad \Longleftrightarrow \quad W = \frac{Y}{1-Y} \quad \text{with} \quad Y \in [0,1]\,,\ W \in [0,\infty)\,.$$

In the given range the two functions are monotonic and one the inverse of the other, which implies that the cumulative distribution function (or probability distribution function) cdf of the two random variables is related by

$$P_Y(y) = \mathrm{P}\left[Y \le \frac{w}{1+w}\right] = \mathrm{P}\left[W \le \frac{y}{1-y}\right] = P_W\left(\frac{y}{y-1}\right) = P_{\mathcal{F}_{\nu_1,\nu_2}}\left(\frac{y}{1-y}\frac{\nu_2}{\nu_1}\right) \tag{4.76}$$

because $W = (\nu_1/\nu_2)Z$, where $Z \in \mathcal{F}_{\nu_1,\nu_2}$. By derivation we obtain

$$p_Y(y) = \frac{y^{\frac{\nu_1}{2}-1}(1-y)^{\frac{\nu_2}{2}-1}}{B(\nu_1/2,\nu_2/2)} 1(y)1(y-1)\,. \tag{4.77}$$

Another way to obtain the cdf is to directly integrate (4.77)

$$P_Y(y) = \int_0^y p_Y(y)\mathrm{d}y = I_y\left(\frac{\nu_1}{2},\frac{\nu_2}{2}\right)$$

where $I_y(u,v)$ is the incomplete Beta function [73, pag. 944]. Since Y is a function of a central F rv Z, it does not depend on the parameter σ^2.

In general, for a beta rv $Y \sim \beta_{p,q}$, the raw moments are

$$\mu'_n(p,q) = \mathrm{E}\left[Y^n\right] = \frac{\Gamma(p+n)\Gamma(p+q)}{\Gamma(p)\Gamma(p+q+n)} \simeq \frac{\Gamma(p+n)}{\Gamma(p)}\frac{1}{(q+p+n)^n} \text{ for } q \to +\infty\,. \tag{4.78}$$

In particular, for a beta rv $Y \sim \beta_{p,q}$, we have

$$\mathrm{E}\left[Y\right] = m_Y = \frac{p}{p+q}\,, \qquad \mathrm{E}\left[|Y-m_Y|^2\right] = \sigma_Y^2 = \frac{pq}{(p+q)^2(p+q+1)} \tag{4.79}$$

asymptotically for $q \to +\infty$

$$\lim_{q\to+\infty} \mathrm{E}\left[Y\right] = 0\,, \qquad \lim_{q\to+\infty} \mathrm{E}\left[|Y-m_Y|^2\right] = 0\,. \tag{4.80}$$

Hence, when q goes to infinity, Y converge to the pseudo-random variable 0 (since the series of rv converges in 2–mean as q goes to infinity). It is likewise possible to prove that when p goes to infinity Y converge to the pseudo-random variable 1.

The non–central beta random variable of parameters $\nu_1/2$, $\nu_2/2$ and non–centrality parameter λ/σ^2, $Y \sim \beta_{\nu_1/2,\nu_2/2}(\lambda/\sigma^2)$ is obtained as

$$Y = \frac{X_1}{X_1+X_2}\,, \qquad X_1 \sim \chi'^2_{\nu_1}(\sigma^2,\lambda)\,,\ X_2 \sim \chi^2_{\nu_2}(\sigma^2) \tag{4.81}$$

If we proceed as before, with $W = (\nu_1/\nu_2)Z$ and $Z \in \mathcal{F}_{\nu_1,\nu_2}(\lambda)$ this time we obtain the cdf

$$P_Y(y) = P_{\mathcal{F}_{\nu_1,\nu_2}(\lambda/\sigma^2)}\left(\frac{y}{1-y}\frac{\nu_2}{\nu_1}\right) = e^{-\frac{\lambda}{2\sigma^2}} \sum_{k=0}^{\infty} \frac{\left(\frac{\lambda/\sigma^2}{2}\right)^k}{k!} I_y\left(\frac{\nu_1}{2}+k,\frac{\nu_2}{2}\right) \tag{4.82}$$

and pdf

$$p_Y(y) = e^{-\frac{\lambda}{2\sigma^2}} \sum_{k=0}^{\infty} \frac{\left(\frac{\lambda}{2\sigma^2}\right)^k}{k!} p_{\beta_{\frac{\nu_1}{2}+k,\frac{\nu_2}{2}}}(y)\,. \tag{4.83}$$

The pdf (4.83) can be generalized by replacing $\nu_1/2$ and $\nu_2/2$ with two real positive parameters p and q and λ/σ^2 woth $\lambda' \geq 0$, in order to obtain the general pdf of a rv $Y \sim \beta_{p,q}(\lambda')$

$$p_Y(y) = e^{-\frac{\lambda'}{2}} \sum_{k=0}^{\infty} \frac{\left(\frac{\lambda'}{2}\right)^k}{k!} p_{\beta_{p+k,q}}(y)\,, \qquad \mu'_n(p,q,\lambda') = \mathrm{E}\left[Y^n\right]. \tag{4.84}$$

From (4.84) the raw moments of a non–central beta rv can be derived from the ones of the correspoding central beta rv

$$\mu'_n(p,q,\lambda') = e^{-\frac{\lambda'}{2}} \sum_{k=0}^{\infty} \frac{\left(\frac{\lambda'}{2}\right)^k}{k!} \mu'_n\left(p+k,q\right) \tag{4.85}$$

If $p+q \in \mathbb{N}$ then a simple expression for the mean exists

$$\begin{aligned} m_Y &= 1 - q\left[\sum_{k=0}^{p+q-1}(-1)^k \tfrac{(p+q-1)!}{(p+q-1-k)!}\left(\tfrac{2}{\lambda'}\right)^{k+1}\right. \\ &\qquad \left. +(-1)^{p+q-1}(p+q-1)!e^{-\frac{\lambda'}{2}}\left(\tfrac{2}{\lambda'}\right)^{p+q}\right] \\ &= 1 - q(p+q-1)!\sum_{k=0}^{\infty}\tfrac{(-1)^k}{(p+q+k)!}\left(\tfrac{\lambda'}{2}\right)^k \end{aligned} \tag{4.86}$$

When $\lambda' = 0$ we obtain a central beta with the same parameters, of course. For large λ' it holds

$$m_Y \simeq 1 - \frac{2q}{\lambda'} \tag{4.87}$$

B Circles

B.1 Parameterization of Complex Hyperspheres

We describe a particular parameterization of the complex hypersphere $\mathbb{U}^T$ with real parameters, which will be useful later on. Let $\mathbf{v}$ belong to $\mathbb{U}^T$. Once fixed an arbitrary unit vector $\mathbf{u}_1$, which takes the role of reference direction, then a vector $\mathbf{v} \in \mathbb{U}^T$ can be expressed as

$$\mathbf{v} = e^{i\xi_1}\cos\theta_1\mathbf{u}_1 + \sin\theta_1\mathbf{v}_1\,, \qquad \mathbf{v}_1 \perp \mathbf{u}\,,\ \|\mathbf{v}_1\| = 1 \tag{4.88}$$

where $\theta_1 \in [0, \pi/2]$ (it is the amplitude of a complex number) and $\xi_1 \in [0, 2\pi)$ (phase degree of freedom). $\theta_1 = 0 = \xi_1$ locate $\mathbf{u}_1$, the reference vector of the parameterization. Equation (4.88) means that $\mathbb{U}^T \simeq \mathbb{S}^{2T}$, the $(2T-1)$–dimensional[2] complex hypersphere, can be parameterized by a $(2T-3)$–dimensional complex hypersphere and two free real parameters θ_1 and ξ_1, which are written in the previous form to satisfy the constraint of the sphere equation. The roles of sine and cosine are equivalent

[2] In real dimensions.

(we can change them and obtain the same surface, even if the reference points do not coincide). Through a slight abuse of notation, for every fixed $\mathbf{u}_1$, we have

$$\mathbb{U}^T = e^{i\xi_1}\cos\theta_1\mathbf{u}_1 + \sin\theta_1\mathbb{U}_T^{T-1}(\mathbf{u}_1)\,, \tag{4.89}$$

where $\mathbb{U}_T^{T-1}$ is a $(T-1)$–dimensional hypersphere[3] in $\mathbb{C}^T$, orthogonal to $\mathbf{u}_1$, i.e. $\mathbb{U}_T^{T-1}(\mathbf{u}_1) = \{\mathbf{v} \in \mathbb{C}^T : \|\mathbf{v}\| = 1, \mathbf{v}^\dagger\mathbf{u}_1 = 0\}$. The process can be repeated, i.e. fix $\mathbf{u}_2$ orthogonal to $\mathbf{u}_1$ and let $\mathbf{v}_2$ run over the $(2T-5)$–dimensional complex hypersphere $\mathbb{U}_T^{T-2}(\mathbf{u}_1, \mathbf{u}_2)$, orthogonal to the subspace spanned by $\mathbf{u}_1$ and $\mathbf{u}_2$, then

$$\mathbf{v} = e^{i\xi_1}\cos\theta_1\mathbf{u}_1 + \sin\theta_1(e^{i\xi_2}\cos\theta_2\mathbf{u}_2 + \sin\theta_2\mathbf{v}_2)\,. \tag{4.90}$$

Generally, if we consider an hypersphere $\mathbb{U}_T^{T-n}(\mathbf{u}_1, \ldots, \mathbf{u}_n)$ with real dimensions $2T-1-2n$ orthogonal to a $2n$–dimensional subspace generated by the orthonormal basis $\{\mathbf{u}_1, \ldots, \mathbf{u}_n\}$, we have

$$\begin{aligned}\mathbf{v} = e^{i\xi_1}\cos\theta_1\mathbf{u}_1 + \sin\theta_1\{e^{i\xi_2}\cos\theta_2\mathbf{u}_2 + \sin\theta_2[\ldots \\ \ldots + \sin\theta_{n-1}(e^{i\xi_n}\cos\theta_n\mathbf{u}_n + \sin\theta_n\mathbf{v}_n)\ldots]\}\end{aligned} \tag{4.91}$$

with $\theta_1, \ldots, \theta_m \in [0, \pi/2]$, $\xi_1, \ldots, \xi_n \in [0, 2\pi)$ and $\mathbf{v}_n \in \mathbb{U}_T^{T-n}(\mathbf{u}_1, \ldots, \mathbf{u}_n)$. When $n = T-1$ parameterization (4.91) becomes

$$\mathbf{v} = e^{i\xi_1}\cos\theta_1\mathbf{u}_1 + \sin\theta_1[\ldots\sin\theta_{T-2}(e^{i\xi_{T-1}}\cos\theta_{T-1}\mathbf{u}_{T-1} + e^{i\xi_T}\sin\theta_{T-1}\mathbf{u}_T)\ldots]\,. \tag{4.92}$$

where $\mathbf{v}_{T-1} = e^{i\xi_T}\mathbf{u}_T$ is the one–dimensional hypershere, i.e. a fixed unit vector $\mathbf{u}_T$ (orthogonal to $\mathbf{u}_t$, $t = 1, \ldots, T-1$) with a free phase factor. We need $2T-1$ real parameters, as required.

Parameterization (4.92) is not unique, it depends for instance on the choice of orthonormal basis $\{\mathbf{u}_1, \ldots, \mathbf{u}_T\}$. Another parameterization is obtained by defining the phase parameters of each couple in relation to the previous one. If we collect the factor inside each parenthesis in (4.92) and rename it, we obtain

$$\mathbf{v} = e^{i\xi_1}\{\cos\theta_1\mathbf{u}_1 + e^{i\xi_2}\sin\theta_1[\ldots e^{i\xi_{T-1}}\sin\theta_{T-2}(\cos\theta_{T-1}\mathbf{u}_{T-1} + e^{i\xi_T}\sin\theta_{T-1}\mathbf{u}_T)\ldots]\}. \tag{4.93}$$

The previous parameterization can be restated in form (4.91)

$$\mathbf{v} = e^{i\xi_1}\{\cos\theta_1\mathbf{u}_1 + e^{i\xi_2}\sin\theta_1[\ldots e^{i\xi_n}\sin\theta_{n-1}(\cos\theta_n\mathbf{u}_n + \sin\theta_n\mathbf{v}_n)\ldots]\}\,. \tag{4.94}$$

where $\mathbf{v}_n \in \mathbb{U}_T^{T-n}(\mathbf{u}_1, \ldots, \mathbf{u}_n)$.

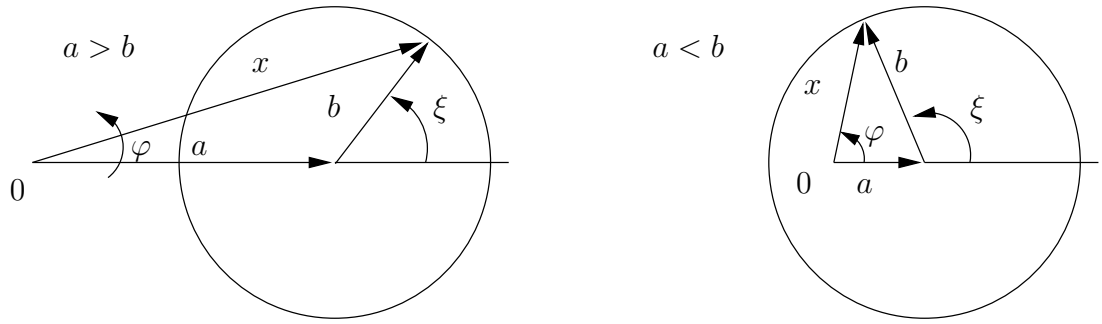

Figure 4.14: Graphical interpretation of the expression $x = a + be^{i\xi}$ for $a > b$ and $a < b$.

B.2 Absolute Value and Phase of Points over a Circle

Let a and b be two real and positive numbers. We want to calculate, module and phase of $x = a + b\,e^{i\xi}$, $\xi \in (-\pi, \pi]$

$$|x| = [a^2 + b^2 + 2ab\cos\xi]^{1/2}\,, \qquad \varphi = \angle x = \begin{cases} \arccos\left(\frac{a+b\cos\xi}{|x|}\right) & , \xi \in [0, \pi] \\ -\arccos\left(\frac{a+b\cos\xi}{|x|}\right) & , \xi \in (-\pi, 0) \end{cases} \tag{4.95}$$

	$a < b$	$a = b$	$a > b$
$\max_\xi\{\lvert x\rvert\}$	$a + b,\ \xi = 0$	$2a,\ \xi = 0$	$a + b,\ \xi = 0$
$\min_\xi\{\lvert x\rvert\}$	$b - a,\ \xi = \pi$	$0,\ \xi = \pi$	$a - b,\ \xi = \pi$
$\max_\xi\{\varphi\}$	$\pi,\ \xi = \pi$	$\pi/2,\ \xi = \pi$	$\bar\varphi = \arcsin(b/a),\ \xi = \pi/2 + \bar\varphi$

Notice that, while the absolute value of x is a continuous function of a and b, its maximum phase has a discontinuity at $a = b$, where it jumps from $\pi/2$ to π.

B.3 On the common phase of points in the preimage of level sets when $\theta_a = \pi/2$.

We can distinguish three case according to the relationship between θ_1 and θ_r.

1. $0 \le \theta_1 \le \theta_r$. In this case the point $\mathbf{0} \in B_{\pi/2}$ is contained in the preimage of the level set. Moreover, the following inequalities hold

$$\sin\theta_1 \sin\theta_r \le \sin\theta_1 \cos\theta_r \le \sin\theta_r \cos\theta_1 \le \cos\theta_1 \cos\theta_r$$

The first term δ (defined in (4.41)) is bounded since $a \ge b_{max}$ (defined in (4.40)): $\delta \in [-\bar\delta, \bar\delta]$ with $\bar\delta$ as in (4.46). We note that, being $\theta_1 \le \theta_r < \pi/4$, then

[3]The subscript T in $\mathbb{U}_T^{T-1}$ means that $\mathbb{U}_T^{T-1}$ vectors' length is T and not $T-1$, because the hypersphere are imbedded in $\mathbb{C}^T$.

$\tan\theta_1 \leq \tan\theta_r < 1$. On the other hand the phase

$$\gamma = \angle(\cos\theta_r \sin\theta_1 - \sin\theta_r \cos\theta_1 \, e^{i\xi_a}) \tag{4.96}$$

can span the whole interval $[0, 2\pi)$ because $\cos\theta_r \sin\theta_1 \leq \sin\theta_r \cos\theta_1$ in this case. This means that the global common phase factor spans $[0, 2\pi)$ but this is not a modulo–$\mathbb{U}$ effect, it is simply due to the fact that the origin of the tangent space is inside the preimage of the level set.

2. $\theta_r < \theta_1 < \pi/2 - \theta_r$. In this case the level set is between the origin and the equator.We have

$$\left.\begin{array}{l} \sin\theta_1 \sin\theta_r \\ \sin\theta_r \cos\theta_1 \end{array}\right\} \leq \sin\theta_1 \cos\theta_r \,, \qquad \sin\theta_1 \sin\theta_r < \cos\theta_1 \cos\theta_r \,.$$

In this case δ is limited with the same expression in (4.46), where $\tan\theta_1 < \tan(\pi/2 - \theta_r) = 1/\tan\theta_r$, assures a real solution. This time γ in (4.96) is limited too

$$\gamma \in [-\bar{\gamma}, \bar{\gamma}] \,, \qquad \bar{\gamma} = \arcsin(\tan\theta_r / \tan\theta_1) \text{ at } \xi_a = \pm(\pi/2 - \bar{\gamma}) \,.$$

hence we do not have modulo–$\mathbb{U}$ effect.

3. $\pi/2 - \theta_r \leq \theta_1 < \pi/2$. The modulo–$\mathbb{U}$ effect is present. In this case $\theta + r < \pi/4 < \pi/2 - \theta_r \leq \theta_1$, we have

$$\sin\theta_r \cos\theta_1 \leq \cos\theta_1 \cos\theta_r \leq \sin\theta_1 \sin\theta_r \leq \sin\theta_1 \cos\theta_r$$

and so γ is bounded as in the previous case, while $\delta_{\pi/2}$ can assume all values in $[0, 2\pi)$.

B.4 Choice of the Spheres for the Case with Modulo Effect

For the case of modulo–$\mathbb{U}$ effect, the common phase phase δ of the origin can be everywhere in $[0, 2\pi)$. However, we chose to use three sphere searches. The first search takes place inside a sphere with center $\mathbf{o}_1 = \mathbf{o}$ as in (4.58) and radius r_{max} (4.57).

What is the common phase $\hat{\delta}$ which bring $\mathbf{o}^e i\hat{\delta}$ on the surface of this first sphere? The solution is $\|\mathbf{o}^{i\hat{\delta}} - \mathbf{o}\| = r_{max}$, i.e. $\|\mathbf{o}\||1 - e^{i\hat{\delta}}| = r_{max}$, i.e. $||1 - e^{i\hat{\delta}}| \leq r_{max}/o$. Solving the latter equation yields

$$\hat{\delta} = \arccos\left[\frac{1}{2\alpha}\left(2 - R^2\right)\right] \,, \qquad R = \frac{r_{max}}{o} \tag{4.97}$$

which is valid for $R < 2$ and which holds true for the values of θ_r we use. Expression (4.97) exactly corresponds to expression (4.61), in which the parameter k artificially scales the radius of the first sphere. Hence if $k = 1$, the common phases $\delta_{2,3}$ are such that $\mathbf{o}_{2,3}$ are located on the surface of the first sphere. If $k < 1$, $\mathbf{o}_{2,3}$ are contained in the first sphere, while if $k > 1$ they are out of the first sphere. In other words, k controls the position of the two spheres with respect to the first one (given by $\delta = 0$).

Chapter 5

Suboptimal Decoding of EP Codes over $G_{T,M}$

We present two simplified decoders for space–time EP codes. We suppose that the receiver has a number of antennas equal or greater than than the number of antennas at the transmiter ($N \geq M$). We will also suppose that the duration of the frame is $T = 2M$, since it is the only case for which we can say something about EP code properties. As a matter of fact, when $M > 1$ analytical investigation of the GLRT rule has proved to be a tough task. This was already proved by Theorem 1: the complex non–linear relationship between $\mathcal{B}$ and $\mathcal{C}$ prevented us to find an analytical relationship between the product distance (for $\mathcal{C}$) and the classical Euclidean distance (for $\mathcal{B}$). Only a local description of EP codes properties around the reference subspace has been found. Even if this description gives some insights in code design, EP codes parameters must be eventually optimized by simulation.

Section 5.1 recalls the GLRT detection rule and introduces a simple subspace estimation when $N > M$. In Section 5.2, some results on product distances are reported under the assumption of small principal angles (between codeword subspaces and the reference subspace). In Section 5.3, we discuss linear approximations of the Grassmannian. We introduce a decoder coming from the geometrical interpretation of the coding procedure and another simplified decoder based on the small principal angle assumption, called local GLRT. A first investigation about the latter decoder is presented as well as a rough complexity study. In Section 5.4 some particular EP codes are presented. The choice of the homothetic factor and of other parameters is discussed under different decoding strategies. Performances are reported and comparisons are performed in particular with training–based codes. The last section contains conclusions.

5.1 Detection Criteria for EP Codes on $G_{T,M}$

We recall the channel model (2.1) with normalization (2.4)

$$\mathbf{Y} = \mathbf{X}\mathbf{H} + \sigma\mathbf{W}\,, \qquad \sigma^2 = \frac{M}{T\rho} \tag{5.1}$$

where ρ is the SNR per receive antenna averaged over supersymbols and channel fadings. GLRT rule is

$$\hat{\mathbf{X}} = \max_{\mathbf{X}\in\mathcal{C}} \|\mathbf{X}^\dagger\mathbf{Y}\|_F^2\,. \tag{5.2}$$

Channel and noise affect sent unitary codewords so that received signals are no longer unitary. As in SIMO case, we also consider the suboptimal criterion

$$\hat{\mathbf{X}}_{sub} = \max_{\mathbf{X}\in\mathcal{C}} \|\mathbf{X}^\dagger\mathbf{Y}_u\|^2\,, \qquad \mathbf{Y}_u^\dagger\mathbf{Y}_u = \mathbf{I}_M\,,\ \mathrm{span}(\mathbf{Y}_u) = \mathrm{span}(\mathbf{Y}) \tag{5.3}$$

replacing $\mathbf{Y}$ with a unitary basis $\mathbf{Y}_u$ spanning the same subspace. The suboptimal criterion (5.3) is not equivalent to GLRT (5.2), of course. This approximation enables to express the decision criterion as a function of the points over the Grassmannian. Nevertheless, the increased complexity of suboptimal GLRT (5.3) geometrical analysis prevented us to lead an in–depth study as in SISO channel case (see Chapter 4). Moreover(5.3) proved to be far less accurate than in SISO/SIMO cases, so we do not report results here.

When $N > M$, received signal $\mathbf{Y}$ can be reduced to $G_{T,M}$ as in SIMO case. From the same correlation matrix reported in expression (4.8), we reduce $T \times N$ received signal matrix $\mathbf{Y}$ to a $T \times M$ matrix $\mathbf{Y}_u$:

$$\mathbf{Y}_u:\ \text{eigenvectors of first } M \text{ greatest eigenvalues of } \mathbf{R}_Y = \frac{1}{N}\mathbf{Y}\,\mathbf{Y}^\dagger\,. \tag{5.4}$$

As a matter of fact, using channel model (5.1)

$$\mathbf{Y}\,\mathbf{Y}^\dagger = \mathbf{X}\,\mathbf{H}\,\mathbf{H}^\dagger\mathbf{X}^\dagger + \sigma\mathbf{W}\mathbf{H}^\dagger\mathbf{X}^\dagger + \mathbf{X}\,\mathbf{H}\sigma\mathbf{W}^\dagger + \sigma^2\mathbf{W}\,\mathbf{W}^\dagger$$

we obtain

$$\mathrm{E}\,[\mathbf{R}_Y] = \mathbf{X}\,\mathbf{X}^\dagger + \sigma^2\mathbf{I}_T\,, \tag{5.5}$$

which is similar to (4.9) (expectation conditioned on sent codeword $\mathbf{X}$). We notice that, if N were strictly smaller than M, $\mathbf{R}_Y$ would have rank $N < M$. Hence, $M - N$ dimensions of the subspace spanned by $\mathbf{X}$ would be lost and conclusion (5.5) is no longer true. In fact, $\mathbf{Y}_u$ is no longer on $G_{T,M}$ but on $G_{T,N}$ and we do not know how this reduction affects the coherent code on the tangent space. In other words, as in coherent systems, our system is under-determined (more variables than observations), and decoding complexity is exponential in $T(M-N)$. One possible strategy to recover the whole sent codeword is to use a channel with greater diversity. For instance, the same codeword $\mathbf{X}$ could be sent over $\lceil M/N \rceil$ independent block fading realizations, so that codeword duration is $T\lceil M/N \rceil$. This case will not be considered here.

5.2 Properties of EP Codes over $G_{T,M}$

EP codes over a Grassmannian $G_{T,M}$ have a far less exploitable structure than codes over $G_{T,1}$. However we succeeded in relating product distance of EP code $\mathcal{C}_{\mathcal{B}}$ to fundamental parameters of coherent code $\tilde{\mathcal{B}}$. The latter is defined from $\mathcal{B}$ as in the proof of Theorem 1: singular value matrix $\mathbf{\Theta}_k$ of $\mathbf{B}_k \in \mathcal{B}$ is replaced by $\tan \mathbf{\Theta}_k$ (see (3.39)). Under the assumption of full diversity (in the coherent sense) of $\mathcal{B}$, we define

$$\Lambda(\mathbf{B}_k, \mathbf{B}_\ell) = \det[(\mathbf{B}_\ell - \mathbf{B}_k)^\dagger (\mathbf{B}_\ell - \mathbf{B}_k)] = |\det(\mathbf{B}_\ell - \mathbf{B}_k)|^2 \tag{5.6}$$

where the second passage is valid only for square matrices. The minimum of these quantities

$$\Lambda(\mathcal{B}) = \min_{k \neq \ell} \Lambda(\mathbf{B}_k, \mathbf{B}_\ell) \tag{5.7}$$

is closely related to the coding gain of STB code $\mathcal{B}$, in the case of flat quasi–static block–fading channel whit no outer code [12].

Given these definitions, we prove

Proposition 8 *Suppose that $T = 2M$. Let $\mathcal{C}_{\mathcal{B}}$ be an EP code derived from coherent code $\mathcal{B}$, and consider also code $\tilde{\mathcal{B}}$. Suppose that all the codes enjoy full diversity. Let $\mathbf{X}_k, \mathbf{X}_\ell \in \mathcal{C}_{\mathcal{B}}$, $\mathbf{B}_k, \mathbf{B}_\ell \in \mathcal{B}$ the corresponding matrices in $\mathcal{B}$ and let $\mathbf{\Theta}_k$ be the singular values of $\mathbf{B}_k \in \mathcal{B}$. Then*

$$d_p(\mathbf{X}_k, \mathbf{X}_\ell) = |\cos \mathbf{\Theta}_k|^{\frac{1}{M}} |\cos \mathbf{\Theta}_\ell|^{\frac{1}{M}} [\Lambda(\tilde{\mathbf{B}}_k, \tilde{\mathbf{B}}_\ell)]^{\frac{1}{2M}} \tag{5.8}$$

Proof. Since $T = 2M$, matrices in $\mathcal{B}$ and $\tilde{\mathcal{B}}$ are square $M \times M$. Under this hypothesis, determinantal formula (2.76) gives

$$\det[(\tilde{\mathbf{B}}_\ell - \tilde{\mathbf{B}}_k)^\dagger (\tilde{\mathbf{B}}_\ell - \tilde{\mathbf{B}}_k)] = \det \left\{ \begin{bmatrix} \mathbf{I}_M & \mathbf{0}_M \\ \tilde{\mathbf{B}}_k & \tilde{\mathbf{B}}_\ell - \tilde{\mathbf{B}}_k \end{bmatrix}^\dagger \begin{bmatrix} \mathbf{I}_M & \mathbf{0}_M \\ \tilde{\mathbf{B}}_k & \tilde{\mathbf{B}}_\ell - \tilde{\mathbf{B}}_k \end{bmatrix} \right\} \tag{5.9}$$

where, from (3.40) and (3.41)

$$\begin{aligned} \begin{bmatrix} \mathbf{I}_M & \mathbf{0}_M \\ \tilde{\mathbf{B}}_k & \tilde{\mathbf{B}}_\ell - \tilde{\mathbf{B}}_k \end{bmatrix} &= \begin{bmatrix} \mathbf{I}_M & \mathbf{I}_M \\ \tilde{\mathbf{B}}_k & \tilde{\mathbf{B}}_\ell \end{bmatrix} \begin{bmatrix} \mathbf{I}_M & -\mathbf{I}_M \\ \mathbf{0}_M & \mathbf{I}_M \end{bmatrix} \\ &= [\mathbf{X}_k \ \mathbf{X}_\ell] \begin{bmatrix} \mathbf{U}_k \mathbf{C}_k^{-1} \mathbf{U}_k^\dagger & \mathbf{0}_M \\ \mathbf{0}_M & \mathbf{U}_\ell \mathbf{C}_\ell^{-1} \mathbf{U}_\ell^\dagger \end{bmatrix} \begin{bmatrix} \mathbf{I}_M & -\mathbf{I}_M \\ \mathbf{0}_M & \mathbf{I}_M \end{bmatrix} \end{aligned}$$

where $\mathbf{C}_k = \cos(\mathbf{\Theta}_k)$. By insertion of the previous identity in (5.9) we obtain

$$\det[(\tilde{\mathbf{B}}_\ell - \tilde{\mathbf{B}}_k)^\dagger (\tilde{\mathbf{B}}_\ell - \tilde{\mathbf{B}}_k)] = \det \left\{ \begin{bmatrix} \mathbf{X}_k^\dagger \\ \mathbf{X}_\ell^\dagger \end{bmatrix} [\mathbf{X}_k \ \mathbf{X}_\ell] \right\} \det \mathbf{C}_k^{-2} \det \mathbf{C}_\ell^{-2}$$

and we conclude the proof thanks to product distance definition (2.26). □

Expression (5.8) is nice but not very useful, because a simple link between $\det[(\tilde{\mathbf{B}}_\ell - \tilde{\mathbf{B}}_k)^\dagger(\tilde{\mathbf{B}}_\ell - \tilde{\mathbf{B}}_k)]$ and $\det[(\mathbf{B}_\ell - \mathbf{B}_k)^\dagger(\mathbf{B}_\ell - \mathbf{B}_k)]$ does not exist. Even if $\mathcal{B}$ has a strong algebraic structure (e.g. it is carved from a lattice), code $\tilde{\mathcal{B}}$ normally looses this structure because of the non–linear operation which produces it from $\mathcal{B}$. This prevented us finding a good homothetic factor via mathematical analysis on distance bounds, as in the case $G_{T,1}$.

However, $\tilde{\mathbf{B}}_k \simeq \mathbf{B}_k$ is valid if singular values $\mathbf{\Theta}_k$ are sufficiently small so that $\tan(\mathbf{\Theta}_k)$ is acceptably approximated by $\mathbf{\Theta}_k$ itself. In this case, identity (5.8) becomes

$$d_p(\mathbf{X}_k, \mathbf{X}_\ell) \simeq |\cos \mathbf{\Theta}_k|^{\frac{1}{M}} |\cos \mathbf{\Theta}_\ell|^{\frac{1}{M}} [\Lambda(\mathbf{B}_k, \mathbf{B}_\ell)]^{\frac{1}{2M}}, \quad \tan(\mathbf{\Theta}_k), \tan(\mathbf{\Theta}_\ell) \simeq \mathbf{\Theta}_k, \mathbf{\Theta}_\ell \,. \tag{5.10}$$

From inequalities $1 - (2/\pi)x \leq \cos x \leq 1$, in $x \in [0, \pi/2]$, and $1 - \theta_{k,m}\pi/2 \geq 1 - \theta_{k,1}\pi/2$, where $\theta_{k,1} = \|\mathbf{B}_k\|_2$ (spectral norm as in (2.74)), we have

$$1 - (2/\pi)\|\mathbf{B}_k\|_2 \leq \Big[\prod_{m=1}^{M} (1 - (2/\pi)\theta_{k,m}) \Big]^{\frac{1}{M}} \leq |\cos \mathbf{\Theta}_k|^{\frac{1}{M}} \leq 1 \,.$$

By combining the previous expression with (5.10), the following bounds are obtained for codewords sufficiently close to the reference space

$$(1 - (2/\pi)\|\mathbf{B}_k\|_2)(1 - (2/\pi)\|\mathbf{B}_\ell\|_2)[\Lambda(\mathbf{B}_k, \mathbf{B}_\ell)]^{\frac{1}{2M}} \lessapprox d_p(\mathbf{X}_k, \mathbf{X}_\ell) \lessapprox [\Lambda(\mathbf{B}_k, \mathbf{B}_\ell)]^{\frac{1}{2M}} \tag{5.11}$$

Suppose now that the homothetic factor is chosen so that all codewords are close to the reference space. We can then minimize the three terms of (5.11) and by defining

$$d_{p,min}(\mathcal{C}_\mathcal{B}) = \min_{\mathbf{X}_k \neq \mathbf{X}_\ell \in \mathcal{C}} d_p(\mathbf{X}_k, \mathbf{X}_\ell) \,, \tag{5.12}$$

we have

$$(1 - (2/\pi) \min_{\mathbf{B}_k \in \mathcal{B}} \|\mathbf{B}_k\|_2)^2 [\Lambda(\mathcal{B})]^{\frac{1}{2M}} \lessapprox d_{p,min}(\mathcal{C}_\mathcal{B}) \lessapprox [\Lambda(\mathcal{B})]^{\frac{1}{2M}} \,. \tag{5.13}$$

We notice that the minimum is not necessarily reached by the same couple, for all terms. For the approximation to be valid, $\|\mathbf{B}_k\|_2$ must be small. Under this assumption we eventually obtain $d_{p,min}(\mathcal{C}_\mathcal{B}) \simeq [\Lambda(\mathcal{B})]^{\frac{1}{2M}}$. Expression (5.13) was obtained supposing small homothetic factors, condition under which performances degrade (as we will see). Therefore, expression (5.13) cannot be used to find homothetic factors for codes which have part of their codewords far away from the reference space.

5.3 Decoder Proposals

5.3.1 About $G_{T,M}$ Linearization around the Received Signal

We have seen in Chapter 4 that the Grassmannian can be linearized around reference space Ω_{ref}: its tangent space $t\pi_{ref}$ is a good approximation (around the reference

space). Now, we suppose that received signal $\mathbf{Y}$ has already been orthonormalized and reduced to CS form (3.20). If $M = N$, at high SNR the sent codeword must be close to the received signal. Our idea is to linearize $G_{T,M}$ around the received signal (not the reference space!), to extract a list of candidate codewords and to perform a local GLRT on that list, with the true GLRT criterion (5.2) (as in the previous chapter). In other words, we would like to map codebook $\mathcal{C}_{\mathcal{B}}$ back to the tangent space at $\mathbf{Y}$ and then to use it as a linear approximation of the Grassmannian around $\mathbf{Y}$.

To this end, we consider a codebook whose codewords give matrices imbedded on the tangent space that satisfy the commutative property ($\mathbf{\Delta}_k\mathbf{\Delta}_l = \mathbf{\Delta}_l\mathbf{\Delta}_k$ for each couple $k \neq l$). As seen in Chapter 4, codes satisfying this property are quite rare. Nevertheless, these strong structured codes allow us to understand linearization issues.

A generic codeword $\mathbf{X} \in \mathcal{C}_{\mathcal{B}}$ is obtained as $\mathbf{X} = \exp(\mathbf{\Delta}_{X,ref})\mathbf{I}_{T,M}$ (see (3.15)), where subscripts X, ref mean that matrix $\mathbf{\Delta}_{X,ref}$ is in $t\pi_{ref}$ and corresponds to $\mathbf{X}$. To deduce which matrix corresponds to $\mathbf{X}$ in the tangent space at $\mathbf{Y}$, we should rewrite $\mathbf{X}$ as (see (3.15))

$$\mathbf{X} = \mathbf{Q}_Y \exp\left(\begin{bmatrix} \mathbf{0} & -\mathbf{B}_{X,Y}^\dagger \\ \mathbf{B}_{X,Y} & \mathbf{0} \end{bmatrix}\right) \mathbf{I}_{T,Y} \tag{5.14}$$

where $\mathbf{Q}_Y = [\mathbf{Y}\ \mathbf{Y}^\perp] \in \mathcal{U}_T$. To this end consider

$$\begin{aligned} \mathbf{X} &= \exp(\mathbf{\Delta}_{X,ref})\mathbf{I}_{T,M} = \mathbf{Q}_Y\mathbf{Q}_Y^\dagger \exp(\mathbf{\Delta}_{X,ref})\mathbf{I}_{T,M} \\ &= \text{(using (3.13) and (3.4))} = \mathbf{Q}_Y \exp(\mathbf{\Delta}_{Y,ref}^\dagger)\exp(\mathbf{\Delta}_{X,ref})\mathbf{I}_{T,M} \\ &= \text{(commuting skew–Hermitian matrices)} = \mathbf{Q}_Y \exp(\mathbf{\Delta}_{X,ref} - \mathbf{\Delta}_{Y,ref})\mathbf{I}_{T,M}\,, \end{aligned}$$

and we obtain (5.14), where

$$\begin{bmatrix} \mathbf{0} & -\mathbf{B}_{X,Y}^\dagger \\ \mathbf{B}_{X,Y} & \mathbf{0} \end{bmatrix} = \mathbf{\Delta}_{X,ref} - \mathbf{\Delta}_{Y,ref} \quad \Longrightarrow \quad \mathbf{\Delta}_{X,Y} = \mathbf{Q}_Y(\mathbf{\Delta}_{X,ref} - \mathbf{\Delta}_{Y,ref})\,. \tag{5.15}$$

It is easy to verify that the block form of $\mathbf{\Delta}_{X,ref} - \mathbf{\Delta}_{Y,ref}$ is correct. Notice that new matrices in the tangent space at $\mathbf{Y}$ are obtained by a linear transformation, which is unique for all matrices and determined by $\mathbf{Y}$.

Unfortunately, when matrices on $t\pi_{ref}$ do *not* commute, it is impossible to draw similar conclusions. Proceeding as before, the step in which commutativity is used must be replaced by explicit calculations. To simplify calculations let us take $T = 2M$. By writing exponential matrices in CS form (see (3.19) and (3.20) for matrix definitions) we have

$$\begin{aligned} \mathbf{X} &= \mathbf{Q}_Y \exp(\mathbf{\Delta}_{Y,ref}^\dagger)\exp(\mathbf{\Delta}_{X,ref})\mathbf{I}_{T,M} \\ &= \mathbf{Q}_Y \begin{bmatrix} \mathbf{U}_Y\mathbf{C}_Y\mathbf{U}_Y^\dagger & \mathbf{U}_Y\mathbf{S}_Y\mathbf{V}_Y^\dagger \\ -\mathbf{V}_Y\mathbf{S}_Y\mathbf{U}_Y^\dagger & \mathbf{V}_Y\mathbf{C}_Y\mathbf{V}_Y^\dagger \end{bmatrix} \begin{bmatrix} \mathbf{U}_X\mathbf{C}_X\mathbf{U}_X^\dagger & -\mathbf{U}_X\mathbf{S}_X\mathbf{V}_X^\dagger \\ \mathbf{V}_X\mathbf{S}_X\mathbf{U}_X^\dagger & \mathbf{V}_X\mathbf{C}_X\mathbf{V}_X^\dagger \end{bmatrix} \mathbf{I}_{T,M}\,, \end{aligned}$$

where matrix subscripts X or Y denote correspondence with $\mathbf{X}$ or $\mathbf{Y}$ represented with respect to $t\pi_{ref}$. For example, consider left top block of the matrix exponential product

$$\mathbf{U}_Y\mathbf{C}_Y\mathbf{U}_Y^\dagger\mathbf{U}_X\mathbf{C}_X\mathbf{U}_X^\dagger + \mathbf{U}_Y\mathbf{S}_Y\mathbf{V}_Y^\dagger\mathbf{V}_X\mathbf{S}_X\mathbf{U}_X^\dagger\,. \tag{5.16}$$

The correct sent codeword is close to the received signal at high SNR. Let us use approximations: $\mathbf{U}_X \simeq \mathbf{U}_Y$, $\mathbf{V}_X \simeq \mathbf{U}_Y$ and $\mathbf{\Theta}_X = \mathbf{\Theta}_Y + \mathbf{\Xi}$, where $\mathbf{\Xi}$ is a diagonal matrix which contains the perturbation of singular values $\mathbf{\Theta}_Y$. If we inject these approximations inside (5.16) we find $\mathbf{U}_Y \cos(\mathbf{\Xi})\mathbf{U}_Y^\dagger$, which has the correct form, but is useless. In fact, the directional information of $\mathbf{X}$ with respect to $\mathbf{Y}$ is lost, since it is contained in TSVD unitary matrices.

However, if $\mathbf{\Theta}_X \simeq \mathbf{\Theta}_Y$ and $\mathbf{U}_X$, $\mathbf{V}_X$ are not approximate, we have

$$\mathbf{U}_Y\mathbf{C}_Y\mathbf{U}_Y^\dagger\mathbf{U}_X\mathbf{C}_Y\mathbf{U}_X^\dagger + \mathbf{U}_Y\mathbf{S}_Y\mathbf{V}_Y^\dagger\mathbf{V}_X\mathbf{S}_Y\mathbf{U}_X^\dagger\,. \tag{5.17}$$

Matrix (5.17) is not in CS form (it should be Hermitian) so that we must find a right unitary transformation to set (5.17) in Hermitian form (see polar decomposition [68]). We do not succeeded in finding such a rotation in close form. Moreover such a rotation generally depends on the TSVD matrices of each codeword $\mathbf{\Delta}_X$ in a non–linear way, while we would like to find a linear expression in $\mathbf{\Delta}_X$ as in (5.15). We explain this fact as a structure loss of code $\mathcal{B}$ when mapped back to the tangent space at a point different from the reference subspace. Once fixed $\mathcal{C}_\mathcal{B}$, the algebraic structure of $\mathcal{B}$ changes if the tangent space changes.

We conclude that Grassmannian linearization is not feasible around the received signal, in the sense that the coherent code has no apparent structure to be exploited.

5.3.2 Simplified Decoding based on Tangent Space Directions

In the previous subsection we did not succeeded in linearizing the Grassmannian and in maintaining a sufficient code structure to decode efficiently at the same time. We propose here a simplified decoder which exploits the geometrical interpretation of matrices $\mathbf{\Delta}$ on $t\pi_{ref}$.

We have seen that the singular values of $\mathbf{B}_k$ are the principal angles between Ω_{ref} and $\Omega_{\mathbf{X}_k}$, while matrix $\mathbf{\Delta}_k \in t\pi_{ref}$ (built from $\mathbf{B}_k$) is the direction of the Grassmannian geodesic passing through Ω_{ref} and $\Omega_{\mathbf{X}_k}$ (see (3.14)).

Our idea is to choose the codeword whose direction in $t\pi_{ref}$ is closest to direction $\mathbf{\Delta}_Y$, corresponding to $\mathbf{Y}_u$ in (5.4). Hence, we maximize the cosine between direction couples, using canonical matrix (3.11) (which is defined in the tangent space)

$$\min_{\mathbf{B}\in\mathcal{B}} \langle \mathbf{\Delta}_Y, \mathbf{\Delta} \rangle / (||\mathbf{\Delta}_Y||_F ||\mathbf{\Delta}||_F) \tag{5.18}$$

(the relationship between $\mathbf{B}$ and $\mathbf{\Delta}$ can be found in formula (3.10)). We do not know how to solve efficiently problem (5.18). But, under assumption

$$\|\mathbf{B}\|_F = \text{ constant}\,, \qquad \forall\, \mathbf{B} \in \mathcal{B} \tag{5.19}$$

from (3.11), it is simple to show that (5.18) is equivalent to the minimization problem

$$\min_{\mathbf{B}\in\mathcal{B}} \frac{\|\mathbf{B}_Y - \mathbf{B}\|_F^2}{\|\mathbf{B}_Y\|_F \|\mathbf{B}\|_F} = \min_{\mathbf{B}\in\mathcal{B}} \|\mathbf{B}_Y - \mathbf{B}\|_F^2\,. \tag{5.20}$$

Matrix $\mathbf{B}_Y$ can be calculated as explained in the proof of Proposition 5, we quickly recall the algorithm. Let $\mathbf{Y}$ be the received signal (not necessarily with orthonormal columns)

1. Find $\mathbf{Y}_u$ from the eigenvector problem (5.4). $\mathbf{Y}_u$ is calculated to have orthonormal columns.
2. Put $\mathbf{Y}_u = [\mathbf{Y}_{u,1}^\dagger \mathbf{Y}_{u,2}^\dagger]^\dagger$ in CS form $\mathbf{Y}_c$ (calculate the SVD of $M \times M$ square upper matrix $\mathbf{Y}_{u,1} = \mathbf{U}_Y \mathbf{C}_Y \tilde{\mathbf{U}}^\dagger$, then calculate $\mathbf{Y}_c = \mathbf{Y}_u \tilde{\mathbf{U}} \mathbf{U}_Y^\dagger$).
3. Calculate $\mathbf{B}_Y$ by inverting the exponential map (from $\mathbf{Y}_c = [\mathbf{Y}_{c,1}^\dagger \mathbf{Y}_{c,2}^\dagger]^\dagger$, calculate TSVD $\mathbf{Y}_{c,2} = \mathbf{V}_Y \mathbf{S}_Y \mathbf{U}_Y^\dagger$, and form $\mathbf{B}_Y = \mathbf{V}_Y \arcsin(\mathbf{S}_Y) \mathbf{U}_Y^\dagger$).

Once obtained $\mathbf{B}_Y$, an efficient method to implement (5.20) is the Schnorr–Euchner algorithm for closest point search, as long as code $\mathcal{B}$ has an adequate algebraic structure [60]. Unfortunately this algorithm is not able to recover diversity, as shown by simulations. This is not a surprise, because the channel effect is disappeared inside decoding rule (5.20). To improve performance, the GLRT metric can be computed on a list of codewords (local GLRT), as in the case of one transmit antenna. This leads to a SNR gain, but simulations show that diversity is not recovered. We do not report this case in simulations.

5.3.3 Decoding on the Tangent Space

We propose another decoder, performing better than the previous one. Our idea is to find an approximated decoding rule for codewords close to the reference subspace. This approximate decoding rule will be applied to all received signals, as it was the case with the coherent ML decoder on the tangent space (4.56). This is naturally a suboptimal strategy because exponential map non–linearity is very important for sent codewords far from the reference subspace. However, we succeeded in obtaining acceptable performances in certain cases.

After calculating $\mathbf{Y}_u$ from (5.4) we reduce it to CS form $\mathbf{Y}_c = \mathbf{Y}_u \tilde{\mathbf{U}} \mathbf{U}_Y^\dagger$, as described in the previous subsection. By exploiting codeword orthogonality, a rough channel coefficients estimation can be easily extracted[1]

$$\mathbf{H}_e = \mathbf{Y}_c^\dagger \mathbf{Y} \tag{5.21}$$

which is a $M \times N$ complex matrix. If no additive noise is on the channel, $\mathbf{Y}_c$ is equal to $\mathbf{X}$ and channel estimation (5.21) coincides with channel realization $\mathbf{H}$.

We use a suboptimal metric coming from a training interpretation of our scheme, for codewords close to the reference subspace. As seen in (3.31), under the latter condition, EP codewords look like training–based codewords $\mathbf{X} \simeq [\mathbf{I}_M \ \mathbf{B}^\dagger]^\dagger$. We propose to use the decoder (2.66)

$$\widehat{\mathbf{B}} = \arg \min_{\mathbf{B} \in \mathcal{B}} \|\mathbf{Y}_2 - \mathbf{B}\mathbf{H}_e\|_F$$

[1] Our proposition has a common point with training–based schemes, even if in our case no training data is sent.

where $\mathbf{Y} = [\mathbf{Y}_1^\dagger \ \mathbf{Y}_2^\dagger]^\dagger$. Since $\mathbf{Y}_2 = \mathbf{Y}_{c,2}\mathbf{H}_e \simeq \mathbf{B}_Y\mathbf{H}_e$ for $\mathbf{Y}_c$ close to Ω_{ref}, we deduce

$$\widehat{\mathbf{B}} = \arg\min_{\mathbf{B}\in\mathcal{B}} \|(\mathbf{B}_Y - \mathbf{B})\mathbf{H}_e\|_F \,. \tag{5.22}$$

We assume that coherent codes are carved from a lattice, in order to exploit efficient closest point search algorithms (sphere decoder). Decoding rule (5.22) preserves diversity of coherent code $\mathcal{B}$, as we have seen in Sect. 2.8 and Proposition 3. However, in our case diversity is no longer assured, since we consider codes with codewords far away from the reference space. As simulations indicate, a performance degradation and a diversity loss is possible if exponential map non–linearity is not mitigated. As a matter of fact, this decoder is similar to the co–ML–tg decoder in SIMO case and exploits similar ideas. We use the same name co–ML–tg (coherent ML decoder of the tangent space) for the generic MIMO case too. We briefly recall the decoding steps

1. Find $\mathbf{Y}_u$ from the received signal $\mathbf{Y}$ (see (5.4)) and reduce it in CS form $\mathbf{Y}_c$. Calculate channel estimation $\mathbf{H}_e$ (see (5.21)).
2. Invert the exponential map to obtain $\mathbf{B}_Y$.
3. Estimate the sent codeword $\widehat{\mathbf{B}}$ by solving problem (5.22) via a closest point search (e.g. by a Schnorr-Euchner strategy).

5.3.4 Local GLRT Decoder

Coherent ML decoders on the tangent space for MIMO and SIMO systems share common problems. In MIMO channels problems are more severe, since diversity is lost (as simulations show). For this reason, we propose to adopt a local GLRT strategy, as in SISO case.

Starting from point $\mathbf{B}_Y$ in the tangent space, a list of candidate codewords is calculated via the Pohst algorithm of closest point search [77] applied to mismatched metric $\|(\mathbf{B}_Y - \mathbf{B})\mathbf{H}_e\|_F$. Since $\mathbf{H}_e$ is present in the metric, it is not possible to control list length as in the previous chapter. Anyway, we would like to control list lengths as much as possible, since this parameter principally determines decoder complexity. A similar problem is investigated is [77]. Through a discussion with the authors of the previous paper and after simulation validation, a practical choice of the radius for the Pohst search was found. We cannot explicate here the sphere decoding algorithm, nevertheless we quickly explain our radius choice using standard notation. For better comprehension see references [60], [65], [77].

The first step of a generic sphere decoding algorithm is to find an upper (or lower) triangular basis of the global lattice. Usually, given a lattice basis $\mathbf{G}$ which depends on channel estimation and code $\mathcal{B}$, a QR factorization is performed $\mathbf{G} = \mathbf{Q}\,\mathbf{R}$ [3] (other algorithm can be used, e.g. a Cholesky factorization). Matrix $\mathbf{Q}$ is unitary and can be seen as a rotation. Matrix $\mathbf{R}$ is the searched basis. We chose as the initial radius r of sphere searches the minimal diagonal entry of $\mathbf{R}$ multiplied by a factor 1.1

$$r = 1.1(\min_{t=1,\dots,2T} R_{t,t}) \,, \tag{5.23}$$

where we suppose to represent $T \times T$ complex matrices with their $2t \times 2T$ real representation. If no point is found by the first search, r is increased of 20%: $r_{new} = r + r/5$. This heuristic management of r provided small candidate lists lengths.

We summarize the steps of the local GLRT decoder

1. Process the received signal $\mathbf{Y}$ to obtain a basis of span$(\mathbf{Y})$ in CS form, called $\mathbf{Y}_c$ and a channel estimation $\mathbf{H}_e$.

2. Inverse the exponential map to obtain $\mathbf{B}_Y$.

3. Search for a list of candidate codewords of $\mathcal{B}$ obtained with the distance definition $\|(\mathbf{B}_Y - \mathbf{B})\mathbf{H}_e\|_F$ via a Pohst search in an hypersphere of radius r chosen as in (5.23). It is possible to iterate the search until a minimum list length $\hat{L}_{min}$ is reached, increasing the radius of 20% at each iteration.

4. Calculate the candidate codewords list $\mathcal{L}_\mathcal{C} \subset \mathcal{C}$ from the candidate codewords list $\mathcal{L}_\mathcal{B} \subset \mathbf{B}$ just found.

5. Solve the local GLRT problem by exhaustive computation of GLRT metrics on the candidate list $\mathcal{L}_\mathcal{C}$.

This decoder is far much complicated than the co–ML–tg. Moreover, lists have variable length since hypersphere radius depends on channel coefficients. To cope with this uncertainty, we fix also the maximum list length $\hat{L}_{max}$. Simulations show that the local GLRT decoder permits to follow GLRT performance at least to a certain extent.

5.3.5 Local GLRT Decoder Complexity

We are giving here a first order investigation about local GLRT decoder complexity.

- Calculation of matrix $\mathbf{R}_Y = \mathbf{Y}\,\mathbf{Y}^\dagger$: $NT(T+1)/2$ complex multiplications and additions. If $N = M$ this step can be avoided.

- Calculation of first M greatest eigenvectors $\mathbf{Y}_u$: about $12T^2$ real multiplications and addition (total) [3, pag. 229]. If $N = M$ this step can be replaced by a Gram–Schmidt orthogonalization algorithm: about $8TM^2$ real multiplications and additions (total) [3, pag. 232].

- Calculation of CS form $\mathbf{Y}_c$: 1) about $88M^3$ real multiplications and additions (total) [3, pag. 254] for the SVD $\mathbf{Y}_{u,1} = \mathbf{U}_Y \mathbf{C}_Y \tilde{\mathbf{U}}^\dagger$, 2) $2M^3 + TM^2$ complex multiplications and additions to calculate $\mathbf{Y}_c = \mathbf{Y}_u \tilde{\mathbf{U}} \mathbf{U}_Y^\dagger$).

- Calculation of $\mathbf{B}_Y$: 1) about $4(14(T-M)M^2 + 8M^3)$ real multiplications and additions (total) for TSVD $\mathbf{Y}_{c,2} = \mathbf{V}_Y \mathbf{S}_Y \mathbf{U}_Y^\dagger$, 2) $M^3 + NM^2$ complex multiplications and additions and M non–linear operations to calculate $\mathbf{B}_Y = \mathbf{V}_Y \arcsin(\mathbf{S}_Y)\mathbf{U}_Y^\dagger$.

- Calculation of $\mathbf{H}_e = \mathbf{Y}_c^\dagger \mathbf{Y}$: MNT complex multiplications and additions.

- Determine candidate codeword list $\mathcal{L}_{\mathcal{B}} = \{\mathbf{B}_{\ell_1}, \ldots, \mathbf{B}_{\ell_{\hat{L}}}\}$ via a Pohst search: $O(8[(T-M)M]^3)$. This step requires also $4\hat{L}(T-M)M$ memory cells.

- Calculate candidate codewords list $\mathcal{L}_{\mathcal{C}} = \{\mathbf{X}_{i\ell_1}, \ldots, \mathbf{X}_{\ell_{\hat{L}}}\}$: this requires $\hat{L}$ SVD and $2\hat{L}$ matrix multiplications for an approximate total of about $70\hat{L}(T-M)M^2$ real multiplications and addition (total) and $4\hat{L}TM$ memory cells.

- Calculate GLRT metrics on the candidate list: $6\hat{L}TNM$ real multiplications and additions (total)

The length $\hat{L}$ of candidate codewords lists is a random variable. In order to roughly understand expected complexity, the average of length $\hat{L}$ should be evaluated via simulation. Anyway, without explicitly computing expected complexity, it is easily found that expected complexity of a training based scheme is far less important. We refer to training model in Sect. 2.8, then the Estimation–Detection decoder complexity of a training based code is

- Extract channel estimation from first M rows of the received matrix: no computations.

- Perform a closest point search (2.66) using the following $T-M$ rows of the received matrix as received data: the expected average complexity is $O(8[(T-M)M]^3)$

With training based system a list of candidate codewords is not needed: decoding is achieved by a unique closest point search and no extra memory is required. It is clear that the whole local GLRT decoder preprocessing due to exponential non–linearity is avoided in training based systems. The local GLRT decoder also recalculates codewords in $\mathcal{L}_{\mathcal{C}}$ from codewords in $\mathcal{L}_{\mathcal{B}}$, for each received signal. This step needs the calculation of the non–linear exponential map again. It is clear that training–based systems are far better than EP codes from a decoding complexity perspective.

5.4 Simulations

In this section coherent space–time block codes are briefly introduced. We also discuss the choice of good homothetic factor α. Simulations results and comparisons are reported.

5.4.1 Coherent Codes for EP codes

We cannot give a complete introduction about the theory of coherent STB codes. We will simply apply to our aims some already built coherent STB codes. Some interesting references are [55, 27, 78]. Coherent STB codes considered here are carved from lattices [27, 78, 32].

Some examples of EP codes are shown for $T = 2M$, where $M = 2, 3$. In this subsection we introduce the coherent codes we will use to generate our EP codes. We recall that a coherent space–time block code of size $(T-M)\times M$ is needed to generate an EP code of size $T \times M$. In our examples, $(T-M)\times M$ coherent codes are obtained from points of a (Q–QAM)$^{(T-M)M}$ constellation which are rotated by an appropriate unitary matrix and opportunely combined. To better understand the principal issues of coherent codes design, please refer to previous (and following) references.

In Sect. 3.3.3 we proved that a coherent code $\mathcal{B}'$ with high minimal singular value should be used to assure diversity control. This kind of codes are not available yet. In our examples coherent codes with non–vanishing determinant are sometimes used [79, 33, 80]. These codes satisfy the very special property that their minimum determinant $\Lambda(\mathcal{B})$ (see (5.7)) does not vanish to zero if the constellation size increases. Moreover they are the current best 2×2 coherent codes. We also considered coherent codes of other propositions [32], [27, pag. 1109]. As a general rule, we chose the best coherent codes available when our research was carried out. Simulations normally confirm that the better the coherent code is, the better the EP code is.

Coherent codes for EP codes on $G_{4,2}$

If $T = 4$ and $M = 2$, we considered two codes. Let us set

$$\mathbf{s} = [s_1\ s_2\ s_3\ s_4]^t\,, \qquad s_i \in 4\text{–QAM},\ 8\text{–QAM}$$

where the average statistical power of the constellation is normalized to 1. The spectral efficiency is 2 bits/s/Hz or 3 bits/s/Hz, if respectively 4–QAM or 8–QAM is used.

Code $\mathcal{B}'_1$ presented in [32] was already applied to build a non–coherent code $\mathcal{C}_1$ in [22]. Code $\mathcal{B}'_1$ will be also called code 1 in the following. Its generic codeword is

$$\mathbf{B}' = \frac{1}{\sqrt{2}} \begin{bmatrix} s_1 + \phi s_2 & \vartheta(s_3 + \phi s_4) \\ \vartheta(s_3 - \phi s_4) & s_1 - \phi s_2 \end{bmatrix}\,, \qquad \vartheta^2 = \phi = e^{i\pi/4}\,. \tag{5.24}$$

Expression (5.24) can be written in the following equivalent form

$$\mathbf{b}' = \mathrm{vec}(\mathbf{B}') = \mathbf{\Phi}_1 \mathbf{s}\,, \qquad \mathbf{\Phi}_1 = \frac{1}{\sqrt{2}} \begin{bmatrix} 1 & \phi & 0 & 0 \\ 0 & 0 & \vartheta & -\vartheta\phi \\ 0 & 0 & \vartheta & \vartheta\phi \\ 1 & -\phi & 0 & 0 \end{bmatrix} \tag{5.25}$$

where $\mathbf{\Phi}_1$ is unitary.

If $s_i \in 4$–QAM, for all constellation points $\|\mathbf{s}\| = 2$ is constant. The suboptimal decoding method (5.20) can be applied (this is no longer true if s_i belongs to 8–QAM). In this simple case, the singular values of $\mathbf{B}'$ can be derived. From (5.25), $\|\mathbf{B}'\|_F^2 = \|\mathbf{b}'\|^2 = \|\mathbf{s}\|^2 = 4$. Identity $\delta = \sqrt{\det(\mathbf{B}'^{\dagger}\mathbf{B}')} = |\det(\mathbf{B}')| = |s_1^2 - \phi^2 s_2^2 - \phi s_3^2 + \phi^3 s_4^2|/2$ [32] takes only two values: $\delta_{1,2} = (1 \pm 1/\sqrt{2})^{1/2}$. Hence, there are only two couples of singular values

$$\lambda_{1,2} = (\sqrt{4 + 2\delta_1} \pm \sqrt{4 + 2\delta_1})/2\,, \qquad \lambda_{3,4} = (\sqrt{4 + 2\delta_2} \pm \sqrt{4 + 2\delta_2})/2$$

This is indicative of code $\mathcal{C}_1$ geometrical structure around the reference space $\mathbf{I}_{4,2}$ and it is useful to fix the maximum valid homothetic factor $\alpha_{max} = (\pi/2)/\max\{\lambda_i\} \simeq 0.793$.

Code $\mathcal{C}_2$, which will be also called code 2, comes from the coherent code $\mathcal{B}'_2$ called golden code, see [33]. Its generic codeword is

$$\mathbf{B}' = \frac{1}{\sqrt{5}} \begin{bmatrix} \phi_r(s_1 + rs_2) & \phi_r(s_3 + rs_4) \\ i\bar{\phi}_r(s_3 - \bar{r}s_4) & \bar{\phi}_r(s_1 + \bar{r}s_2) \end{bmatrix} \tag{5.26}$$

with

$$r = \frac{1+\sqrt{5}}{2},\ \bar{r} = \frac{1-\sqrt{5}}{2},\ \phi_r = 1 + i(1-r),\ \bar{\phi}_r = 1 + i(1-\bar{r})$$

Expression (5.26) can be written in the following equivalent form

$$\mathbf{b}' = \mathrm{vec}(\mathbf{B}') = \mathbf{\Phi}_2 \mathbf{s}\,, \qquad \mathbf{\Phi}_2 = \frac{1}{\sqrt{5}} \begin{bmatrix} \phi_r & r\phi_r & 0 & 0 \\ 0 & 0 & i\bar{\phi}_r & -i\bar{\phi}_r\bar{r} \\ 0 & 0 & \phi_r & r\phi_r \\ \bar{\phi}_r & \bar{r}\bar{\phi}_r & 0 & 0 \end{bmatrix} \tag{5.27}$$

where $\mathbf{\Phi}_2$ is unitary and hence, if symbols s_i are drawn from 4–QAM, decoding method (5.20) can be applied. δ takes 5 values $\delta \in \{\sqrt{2/5}, 2/\sqrt{5}, \sqrt{8/5}, \sqrt{2}, \sqrt{18/5}\}$, and there are 5 classes of singular values. The maximum homothetic factor in this case is $\alpha_{max} = 0.796$.

If 8–QAM constellations are used to build the EP code, maximal homothetic factor are obtained via numerical search.

Both codes have full diversity (in the coherent sense) ans also $\Lambda(\mathcal{B}'_1)$ and $\Lambda(\mathcal{B}'_2)$ can be calculated, but we will see that they are of no use for the practical choice of the homothetic factor.

Coherent code for EP codes on $G_{6,3}$

If $M = N = 3$ and $T = 6$), the Threaded Algebraic Space–Time (TAST) code $\mathcal{B}'_3$ presented in [27, pag. 1109] was applied. Symbols s_i are drawn from a 4–QAM constellation so that $\eta = 3$ bit/s/Hz. The generic codeword is

$$\mathbf{B}' = \begin{bmatrix} u_1 & \phi^{2/3}u_8 & \phi^{1/3}u_6 \\ \phi^{1/3}u_4 & u_2 & \phi^{2/3}u_9 \\ \phi^{2/3}u_7 & \phi^{1/3}u_5 & u_3 \end{bmatrix}, \qquad \mathbf{u} = (\mathbf{I}_3 \otimes \mathbf{M})\mathbf{s}$$

where $\phi = e^{i\pi/5}$ and the 3×3 optimal real rotation $\mathbf{M}$ is obtained by the so–called "cyclotomic construction" given in [81, Sect. IV]. The maximal homothetic factor can be obtained via numerical search on the singular values of all codewords.$\mathcal{B}'_3$ has full diversity.

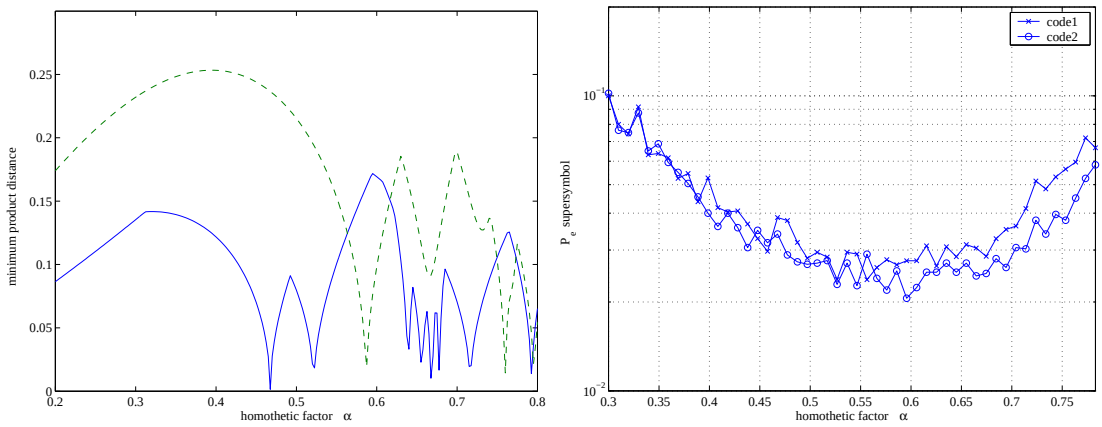

Figure 5.1: Left plot: minimal product distance of code 1 ($\mathcal{C}_1(\alpha)$) and code 2 ($\mathcal{C}_2(\alpha)$), $\eta = 2$ bits/s/Hz), as a function of homothetic factor α. Right plot: for the same codes, average supersymbol error probability (FER) at 15 dB with respect to GLRT detection solved by exhaustive search.

5.4.2 The Homothetic Factor Choice

In this subsection we discuss different criteria to choose a good homothetic factor. We see that numerical optimization method must be adopted. In any case the numerical algorithm is very simple (e.g. minimizing error probabilities via transmission simulation). Details are provided for the case of $\mathcal{C}_1$ and $\mathcal{C}_2$ with spectral efficiency 2 bits/s/Hz (4–QAM).

Theorem 1 states conditions under which the diversity of codes $\mathcal{C}_1, \mathcal{C}_2$ is greater or equal to the diversity of $\mathcal{B}_1 = \alpha\mathcal{B}'_1, \mathcal{B}_2 = \alpha\mathcal{B}'_2$. In the case of coherent codes $\mathcal{B}'_1$ and $\mathcal{B}'_2$ coming from 4–QAM, by extensive computer search we found that the maximal homothetic factors to get full diversity according to Theorem 1 are $\alpha = 0.0950$ for $\mathcal{C}_1$ and $\alpha = 0.2125$ for $\mathcal{C}_2$ (step of 0.0025 in the numerical search). We notice that the homothetic factor of $\mathcal{C}_2$ (coming from golden code) is more than the double of the homothetic factor of $\mathcal{C}_1$. This is due to the code structure.

However, the homothetic factors above are unnecessarily small. Hence, we choose α not satisfying assumptions of Theorem 1. Then, diversity is no longer guaranteed but can be verified by measuring performance curve slope.

What is the best criterion to choose α? This question has not an immediate answer. A similar problem in literature is codebook design via numerical methods [9], [13], [15]. These papers tell us that minimizing codeword distances (e.g. the product distance or the chordal distance) often gives worse results than directly minimizing the BER (Bit Error Rate) or the FER (Frame Error Rate, or also supersymbol error probability). The same conclusion can be drawn for our two codes.

The minimal product distance (2.26) is plotted in Fig. 5.1 at the left. For each value of α we generated the corresponding codes $\mathcal{C}_1(\alpha)$, $\mathcal{C}_2(\alpha)$, and calculated $d_{p,min}(\mathcal{C}_1(\alpha))$

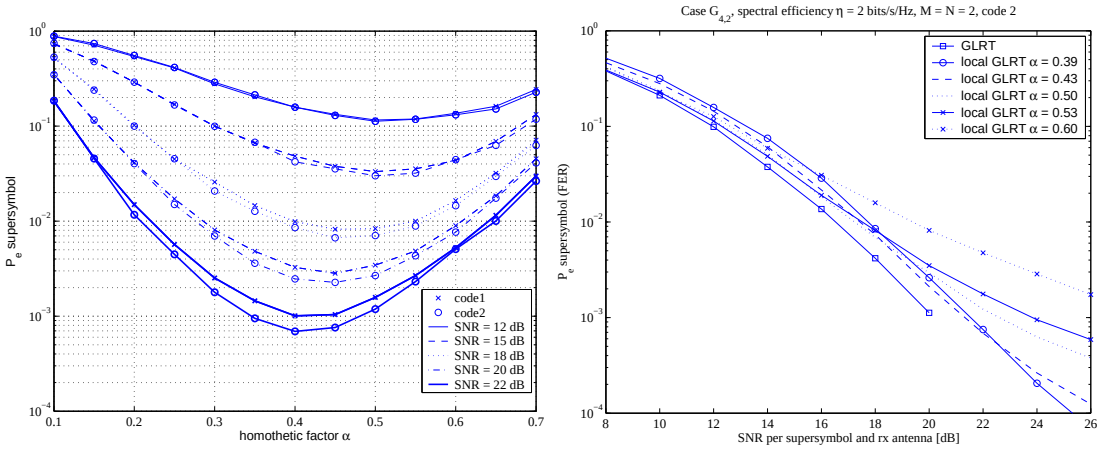

Figure 5.2: Left Plot. Local GLRT average supersymbol error probability (FER) as a function of the homothetic factor α, at different SNR; candidate lists have length between 10 and 30 and spectral efficiency $\eta = 2$ bits/s/Hz. Right plot. FER of EP codes generated by $\mathcal{B}_2'$ (golden code, $\eta = 2$ bits/s/Hz). The EP code $\mathcal{C}_2$ combined with GLRT detection (exhaustive search) was generated for $\alpha = 0.6$. The other EP codes $\mathcal{C}_2(\alpha)$ are decoded by a local GLRT decoder with candidate codewords lists of length between 10 and 30.

and $d_{p,min}(\mathcal{C}_2(\alpha))$ with definition (5.12). For code $\mathcal{B}_1'$ (4–QAM), $\max_\alpha d_{p,min}(\mathcal{C}_1(\alpha)) = 0.172$ reached at $\alpha_{1,max} = 0.595$. For code $\mathcal{B}_2'$ (4–QAM), $\max_\alpha d_{p,min}(\mathcal{C}_2(\alpha)) = 0.2530$ reached at $\alpha_{2,max} = 0.395$. Step of 0.0025 on α are used in calculations. In Fig. 5.1 at the right, for each code $\mathcal{C}_1(\alpha)$, $\mathcal{C}_2(\alpha)$, average supersymbol error probability (FER) was calculated via simulation. Simulation parameters are: 15 dB SNR, GLRT detection, implemented with exhaustive search, minimum number of supersymbol errors 500. There exists an interval of good values, approximatively $\alpha \in (0.5, 0.7)$. We notice that the homothetic factor $\alpha_{1,max}$, which maximizes the product distance of $\mathcal{C}_1$, falls inside this interval, but $\alpha_{2,max}$ of $\mathcal{C}_2$ does not belong to this interval. Nevertheless, $\mathcal{C}_2(\alpha)$ performs better than $\mathcal{C}_1(\alpha)$ for all values of α! This can be explained by a better distribution of codeword distances. In the following, we chose the homothetic factor according to the minimum FER criterion.

Minimum FER criterion depends on the implemented decoder. For instance, when a local GLRT strategy is adopted, the optimal homothetic factor does not necessarily coincide with the value found for GLRT detection. For the local GLRT decoder, optimal α depends on the SNR level and on decoder parameters, i.e. candidate list length. In Fig. 5.2 at the left, we plotted the FER as a function of the homothetic factor at different SNR, where the candidate lists can have length between 10 and 30 codewords. The optimal α depends on the SNR. The higher the SNR is, the lower the homothetic factor is. In fact, for low–power noise, the exponential map non–linearity is important. If we decrease α, the non–linearity effect is reduced for constant SNR. Besides, given a constant homothetic factor, the non–linearity effect is much more important at high

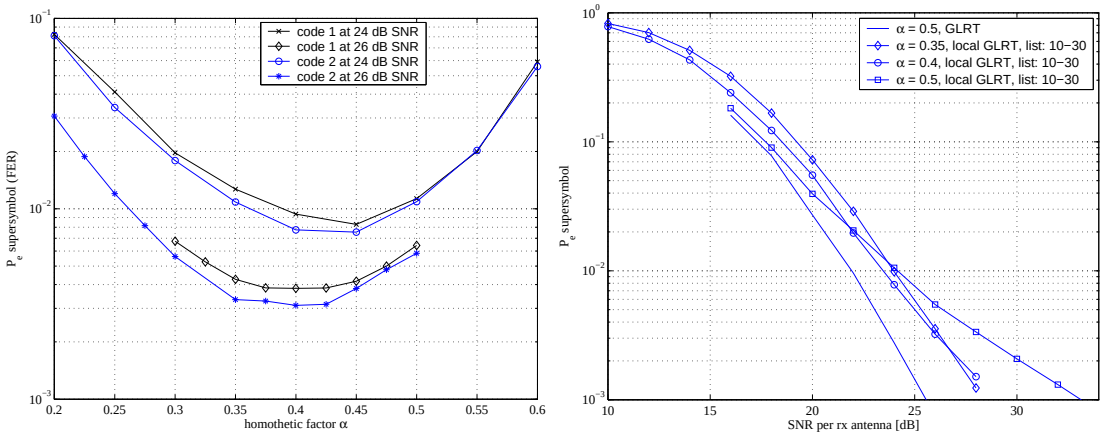

Figure 5.3: Left plot. Local GLRT average supersymbol error probability (FER) as a function of the homothetic factor α, at different SNR; candidate lists have length between 10 and 30 and spectral efficiency $\eta = 3$ bits/s/Hz. Right plot. FER of EP codes generated by $\mathcal{B}_2'$ (golden code, $\eta = 3$ bits/s/Hz). The EP code $\mathcal{C}_2$ combined with GLRT detection (exhaustive search) was generated for $\alpha = 0.5$. The other EP codes $\mathcal{C}_2(\alpha)$ were decoded by a local GLRT decoder with candidate codewords lists of length between 10 and 30.

SNR, where the channel estimation is good and the noise can be neglected. This is why the optimal homothetic factor moves to the left when the SNR increases. However, if α decreases, codewords distances decrease too. When α goes out of the interval of optimal values $(0.5, 0.7)$ found in the GLRT case, important performance degradation is expected (with respect to the GLRT performances).

This trade–off can be straightforwardly appreciated in the right plot of Fig. 5.2. The local GLRT performances of codes $\mathcal{C}_2(\alpha)$ are closer to the GLRT performance at low SNR, if α is close to 0.6 (i.e. the homothetic factor which we adopted to trace the curve of GLRT performance). At high SNR, the local GLRT performances and the GLRT ones diverge: the decoder is not able to recover diversity! This effect can be mitigated setting a lower α, as previously discussed. The price to pay is a performance loss at low SNR.

Denser codes was obtained from codes $\mathcal{B}_1'$ and $\mathcal{B}_2'$ by using $(8\text{–QAM})^4$ symbols (spectral efficiency $\eta = 3$ bits/s/Hz). Results are similar to the previous case with $\eta = 2$ bits/s/Hz. In Fig. 5.3 at the left, the same trend of optimal α can be appreciated: for growing SNR, the optimum homothetic factor decreases. At the right, the performance loss with respect to the best GLRT performance (obtained for $\alpha = 0.5$) is greater than in the case of Fig. 5.2. We notice that code $\mathcal{C}_2(0.35)$ ($\eta = 3$ bits/s/Hz) looses about 2 dB at 10^{-3} FER, while code $\mathcal{C}_2(0.39)$ ($\eta = 2$ bits/s/Hz) looses 1 dB. However, for the latter code the maximal relative length of candidate lists with respect to the code cardinality L is $\hat{L}_{max}/L = 30/256 = 11\%$, while for the code at higher spectral efficiency the maximal relative length is $\hat{L}_{max}/L = 30/4096 = 0.73\%$. For the same relative length

performance loss is naturally smaller. Anyway, we deduce that when the dimension of the Grassmannian grows the non–linearity effect increases.

Following previous considerations, the homothetic factor is chosen by a numerical optimization, usually minimizing FER and it can be made "off–line". This process must be iterated for each different code and it is better optimized if the SNR working level of the system is known.

5.4.3 Decoders Parameters and Performances

In this subsection we compare the different decoders we proposed and we illustrate the behaviour of the candidate list lengths of the local GLRT decoder.

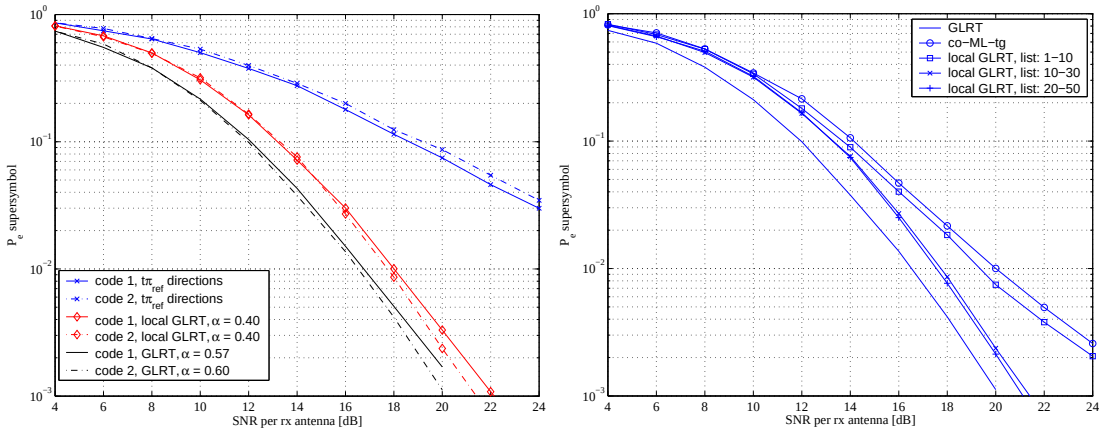

Figure 5.4: Left plot. GLRT, local GLRT and simplified decoder (5.20) FER performance at $\eta = 2$ bits/s/Hz. EP codes are obtained from code $\mathcal{B}'_1$ and golden code $\mathcal{B}'_2$, with parameters in the legend. For the local GLRT decoder, candidate lists lengths are between 10 and 30. Right plot. GLRT, local GLRT and co–ML–tg decoder FER performance at $\eta = 2$ bits/s/Hz. For GLRT decoder, code $\mathcal{C}_2$ was obtained from golden code $\mathcal{B}'_2$ and $\alpha = 0.6$; for the other decoders EP codes have $\alpha = 0.4$.

When codes $\mathcal{B}'_1$ and $\mathcal{B}'_2$ are obtained from $(4$–QAM$)^4$, codes $\mathcal{C}_1$ and $\mathcal{C}_2$ satisfy condition (5.19), and decoding rule (5.20) can be used. Moreover rule (5.20) can be simplified because $\|\mathbf{B}_Y - \mathbf{B}\|_F = \|\mathrm{vec}(\mathbf{B}_Y) - \mathrm{vec}(\mathbf{B})\|$ and, if we let $\mathbf{s}_{y,1,2} = \mathbf{\Phi}^{\dagger}_{1,2}\,\mathrm{vec}(\mathbf{B}_Y)$, then $\|\mathbf{B}_Y - \mathbf{B}\|_F = \|\mathbf{s}_{y,1,2} - \mathbf{s}\|$. Hence, (5.20) can be implemented by a simple threshold detector. In Fig. 5.4 at the left, the performance of this simplified decoder (named "$t\pi_{ref}$ directions" in the legend) is very deceiving, due to the fact that channel influence is neglected.

At the right of Fig. 5.4, performances of different decoders for EP codes coming from golden code $\mathcal{B}'_2$ are shown. GLRT performances are calculated by exhaustive search for an EP code obtained with $\alpha = 0.6$. Local GLRT performances and co–ML–tg performances are calculated for an EP codes $\mathcal{C}_2$ obtained for $\alpha = 0.4$. We have chosen such homothetic factor to assure acceptable performances at 10^{-3}, which

is a good FER for transmission system without outer code. The co–ML–tg decoder does not recover code diversity, as it can be guessed. As seen in the previous subsection, local GLRT decoder approaches to GLRT performance. Increasing minimal and maximal length of candidate lists above respectively 10 and 30 does not recover the performance loss (to approach GLRT performance α must be changed).

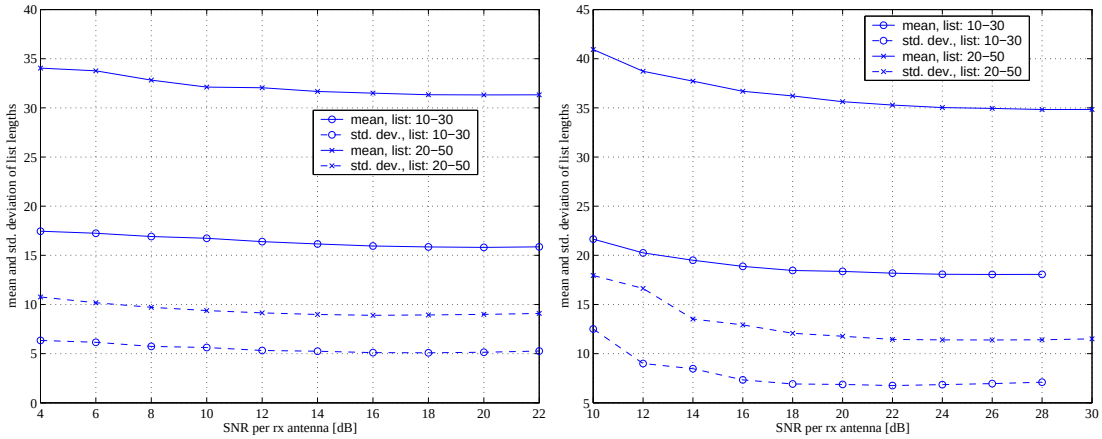

Figure 5.5: Left plot. Mean and standard deviation of candidate lists length as a function of the SNR, for EP code $\mathcal{C}_2$ obtained for $\alpha = 0.4$ at $\eta = 2$ bits/s/Hz. Right plot. Mean and standard deviation of candidate lists length as a function of the SNR, for EP code $\mathcal{C}_2$ obtained for $\alpha = 0.35$ at $\eta = 3$ bits/s/Hz.

In Fig. 5.5, mean and standard deviation of candidate lists are reported, for EP codes $\mathcal{C}_2$ and $\eta = 2, 3$ bits/s/Hz. Concerning local GLRT decoding, the Pohst search was stopped when lists length were greater than $\hat{L}_{min}$. Even if lists longer than $\hat{L}_{max}$ were truncated to calculate the GLRT metrics, length statistics were calculated without top truncation. As it can be appreciated, list mean is stable all over the SNR interval and just a little bit higher than $\hat{L}_{min}$. Hence, the initial hypersphere radius choice and its increase policy are correct, both for a relatively small codebook ($\eta = 2$ bits/s/Hz corresponds to code cardinality $L = 256$) and a relatively big code ($\eta = 3$ bits/s/Hz corresponds to code cardinality $L = 4096$). Lists standard deviations hold almost constant with increasing SNR too.

When the dimension of the Grassmannian grows, the exponential map non–linearity becomes more severe. FER performances of EP code $\mathcal{C}_3$ obtained from $\mathcal{B}'_3$ are reported in Fig. 5.6. The homothetic factor is chosen equal to 0.41 in order to optimize approximatively code GLRT performance. Once set the homothetic factor, we tried the local GLRT decoder with different interval of candidate lists lengths. Results are not good because the optimal homothetic factor for local GLRT decoders is surely not 0.41. Anyway, we can appreciate that the sensitivity to non–linearity grows with the manifold dimension. We have also verified that the initial value of the Pohst search radius gives list of about 8000 codewords. Then, search–radius initial value should be optimized again when increasing manifold dimensions, if we want to obtain short list

lengths.

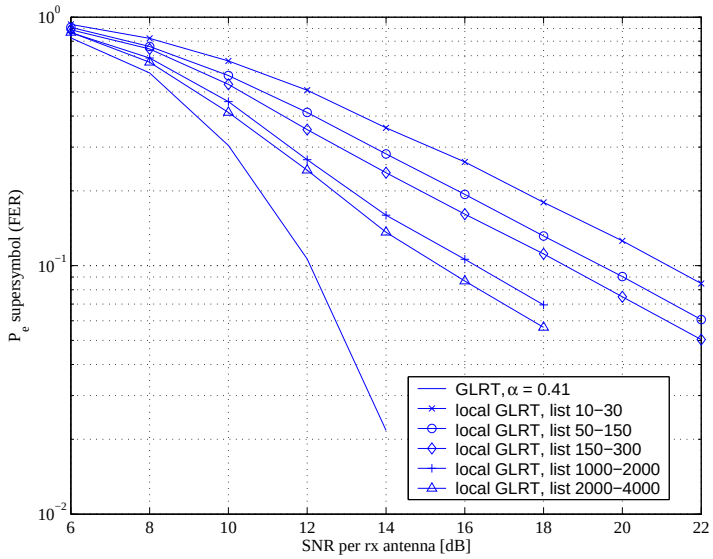

Figure 5.6: FER performance of EP code $\mathcal{C}_3$ obtained from $\mathcal{B}'_3$ with $\alpha = 0.41$. GLRT decoding is performed by exhaustive search. For local GLRT decoders, lists length intervals are reported.

5.4.4 Comparisons

Comparisons are mainly performed with respect to training–based codes for two reasons. The first one is that they are currently one of the best propositions in term of performance–complexity trade-off. The latter is that many other propositions are not simple to implement since they are obtained by numerical optimization. For all training–based codes we considered optimal power allocation (in our particular cases, the training and data phase must have equal power).

FER performances of EP codes $\mathcal{C}_1$ and $\mathcal{C}_2$ with respect to GLRT detection are compared to the training–based code obtained from the golden code $\mathcal{B}'_2$ in the left plot of Fig. 5.7. GLRT performance of the training code is almost identical to the one of the EP code coming from the same coherent code. The same situation can be appreciated in the right plot of Fig. 5.7: the EP code and training code coming from $\mathcal{B}'_1$ have equivalent performance.

Training codes suboptimally decoded with the estimation–detection (E–D) rule (2.66) maintain diversity as claimed by Proposition 3. They also exhibit small SNR loss (less than 1 dB) with respect to GLRT performance. The proposed local GLRT decoder managed to follow the GLRT performance, however they experience greater SNR loss with respect to the corresponding GLRT performance. They loose at least 1 dB with respect to the simplified E–D decoder of training–based codes and they have greater complexity.

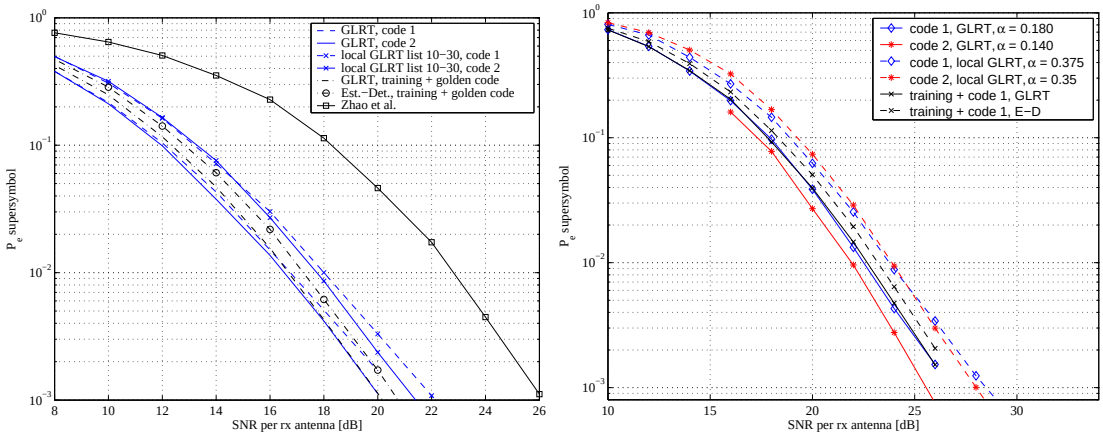

Figure 5.7: Left plot. FER performances for EP codes $\mathcal{C}_1$ and $\mathcal{C}_2$ are compared to training-based code obtained from the same golden code $\mathcal{B}_2'$ and proposition of Zhao et al. [24]. Candidate lists length belong to the interval $(10, 30)$. All codes have spectral efficiency $\eta = 2$ bits/s/Hz. Right plot. FER performances for EP codes $\mathcal{C}_1$ and $\mathcal{C}_2$ are compared to training-based code obtained from the same golden code $\mathcal{B}_1'$. Candidate lists length belong to the interval $(20, 50)$. All codes have spectral efficiency $\eta = 3$ bits/s/Hz.

In the case $G_{6,3}$ the behaviour is similar to the case $G_{4,2}$, as shown in Fig. 5.8. In fact, it is possible to find homothetic factors for which the EP codes decoded with local GLRT follow the GLRT performance and the training–based code performance. About 1 dB loss with respect to the training–based code is reported for FER above 10^{-3} with relatively small candidate list relative length $\hat{L}_{max}/L = 300/4^9 \simeq 1.1\%$. However, the expected complexity of the local GLRT is higher than the one of the estimation–detection process.

5.5 Conclusions

We presented two simplified decoding techniques for noncoherent space–time EP codes over $G_{T,M}$. The most promising one is the so–called local GLRT decoder. The receiver reduces the received signal onto $G_{T,M}$, if the number of receive antennas is greater or equal to the number of transmit antennas. Then, a linearization of the Grassmannian around the reference space permitted to decode through the closest point search algorithms developed for algebraic coherent space–time block codes. Anyway, the neglected non–linearity deteriorated performances. We coped with this degradation by opportunely setting the homothetic factor α of the code and by increasing the receiver complexity. Final comparisons showed that the training-based codes and EP codes obtained from the same coherent code perform in a similar way, as long as they are opportunely designed according to their corresponding criteria.Training–based codes

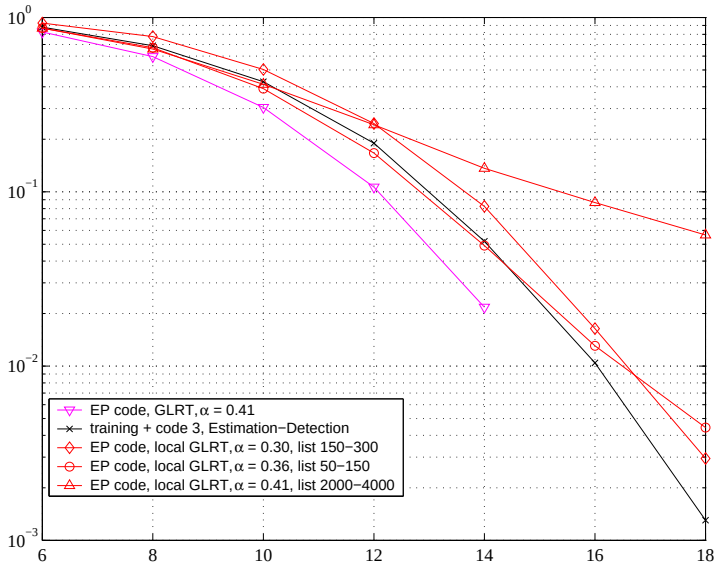

Figure 5.8: FER performances of EP codes $\mathcal{C}_3$ over $G_{6,3}$ and training-based code obtained from the same code $\mathcal{B}'_3$. Parameters are reported in the legend and all codes have spectral efficiency $\eta = 3$ bits/s/Hz.

eventually achieve the same performance with lower expected complexity and with less decoder tuning operations.

Chapter 6

Minimal PAM Decompositions of CPM Signals

Continuous Phase Modulation (CPM) is often used in both power and bandwidth limited communication links [82, 83, 84]. It has recently been combined with space–time codes [85]. CPM is particularly attractive for radio transmitters employing non–linear amplifiers since it produces a constant envelope signal [86]. However, CPM is a non–linear format with memory and the ML receiver can be quite complex. In 1986, Laurent [34] has shown that binary CPM signals can be decomposed into a finite number of PAM signals. This result was extended by Mengali and Morelli [35] to a generic M-ary CPM signal. More recently, a PAM decomposition for binary CPM signals with integer modulation index has been proposed [36].

These decompositions allow to describe CPM signals as linear combination of pulses and permit to reduce receiver complexity at the same times. For instance, in the case of coherent receivers, PAM decompositions have a beneficial effect both on suboptimal ML receivers (reduction of the number of matched filters and trellis states) [37, 39] and on synchronization issues (see [37, 40] and references therein).

CPM is also considered for non–coherent systems [87]. PAM decompositions allow to propose simplified receivers [88, 36], and permit to re–use knowledge about receivers for linear modulations [38, 37].

In this chapter, we deal with PAM decompositions of a certain class of CPM signals, being aware of the fact that improvements on this topic can lead to improvements in receiver realizations or in system and code analysis (for example PAM decompositions are used to derive design criteria of space–times codes for CPM signals in [85]).

For this class, which includes the L–REC signals and several other CPM formats, we pointed out a procedure to generate a decomposition with cardinality given by

$$N_c = L(M-1)\,, \tag{6.1}$$

where M is the alphabet size. N_c in (6.1) only grows linearly with respect to the signal memory length L. This is to be compared to the cardinality of the Laurent–Mengali–Morelli decomposition (LMMD) given by $N_d = M^L - M^{L-1}$, which grows exponentially with respect to L. For separable–phase CPM signals we shall prove that

the cardinality given by (6.1) represents the *minimal cardinality*, which means that it is not possible to decompose a separable–phase CPM signal with less than N_c PAM waveforms. CPM signals with $L = 1$ are also called full response signals. In this case, the separability condition is always satisfied, thus full response CPM signals with arbitrary phase response fall into this framework.

This chapter is organized as follows. In Section 1, a brief recall of the CPM format is reported as well as the definition and some properties of the CPM signal class investigated in this study. In Section 2, a preliminary decomposition, called Compact Decomposition (CD), is presented. The CD is modified by an arbitrary linear transformation, thus obtaining infinitely many decompositions of the same CPM signal. In Section 3, the decomposition with minimum cardinality is derived. Evetually, in Section 4 the pulses are obtained as closed form expressions for small cardinalities.

We recall that notation used in previous chapters is not valid in this part, symbols will be redefined here!

6.1 CPM Signal Model

The complex envelope of a CPM signal has the form

$$v(t) = \exp\left[j2\pi h \sum_{n=-\infty}^{+\infty} a_n\, \varphi(t - nT)\right] \tag{6.2}$$

where h is the *modulation index*, $\varphi(t)$ is the normalized *phase response* and a_n is the n–th input data. The data a_n belong to an M-ary balanced alphabet $\mathcal{A}_M = \{\pm 1, \pm 3, \ldots, \pm(M-1)\}$ for M even and $\mathcal{A}_M = \{0, \pm 2, \ldots, \pm(M-1)\}$ for M odd. The phase response $\varphi(t)$ is an increasing function of $t \in [0, LT]$ and is equal to 0 for $t \leq 0$ and equal to $\varphi(LT) = 1/2$ for $t > LT$. With these properties the expression of $v(t)$ in the n–th time slot $\mathcal{I}_n = [nT, (n+1)T)$ becomes

$$v(t) = \exp\left[j2\pi h\Big(\frac{1}{2}\theta_{n-L+1} + \sum_{i=0}^{L-1} a_{n-i}\, \varphi(t - nT + iT)\Big)\right], \tag{6.3}$$

where θ_{n-L+1} is the *phase state* of the modulator at time $n - L + 1$ given by $\theta_{n-L+1} = \sum_{m=-\infty}^{n-L} a_m$. Hence, in $\mathcal{I}_n$ the "past" data $\{a_m,\ m \leq n - L\}$ are no more "active" since they are incorporated into the phase state θ_{n-L+1} and only the "present" data $(a_n, a_{n-1}, \ldots, a_{n-L+1})$ are active. The phase state is renewed at each time mT according to the state equation $\theta_{m+1} = \theta_m + a_m$.

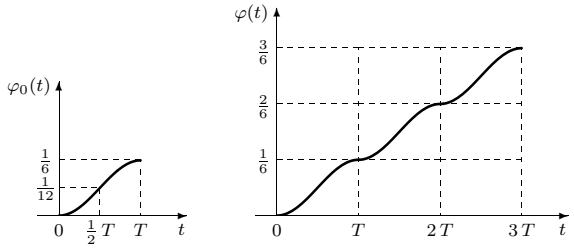

Figure 6.1: Construction of a separable phase response, for $L = 3$.

6.2 Separable CPM Signals

6.2.1 The Separability Condition and the Equivalence Principle

This work does not deal with general CPM signal but focusses on a class of M–ary CPM signals whose phase response $\varphi(t)$ satisfies the following *separability* property

$$\varphi(t + iT) = \varphi_0(t) + \frac{i}{2L}\,, \qquad i = 0, 1, \ldots, L-1,\ t \in [0, T) \tag{6.4}$$

where $\varphi_0(t)$ is monotonic in $[0, T]$ with $\varphi_0(t) = 0$ for $t \leq 0$ and $\varphi_0(t) = 1/(2L)$ for $t \geq T$. L is the memory length of the CPM signal. An example of construction of a separable phase $\varphi(t)$ starting from the *elementary* phase $\varphi_0(t)$ is illustrated in Fig. 6.1 for $L = 3$. This class includes L–REC signals and several other CPM formats, but it does not contain L–RC signals or GMSK signals.

Let's consider a CPM signal with a separable phase response $\varphi(t)$ as in (6.4). Then, the normalized phase in (6.3) becomes

$$\begin{aligned}\alpha_n(t) &= \frac{1}{2}\,\theta_{n-L+1} + \sum_{i=0}^{L-1} a_{n-i}\,\varphi(t + iT - nT) \\ &= \frac{1}{2L}\,\Theta_n + A_n\,\varphi_0(t - nT)\end{aligned}$$

where

$$\boxed{A_n = \sum_{i=0}^{L-1} a_{n-i}} \tag{6.5}$$

represents the "compact" symbols and $\Theta_n = L\,\theta_{n-L+1} + \sum_{i=0}^{L-1}(i/2L)\,a_{n-i}$ is the "compact" phase state. In terms of "compact" parameters, the CPM signal becomes

$$v(t) = \exp\left[j2\pi h\Big(\frac{1}{2L}\Theta_n + A_n\,\varphi_0(t - nT)\Big)\right], \qquad t \in \mathcal{I}_n\,. \tag{6.6}$$

Note that L consecutive input data $a_{n-L+1}, \ldots, a_n$ are "compacted" into a single symbol A_n. The alphabet of A_n is equal to $\mathcal{A}_M$ itself for $L = 1$, to $\mathcal{A}_M + \mathcal{A}_M = \{a_{n-1} +$

$a_n,\, a_{n-1} \in \mathcal{A}_M \,|\, a_n \in \mathcal{A}_M\} = \mathcal{A}_{2M-1}$ for $L = 2$, to $\mathcal{A}_M + \mathcal{A}_M + \mathcal{A}_M = \mathcal{A}_{3M-2}$ for $L = 3$, and to $\mathcal{A}_N$ with $N = L(M-1)+1$ for generic L. Since $\theta_{m+1} = \theta_m + a_m$, we find that the compact phase state Θ_n is renewed according to $\Theta_{m+1} = \Theta_m + A_m$.

Let us compare the original expressions governing a CPM modulator with memory $L = 1$ with respect to the "compact" expressions obtained with a separable phase response

original expressions	"compact" expressions
$v(t) = e^{j2\pi h[\frac{1}{2}\theta_n + a_n \varphi(t-nT)]}$	$v(t) = e^{j2\pi \frac{h}{L}[\frac{1}{2}\Theta_n + A_n L \varphi_0(t-nT)]}$
$a_n \in \mathcal{A}_M$	$A_n \in \mathcal{A}_N\,,\ N = L(M-1)+1$
$\theta_{m+1} = \theta_m + a_m$	$\Theta_{m+1} = \Theta_m + A_m$

Considering that $\varphi_1(t) = L\,\varphi_0(t)$ is a valid phase response and setting $h_1 = h/L$, we obtain the following Equivalence Principle [89]

Proposition 9 *Let $\mu_L(M)$ be a separable CPM modulator with parameters M, L, h and $\varphi(t)$, where $\varphi(t)$ is generated by an arbitrary elementary phase $\varphi_0(t)$. Then, $\mu_L(M)$ is equivalent to a CPM modulator $\mu_1(N)$ with parameters: $M_1 = N = L(M-1)+1, L_1 = 1, h_1 = h/L$, and $\varphi_1(t) = L\,\varphi_0(t)$. The input data $A_n \in \mathcal{A}_N$ of $\mu_1(N)$ is obtained from the input data $a_n \in \mathcal{A}_M$ of $\mu_L(M)$ by (6.5).* □

The relevant consequence of the Equivalence Principle is that every CPM modulator $\mu_L(M)$ with arbitrary L and M, but with a separable phase response, can be implemented by a CPM modulator $\mu_1(N)$ with a unitary memory but with a bigger alphabet $\mathcal{A}_N$. In other words, there is an equivalence between separable CPM signals and full response CPM signals (i.e. signals with $L = 1$) as long as the alphabet, modulation index and phase response of the full response signal are properly derived from the corresponding parameters of the separable signal.

Observe that several modulators $\mu_L(M)$ with different L and M may be related to a same modulator $\mu_1(N)$ with the adjustment of the modulation index. Table 6.1 collects this equivalence for the first orders N. For instance, a binary modulator with $L = 4$ ($\mu_4(2)$) and a ternary modulator with $L = 2$ ($\mu_2(3)$) are both equivalent to a five–symbol modulator with $L = 1$, that is $\mu_1(5)$, provided that each one is preceded by the appropriate compactor. Vice versa, a CPM signal with a large alphabet (for example $M = 9$) can be obtained by a CPM signal with smaller alphabet ($M = 2$). This idea can be generalized by relating $\mu_{L_1}(N_1)$ to some $\mu_{L_2}(N_2)$, where both L_1 and L_2 are not unitary. For instance, $\mu_8(2)$ can be implemented through $\mu_4(3)$, preceded by an appropriate block converting symbols in the correct alphabet.

6.2.2 Dimension of the CPM signal space

Let us fix the CPM parameters M, L, h and $\varphi(t)$ and let us consider the equivalent full response CPM signal $v(t)$ of Proposition 9 with N, h/L and $L\varphi_0(t)$. Let $\mathcal{T}$ be the set of all the trajectories of $v(t)$ in the time period $\mathcal{I}_n = [nT, (n+1)T)$, i.e. the *eye diagram*. Equation (6.6) implies $\mathcal{T} = \left\{ S_n\, e^{j\,2\pi\, h\gamma\, \varphi_0(t)} \;|\, \gamma \in \mathcal{A}_N \right\}$, where the state

N	$M=2$	$M=3$	$M=4$	$M=5$	$M=6$	$M=7$	$M=8$
2	$L=1$						
3	$L=2$	$L=1$					
4	$L=3$		$L=1$				
5	$L=4$	$L=2$		$L=1$			
6	$L=5$				$L=1$		
7	$L=6$	$L=3$	$L=2$			$L=1$	
8	$L=7$						$L=1$
9	$L=8$	$L=4$		$L=2$			
10	$L=9$		$L=3$				
11	$L=10$	$L=5$			$L=2$		
12	$L=11$						
13	$L=12$	$L=6$	$L=4$	$L=3$		$L=2$	
14	$L=13$						
15	$L=14$	$L=7$					$L=2$
16	$L=15$		$L=5$		$L=3$		

Table 6.1: Equivalence Table.

$S_n = e^{j\pi\frac{h}{L}\Theta_n}$ depends on the data but not on t. We search for the minimum number of waveforms whose linear combination generates all trajectories in $\mathcal{T}$, i.e. for a basis of the vector space $V = \operatorname{span}\mathcal{T}$. To this end, we consider the set of *expurgated–state* trajectories

$$\mathcal{Q}_{\mathcal{P}} = \{f_\gamma(t)\,|\gamma \in \mathcal{A}_N\} = \left\{e^{j\,2\pi\,h\gamma\,\varphi_0(t)}\,|\,\gamma \in \mathcal{A}_N\right\}\,. \tag{6.7}$$

Since the state dependence S_{n-L+1} is a scalar factor, $V = \operatorname{span}\mathcal{T} = \operatorname{span}\mathcal{Q}_{\mathcal{P}}$. We showed in Appendix A that functions belonging to $\mathcal{Q}_{\mathcal{P}}$ are *linearly independent*. Hence, the dimension of $\operatorname{span}\mathcal{T}$ is just the cardinality of $\mathcal{Q}_{\mathcal{P}}$, which is

$$\dim(V) = N = L(M-1)+1\,. \tag{6.8}$$

6.3 Two PAM Decompositions

6.3.1 The Compact Decomposition (CD)

We are now formulating a CPM decomposition with cardinality given by (6.8) that is

$$N = L(M-1)+1\,. \tag{6.9}$$

Our mind is to associate the appropriate coefficients to the expurgated trajectories, in order to obtain a decomposition with the same number of PAM signals. Note that (6.6) can be rewritten as

$$v(t) = S_n\,e^{j\,2\pi\,h\,A_n\varphi_0(t)}\,, \qquad t \in \mathcal{I}_n \tag{6.10}$$

where $A_n \in \mathcal{A}_N$ are the compact symbols defined in (6.5) and S_n is the "compact" state $S_n = e^{j\pi\frac{h}{L}\Theta_n}$, which is renewed according to

$$S_{n+1} = S_n \, Z^{A_n} \quad \text{with} \quad Z = e^{j\,\pi\frac{h}{L}} \,. \tag{6.11}$$

Expression (6.10) can be rewritten as a sum of PAM pulses. In fact, let $\gamma \in \mathcal{A}_N = \{\gamma_1, \ldots, \gamma_N\}$ and

$$e_n(\gamma) = S_n \, \delta_{A_n,\gamma} \,, \qquad f_\gamma(t) = \eta(t) \, e^{j\,2\pi\,h\,\gamma\,\varphi_0(t)} \tag{6.12}$$

where $\delta_{A_n,\gamma} = 1$ when $A_n = \gamma$ and zero otherwise and $\eta(t) = 1$ when $t \in [0, T)$ and zero otherwise. So that we obtain

$$\boxed{v(t) = \sum_n \mathbf{e}_n^t \; \mathbf{f}(t - nT) \,,} \tag{6.13}$$

where $\mathbf{e}_n$ is the column vector with entries $e_n(\gamma)$, $\mathbf{f}(t)$ is the column vector of the $f_\gamma(t)$, both of them have size N. $(\cdot)^t$ denotes transposition. (6.13) represents the Compact Decomposition (CD).

We have shown that a separable CPM signal can be decomposed using only N PAM waveforms, whose duration is T, by construction, as stated in (6.12). Therefore, considerations in Sect. 6.2.2 prove that N is the minimal cardinality within the class of decompositions with pulses of duration T.

6.3.2 The Modified Compact Decomposition (mCD)

We are now modifying the CD by means of a linear transformation, in order to obtain a modified Compact Decomposition (mCD). This linear transformation can be seen as a change of basis in the vector space V and permits to further reduce the cardinality of the PAM decomposition (see next section).

Let $\mathbf{P} = [p_{\gamma,k}]$, $\gamma \in \mathcal{A}_N$, $k \in \mathcal{K}_N = \{0, 1, \ldots, N-1\}$ be an invertible $N \times N$ matrix and let $\mathbf{R} = \mathbf{P}^{-1} = [r_{k,\gamma}]$ be its inverse. Then, inserting the product $\mathbf{P}\,\mathbf{R}$ in (6.13) gives

$$\boxed{v(t) = \sum_n \mathbf{c}_n^t \; \mathbf{g}(t - nT)} \tag{6.14}$$

where

$$\mathbf{c}_n^t = \mathbf{e}_n^t \, \mathbf{P} \,, \qquad \mathbf{g}(t) = \mathbf{R} \; \mathbf{f}(t) \tag{6.15}$$

are the *modified words* and the *modified pulses*, respectively, and they form a modified Compact Decomposition (mCD) of the CPM signal. The transformation matrix $\mathbf{P}$ is arbitrary so that infinitely many mCDs can be found for the same CPM signal. As long as $\mathbf{P}$ is invertible, a basis of V is transformed into another basis of V, with the same cardinality N given by (6.9). Therefore, all the mCDs share the same property of minimality and the same pulse duration T as the CDs.

If we replace (6.12) in (6.15), we obtain the modified symbols

$$c_n(k) = S_n \, p_{A_n,k} \,, \quad k \in \mathcal{K}_N \,, \tag{6.16}$$

that is, the k–th symbol is given by the $(A_n; k)$ entry of the matrix $\mathbf{P}$ multiplied by the current state S_n. The k–th pulse assumes the explicit form

$$g_k(t) = \eta(t) \sum_{\gamma \in \mathcal{A}_N} r_{k,\gamma} \, e^{j2\pi \, h \, \gamma \, \varphi_0(t)} \,, \quad k \in \mathcal{K}_N \,. \tag{6.17}$$

where $r_{k,\gamma}$ are the entries of $\mathbf{R}$. Hence, the compact pulses are linear combinations of complex exponentials truncated to the interval $[0, T)$.

If we choose an appropriate matrix $\mathbf{P}$ or $\mathbf{R} = \mathbf{P}^{-1}$, it is possible to impose some properties, in particular:

Proposition 10 *The mCD pulses $g_k(t)$ are real if and only if $\mathbf{P} = [p_{\gamma,k}]$ is column Hermitian, namely $p_{-\gamma,k} = p^*_{\gamma,k}$ or, equivalently, $\mathbf{P}^{-1} = \mathbf{R} = [r_{k,\gamma}]$ is row Hermitian, namely $r_{k,-\gamma} = r^*_{k,\gamma}$.* □

Proof. It is trivial to show that if $\mathbf{R}$ is row Hermitian then the pulses are real. This is due to the fact that the alphabet $\mathcal{A}_N$ is balanced and naturally ordered (from the smallest to the greatest element). The contrary is simple. Pulses $\mathbf{g}(t)$ are real if and only if $\mathbf{g}(t) = \mathbf{g}^*(t)$ for all $t \in [0, T)$, where $(\cdot)^*$ denotes the complex conjugate matrix. Since $\mathbf{g}(t) = \mathbf{R}\,\mathbf{f}(t)$, we have $\mathbf{g}^*(t) = \mathbf{R}^* \, \mathbf{f}^*(t)$. Since $\mathcal{A}_N$ is balanced and the basic pulses $\mathbf{f}(t)$ are complex exponentials, $\mathbf{f}^*(t) = \mathbf{\Pi}\,\mathbf{f}(t)$ holds, where $\mathbf{\Pi}$ is the anti–diagonal matrix which turns upside down $\mathbf{f}(t)$. Now

$$\mathbf{g}(t) - \mathbf{\Pi}\,\mathbf{g}(t) = 0 \iff (\mathbf{R} - \mathbf{R}^* \, \mathbf{\Pi})\,\mathbf{f}(t) = 0 \,, \; t \in [0, T)$$

Since $\mathbf{f}(t)$ are linearly independent signals, as shown in Appendix A, no linear combination annihilates them all over the support. Thus $\mathbf{R} = \mathbf{R}^* \, \mathbf{\Pi}$, i.e. $\mathbf{R}$ is row Hermitian. It is easy to prove [90] that, if $\mathbf{P}$ is column Hermitian, then the inverse $\mathbf{R} = \mathbf{P}^{-1}$ is row Hermitian and vice versa. The same holds for Anti–Hermitian matrices.□

6.3.3 A Useful Class of Transformation Matrices

Any invertible $N \times N$ complex matrix $\mathbf{P}$ gives a valid mCD. We are now focussing on the particular subclass $\mathcal{M}_{\mathrm{H}}(N)$ of column Hermitian matrices and on the subclass $\mathcal{M}_{\mathrm{P}}(N)$ whose entries are integer powers of $Z = e^{j\pi \, h/L}$ and, in particular, on the subclass $\mathcal{M}_{\mathrm{HP}}(N) = \mathcal{M}_{\mathrm{H}}(N) \cap \mathcal{M}_{\mathrm{P}}(N)$. Although restricted, the class $\mathcal{M}_{\mathrm{HP}}(N)$ is still broad and has some interesting properties. In the following, we shall further restrict the investigation to transformation matrices which lead to recursion formula between pulses and permit building the Minimal Decomposition.

The class $\mathcal{M}_{\mathrm{P}}(N)$ imposes the following properties: 1) the modified words $\mathbf{c}_n$ are polynomial in Z; 2) the determinant of $\mathbf{P}$ is a polynomial in Z; 3) the entries of the inverse matrix $\mathbf{R} = \mathbf{P}^{-1}$ are rational functions of Z. The poles of the determinant of $\mathbf{P}$

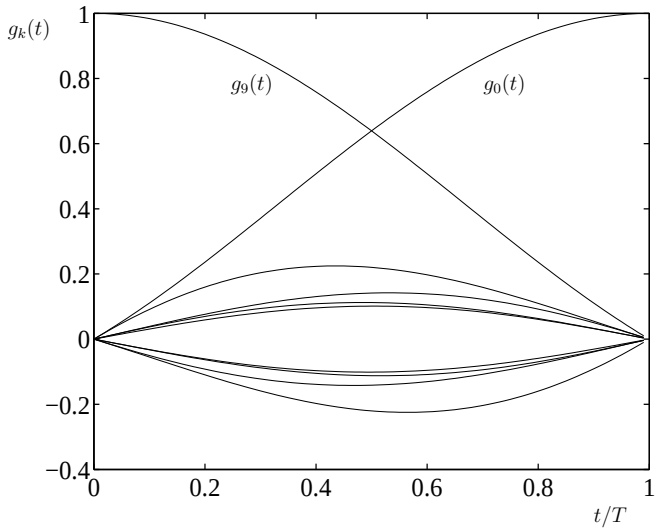

Figure 6.2: All 10 mCD pulses $g_k(t)$ with $M = 4$, $L = 3$ and transformation matrix specified by (6.18) for $h = 0.3$.

determine the *forbidden values* of the modulation index h, values at which $\mathbf{P}$ becomes singular and the mCD can not be carried out. For the subclass $\mathcal{M}_{\mathrm{HP}}(N)$, the determinant of $\mathbf{P}$ is a rational function $\Delta(Z)$, which satisfies also $\Delta(Z) = \Delta(Z^{-1})$.

Example 1. The Vandermonde matrix (for arbitrary M and L) can be taken as a transformation matrix with the first column equal to $[Z^{\gamma}]$, $\gamma \in \mathcal{A}_N$. We assume $Z^{\gamma_1} \neq Z^{\gamma_2}$ for all $\gamma_1 \neq \gamma_2$, so that $\mathbf{P}$ is invertible. Therefore, the forbidden values of h are $\{Lk/n,\, n = 1, 2, \ldots, N-1,\ k \in \mathbb{N}\}$. For instance, if $M = 4$ and $L = 3$ ($N = 10$) the first column of the Vandermonde matrix is given by

$$\begin{bmatrix} Z^{-9} & Z^{-7} & Z^{-5} & Z^{-3} & Z & Z^{1} & Z^{3} & Z^{5} & Z^{7} & Z^{9} \end{bmatrix}^t . \tag{6.18}$$

and the corresponding pulses are shown in Fig. 6.2. If $Z = e^{j\pi\, h/3}$, in the interval $(0, 1)$ we find five forbidden values for h, namely $\left\{\frac{3}{8},\, \frac{3}{7},\, \frac{1}{2},\, \frac{3}{4},\, \frac{3}{5}\right\}$.

6.4 The Minimal Decomposition (MD)

We saw that every mCD has cardinality $N = L(M-1)+1$. A further reduction is possible if we choose such transformation matrices that provide recursive updates for the modified symbols $c_n(k)$. For example, for $N = 4$ the mCD is $v(t) = v_0(t)+v_1(t)+v_2(t)+v_3(t)$, where $v_k(t) = \sum_n c_n(k)\, g_k(t-nT)$. If the recursion $c_n(3) = c_{n-1}(0)$ is valid for all n, we can combine $v_0(t)$ and $v_3(t)$ into a single PAM waveform, namely $v_0(t)+v_3(t) = \sum_n c_n(0)\, h_0(t-nT)$, with $h_0(t) = g_0(t)+g_3(t-T)$. The cardinality decreases from 4 to 3, and the pulse $h_0(t)$ has support $[0, 2T)$.

This method can only reduce the cardinality by one. In fact, Proposition 9 states that the separable CPM signals are equivalent to full response CPM signals. Mengali and Morelli [35] showed that, in general, only one pulse of length $(L+1)T$ exists, due to the memory of the signal. From this argument and the fact that the CD has the same cardinality of the CPM signal space in $[0, T)$, we conclude that the MD has minimal cardinality.

6.4.1 Conditions for recursions

We are now establishing the conditions on $\mathbf{P}$ which produce the following recursion

$$c_n(k_1) = c_{n-1}(k_0)\,, \qquad k_1 \neq k_0\,. \tag{6.19}$$

When $Z \neq 0$, combination of (6.16) and (6.11) implies

$$p_{A_n,k_1} = Z^{-A_{n-1}} p_{A_{n-1},k_0}\,, \quad k_1 \neq k_0 \tag{6.20}$$

where the selection of the entries p_{A_n,k_1} and p_{A_{n-1},k_0} of the same fixed matrix $\mathbf{P}$ depends on two distinct compact symbols A_{n-1} and A_n. Recursion (6.20), which has to hold true for all input data sequences, imposes the following form on the columns k_0 and k_1 of $\mathbf{P}$ (see Appendix B for a proof)

$$p_{\gamma,k_0} = \pi_0\, Z^{\gamma}\,, \qquad p_{\gamma,k_1} = \pi_0\,, \qquad \forall\, \gamma \tag{6.21}$$

where $\pi_0 \neq 0$ is an arbitrary constant.

Without loss of generality, we may set $k_0 = 0$, $k_1 = N-1$ and $\pi_0 = 1$. Then, the matrix $\mathbf{P}$, if compatible with condition (6.19), takes the form

$$\mathbf{P} = \begin{bmatrix} Z^{-N+1} & p_{0,1} & \cdots & p_{0,N-2} & 1 \\ Z^{-N+3} & p_{1,1} & \cdots & p_{1,N-2} & 1 \\ \vdots & \vdots & \ddots & \vdots & \vdots \\ Z^{N-1} & p_{N-1,1} & \cdots & p_{N-1,N-2} & 1 \end{bmatrix} \tag{6.22}$$

where inner columns can be chosen arbitrarily, as long as $\mathbf{P}$ is invertible. A transformation matrix of the above form will be called a standard transformation matrix. Moreover, it is clear that only one recursion of the form (6.21) can be imposed, otherwise two columns in $\mathbf{P}$ would be proportional to another one and $\mathbf{P}$ would be no longer invertible.

6.4.2 Formulation of the MD

If we apply condition (6.19) to the mCD we obtain the MD, namely

$$\boxed{v(t) = \sum_n \mathbf{d}_n^t\, \mathbf{h}(t - nT)} \tag{6.23}$$

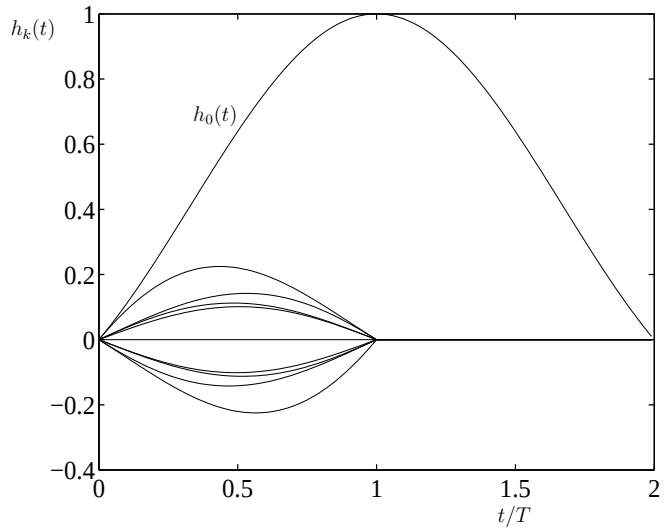

Figure 6.3: MD pulses $h_k(t)$ with $M = 4$, $L = 3$ and $h = 0.3$.

where $\mathbf{d}_n$ is obtained from $\mathbf{c}_n$ by dropping the last symbol $c_n(N-1)$ and

$$h_k(t) = \begin{cases} g_0(t) + g_{N-1}(t-T), & k = 0 \\ g_k(t), & k = 1, \ldots, N-2 \end{cases} \tag{6.24}$$

We notice that the support of $h_0(t)$ is equal to $[0, 2T)$ while the support is $[0, T)$ for the others $h_k(t)$. For all valid matrices $\mathbf{P}$, the pulses created with this procedure are continuous functions of t, as can be easily seen considering the limits at the points $0, T, 2T$ and using definitions (6.12), (6.15), (6.17) and (6.24). In Example 1 (where $M = 4$, $L = 3$ and $N_c = 9$), the corresponding MD pulses are shown in Fig. 6.3.

It is clear that the MD cardinality is $N_c = N - 1$, as claimed in (6.1). Therefore N_c represents the true minimal cardinality of all possible decompositions of a separable–phase CPM signal. In Table 6.2, the cardinality of the new PAM decompositions of separable phase CPM signals are compared to the cardinality of the Mengali–Morelli decomposition [35]. We see that the cardinality of the proposed decompositions increases only linearly with the memory of the original CPM signal. If the constraint on separable phase is relaxed, our decomposition is still valid for full response CPM signals with $L = 1$. In Table 6.3 a comparison with the Mengali–Morelli decomposition is presented.

6.4.3 Step–by–step procedure to evaluate an MD

The complete procedure for obtaining a MD is presented hereafter. Let us consider a CPM signal with separable phase, parameters L, h, M and elementary phase $\varphi_0(t)$. The procedure to obtain the MD is as follows

1. set $N = L(M-1) + 1$;

$M = 4$, separable phase			
decomp. cardinality	LMMD $M^L - M^{L-1}$	CD, mCD $L(M-1)+1$	MD $L(M-1)$
$L = 1$	3	4	3
$L = 2$	12	7	6
$L = 3$	48	9	8
$L = 4$	208	13	12
$L = 5$	768	16	15

Table 6.2: Cardinality of different decompositions with separable phase, for $M = 4$ and some L.

$L = 1$, no phase constraint			
decomp. cardinality	LMMD $2^{\lceil \log_2 M \rceil} - 1$	CD, mCD M	MD $M-1$
$M = 2$	1	2	1
$M = 4$	3	4	3
$M = 6$	7	6	5
$M = 8$	7	8	7
$M = 10$	15	10	9

Table 6.3: Cardinality of different decompositions with no phase constraint, for $L = 1$ and some M.

2. choose an $N \times N$ standard transformation matrix $\mathbf{P}$ according to (6.22);

3. compute its inverse $\mathbf{R} = [r_{\gamma,k}]$ and check that it is regular for the given value of h;

4. evaluate the mCD symbols $c_n(k)$ from (6.16) and the mCD pulses $g_k(t)$ from (6.15);

5. the MD symbols coincide with the first $N-1$ mCD symbols, i.e. $d_n(k) = c_n(k)$, for $k = 0, 1, \ldots, N-2$;

6. evaluate the MD pulses using (6.24).

When real pulses are required, in step 2) $\mathbf{P}$ must be chosen column Hermitian.

6.5 Explicit pulse expressions

Pulse evaluation of mCD and MD requires the inversion of standard transformation matrix $\mathbf{P}$. This can be done in exact (non numerical) form for small values of N. We found the CD pulses for $N = 2,\ 3,\ 4$.

In order to get the general formulas, we set $h_1 = h/L$, $\varphi_1(t) = L\varphi_0(t)$. For $N = 2$, the only possibility is $M = 2$, $L = 1$, and we obtain the well-known MSK modulation.

The standard transformation matrix is unique, for the two columns of $\mathbf{P}$ are determined by condition (6.21),

$$\mathbf{P} = \begin{bmatrix} Z^{-1} & 1 \\ Z & 1 \end{bmatrix}, \qquad \mathbf{R} = \frac{1}{\Delta} \begin{bmatrix} 1 & -1 \\ -Z & Z^{-1} \end{bmatrix}, \tag{6.25}$$

where $Z = e^{j\pi h_1}$ and $\Delta = \det \mathbf{P} = Z^{-1} - Z = -2j\, \sin(\pi\, h_1)$. The mCD pulses can be written in the form

$$\begin{aligned} g_0(t) =& \eta(t) \sin[2\pi\, h_1 \varphi_1(t)] / \sin(\pi\, h_1) \\ g_1(t) =& \eta(t) \sin[2\pi\, h_1 (1/2 - \varphi_1(t))] / \sin(\pi\, h_1) \end{aligned}$$

If $N = 3$ the standard transformation matrix is no longer unique. We choose

$$\mathbf{P} = \begin{bmatrix} Z^{-2} & Z^{-1} & 1 \\ 1 & 1 & 1 \\ Z^2 & Z & 1 \end{bmatrix}, \qquad \mathbf{R} = \frac{1}{\Delta} \begin{bmatrix} 1 - Z & Z - Z^{-1} & Z^{-1} - 1 \\ Z^2 - 1 & Z^2 - Z^{-2} & 1 - Z^{-2} \\ Z - Z^2 & Z - Z^{-1} & Z^{-2} - Z^{-1} \end{bmatrix}$$

where $\Delta = 4j\, \sin(\pi h_1)[1 - \cos(\pi h_1)]$. If we set $\mathrm{c}(x) = \cos(2\pi\, h_1 x)$, we obtain the following mCD pulses

$$\begin{aligned} g_0(t) =& \eta(t) \frac{\mathrm{c}(1/4) - \mathrm{c}(2\varphi_1(t) - 1/4)}{2\,\mathrm{c}(1/4)\,[1 - \mathrm{c}(1/2)]} \\ g_1(t) =& \eta(t) \frac{\mathrm{c}(1/2) + \mathrm{c}(2\varphi_1(t) - 1/2)}{1 - \mathrm{c}(1/2)} \\ g_2(t) =& \eta(t) \frac{\mathrm{c}(1/4) - \mathrm{c}(2\varphi_1(t) - 3/4)}{2\,\mathrm{c}(1/4)\,[1 - \mathrm{c}(1/2)]} \end{aligned}$$

For $N = 4$ we choose

$$\mathbf{P} = \begin{bmatrix} Z^{-3} & Z^{-1} & Z^{-2} & 1 \\ Z^{-1} & Z^{-1} & 1 & 1 \\ Z & Z & 1 & 1 \\ Z^3 & Z & Z^2 & 1 \end{bmatrix}, \qquad \mathbf{R} = \frac{1}{\Delta} \begin{bmatrix} Z & -Z & -Z^{-1} & Z^{-1} \\ -Z & Z^{-1} & Z & -Z^{-1} \\ -Z^2 & Z^2 & Z^{-2} & -Z^{-2} \\ Z^2 & -1 & -1 & Z^{-2} \end{bmatrix}$$

where $\Delta = (Z^{-1} - Z)^2 = -4 \sin^2(\pi\, h_1)$. The mCD pulses are

$$\begin{aligned} g_0(t) &= \eta(t) \{-\mathrm{c}[\varphi_1(t) - 1/2] + \mathrm{c}[3\varphi_1(t) - 1/2]\} / \Delta \\ g_1(t) &= \eta(t) \{\mathrm{c}[\varphi_1(t) + 1/2] - \mathrm{c}[3\varphi_1(t) - 1/2]\} / \Delta \\ g_2(t) &= \eta(t) \{\mathrm{c}[\varphi_1(t) - 1] - \mathrm{c}[3\varphi_1(t) - 1]\} / \Delta \\ g_3(t) &= \eta(t) \{-\mathrm{c}[\varphi_1(t)] + \mathrm{c}[3\varphi_1(t) - 1]\} / \Delta \end{aligned}$$

6.6 Conclusions

This work analyzies the problem of PAM decomposition of CPM signals. In particular, the attention is focused on CPM signals with a separable phase. This property allows us to find the exact signal space dimension and to derive PAM decompositions with minimal cardinality. The procedure to obtain such decompositions is new and original compared to previous works [34], [35], [36] and gives insight on the relationship between the signal space bases and the final PAM waveforms. Further work needs to be performed to understand the consequences of these decompositions on the implementation of simplified receivers.

A Appendix: the dimension of $\mathrm{span}\,\mathcal{Q}_{\mathcal{P}}$

We want to show that the functions in $\mathcal{Q}_{\mathcal{P}}$ are linearly independent,in order to conclude that the dimension of $\mathrm{span}\,\mathcal{T}$ is the cardinality of $\mathcal{Q}_{\mathcal{P}}$. More precisely we have the following

Theorem 2 *Let $\mathcal{Q}_{\mathcal{P}}$ be the class of the expurgated–state trajectories generated by a separable phase response and let $S = \mathrm{span}\,\mathcal{Q}_{\mathcal{P}}$. Then, a base for S is given by the pulses $f_\gamma(t) = e^{j2\pi h\,\gamma\,\varphi_0(t)}\,,\ \gamma \in \mathcal{A}_N\,,\ t \in [0,T)$ and its dimension is $N = L(M-1)+1$.*

Proof. We show that the functions $f_\gamma(t)$ are linearly independent. Since $\varphi_0(t)$ is continuous and monotonic in $[0,T)$ from 0 to $1/(2L)$, it is always possible to find N instants t_i so that $\varphi_0(t_i) = i/N_1\,,\ i = 0,\,1,\ldots,N-1 = L(M-1)$, provided that $N_1 > 2L^2(M-1)$. Let's sample $f_\gamma(t)$ over $\{t_i\}$ and store the samples in a $N \times N$ matrix $\mathbf{F}$. This is a Vandermonde matrix

$$[\mathbf{F}]_{i,\gamma} = f_\gamma(t_i) = e^{j2\pi\,h\,\gamma\frac{i}{N_1}} = Q_\gamma^i\,, \qquad Q_\gamma = e^{j2\pi h\frac{\gamma}{N_1}}\,,$$

and it is non–singular if and only if the N complex numbers Q_γ are pairwise distinct and non-zero [68]. This is achieved by setting $N_1 > 2\,h\,L(M-1)$ so that the phases of each Q_γ are all distinct and contained in the interval $[-\pi,\pi)$. Therefore, choosing

$$N_1 > \max\{\,2L^2(M-1),\,2\,h\,L(M-1)\,\}$$

we can always find an N–tuple $(t_1,\ldots,t_n)$ such that the N vectors $\mathbf{f}_\gamma = [f_\gamma(t_1),\,\ldots,\,f_\gamma(t_N)]$, $\gamma \in \mathcal{A}_N$ are linearly independent. Note that this choice is always possible since M, L and h are finite.

Since the sampled vectors $\{\mathbf{f}_\gamma\}$ are linearly independent, the continuous functions $\{f_\gamma(t)\}$, $t \in [0,T)$, $\gamma \in \mathcal{A}_N$ are also linearly independent. As a matter of fact, if we could find a non–null linear combination $\sum_\gamma c_\gamma f_\gamma(t) = 0$ for all $t \in [0,T)$, then $\sum_\gamma c_\gamma f_\gamma(t_i) = 0$, which is not possible. □

B Appendix: Recurrence Solution

We want to prove that equation (6.20) has solutions of the form (6.21).

Considering that $A_n - A_{n-1} = a_n - a_{n-L}$, from (6.20) we obtain

$$p_{A_{n-1}+a_n-a_{n-L},k_1} = Z^{-A_{n-1}}p_{A_{n-1},k_0}\,, \tag{6.26}$$

which has to be satisfied for all input sequences $\{a_n\}$. Now, given a generic $\gamma \in \mathcal{A}_N$, $\gamma < N-1$, there exists a fixed sequence $\tilde{\mathbf{a}}_{n-1} = (\tilde{a}_{n-L},\ldots,\tilde{a}_{n-1})$ so that $A_{n-1} = \sum_{i=1}^{L}\tilde{a}_{n-i} = \gamma$ and $\tilde{a}_{n-L} < M-1$. The sequence $\tilde{\mathbf{a}}_{n-1}$ fixes the second term of (6.26). Now, if the input data $a_n = \tilde{a}_{n-L}$, then $A_n = A_{n-1} = \gamma$; if $a_n = \tilde{a}_{n-L}+2$ we have

$A_n = A_{n-1} + 2 = \gamma + 2$. Hence, in the first case $p_{\gamma,k_1} = Z^{-\gamma} p_{\gamma,k_0}$, while in the latter $p_{\gamma+2,k_1} = Z^{-\gamma} p_{\gamma,k_0}$. Therefore

$$p_{\gamma+2,k_1} = p_{\gamma,k_1}\,, \qquad \forall\, \gamma \in \mathcal{A}_N,\ \ \gamma < N-1\,. \tag{6.27}$$

The $N-1$ equalities (6.27) state that all the entries p_{γ,k_1}, for all $\gamma \in \mathcal{A}_N$, are equal to a constant, say π_0. From the latter statement and from (6.26) we have, $\pi_0 = Z^{-\gamma} p_{\gamma,k_0}$, which is satisfied for all $\gamma \in \mathcal{A}_N$, finally obtaining $p_{\gamma,k_0} = \pi_0 Z^{\gamma}$. This completes the proof. □

Conclusions

This thesis mainly investigated coding and decoding problems of noncoherent space–time codes. Our attention focused on unitary codes obtained via the exponential map. This specific topic requires an important mathematical background: space–time code theory, matrix theory and differential manifold basics.

One important contribution of this thesis is the collection and organization of the basic mathematical tools we need to understand EP codes. In particular, we hope to have provided a sufficiently clear description of the geometrical interpretation of the coding procedure in Chapter 3. In that chapter, one original and important contribution is Theorem 1, which relates the non–coherent code diversity to the diversity of the corresponding coherent code. This was a particularly hard task for two reasons: the first one is the non–linearity of the exponential map, the latter is the fact the the diversity is defined with respect to different detection criteria. Besides, the proof of Theorem 1 suggested relationships between training codes and EP codes. The example with commuting matrices at the end of Chapter 3 is original and the remark about generalized PSK codes and Givens codes too.

We believe that, in SISO case, the derivation of the new simplified decoder based on geometrical investigation in Chapter 4 is original. The application of the new simplified decoder to a SIMO systems is original too. Detailed discussions about the difficulties which prevented us from finding performing decoders for MIMO EP codes were never reported before (see Chapter 5). We hope that they can be helpful to other researchers who want to pursue this goal. The simplified decoders described in Chapter 5 are worth of attention as well as the discussion of the parameters choice, since they can be source of inspiration to ameliorate decoder performance.

Simulations show that GLRT performances of EP codes are substantially equivalent or slightly better than training–based codes performances, specially in SISO case for intermediate spectral efficiencies. When suboptimal and simplified decoding is applied, training–based codes seem to perform slightly better and to have smaller computational complexity. One of the possible research directions is to further develop EP code design and decoding, to reduce decoder complexity and to maintain diversity at the same time. We believe that the remarks about the relationship between EP codes and training–based codes quoted above can constitute a promising tool to cope with the search for new suboptimal efficient decoders or to understand in deep the reasons why one proposition eventually works better than the other.

Another topic which would be interesting to investigate is the theoretical upper and lower bound of error rate performances with respect to the local GLRT decoder here

proposed. For instance, such a study concerning the local GLRT could clarify if this suboptimal decoder have some floor and how much diversity is lost. Our simulations in fact show only performance behaviours in some particular cases, but they are not a proof. It would be interesting also to simulate performances in the general MIMO case when the number of receive antennas is greater that the number of transmit antennas ($N > M$), by applying the subspace basis estimation algorithm reported in this thesis. Another important point is to propose strategies to use more transmit antennas than receive ones ($M > N$), issue which is not treated in this thesis. The optimal number of active antenna M^* was chosen according to results of the ergodic channel. M^* should actually be revisited under the perspective of quasi–static or generic block fading channel, a more realistic channel model, which can lead to different strategies. This is a short list of issues which in my opinion should be addressed first. The solution to these problems can lead to the proposition of more flexible EP codes, and is an inevitable step toward practical implementations.

The original contributions of Chapter 6 are the equivalence principle for separable CPM signals and the new method to obtain PAM decompositions. This method also shows that these decompositions have minimal cardinality: it is not possible to find PAM decompositions with fewer pulses. Many topics can be further investigated. For instance, PAM decompositions have been recently applied to space–time coding, so that our decomposition can be a useful tool to design space–time codes for CPM system with linear phase response. Our decomposition can be applied to "classic" investigations: the simplification of the optimal CPM receiver, synchronization issues, etc.. The method to create PAM decompositions we propose can be generalized to CPM with general phase response. In this case the equivalence principle is no longer valid so that the decompositions cardinality is not linear with respect to the CPM signal memory. Therefore, for generic CPM signals our method does not produce decompositions more compact than the other ones proposed in literature. Anyway, the generation method itself is interesting and gives insights in the CPM signal structure. This understanding can be eventually a useful tool to deal with the above quoted problems.

Bibliography

[1] E. Biglieri, J. Proakis, and S. S. (Shitz), "Fading channels: Information–theoretic and communications aspects," *IEEE Trans. Inform. Theory*, vol. 44, no. 6, pp. 2619–2692, October 1998.

[2] E. Biglieri, G. Caire, and G. Taricco, "Limiting performance for block-fading channels with multiple antennas," *IEEE Trans. on Inform. Theory*, vol. 47, no. 4, pp. 1273–1289, May 2001.

[3] G. H. Golub and C. F. Van Loan, *Matrix Computations*, 3rd ed. Johns Hopkins University Press, 1996, ISBN 0-8018-5414-8.

[4] A. Edelman, T. A. Arias, and S. T. Smith, "The Geometry of Algorithms with Orthogonality Constraints," *Siam J. Matrix Anal. Appl.*, vol. 20, no. 2, pp. 303–353, 1998.

[5] A. Barg and D. Y. Nogin, "Bounds on packings in the Grassmann manifold," *IEEE Trans. Inform. Theory*, vol. 48, no. 9, pp. 2450–2454, Sep. 2002.

[6] D. Warrier and U. Madhow, "Spectrally Efficient Noncoherent Communication," *IEEE Trans. Inform. Theory*, vol. 48, no. 3, pp. 651–668, March 2002.

[7] A. Lapidoth and P. Narayan, "Reliable Communications Under Channel Uncertainty," *IEEE Trans. on Inform. Theory*, vol. 44, no. 6, pp. 2148–2177, October 1998.

[8] J. G. Proakis, *Digital Communications*, 4th ed. McGraw-Hill, 2000.

[9] B. M. Hochwald and T. L. Marzetta, "Unitary Space–Time Modulation for Multiple-Antenna Communications in Rayleigh Flat Fading," *IEEE Trans. Inform. Theory*, vol. 46, no. 2, pp. 543–564, March 2000.

[10] A. Dogandžiċ, "Chernoff Bounds on Pairwise Error Probabilities of Space–Times Codes," *IEEE Trans. Inform. Theory*, vol. 49, no. 5, pp. 1327–1336, May 2003.

[11] M. Brehler and M. K. Varanasi, "Asymptotic Error Probability Analysis of Quadratic Receivers in Rayleigh–Fading Channels with Applications to a Unified Analysis of Coherent and Noncoherent Space–Time Receivers," *IEEE Trans. Inform. Theory*, vol. 47, pp. 2383–2399, Sep. 2001.

[12] V. Tarokh, N. Seshadri, and A. R. Calderbank, "Space–time codes for high data rate wireless communications: Performance Criterion and code construction," *IEEE Trans. Inform. Theory*, vol. 44, no. 2, pp. 744–765, March 1998.

[13] D. Agrawal, T. J. Richardson, and R. L. Urbanke, "Multiple-Antenna Signal Constellations for Fading Channels," *IEEE Trans. Inform. Theory*, vol. 47, no. 6, pp. 2618–2626, September 2001.

[14] R. H. Gohary and T. N. Davidson, "Non-Coherent MIMO Communication: Grassmannian Constellation and Efficient Detection," in *Proc. of the International Symposium of Information Theory 2004 (ISIT2004)*, Chicago, USA, June 27 – July 2 2004, p. 65.

[15] M. L. McCloud, M. Brehler, and M. K. Varanasi, "Signal Design and Convolutional Coding for Noncoherent Space-Time Communication on the Block-Rayleigh-Fading Channel," *IEEE Trans. Inform. Theory*, vol. 48, no. 5, pp. 1186–1194, May 2002.

[16] M. Brehler and M. K. Varanasi, "Training-Codes for the Noncoherent Multi-Antenna Block-Rayleigh-Fading Channel," in *Proc. of the Conf. Inform. Sciences and Systems*, Johns Hopkins University, March 2003.

[17] M. J. Borran, A. Sabharwal, and B. Aazhang, "On Design Criteria and Construction of Noncoherent Space-Time Constellations," *IEEE Trans. Inform. Theory*, vol. 49, no. 10, pp. 2332–2351, October 2003.

[18] B. M. Hochwald, T. L. Marzetta, T. J. Richardson, W. Sweldens, and R. Urbanke, "Systematic design of Unitary Space–Time Constellations," *IEEE Trans. Inform. Theory*, vol. 46, no. 6, pp. 1962–1973, September 2000.

[19] Y. Jing and B. Hassibi, "Unitary Space–Time Modulation via Cayley Transform," *IEEE Trans. Signal Processing*, vol. 51, no. 11, pp. 2891–2904, Nov. 2003.

[20] J. Wang, X. Wang, and M. Madihian, "Optimum Design of Noncoherent Cayley Unitary Space–Time Codes," *IEEE Trans. Wireless Commun.*, submitted for pubblication, 2004.

[21] I. Kammoun, "Codage Spatio–temporel sans connaissance à priori du canal," Ph.D. dissertation, Ecole Nationale Supérieure des Télécommunications, Paris, 2004.

[22] I. Kammoun and J.-C. Belfiore, "A new family of Grassmannian space-time codes for non-coherent MIMO systems," *IEEE Comm. Letters*, vol. 7, pp. 528–530, Nov. 2003.

[23] V. Tarokh and I.-M. Kim, "Existence and Construction of Noncoherent Unitary Space-Time Codes," *IEEE Trans. Inform. Theory*, vol. 48, no. 12, pp. 3112–3117, December 2002.

[24] W. Zhao, G. Leus, and G. Giannakis, "Orthogonal design of unitary constellations for uncoded and trellis coded non–coherent space–time systems," *IEEE Trans. Inform. Theory*, vol. 50, no. 6, pp. 1319–1327, June 2004.

[25] F. Oggier, N. Sloane, A. Calderbank, and S. Diggavi, "Nonintersecting Subspaces Based on Finite Alphabets," submitted to *IEEE Trans. Inform. Theory*. [Online]. Available: http://www.research.att.com/~njas/

[26] P. Dayal, M. Brehler, and M. K. Varanasi, "Leveraging coherent space-time codes for noncoherent communication via training," *IEEE Trans. Inform. Theory*, vol. 50, no. 9, pp. 2058–2080, September 2004.

[27] H. E. Gamal and M. O. Damen, "Universal Space–Time Coding," *IEEE Trans. Inform. Theory*, vol. 49, no. 5, pp. 1097–1119, May 2003.

[28] H. E. Gamal, D. Aktas, and M. O. Damen, "Coherent Space–Time Codes for Noncoherent Channels," in *Proc. IEEE Global Telecommunications Conference*, San Francisco, CA, December 7–10 2003.

[29] ——, "Noncoherent Space–Time Coding: an Algebraic Perspective," *IEEE Trans. Inform. Theory*, submitted for pubblication, 2003.

[30] L. Zheng and D. N. C. Tse, "Communication on the Grassmann Manifold: A Geometric Approach to the Noncoherent Multiple–Antenna Channel," *IEEE Trans. Inform. Theory*, vol. 48, no. 2, pp. 359–383, February 2002.

[31] I. Kammoun and J.-C. Belfiore, "Grassmann-based signal design for noncoherent reception," in *Proc. of the IV IEEE International Workshop on Signal Processing Advances for Wireless Communications (SPAWC2003)*, Rome, Italy, June 2003, pp. 564–568.

[32] M. O. Damen, A. Tewfik, and J.-C. Belfiore, "A Construction of a Space–Time Code Based on Number Theory," *IEEE Trans. Inform. Theory*, vol. 48, no. 3, pp. 753–760, Mar. 2002.

[33] J.-C. Belfiore, G. Rekaya, and E. Viterbo, "The Golden Code: a 2×2 Full–Rate Space–Time Code with Non–Vanishing Determinants," *IEEE Trans. Inform. Theory*, submitted for publication. [Online]. Available: http://www.comelec.enst.fr/~belfiore/

[34] P. A. Laurent, "Exact and approximate construction of digital phase modulations by superposition of amplitude modulated pulses," *IEEE Trans. Commun.*, vol. 34, pp. 150–160, February 1986.

[35] U. Mengali and M. Morelli, "Decomposition of M-ary CPM Signals into PAM Waveforms," *IEEE Trans. Inform. Theory*, vol. 41, pp. 809–820, September 1995.

[36] X. Huang and Y. Li, "The PAM Decomposition of CPM Signals with Integer Modulation Index," *IEEE Trans. Commun.*, vol. 51, pp. 543–546, April 2003.

[37] G. Colavolpe and R. Raheli, "Reduced-Complexity detection and phase synchronization of CPM Signals," *IEEE Trans. Commun.*, vol. 45, pp. 1070–1079, September 1997.

[38] ——, "Noncoherent Sequence Detection," *IEEE Trans. Commun.*, vol. 47, pp. 1376–1385, September 1999.

[39] G. K. Kaleh, "Simple coherent receivers for partial response continuous phase modulation," *IEEE J. Select. Areas Commun.*, vol. 7, pp. 1427–1436, September 1989.

[40] A. N. D'Andrea, A. Ginesi, and U. Mengali, "Frequency detectors for CPM signals," *IEEE Trans. Commun.*, vol. 43, pp. 1828–1837, Feb.-Mar.-Apr. 1995.

[41] T. L. Marzetta and B. M. Hochwald, "Capacity of a Mobile Multiple–Antenna Communication Lynk in Rayleigh Flat Fading," *IEEE Trans. Inform. Theory*, vol. 45, no. 1, pp. 139–157, Jan. 1999.

[42] R. G. Gallager, *Information Theory and Reliable Communications*. New York: Wiley, 1968.

[43] L. H. Ozarow, S. Shamai, and A. D. Wyner, "Information Theoretic Considerations for Cellular Mobile Radio," *IEEE Trans. Inform. Theory*, vol. 43, no. 2, pp. 359–378, May 1994.

[44] E. Telatar, "Capacity of multi–antenna gaussian channels," *European Transaction on Telecommunications (ETT)*, vol. 10, no. 6, November/December 1999.

[45] L. Zheng, "Diversity-Multiplexing Tradeoff: A Comprehensive View of Multiple Antenna Systems," Ph.D. dissertation, University of California, Berkeley, 2002. [Online]. Available: http://web.mit.edu/lizhong/www/

[46] I. C. Abou-Faycal, M. D. Trott, and S. Shamai, "The capacity of discrete–time rayleigh–fading channels," *IEEE Trans. Inform. Theory*, vol. 47, no. 4, pp. 1290–1301, May 2001.

[47] G. Taricco and M. Elia, "Capacity of fading channel with no side information," *IEE Electron. Lett.*, vol. 33, no. 16, pp. 1368–1370, July 1997.

[48] B. Hassibi and T. L. Marzetta, "Multiple–Antennas and isotropically random unitary inputs: the received signal density in closed form," *IEEE Trans. Inform. Theory*, vol. 48, no. 6, pp. 1473–1484, June 2002.

[49] L. Zheng and D. N. C. Tse, "Diversity and multiplexing: a fundamental tradeoff in multiple–antenna channels," *IEEE Trans. Inform. Theory*, vol. 49, no. 5, pp. 1073–1096, May 2003.

[50] G. Bauch, "Introduction to Multi-Antenna Systems and Space-Time Codes," in *Proc. of the 3rd International Workshop on Commercial Radio Sensors and Communication Techniques*, Linz, Austria, Aug. 2001, pp. 50–56.

[51] S. Siwamogsatham, M. P. Fitz, and J. H. Grimm, "A New View of Performance Analysis of Transmit Diversity Schemes is Correlated Rayleigh Fading," *IEEE Trans. Inform. Theory*, vol. 48, no. 4, pp. 950–956, April 2002.

[52] D. Tse and P. Viswanatan, "Fundamentals of Wireless Communication Course Notes," Fall 2002, U.C. Berkeley.

[53] A. Paulraj, R. Nabar, and D. Gore, *Introduction to Space-Time Wireless Communications*. Cambridge Univ. Press, May, 2003.

[54] S. M. Alamouti, "A simple transmit diversity technique for Wireless Communications," *IEEE J. Select. Areas Commun.*, vol. 16, no. 8, pp. 1451–1458, October 1998.

[55] A. Paulraj and C. B. Papadias, "Space–Time Processing for Wireless Communications," *IEEE Signal Processing Mag.*, vol. 14, no. 5, pp. 49–83, November 1997.

[56] S. G. Wilson, *Digital modulation and coding*. Prentice Hall, 1996.

[57] J. H. Conway, R. H. Hardin, and N. J. A. Sloane, "Packing Lines, Planes, etc.: Packings in Grassmannian Spaces," *Experimental Mathematics*, vol. 5, no. 2, pp. 139–159, 1996.

[58] T. M. Cover, J. A. Thomas, *Elements of Information Theory*. New York: Wiley, 1991.

[59] T. L. Marzetta, B. Hassibi, and B. M. Hochwald, "Structured Unitary Space–Time Autocoding Constellations," *IEEE Trans. Inform. Theory*, vol. 48, no. 4, pp. 942–950, April 2002.

[60] E. Agrell, T. Eriksson, A. Vardy, and K. Zeger, "Closest Point Search in Lattices," *IEEE Trans. Inform. Theory*, vol. 48, pp. 2201–2214, Aug. 2002.

[61] B. Hassibi and B. M. Hochwal, "Cayley Differential Unitary Space–Time Codes," *IEEE Trans. Inform. Theory*, vol. 48, no. 6, pp. 1485–1503, June 2002.

[62] V. Tarokh, H. Jafarkhani, and A. R. Calderbank, "Space–time block codes from orthogonal–designs," *IEEE Trans. Inform. Theory*, vol. 45, no. 5, pp. 744–765, July 1999.

[63] B. Hassibi and B. M. Hochwald, "How much Training is Needed in Multiple-Antenna Wireless Links?" *IEEE Trans. Inform. Theory*, vol. 49, no. 4, pp. 951–963, April 2003.

[64] E. Viterbo and J. Boutros, "A universal Lattice Decoder for Fading Channels," *IEEE Trans. Inform. Theory*, vol. 45, pp. 1639–1642, July 1999.

[65] M. O. Damen, H. E. Gamal, and G. Caire, "On Maximum–Likelyhood Detection and the Search for the Closest Lattice Point," *IEEE Trans. Inform. Theory*, vol. 49, pp. 2389–2402, Oct. 2003.

[66] B. Hassibi and H. Vikalo, "On the Sphere Decoding Algorithm. I. Expected Complexity," *IEEE Trans. Signal Processing*, submitted for pubblication.

[67] H. Vikalo and B. Hassibi, "On the Sphere Decoding Algorithm. II. Generalizations, Second Order Statistics, and Applications to Communications," *IEEE Trans. Signal Processing*, submitted for pubblication.

[68] R. A. Horn and C. J. Johnson, *Matrix Analysis*. New York: Wiley, 1958.

[69] N. Benvenuto and G. Cherubini, *Algorithms for Communications Systems and their applications*. Wiley, 2003.

[70] F. W. Warner, *Foundations of Differentiable Manifolds and Lie Groups*. Scott, Foresman and Company, 1971.

[71] S. A. Gaal, *Linear Analysis and Representation Theory*. Springer-Verlag, 1973.

[72] Wolfram, "Mathworld," maintained by Eric Weisstein. [Online]. Available: http://mathworld.wolfram.com

[73] M. Abramowitz and I. A. Stegun, *Handbook of Mathematical Functions*. New York: Dover Publications, 1972.

[74] W. Sweldens, "Fast Block Noncoherent Decoding," *IEEE Commun. Lett.*, vol. 5, no. 4, pp. 132–134, April 2001.

[75] C. M. Monti, G. Pierobon, *Esercitazioni di Teoria della Probabilità: Vettori Aleatori*. Padova: Progetto, 1992, in italiano.

[76] Steven M. Kay, *Fundamentals of statistical signal processing: detection theory*. Upper Saddle River, NJ: Prentice Hall, 1998.

[77] J. Boutros, N. Gresset, L. Brunel, and M. Fossorier, "Soft–input soft–output lattice sphere decoder for linear channels," in *Globecom'03*, Linz, Austria, August 2001, pp. 50–56.

[78] F. Oggier and E. Viterbo, "Algebraic Number Theory and its Applications to code design of Rayleigh fading channels," 2004, book to be published.

[79] J.-C. Belfiore and G. Rekaya, "Quaternionic lattices for space–time coding," in *Proc. of the Information Theory Workshop (ITW 2003)*, Paris. France, March 2004. [Online]. Available: http://www.comelec.enst.fr/~rekaya/

[80] F. Oggier, G. Rekaya, J.-C. Belfiore, and E. Viterbo, "Perfect Space Time Block Codes," *IEEE Trans. Inform. Theory*, submitted for publication. [Online]. Available: http://www.comelec.enst.fr/~rekaya/

[81] E. Bayer-Fluckiger, F. Oggier, and E. Viterbo, "New Algebraic Constructions of Rotated Z^n–Lattice Constellations for the Rayleigh Fading Channel," *IEEE Trans. Inform. Theory*, vol. 50, no. 4, pp. 702–714, April 2004.

[82] N. Rydbeck, T. Aulin, and C. W. Sundberg, "Continuous Phase Modulation: Part I and II," *IEEE Trans. Commun.*, vol. COM-29, pp. 196–225, March 1981.

[83] T. Aulin, J. B. Anderson, and C. W. Sundberg, *Digital Phase Modulation*. New York: Plenum, 1986.

[84] J. H. Lodge and M. L. Moher, "Maximum-Likelihood Sequence estimation of CPM signals transmitted over Rayleigh Flat-Fading Channels," *IEEE Trans. Commun.*, vol. 41, no. 6, pp. 787–794, January 1990.

[85] X. Zhang and M. P. Fitz, "Space–time code design with continuous phase modulation," *IEEE J. Select. Areas Commun.*, vol. 21, no. 5, pp. 783–792, September 2003.

[86] J. B. Anderson and C. E. W. Sundberg, "Advances in constant envelope coded modulation," *IEEE Commun. Mag.*, vol. 29, pp. 36–45, December 1991.

[87] M. K. Simon and D. Divsalar, "Maximum-Likelihood Block Detection of Noncoherent Continuous Phase Modulation," *IEEE Trans. Commun.*, vol. 41, no. 1, pp. 90–98, January 1993.

[88] G. K. Kaleh, "Differential Detection via the Viterbi Algorithm for offset modulation and MSK-type signals," *IEEE Trans. Veh. Technol.*, vol. 41, pp. 401–406, November 1992.

[89] G. Cariolaro and A. M. Cipriano, "An Equivalence Principle for Separable CPM Signals," in *Proc. 15th IEEE Intl. Symp. on Personal, Indoor and Mobile Radio Communications (PIMRC'04)*, vol. 2, Barcelona, Spain, September 2004, pp. 1347–1350.

[90] E. Obetti, "The Decomposition of CPM Signals into PAM Waveforms," Ph.D. dissertation, University of Padua, Padua, Italy, December 2001.